AD NUMBER

AD894052

LIMITATION CHANGES

TO:

Approved for public release; distribution is unlimited. Document partially illegible.

FROM:

Distribution authorized to U.S. Gov't. agencies only; Test and Evaluation; MAR 1962. Other requests shall be referred to Army Materials and Mechanics Research Center, Attn: AMXMR-STL, Watertown, MA 02172. Document partially illegible.

AUTHORITY

darpa ltr, 19 dec 1974

AD

AMMRC CTR 72-3

BRITTLE MATERIALS DESIGN, HIGH TEMPERATURE GAS TURBINE

Technical Report By:

Arthur F. McLean, Ford Motor Company, Dearborn, Michigan 48121
Eugene A. Fisher, Ford Motor Company, Dearborn, Michigan 48121
Don E. Harrison, Westinghouse Electric Corporation, Pittsburgh, Pennsylvania 15235

March, 1972

Interim Report, July 1, 1971 to December 31, 1971

Contract Number DAAG 46-71-C-0162

ARPA Order Number 1849

Project Code Number 1D10

Agency Accession Number DA OD 4733

Prepared for

ARMY MATERIALS AND MECHANICS RESEARCH CENTER
Watertown, Massachusetts 02172

DISCLAIMER NOTICE

THIS DOCUMENT IS THE BEST QUALITY AVAILABLE.

COPY FURNISHED CONTAINED A SIGNIFICANT NUMBER OF PAGES WHICH DO NOT REPRODUCE LEGIBLY.

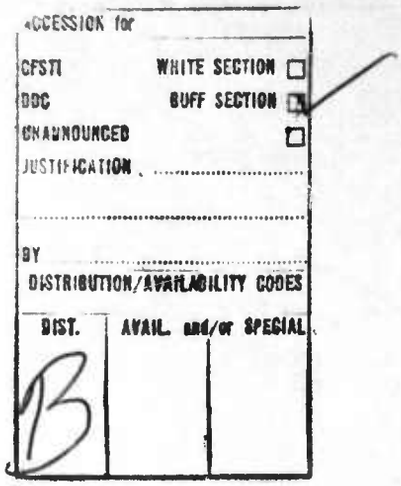

AMMRC CTR 72-3

BRITTLE MATERIALS DESIGN, HIGH TEMPERATURE GAS TURBINE

Technical Report By:

Arthur F. McLean, Ford Motor Company, Dearborn, Michigan 48121
Eugene A. Fisher, Ford Motor Company, Dearborn, Michigan 48121
Don E. Harrison, Westinghouse Electric Corporation, Pittsburgh, Pennsylvania 15235

March, 1972

Interim Report, July 1, 1971 to December 31, 1971

Contract Number DAAG 46-71-C-0162

ARPA Order Number 1849

Project Code Number 1D10

Agency Accession Number DA OD 4733

Prepared for:

ARMY MATERIALS AND MECHANICS RESEARCH CENTER
Watertown, Massachusetts 02172

ABSTRACT

The "Brittle Materials Design, High Temperature Gas Turbine" program is to demonstrate successful use of brittle materials in demanding high temperature structural applications. A small vehicular gas turbine and a large stationary gas turbine, each utilizing uncooled ceramic components, will be used in this iterative design and materials development program. Both the contractor, Ford Motor Company, and the prime subcontractor, Westinghouse Electric Corporation, have had in-house research programs in this area prior to this contract.

In the vehicular gas turbine project, ceramic turbine components of improved design were fabricated and engine testing was started. During the first contract reporting period, silicon nitride turbine stators of the new design have shown considerably improved durability in testing to date. New design silicon nitride nose cones were fabricated by injection molding. Design studies on ceramic turbine rotors have shown that computed operating stresses can be withstood by dense silicon carbide and dense silicon nitride. Development programs were started to fabricate rotors in these materials.

Work on the stationary turbine project has concentrated on materials evaluation and initial design of ceramic stator vanes. Maximum calculated vane stresses were reduced 40% by decreasing the stator vane chord. The strength of hot-pressed silicon nitride, one of the candidate materials, has been significantly improved. A variety of microstructural details of this material have been identified. Physical property data were obtained on hot pressed silicon nitride.

FOREWORD

This report is the first semi-annual technical report of the "Brittle Materials Design, High Temperature Gas Turbine" program initiated by the Advanced Research Projects Agency, ARPA Order Number 1849, and monitored by the Army Materials and Mechanics Research Center, under Contract Number DAAG-46-71-C-0162. This is an incrementally-funded five year program.

Since this is an iterative design and materials development program, design concepts and materials selection and/or properties presented in this report will probably not be those finally utilized. Thus all design and property data contained in the semi-annual reports must be considered tentative, and the reports should be considered to be illustrative of the design, materials processing and NDT techniques being developed for brittle materials.

The principal investigator of this program is Mr. A. F. McLean, Ford Motor Company, and the technical monitor is Dr. A. E. Gorum, AMMRC. The authors would like to acknowledge the valuable contributions in the performance of this work by the following people:

Ford Motor Company

D. J. Cassidy, J. J. Charneski, D. A. Davis, G. C. DeBell, P. H. Havstad, E. R. Herrmann, C. F. Johnson, J. A. Mangels, W. E. Meyer, J. J. Mittman, P. F. Nicholls, A. Paluszny, J. J. Schuldies, J. M. Scofield, K. H. Styhr, W. Trela.

Westinghouse Electric Corporation

R. J. Bratton, C. R. Booher, S. M. DeCorso, W. C. Frazier, A. N. Holden, L. Kish, R. Kossowski, F. F. Lange, S. Y. Lee, S. Leshnoff, D. G. Miller, T. J. Rahaim, J. D. Roughgarden, S. G. Singhal, C. Visser, W. E. Young.

TABLE OF CONTENTS

LIST OF ILLUSTRATIONS

LIST OF TABLES

1. INTRODUCTION

As stipulated by the Advanced Research Projects Agency of the Department of Defense, the major purpose of this program is to demonstrate that brittle materials can be successfully utilized in demanding high temperature structural applications. The gas turbine engine, utilizing uncooled ceramic components in the hot flow path, was chosen as the vehicle for this demonstration. Two hundred hours of operation over a representative duty cycle at ceramic temperatures up to 2500°F is required for the demonstration.

It is the further purpose of this program to develop design technology for ceramic materials on a systems basis requiring close integration of design, engineering, materials selection, materials processing and fabrication, testing and evaluation.

The progress of the gas turbine engine has been closely related to the development of materials capable of withstanding the engine's environment at high operating temperature. Since the early days of the jet engine, new metals have been developed which have allowed a gradual increase in operating temperatures. Today's nickel-chrome superalloys are in use without cooling at turbine inlet gas temperatures of 1800° to 1900°F.[1] However, there is considerable incentive to further increase turbine inlet temperature to improve specific air and fuel consumptions. The use of ceramics in the gas turbine engine as a demonstration vehicle for this program promises to make a major step in increasing turbine inlet temperature. Success will offer significant advances in engine efficiency, power per unit weight, cost, pollution abatement, and fuel utilization.

This program will demonstrate the use of ceramics in two demanding gas turbine applications:

(1) A small-vehicular type of engine (Ford). Such an engine would have a major impact on the technology of mobile field power units, military vehicles and craft. As a consequence of its significantly increased operating temperature it would not only provide more horsepower/unit weight than current engines, but would also provide improved fuel economy. In addition, the benefits of low emissions and multi-fuel capability are attained. A simplified schematic of the flow path of this regenerative type of engine is shown in Figure 1.1. A brief explanation of this flow path will be given to familiarize the reader with the various components considered for ceramics. Air is induced through an intake silencer and filter into a radial compressor, and then is compressed and ducted through one side of each of two rotary regenerators. The hot compressed air is then supplied to a combustion chamber where fuel is added and combustion takes place.

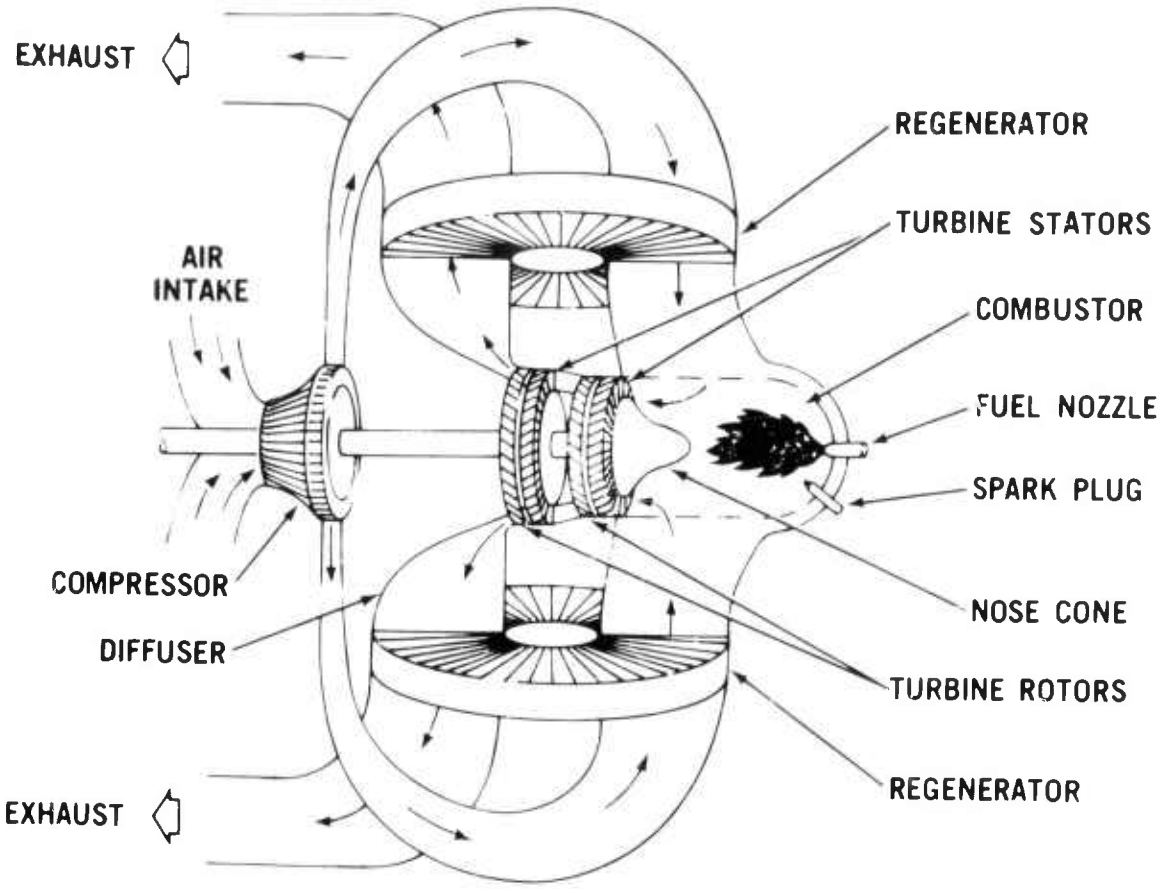

Figure 1.1 — Flow Path Schematic of Vehicular Gas Turbine

The hot gas discharging from the combustor is then directed into the turbine stages by a turbine inlet structure, in this case shown as a nose cone. The gas then passes through the turbine stages which comprise two turbine stators, each having stationary airfoil blades which direct the gas onto each corresponding turbine rotor. In passing through the turbine, the gas expands and generates work to drive the compressor and supply useful power. The expanded turbine exhaust gas is then ducted through the hot side of each of the two regenerators which, to conserve fuel consumption, transfer much of the exhaust heat back into the compressed air.

The parts which are subject to the peak cycle temperature and are made out of superalloys in today's gas turbine are the combustor, the turbine inlet nose cone, the turbine stators and the turbine rotors. These are areas where ceramics could be exploited to the fullest and have been selected for application in the vehicular turbine project.

(2) A large-stationary gas turbine for electric power production (Westinghouse). Such an engine would be most desirable for DOD installations requiring on site power generation. Not only will ceramics facilitate significantly increased operating temperatures with attendant improvement in power and fuel economy, but, because of their improved corrosion-erosion resistance they will also facilitate use of low cost residual fuel. In addition, the environmental benefits of low emissions and lack of cooling water (with its attendant thermal pollution problems) are attained. A simplified sketch of the hot flow path of the engine is shown in Figure 1.2. As with the vehicular turbine project, a brief explanation of the flow path of the stationary turbine will be given to help the reader understand the function of the components to be made from ceramic materials.

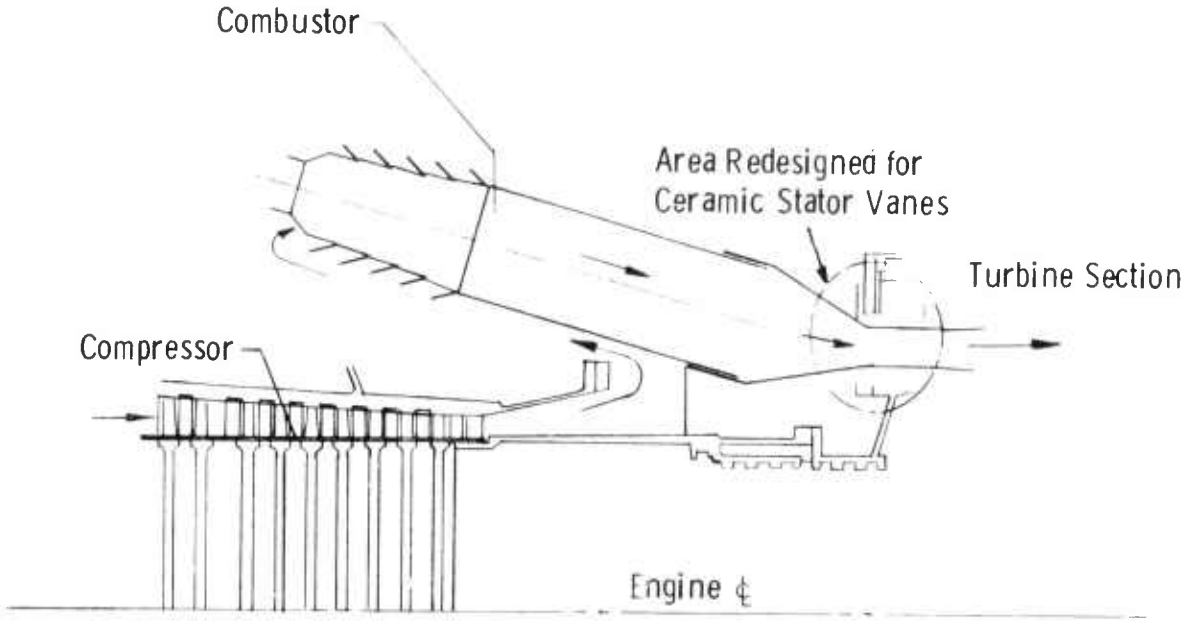

Figure 1.2 — 30 Mw Test Turbine Flow Path

Air is induced through a large intake silencer and filter into an 18 stage axial compressor where it is compressed before entering the combustor housing. The combustor housing supplies air at 650°F to combustion cans assembled in a circumferential array. Air is mixed with distillate fuel or natural gas and ignited in the primary combustion zone. The gas passes down stream through the combustors mixing with secondary air. Flow continues from the combustion section, through the transition zone, and enters the power turbine at a gas temperature of 2500°F. The hot gases expand through the three stage turbine section and are either exhausted through a stack or ducted into a reheat boiler as part of a combined cycle power generating unit.

The parts, where ceramics could be exploited to the fullest, selected for application in the stationary turbine project are the first stage turbine stator vanes and the first stage turbine rotor.

To maintain coherence, progress on the vehicular and stationary turbine projects are reported separately. Also reported separately is the common link between these two programs, materials technology. Information presented under materials technology is general, and does not specifically apply to one or the other of the gas turbine engines. On the other hand, items reported under the vehicular and stationary turbine projects are categorized by components and therefore relate directly to those projects (even these items, however, are indirectly related when it comes to such considerations as design techniques, etc.). Figure 1.3 has been prepared to help the reader understand the interrelationship between the major elements of the report.

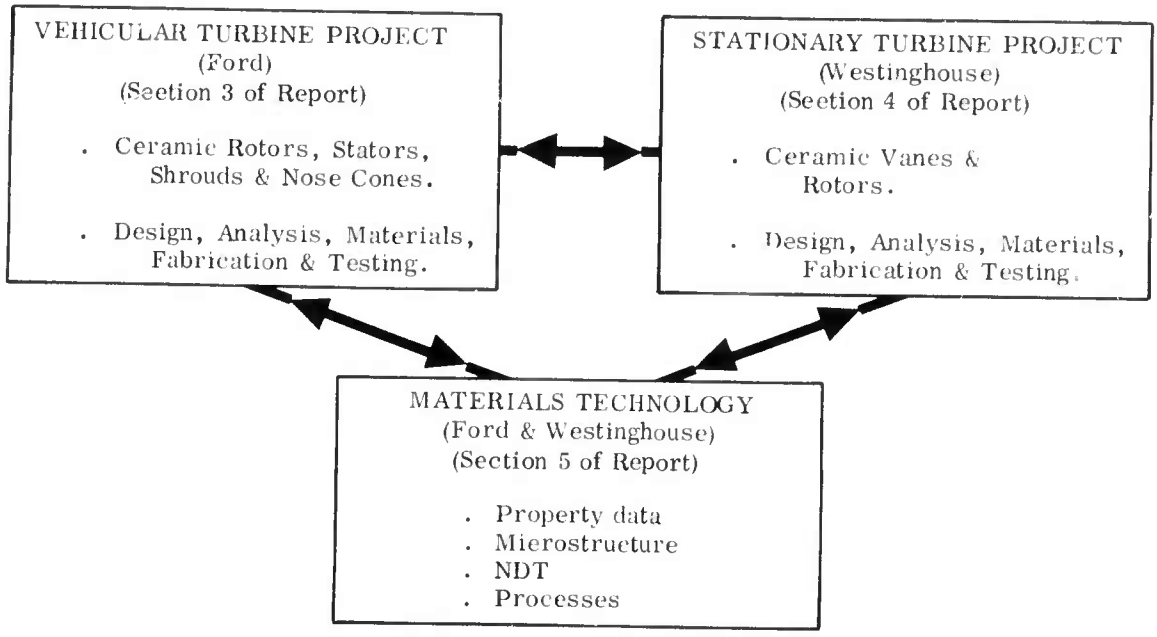

Figure 1.3 — Brittle Material Design/High Temperature Gas Turbine - Breakdown of Major Elements Reported

Successful demonstration of a high temperature gas turbine engine will involve a complex iterative development. One cannot divorce the development of ceramic materials from processes for making parts; no more so can one isolate the design of those parts from how they are made or from what they are made. Likewise, the design of mountings and attaehments between metal and ceramic parts within the engine are equally important. Innovation in the control of the environment of critical engine components is another link in the chain. Each of these factors has a relationship with the others, and to obtain success in any one may involve compromises in the others. Testing plays an important role during the iterative development sinee it provides a positive, objective way of evaluating the various combinations of factors involved. If successful, the test forms the credibility to move on to the next link in the development chain. If unsuccessful, the test flags a warning and prompts feedback to earlier developments to seek out and solve the problem which has resulted in failure. Finally, all of the links in the chain are evaluated by a complete engine test, by which means the ultimate objective of the program will be demonstrated.

Figure 1.4 shows a block diagram flow chart of the major factors involved including the feedback loops, which serves to illustrate this complex and comprehensive iterative development program. The starting point is the concept of a design to use brittle materials. From this, a design layout is prepared and analyzed leading to the detailed design and analysis of the gas turbine engine components made of or involving ceramics. In parallel with the design phase, ceramic materials are developed and screened for application to the gas turbine engine. Process development of candidate ceramics then takes place and material science and property evaluation are used to improve materials and processes, and to feed information back into the design phase. Next with the first detail designs completed and with the process for the selected ceramics reasonably developed, tooling can be designed and fabrication development started to make actual ceramic turbine engine components. Non-destructive testing of these parts will be developed to form a feedback for improving material and fabrication methods. In conjunction with non-destructive evaluation, techniques will be developed for proof testing ceramic components prior to use in engines. In parallel with ceramic part fabrication, proof testing, and non-destructive evaluation, metal parts for the ceramic turbine engine and test rigs are made per the detail design requirements. The ceramic and metal parts are then dimensionally inspected and instrumented for engine testing. Assembly techniques for brittle materials are developed, and testing and durability developments in both test rigs and engines are performed. Failure analysis from test rig and engine testing forms the feedback loops for corrective action; almost all of the factors involved in the development could be affected by experience learned in the test phase of the program. Finally, when engine durability has reached a given level of development, the 200 hour demonstration test will be conducted to meet the program objective.

It should be noted that both the contractor and the prime subcontractor have had in-house research programs in this area prior to the initiation of the current program. Many ceramic materials were extensively tested and screened leading to the selection of silicon nitride and silicon carbide.[1] In the stationary turbine program, preliminary design concepts were in existence before the award of the contract. In the vehicular turbine program, development was fairly well along and at least one pass had been completed through all of the factors shown in Figure 1.4 prior to the initiation of this program. Although there have been many minor iterations, the design configuration of the first major iteration is referred to as Design 'A.' Based on the experience gained during this development, a Design 'B' configuration was generated and is currently under evaluation. Both Design 'A' and Design 'B' will be referred to in the report under the Vehicular Turbine Project.

This report covers the progress in the period July 1, 1971 to December 31, 1971 plus background information where required.

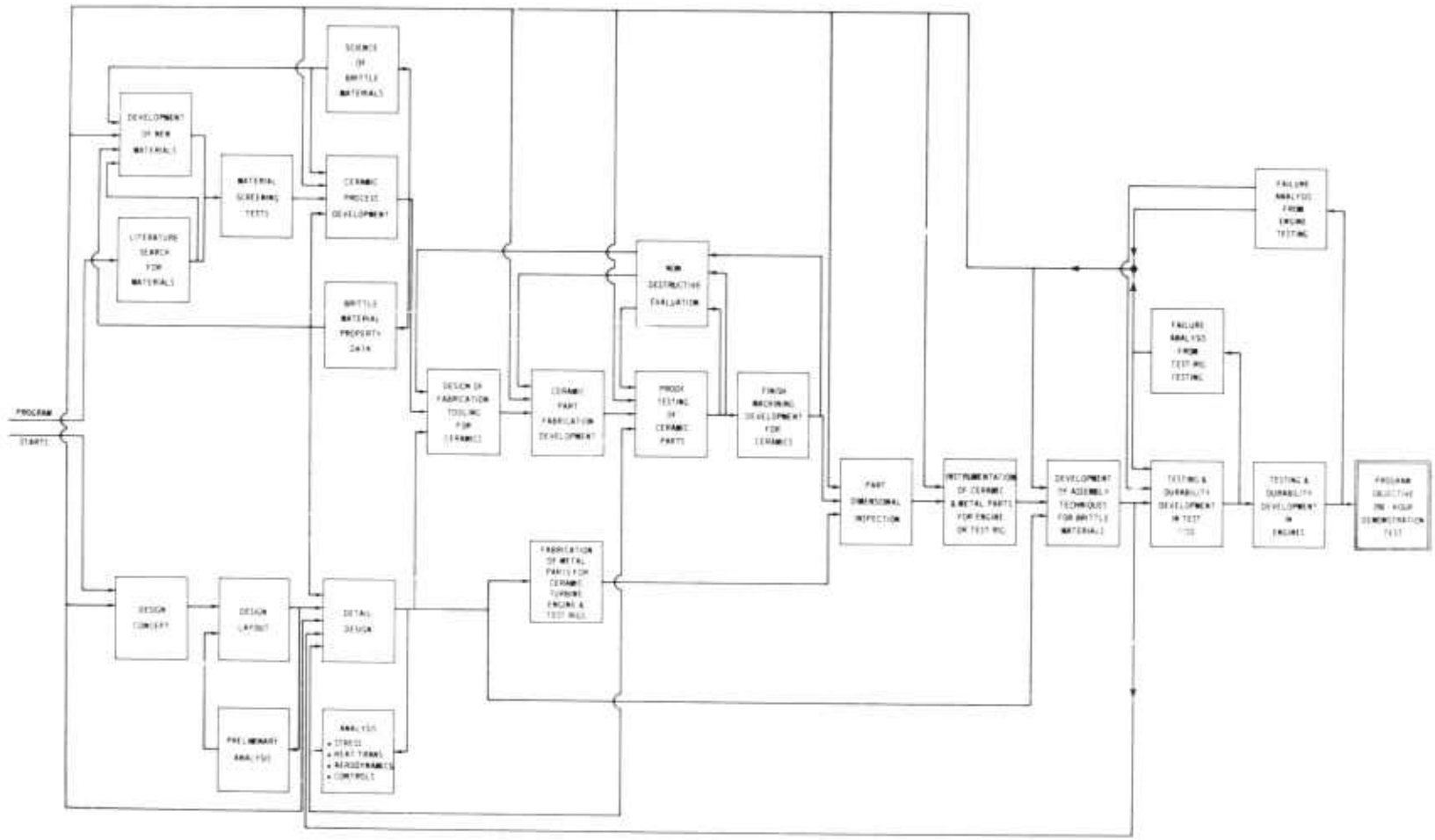

Figure 1.4 — Brittle Material Design/High Temperature Gas Turbine - Block Diagram Flow Chart of Iterative Development

2. SUMMARY OF PROGRESS

2.1 VEHICULAR TURBINE PROJECT

Progress was made on a broad front in all the major task areas which make up the vehicular turbine project. (1) Based upon previous experience gained in design technology and ceramic material and process development, ceramic turbine engine components of improved efficiency and durability were designed, fabricated and have undergone initial testing. (2) Design and material studies in the development of ceramic turbine rotors show promise that performance and durability goals can be met. (3) Ultrasonic defect detection and acoustic emissions testing show promise as analytical tools.

(1) Modified ceramic stators (Design B) were designed and analyzed, tooling procured, and components successfully fabricated in reaction-sintered silicon nitride. Test results to date indicate improved efficiency and durability.

(2) Turbine rotor design studies showed that the calculated maximum tensile stresses in a dense silicon nitride turbine wheel were 56,000 psi; this is well below the current material flexural strength. A preliminary design with acceptable stress levels was conceived for rotors made from chemically vapor deposited silicon carbide. Work was started in-house, with the Norton Company, and with Energy Research Corporation to develop rotor fabrication methods using these materials. A study of the attachment of the ceramic rotors to the metallic turbine shaft resulted in the identification of problem areas.

(3) Ultrasonic defect detection techniques applied to turbine ceramic materials were found to be capable of locating internal flaws with a high degree of sensitivity. Acoustic emission testing of ceramic was initiated, and showed promise of measuring the onset of dangerous stress levels in ceramic materials.

2.2 STATIONARY TURBINE PROJECT

Progress was made in three areas of importance to the successful utilization of uncooled ceramic stator vanes: (1) a stator vane design that operates at stress levels well within the capability of currently available materials, (2) a capability for making sufficiently strong ceramics of the required size, and (3) a characterization of the engineering properties of silicon carbide and silicon nitride.

(1) Analysis of the transient thermal stresses in stator vanes revealed that the maximum thermal stresses could be reduced by 40% through halving the chord of current designs. The maximum transient stress is then 25,000 psi which appears to be well below the ultimate strength of hot-pressed silicon nitride.

Several three-piece stator vane design concepts which can be fabricated by available diamond-grinding techniques are being evaluated to minimize stress concentrations.

(2) During the last year, the Norton Company has made substantial improvements in the high-temperature strength properties of silicon nitride billets of sufficient size for stator vanes. This material should be capable of withstanding turbine inlet temperatures of at least 2200°F. A creep problem may occur at higher temperatures due to the MgO additives used for the hot pressing process. In this temperature range, silicon carbide holds considerable promise, although its fabrication technology is not as far advanced.

Energy Research Corporation is developing a capability for making in-situ vanes of silicon carbide by Chemical Vapor Deposition and Norton is developing hot-pressed silicon carbide on a privately funded program.

(3) Physical property data were obtained from the first lot of hot-pressed silicon nitride supplied by Norton. Tensile strength is about 60% of the flexural strength which is at the 100,000 psi level. Fatigue endurance limits (using 10^7 cycles as a practical limit) were 70,000 psi at 250°F, 30,000 psi at 1800°F, and 20,000 psi at 2200°F. These limits are again about 60% of the flexural strength at temperature.

A variety of microstructural details such as grain size, phase composition, dislocation arrays, stacking faults, and impurity agglomerates were identified using electron microscopy techniques. Since most of these microstructural effects have never been studied, their significance to the engineering performance of silicon nitride and silicon carbide has yet to be established.

Extended corrosion-erosion test periods of up to 125 hrs continue to reflect the outstanding oxidation resistance of silicon nitride at 2000°F.

3. PROGRESS ON VEHICULAR TURBINE PROJECT

3.1 CERAMIC ROTORS

3.1.1 DESIGN AND ANALYSIS

SUMMARY

A design concept for dense Si_3N_4 turbine rotors has been selected. The concept features two turbine stages, with individual disks of modified hyperbolic profile made integrally with blades. Coupling between disks and the turbine shaft is accomplished by means of a central tension bolt. Candidate concepts for the attachment bolt have been identified and are being evaluated. An air cooled bolt was selected as the best candidate for development. Immediate plans call for reassessment of transient and steady state rotor stresses with consideration of effects of bolt cooling and loading.

Introduction

Design of turbine rotors for a vehicular gas turbine is an involved process of optimizing trade-offs between aerodynamic and performance requirements on one hand and the limitations imposed by either material properties and/or fabrication processes on the other. These trade-offs are particularly critical in the case of brittle materials such as ceramics. Complete lack of ductility leaves little room for error, so that extreme care must be exercised in determining boundary conditions and loading modes. Often seemingly insignificant changes in fabrication parameters may profoundly affect material strength.

The design concepts currently being investigated are the results of such an optimization process. With the exception of transient operating conditions, which were conservatively simplified to reduce computational time, all pertinent trade-off parameters were duly considered in the selection of prospective design concepts for ceramic rotors.

Throughout the report, reference will be made to metallic rotors, which are used in some parallel Ford programs. Though not specifically part of this contract, metal turbines will be used in test programs of stationary ceramic parts until ceramic turbine rotors have been developed.

As much of the design work on ceramic turbine rotors was done prior to the contract, only a cursory review of aerodynamic and mechanical considerations will be presented.

Turbine rotors and stators are intimately related aerodynamically and are influential in the design of the entire hot flow path. For convenience and clarity, therefore, aerodynamic design aspects for all of the hot flow path are discussed in this section.

The main difference between ceramic and metallic turbine blade designs, from an aerodynamic point of view, is the increased flow area blockage due to the need to avoid unusually thin blade trailing edges in the ceramic blades. A stator vane trailing edge thickness of 0.020 inches was selected as the minimum desirable in the initial stages of ceramic blade development. This resulted in a flow area blockage 2 to 3 times greater than normally obtained in metal designs. All other aspects of the design have so far followed along conventional lines, with a "free vortex" flow distribution being used to determine the velocity triangles. Efficiency estimates and off-design characteristics were determined using a revised version of the Ainley-Mathieson method.[2]

The first hot flow path design is referred to as Design A, and includes two axial turbine stages comprising ceramic stators and metallic rotors. Simplifications, permitted in the flow path to facilitate ceramic fabrication, represented some compromise in turbine efficiencies.

Modifications were made to the Design A hot flow path to eliminate some structural ceramic components to improve stator thermal shock resistance, and to re-stagger the stator vanes. This modification is referred to as Design B and represents an efficiency improvement over Design A.

A third modification, Design C, may be necessary depending on feedback from test programs. Should this occur, an aerodynamic modification to favor high efficiency at low speeds and to limit trailing edge thicknesses to 0.022 inches maximum may be implemented.

For a ceramic rotor to be feasible it is necessary to use a material which has high specific strength at temperatures up to 2500°F. Candidate materials also must resist thermal shock, survive in a corrosive environment, maintain good dimensional stability, have high specific damping capacity, withstand small particle (carbon deposits and ceramic fragments) impact have an adequate endurance limit for fatigue resistance, and be readily available at a reasonable cost. A program was initiated to select candidate materials and to generate specific strength goals for these materials. Two basic ceramic materials met the general requirements described above, dense silicon nitride and dense silicon carbide.

Theoretically dense silicon nitride has ample specific strength to consider a conventional one-piece rotor design with integrated blades and disk. Thermal shock, oxidation, and sulfidation resistance appeared adequate for this material. Thermal stresses in dense silicon nitride are lower than in many other ceramic candidate materials due to a higher thermal conductivity and a low coefficient of thermal expansion which offsets a moderately high modulus of elasticity.

Preliminary analysis of the monolithic turbine rotor design was performed using a finite element axisymmetric two-dimensional stress program[3] and a supplemental finite element heat transfer program[4] modified for our specific needs.

A contour plotting program was added to the system to facilitate extrapolation of the stresses to the outer fibers of the rotors and to highlight areas of stress concentration. The basic finite element grid was common for all three programs used in this analysis. Boundary conditions for the heat transfer program had been previously established from a finite difference heat transfer analysis of the entire hot flow section, i.e., the section from the combustor exit to the regenerator entrance including the bearing carrier and housing, the rotor shaft, bearings and mounting structure. This analysis assumed 0.3% compresser discharge cooling air bled from the labyrinth seal located adjacent to the second stage rotor disk where a heat balance was performed. Purely elastic material behavior was assumed in the calculation of the ceramic rotor and blade stresses.

The blade loads were calculated with a time-sharing computer program which integrated the blade cross-sectional area as a function of radial position. In addition, this program calculated the centrifugal blade stresses. In computing disk stress, the blade load was assumed carried over the entire rotor circumference. A half-inch center bore was placed in the disks to accommodate a rotor attachment bolt. As is customary for disks with a central hole, a hyperbolic profile was used as the basic geometry. The disk contours were then modified to optimize the stresses using 10% overspeed and 2500°F turbine inlet temperature operating conditions. The blades were offset from the disk centerline to counterbalance the overhung rim and balancing rings were placed on both sides of the disk at the radius of gyration to minimize their effect on hub stresses. The final disk geometry for the Design B first stage rotor is shown in Figure 3.1.

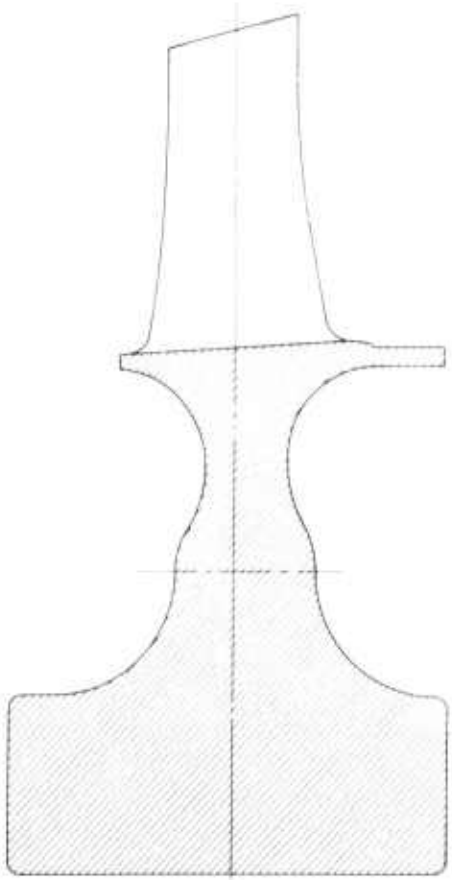

Figure 3.1 — Disk Geometry of First Stage Turbine Rotor

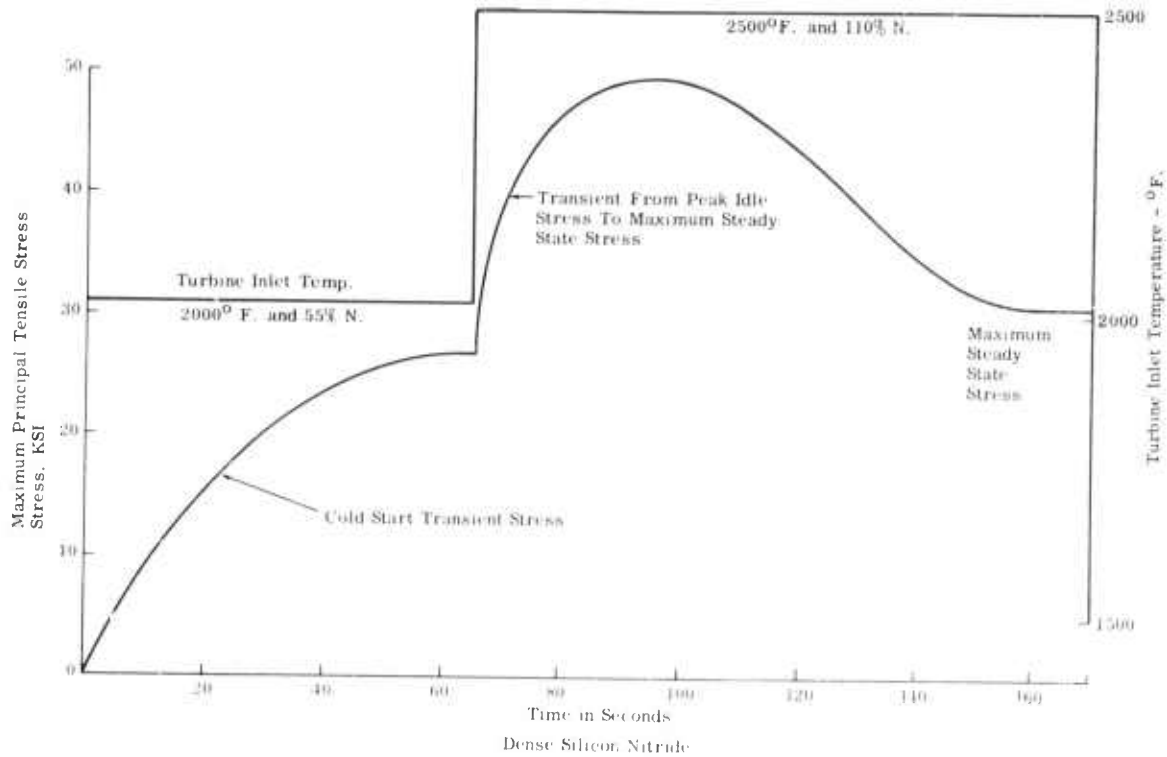

Figure 3.2a

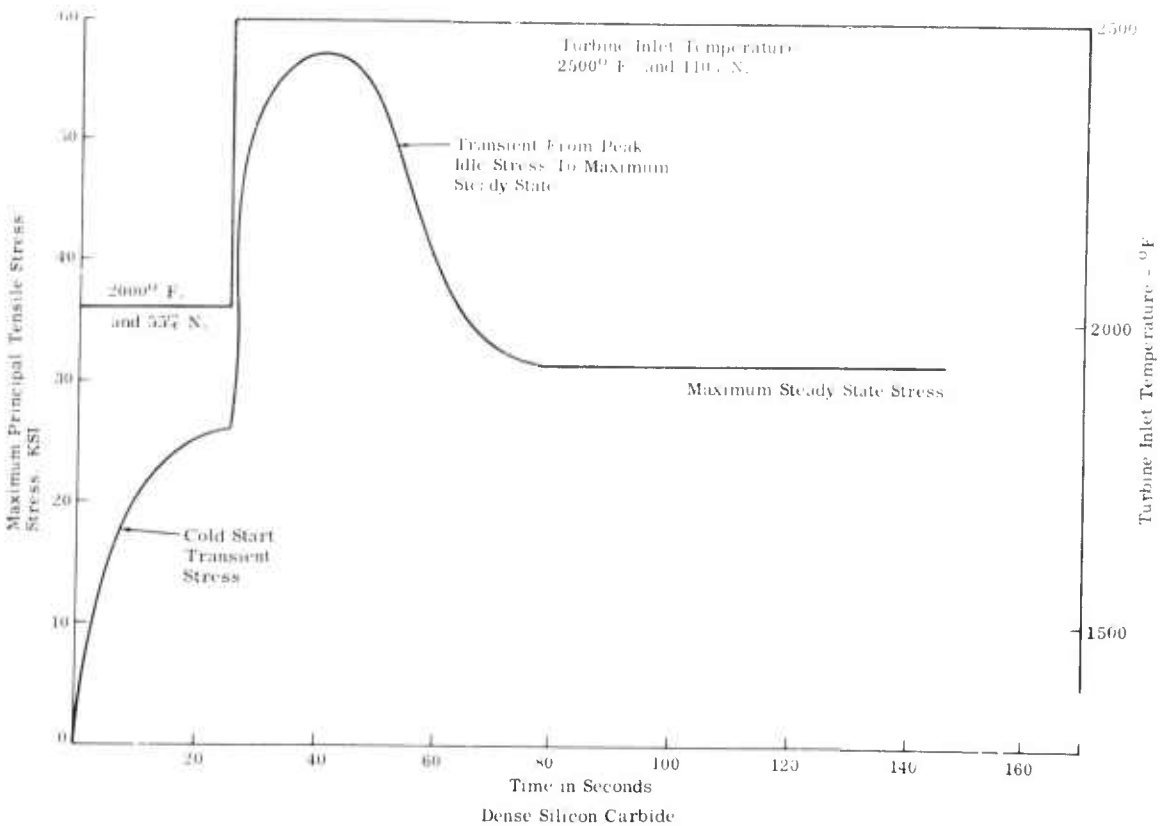

Figure 3.2b

Figure 3.2 — Effect of Assumed Engine Operating Conditions on Rotor Disk Stresses

The maximum principal disk stresses for dense silicon nitride and dense silicon carbide were calculated on a preliminary basis for several operating conditions, as shown graphically in Figure 3-2a and 3.2b respectively. Two basic transients were analyzed:

1. A cold start transient from room temperature to idle speed (55%) at 2000°F turbine inlet temperature. A peak stress occurs in this transient at approximately 65 seconds after light-off for dense silicon nitride, (Figure 3.2a) and 25 seconds after light-off for dense silicon carbide (Figure 3.2b).

2. A transient from the peak stress cold start transient point to maximum overspeed (110%) and temperature (2500°F turbine inlet temperature). The maximum stress obtained in this analysis occurred in this transient condition at approximately 30 seconds after initiation of the transient for dense Si_3N_4 (Figure 3.2a) and 15 seconds after initiation of the transient for dense SiC (Figure 3.2b).

Also analyzed were the steady state operating points shown in Figures 3.2a and 3.2b. A maximum envelope of these stresses vs temperature for dense Si_3N_4 is shown in Figure 3.3. Superimposed is the average modulus of rupture of hot pressed silicon nitride as reported by the Norton Company(5) indicating this material to be a very attractive ceramic for rotor disks. More analytical and experimental work will be required, to determine the actual margin of safety (or probability of failure). This work will also determine the relationship between tensile strength in a spinning mode to modulus of rupture obtained from bending fracture tests. Spin testing of ceramic disks is considered an attractive method to provide this relationship.

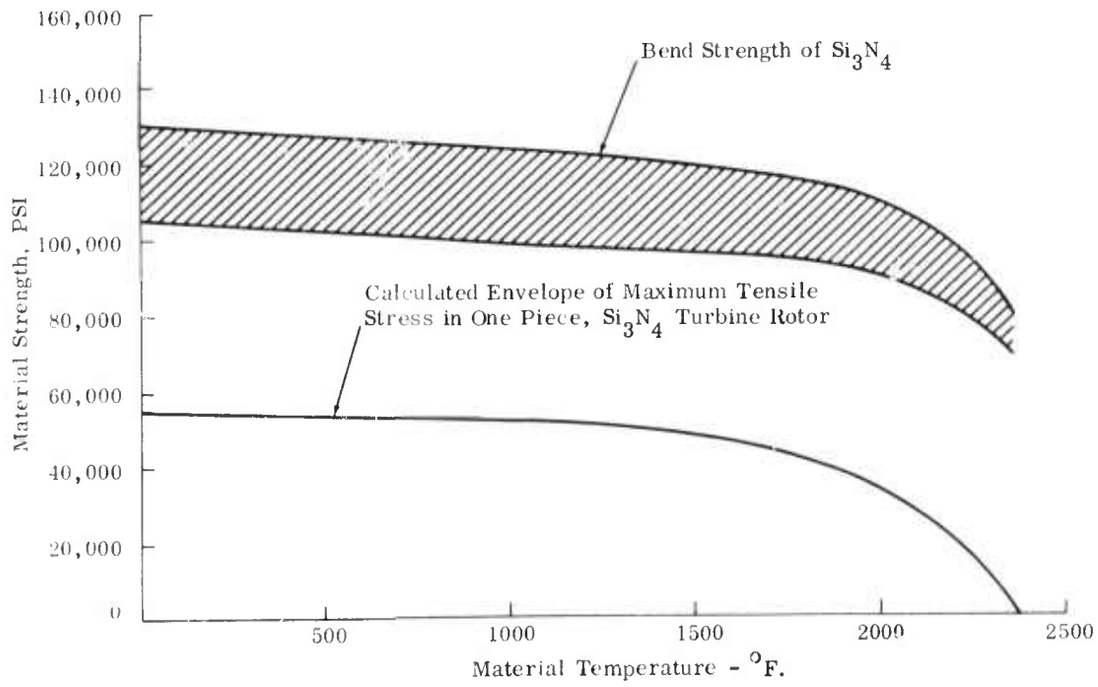

Figure 3.3 — Maximum Disk Tensile Stresses Compared to Bend Strength of Hot Pressed Silicon Nitride

A second basic rotor design concept has been conceived using chemically vapor deposited silicon carbide as the primary material. This turbine wheel concept consists of a rotating shell structure with integral blades. While the analysis is still preliminary, the mechanical stress levels in this concept were estimated to be below the reported modulus of rupture values.

Attachment Methods

A major problem with a ceramic turbine rotor is how to attach it to a metal shaft.

The function of any rotor attachment method is to successfully transmit the torque from the ceramic rotor to the metallic turbine shaft. There is considerable mismatch in thermal growth between the ceramic rotor and metal shaft in both the axial and radial directions. There will be centrifugal and gyroscopic forces to which the attachment method must react. It is also of utmost importance that concentricity be maintained between the rotor and the turbine shaft under all conditions in order to prevent damage from interference between the rotor and other components of the engine.

Axial load and differential thermal growth requirements can be met by a bolt clamping the rotors to the turbine shaft. Torque can be transmitted between rotors and from the second stage rotor to the turbine shaft by radial face splines at the interfaces. The face spline between rotor stages must be designed such that bearing stresses are acceptable for the brittle material used and concentricity is maintained at all times. The face spline between the second stage rotor and the turbine shaft must have the same capabilities in addition to allowing differential thermal growth in the radial direction. These requirements are all met by use of specially designed Curvic couplings.

Rotor Bolt Material

The material chosen for the rotor bolt was Inconel alloy X-750 with a heat treatment of 2100°F for 2 hours followed by slow step-wise cooling. This heat treatment is recommended for service in excess of 1100°F where loads are to be sustained for long periods of time. For these conditions the room temperature yield stress is 93,000 psi. In order to achieve negligible creep, temperature and stress should not exceed 1100°F and 60,000 psi respectively.

Preliminary investigation showed that the average bolt temperature, without cooling, would be in excess of 1500°F. Material characteristics at these temperatures are unacceptable; therefore, the rotor bolt must be cooled or the material changed. A ceramic bolt would eliminate the need for cooling but would likely be subjected to conditions of point loading. It was, therefore, decided to investigate a cooled metal bolt.

Rotor Bolt Cooling

Two methods of cooling the rotor bolt were considered, (1) reversed oil cooling and (2) straight through air cooling.

In the case of oil cooling the oil was supplied through the center of the bolt to the front of the first stage then reversed back by annular flow and dumped between the turbine end labyrinth seal and bearing.

Two methods were studied using air cooling, (1) air supplied from the front of the rotor bolt and (2) air supplied from the rear of the rotor bolt. For rear air cooling, compressor air was supplied to the bolt from the cavity between the diffuser and the bearing carrier housing to the front labyrinth seal and through the turbine shaft Curvic coupling. The air would then exit from the bolt at the front of the first stage rotor and wash up the rotor face. For front air cooling, compressor air was supplied to the outer annulus of the nose cone, and then traveled through the hollow nose cone struts and the center nose cone annulus, to the rotor bolt. The cooling air was discharged from the bolt through the turbine shaft Curvic coupling to the turbine exhaust.

Analytical Methods

The analysis of rotor bolt cooling methods was accomplished by the use of finite difference and finite element heat transfer computer programs and a finite element stress analysis computer program. The heat transfer programs have both transient and steady state solution capabilities. The finite difference program was used with a coarse grid of the entire hot flow section in order to establish realistic boundary conditions for the rotor bolt and rotors.

The finite difference heat transfer program determined the temperature of a coolant stream given the mass flow rate and convective heat transfer coefficient of the adjacent walls. In this way the program lent itself to a study including axial coolant flows. The finite element program could not handle axial flows but would generate convection coefficients for disks with a coolant stream emerging from the disk center. The finite element program was used with a fine grid of the rotors and attachment with the boundary conditions generated by the finite difference model.

The general correlating equation used to determine the Nusault Number, and subsequently the convection coefficient, unless otherwise stated, was as follows:

$$Nu = C\ Pr^{m}\ Re^{n}$$

The constants C, m and n depend on the type of flow in question and the Reynolds Number (Re). The definition of the Reynolds Number is also determined by the type of flow. Pr is the Prandtl Number of the fluid flowing. The Nusault Number (Nu) is a ratio of the convective heat transfer coefficient (h) of the surface and the thermal conductivity (k) of the fluid flowing multiplied by some characteristic length which is a function of the flow geometry. The value of the constants and definition of the parameters will follow in the description of each important heat transfer surface.

The convective heat transfer coefficients for the face of the rotors were determined assuming the rotors to be disks rotating in a hot gas. The correlating equation used was as follows:

$$h = \frac{k}{r} \, Nu$$

where:

Re	=	$\omega \, r^2/\nu$
r	=	radial distance to point where h is required
ν	=	kinimatic viscosity of hot gas at point where h is required
ω	=	angular velocity of rotor

for Re $\leq$ 250,000	C = 0.35	m = 0	n = 0.5
for Re $>$ 250,000	C = 0.0195	m = 0	n = 0.8

The convection coefficient was determined for a finite number of elements on the rotor face and was used in both heat transfer programs.

An equivalent heat transfer coefficient heq, was determined for that portion of the rotor with blades. The turbine blades were treated as fins and the following correlation was used:

$$heq = h_p \left[1 - \frac{N}{\pi} \sin^{-1}\left(\frac{W}{2R}\right) \right] + \frac{NL}{\pi R} \eta \, h_b$$

where:

h_p	=	convection coefficient of platform area without any blades
h_b	=	convection coefficient of blade
N	=	number of blades on rotor
L	=	blade height
W	=	average blade width at platform
R	=	radius of platform
η	=	efficiency of blade as a fin[6]
π	=	3.14159

The convection coefficient for the blades (h_b) was determined as follows:

$$h_b = \frac{\pi K}{P_w} \, Nu$$

where:

R_e	=	$(VP_w)/(\pi \nu)$
V	=	velocity of hot gas relative to blade at point where h is required
P_w	=	wetted perimeter of blade at point where h is required

for Re $<$ 30,000	C = 0.664	m = 0.3	n = 0.5
for Re $\geq$ 30,000	C = 0.11	m = 0.3	n = 0.69

(Other symbols as previously explained.)

The blade area was divided into a finite number of areas and h was determined for each. The average h_b was found for the entire blade.

The convection coefficient for the rotor platform (h_p) was determined as follows:

$$h_p = \frac{k}{R} \text{ Nu}$$

where:

$$\text{Re} = 4 \text{ VR}/\nu$$

for all Re $\quad C = 0.085 \quad m = 0.35 \quad n = 0.7$

(Other symbols as previously described.)

The convective heat transfer coefficients for the rotor bolt were determined as follows:

$$h = \frac{K}{d} \text{ Nu}$$

For cases with Re $\leq$ 5000 the following correlation was used to determine the Nusault Number:

$$\text{Nu} = 3.66 + \frac{.0668 \text{ (d/L) Pr Re}}{1 + .04 \left[\text{(d/L) Pr Re}\right]^{2/3}}$$

where:

Re	=	$(\dot{m}d)/\mu A$
d	=	inside diameter of bolt (characteristic length)
A	=	flow area
L	=	length of flow channel
$\dot{m}$	=	mass flow rate of cooling fluid
μ	=	absolute viscosity of cooling fluid

for Re $\geq$ 5000 $\quad C = 0.023 \quad m = 0.3 \quad n = 0.8$

(Other symbols as previously explained.)

Convection coefficients for flows between the diffuser and bearing carrier housing were determined using the above correlations assuming annular flow. For annular flow the characteristic length was the radial separation of the annulus. The surfaces of cavities used for oil return were assumed to have convection coefficients as determined by the following correlation:

$$h = \frac{K}{L} \text{ Nu}$$

where:

$$\text{Nu} = \frac{4}{3}\left[\frac{.508 \text{ Pr}^{1/2} \text{ Gr}^{1/4}}{(.952 + \text{Pr})^{1/4}}\right]$$

L	=	height of surface
Gr	=	Grashof number based on height of surface

(Other symbols as previously described.)

The mass flow rate for each method of cooling was determined by trial and error with different criteria governing each case. For oil cooling the important factor was oil temperature. The temperature of the cooling oil was not to exceed 300°F; this required an oil flow rate of 0.004 lbm/sec. For air cooling the major design consideration was to maintain an average bolt temperature of 1100°F maximum. The air-in-the-front bolt method was calculated to require 1.0% compressor air while the air-in-the-rear bolt design was calculated to cool the bolt to the required temperature with only 0.1% compressor air.

Due to the low coolant temperature for oil cooling relative to air cooling, the resulting temperature gradient over the rotor radius was shown to be higher in the case of oil cooling. Higher thermal stresses therefore resulted in the ceramic rotors with oil cooling. Rear air cooling caused cool air to wash the front face of the first stage rotor and the rear face of the second stage rotor. This resulted in higher thermal stresses in the rotors for rear cooling as opposed to front cooling.

The rotor bolt must be capable of maintaining contact between the coupling faces under all conditions. Due to the difference in coefficients of thermal expansion the rotor bolt will expand, in the axial direction, considerably more than the rotors during steady state conditions. Therefore, the bolt must be prestressed cold to offset the load relaxation that will occur after the bolt heats up. During transient warm-up conditions the rotors will grow faster than the rotor bolt and add a load to the bolt in addition to the preloads required to offset thermal relaxation and maintain coupling forces.

The minimum bolt load is the sum of three separate forces, the coupling separating force, the gyroscopic forces and centrifugal forces of the rotors. The coupling separating force is as follows:

$$F_1 = (T/R_m) \tan \phi$$

where:

F_1	=	separating force
T	=	torque being transmitted
R_m	=	mean radius of coupling face
ϕ	=	pressure angle of face spline

The gyroscopic moment must be offset by the moment of the bolt force acting through the coupling radius. The gyroscopic moment is as follows:

$$M_g = (I_z \omega \Omega - I_d \Omega^2) \theta$$

where:

M_g	=	gyroscopic moment of the combined rotors
I_z	=	mass moment of inertia of the combined rotors about their axis of spin
I_d	=	mass moment of inertia of combined rotors about a diametral axis
ω	=	angular spin velocity of rotors
Ω	=	angular precession velocity of rotor shaft
θ	=	angular eccentricity of shaft axis

The precession velocity may either be forward, (same sense as spin velocity ω) or backward (opposite spin veloeity). The most likely case will be forward preeession with $\omega = \Omega$. However, baekward preeession eould oeeur and the gyroscopic bolt load will be determined assuming $\Omega = -\omega$. Therefore, the bolt load required to offset the gyroseopie moment is:

$$F_g = \frac{\theta \omega^2}{R} (I_Z + I_d)$$

where:

F_g = gyroscopic bolt force
R = outer radius of eoupling face

(Other symbols as previously explained.)

It is assumed that $|\Omega|$ will not exceed $|\omega|$ in baekward precession. This may be conservative.

Coupled with any gyroscopic moments are centrifugal moments due to the precessional velocity. Each rotor will contribute separately to this moment. The rotor bolt in turn must offset this moment for each rotor by acting through the coupling radius. The eentrifugal moment vector for each rotor may be expressed as follows:

$$\bar{M} = m \left\{ \bar{r} \times \left[\bar{\Omega} \times (\bar{\Omega} \times \bar{r}) \right] \right\}$$

where:

$\bar{M}$ = moment caused by centrifugal forces of rotor
m = mass of rotor
$\bar{r}$ = position vector locating center of gravity of rotor with respect to bolt axis at coupling
$\bar{\Omega}$ = preeession velocity of rotor
x = vector cross product operator

The rotor hubs will undergo axial deformation resulting from Poisson's effects under a state of triaxial stress. This complex state of stress is a function of thermal gradients and centrifugal forecs.

The rotor bolt in turn must be prestressed to take up any relaxation due to this effect.

The stress in the rotor bolt is a function of eross seetional area and strained length. The bolt stress required to offset coupliug separating forees and gyroscopic forces is a funetion of stressed area. The prestress required to offset bolt force relaxation and rotor hub deformation is a funetion of strained length as is the transient stress due to exeess growth of the wheels. In order to stay within the stress limitations of the bolt material, a bolt with low elastie stiffness is required.

Types of Rotor Bolts

Three types of bolts were studied. The straight hollow bolt shown in Figure 3.4 must be recessed deep into the turbine shaft. Air cools the front portion of the bolt while bearing supply oil cools the rear portion of the bolt. This design presents problems of sealing the air and oil ports. The long slender tube must also be supported in order to avoid addition of unwanted vibrations to the shaft as a whole.

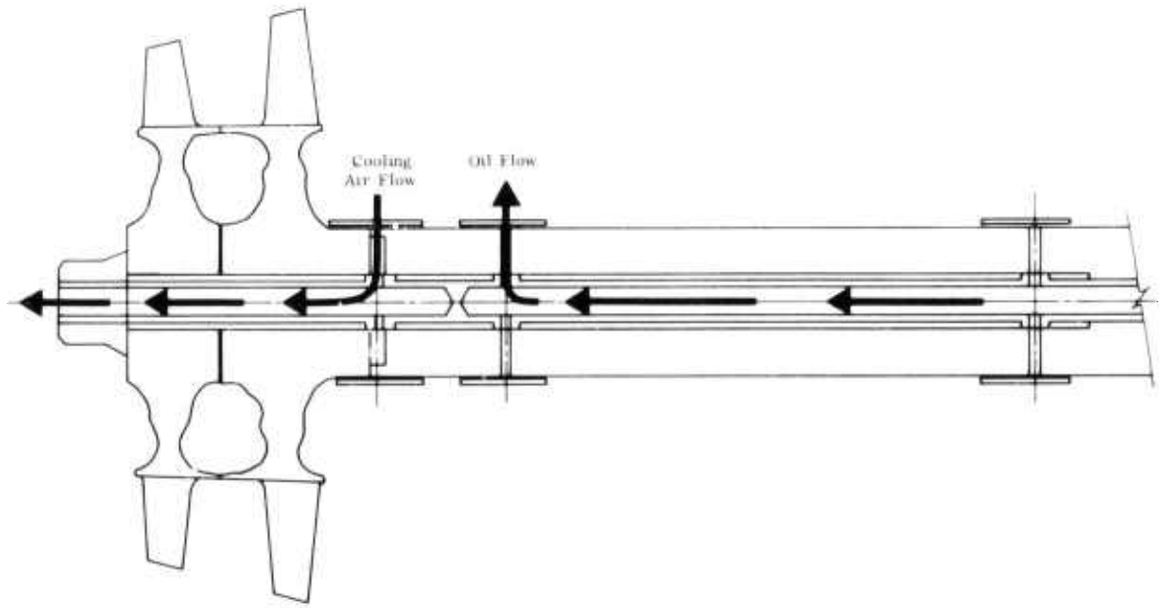

Figure 3.4 — Straight Hollow Bolt

The solid folded bolt shown in Figure 3.5 has air cooling at the front portion by annular flow inside a shield which protects the rotor bore from the coolant. The strain length of the bolt is made up of the solid tension member and the hollow compression member. This bolt must be recessed into the shaft and may also require intermediate support.

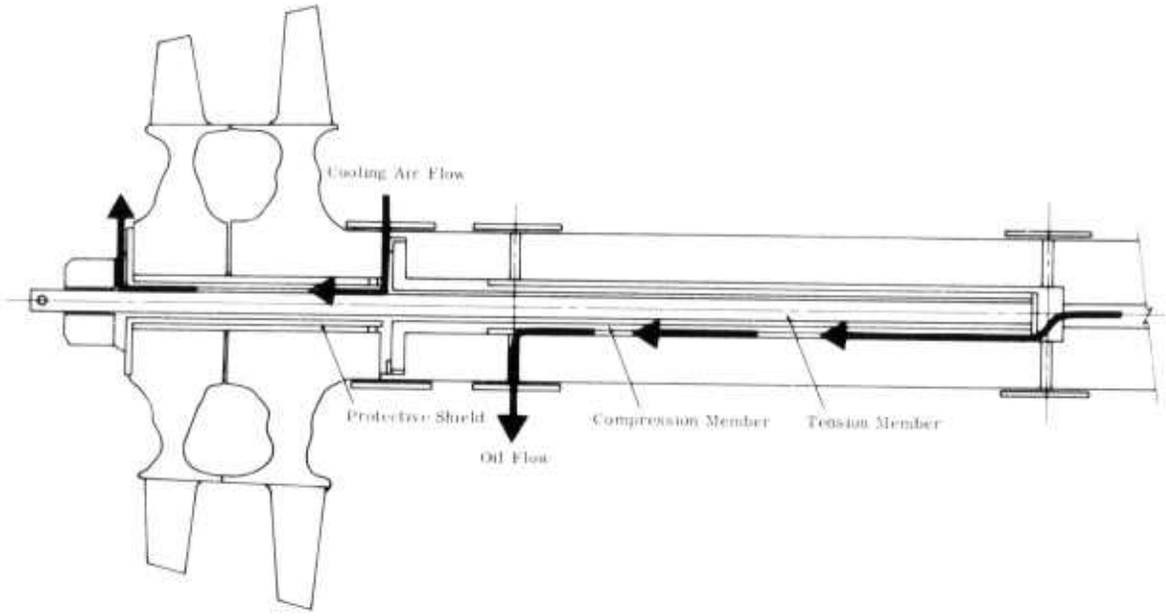

Figure 3.5 — Solid Folded Bolt

The hollow folded bolt shown in Figure 3.6 is cooled entirely by air. Again the strain length is that of the tension and compression members together. This bolt requires the minimum recess but may also require intermediate support.

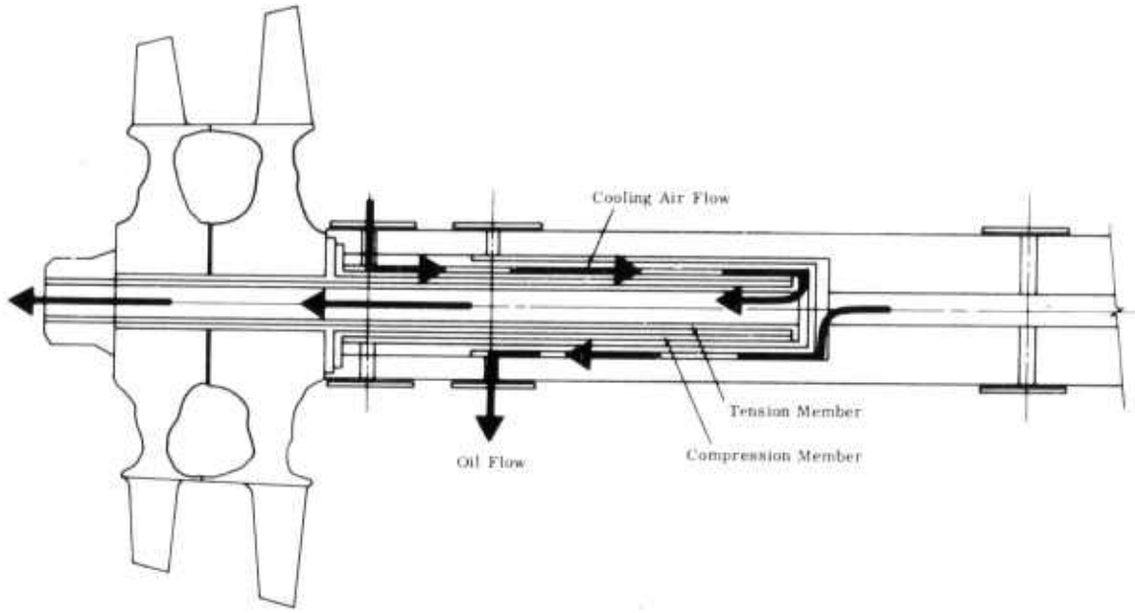

Figure 3.6 — Hollow Folded Bolt

The length of the recess for the folded bolts shown may be decreased considerably by changing the material of the compression member of the bolt. By using a material whose rate of thermal expansion exceeds that of the tension member, the compression member can effectively decrease the coupling force relaxation during steady state operation.

Conclusions

At present the folded bolts appear the most promising for an immediate solution to the attachment problem. A study is being conducted to determine the effects of bolt design on cooling requirements and dynamic stability. When the final bolt design is determined a transient heat transfer analysis of the engine as a whole during shutdown will be conducted to determine the effects of soak-back heating on the attachment mechanism.

3.1.2 MATERIALS AND FABRICATION

SUMMARY

Four parallel efforts directed at producing ceramic turbine rotors are described. The first effort is (1) hot press rotors from high strength silicon nitride by a two step process, in which the turbine blades are first individually hot pressed and then formed into the rotor by a second hot pressing operation. A successful attachment of a simulated blade to a simulated hub section has shown promise of success.

(2) A process is being developed in which a turbine rotor is molded of silicon powder, nitrided to the reactive high alpha phase form of Si_3N_4, and densified by a pseudo-isostatic hot pressing method. Preforms of the rotor have been molded, assembled and nitrided, while pseudo-isostatic hot pressing techniques require further development.

(3) A chemical vapor deposition method is being developed for forming a turbine rotor from dense silicon carbide. Strength of deposited SiC is shown to be near 100,000 psi and limited feasibility is demonstrated by the successful forming of one turbine rotor blade.

(4) The fourth effort involves hot pressing a solid billet of dense Si_3N_4 and machining a turbine rotor. An ultrasonic method appears most promising with a cutting rate of the ceramic 150 times faster than the tool wear rate.

Introduction

It was noted in the preceeding section, 3.1.1 on Design and Analysis that dense silicon nitride (Si_3N_4) and dense silicon carbide (SiC) are candidate materials for ceramic turbine rotors. However, it must be remembered that each of these compounds is a family of materials with properties highly dependent upon starting raw materials and processing techniques.[7]

Silicon nitride, the more recently developed of the two materials, is commonly "reaction sintered" to 70-80% of theoretical density and exhibits strengths of 20-25,000 psi.[8] The nitrogen diffusion process into a silicon compact appears to be self-limiting at about this level. However, such material, with the addition of a suitable densification aid, may be hot pressed to theoretical density with an increase in strength by a factor of three or more.

Carefully controlled reactive silicon nitride powder has recently become available which can be hot pressed, with a suitable densification aid, into material of theoretical density (3.186 gm/cc) exhibiting strengths up to 130,000 psi.[9] Much of the early work was done using 5% MgO as the densification aid. However, tests indicate a severe loss in high temperature strength and creep resistance perhaps related to the second phase formed from MgO at the grain boundaries.

The bulk of silicon carbide shapes produced commercially are fabricated from relatively impure SiC grain bonded by clay compositions, organics, silicate glasses, etc. and are unusable even under moderate loads at turbine operating temperatures. Sintered silicon carbide material available commercially has a strength of 15 to 25,000 psi at turbine operating temperature and is 80% of theoretical density. Other forms of silicon carbide currently being developed appear to possess properties suitable for use for turbine rotors. These include hot pressed,[10] chemically vapor deposited[11] and reaction sintered SiC.[12]

Several programs are in progress aimed at developing materials and forming processes suitable for vehicular turbine rotors.

Ford-Norton Turbine Rotor Program

The development of reactive silicon nitride powder and subsequent pressure sintering (hot pressing) of the powder to dense, high strength material has been progressing in this country and in England. Recently the technology developed by Joseph Lucas Limited in England was transmitted under license to the Norton Company. The development program to be performed by the Norton Company under subcontract to Ford began in September 1971 with two objectives. The primary objective is to hot press individual turbine rotor blades, as close to finished dimension as possible, followed by a second hot pressing which will form the rotor hub around the blade roots and "weld" all of the assembled blades into a monolithic rotor. The secondary objective is to explore the feasibility of directly hot pressing in one step, a simplified wheel with straight-sided by angled blades.

A typical hot pressed billet (Norton No. HS-110) received from the Norton Company in October, 1971 exhibited room temperature modulus of rupture (MOR) highly dependent upon sample size and test fixtures as indicated by Table 3.1.

TABLE 3.1

ROOM TEMPERATURE STRENGTH OF NORTON HOT PRESSED Si_3N_4

Where Tested	No. of Samples	Sample Size (in)	Span (in)	Type of Load	MOR (psi)	1 Std. Dev.
Norton	84	1/8x1/8x1"	3/4	3 Point	123,000	9458
Ford	6	1/4x1/4x4"	2 x 1	4 Point	90,500	5850
Ford	6	1/4x1/4x4"	1-3/4	3 Point	96,400	7247
Ford	6	1/8x1/8x1"	3/4	3 Point	123,800	--

Norton first sliced 1/8" square bars, 1 inch long from the billet and measured strength in 3 point bending on a 3/4" span. Average strength from 84 specimens was 123,000 psi. Norton then sliced 1/4" square bars, 4 inches long and delivered them to Ford, where six bars were broken in 4 point bending using a 2" lower span and 1" upper span. An average strength of 90,500 psi prompted six more bars to be measured in 3 point bending on a standard Instron 1-3/4" span fixture. The strength of 96,400 psi suggested a verification of the Norton test so end portions of the twelve 1/4 inch bars already tested were machined to 1/8" square specimens, one inch long. Norton supplied details of their test fixture and procedures which were duplicated at Ford. The result of 123,800 psi clearly shows that strength of this material is dependent upon sample size and test method.

The electron microscope reveals (Figure 3.7) that the grain size of the material generally ranges from 0.2 to 4 μ m with some grains reaching 7 μ m. Specimens were prepared by mounting and polishing, then etching for 7 minutes in a boiling mixture of 30 parts HF, 25 parts H_2O_2 and 5 parts HNO_3. A negative replication process was then used, shadowing at 45° with platinum followed by carbon applied normal to the surface.

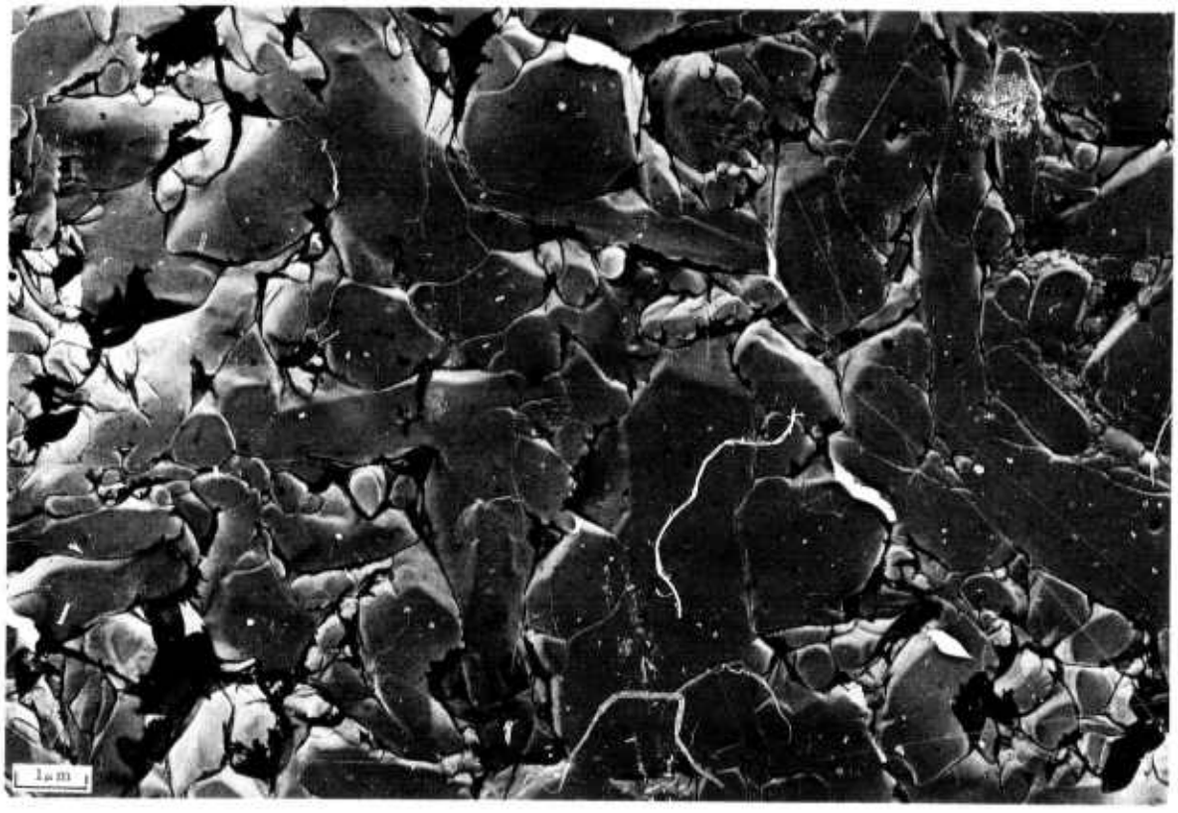

Figure 3.7 — Electron Micrograph 17,300X of Etched Norton Hot Pressed Silicon Nitride

Electron micrographs of the non-polished or etched fractured surfaces after testing to failure revealed numerous microcracks in the area of the origin of fracture. There is strong evidence that the origin of failure is associated with the unusually large grains, confirmed by electron diffraction to be beta silicon nitride.[13] Figure 3.8 reveals a microcrack originating from an unusually large grain in the origin area. This characteristic is typical of several specimens examined.

Figure 3.8 — Electron Micrograph, 13,300X of Fracture Specimen of Norton Hot Pressed Silicon Nitride Showing Miicrocracks Near Origin of Fracture

Although the Norton material is similar to that made by Lucas prior to the Lucas/Norton license agreement, Figure 3.9 shows the grain size of the earlier Lucas material to be somewhat smaller and have a more needle-like structure. The heavier platinum shadowing, which yields a more dramatic grain boundary definition, should not be confused with structure differences. Although selected electron diffraction on extracted needle-like crystals show that while a few are alpha silicon intride (α Si_3N_4) or silicon oxynitride (Si_2ON_2) the bulk are beta silicon nitride (β Si_3N_4). Other characteristics of the two materials are compared in Table 3.2.

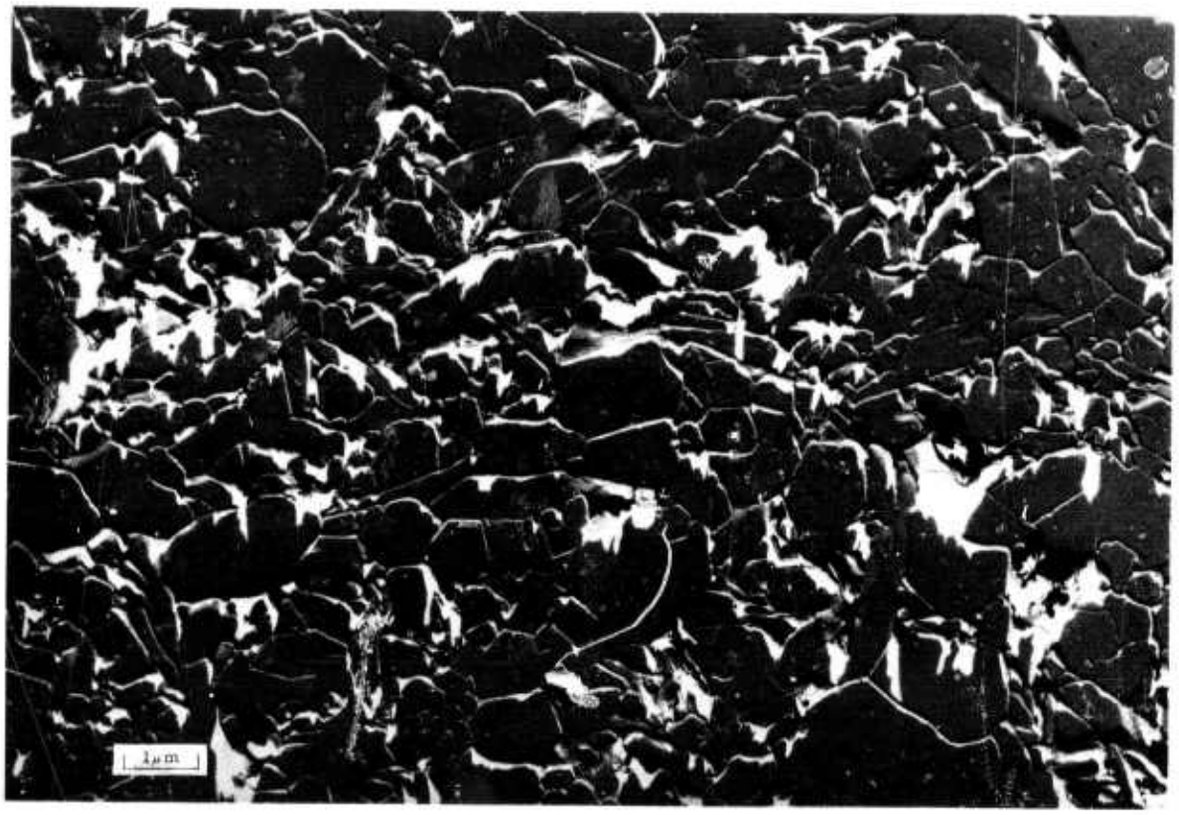

Figure 3.9 — Electron Micrograph, 18,800X of Etched Lucas Hot Pressed Silicon Nitride

TABLE 3.2

CHARACTERISTICS OF LUCAS AND NORTON Si_3N_4

1. Composition (ppm)

Spectrographic	Lucas	Norton
Iron	4300	4500-6000
Nickel	200	200
Copper	1000	300
Chromium	300	100
Molybdenum	NA	100
Manganese	200	100
Titanium	300	400
Aluminum	5000	5500
Calcium	7000	5000-7000
Vanadium	NA	20
Magnesium	4000	12000
Atomic Absorption (ppm)		
Magnesium	5500	7500

2. Phases Present

X-Ray (Peak Height %)	Lucas Bar	Lucas Blades	Norton Bars
α Si_3N_4	13	-	-
β Si_3N_4	82	90 +	84
Si_2ON_2	5	-	8
SiC	-	5	8
W Si	-	Trace	-
Fe Si	-	Trace	-

3. Density (ASTM-C-373) (g/cc)	3.15 to 3.178	2.76 to 2.89	3.06 to 3.12

During the first quarter of the program, Norton completed a study on the effect of small changes in temperature, pressure and holding times on hot pressed thin sections. In thin sections the surface reaction layer between the graphite die and the Si_3N_4 part represents a significant portion of the total volume. The thickness of the layer affects both the surface finish and control of the thickness dimension as well as affecting structure and strength. Minimum reaction layers were obtained by a combination of an interface barrier system and optimized pressing parameters.

Trials were also completed on hot pressing a simulated hub section around a previously hot pressed simulated blade segment. After the second pressing, an assembly was sectioned and test specimens 1/8" x 1/8" x 1" cut with the welded blade root in the center where the interface would be in the plane of maximum stresses when loaded in 3 point bending. Specimens were also cut from the blade section which was subjected to two pressing cycles, and from the hub section

which had been hot pressed only once. Tests indicate the strength of the weld is the same as that of the hub material (70,000 psi), although both were lower than normal for dense silicon nitride. It is interesting to note that the fracture was not along the weld line but adjacent to it. Optical macrographs of the test assembly and the weld line are shown in Figure 3.10a and 3.10b.

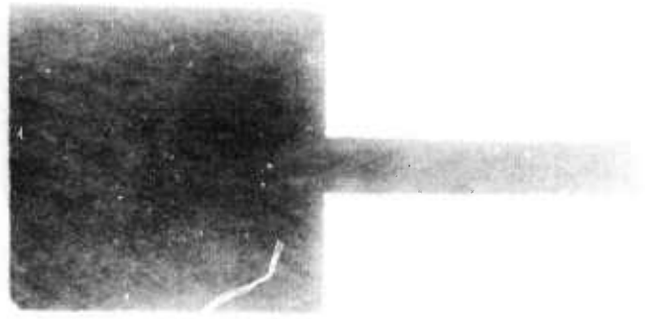

Cross Section

Figure 3.10a

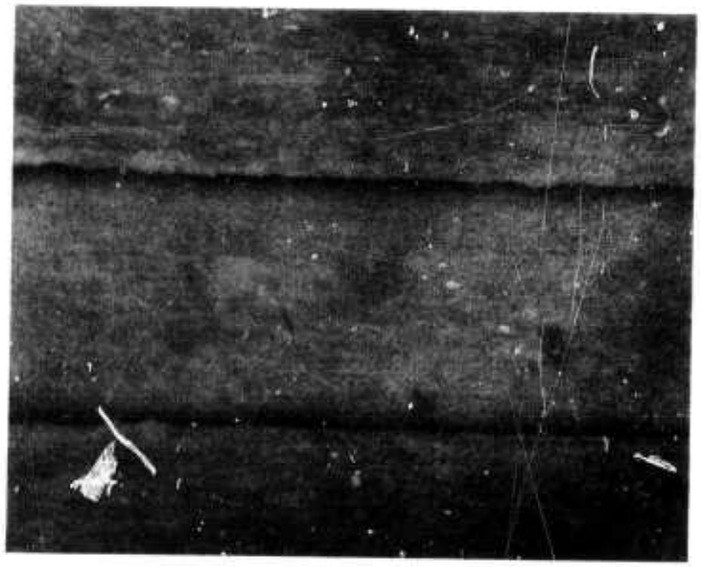

Interface Region Polished And Etched

Figure 3.10b

Figure 3.10 — Norton Hot Pressed Blade and Hub Assembly
(Courtesy of Norton Co., Worcester, Mass.)

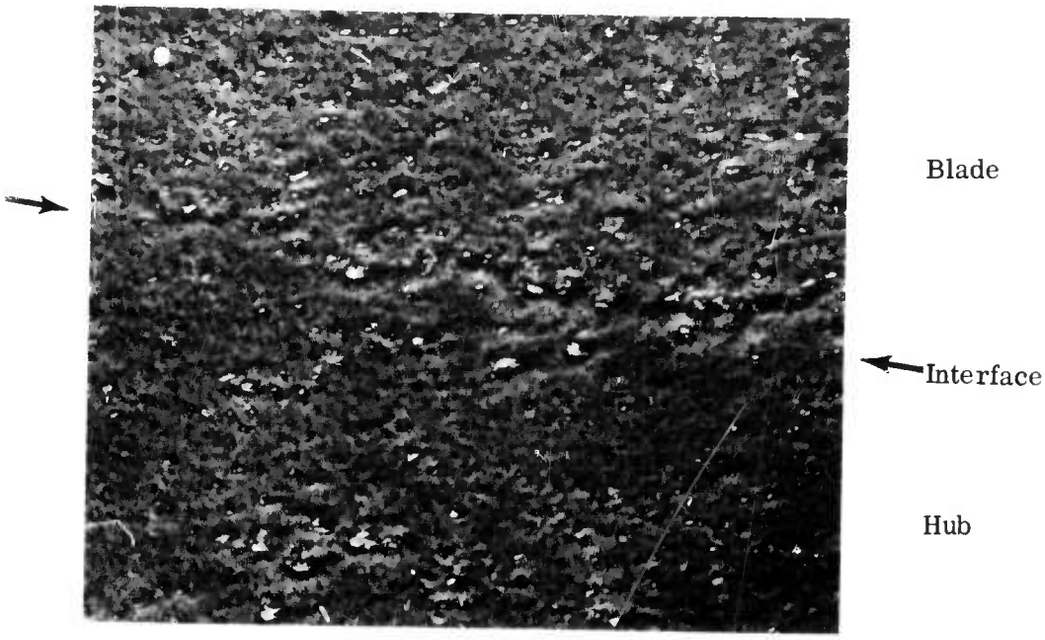

Figure 3.11a

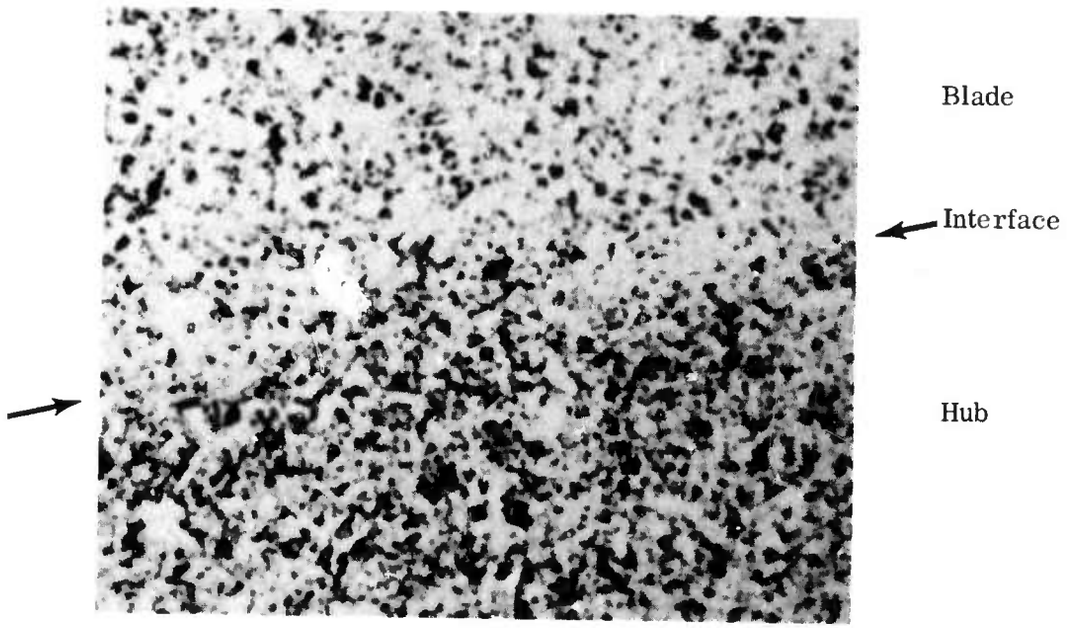

Figure 3.11b

Figure 3.11 — Norton Hot Pressed Blade and Hub Interface

Closer examination of the weld line was accomplished using both the optical and electron microscope. The interface could be detected on the polished and etched sample at 186X under phase contrast conditions (Figure 3.11a). At 930X (Figure 3.11b) it was apparent that the blade area had somewhat larger and deeper pores, and more pull-out, than the hub region. Replicas of the unetched interface examined using the electron microscope showed very little structure and no resolvable weld line. Replicas of the etched surface did reveal the interface but only under relative low (7,100X) magnification (Figure 3.12).

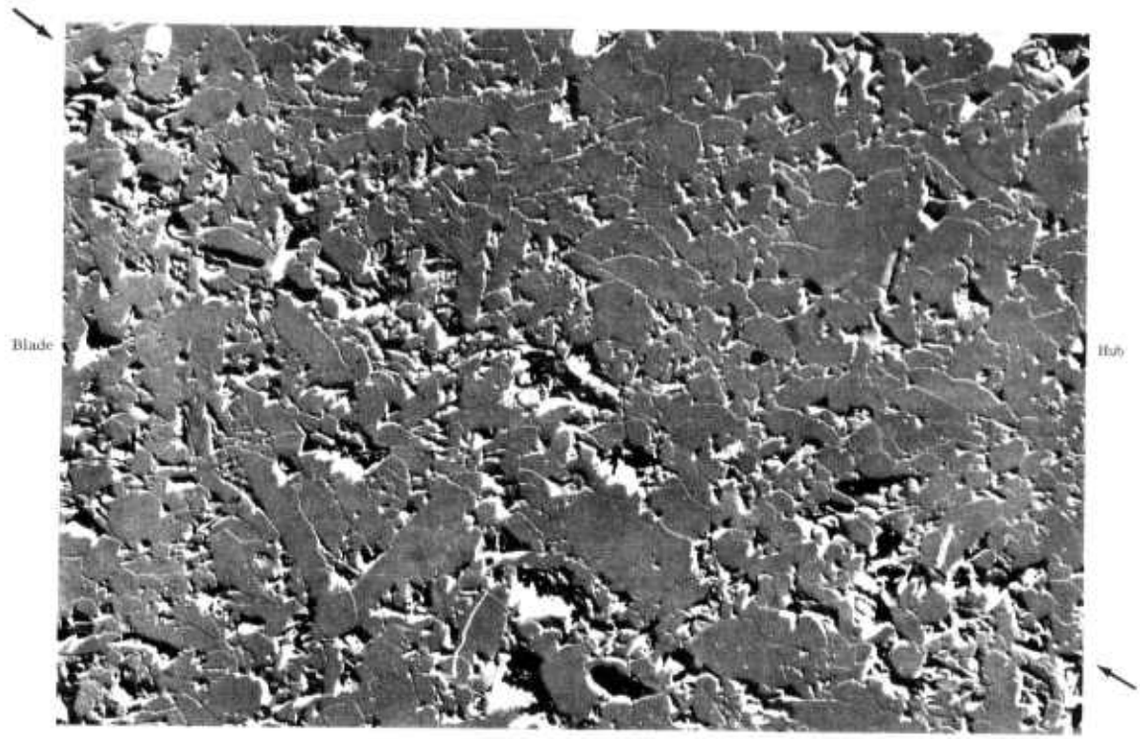

Figure 3.12 — Electron micrograph 7, 100X of Norton hot pressed blade and hub interface showing higher porosity in blade region Arrow denotes location of interface

The small porosity difference noted under the optical microscope were confirmed. It is encouraging that even when carefully examined using the 10 angstrom resolving power of the electron microscope, no separation or distortion of the microstructure could be detected between the blade and the hub interface anywhere on the sample.

Additional progress reported by Norton for the first quarter included completion of the design and ordering of tooling for producing plungers plus male and female dies for preformed blades. Other tools for an untwisted blade airfoil section are being obtained. The initial attempt at "welding" several simple curved blades onto a hub is scheduled for late March, 1972. Graphite mold tooling design for the one step process has been started with the first attempt at hot pressing some simple blades and a hub simultaneously scheduled for May, 1972.

Ford Pseudo - Isostatic Hot Press Method

A non-conventional forming method is under development, consisting of the following three steps:

1. Molding preformed but oversize rotors from silicon, to allow for anisotropic shrinkage during further processing.

2. Nitriding the preformed rotors to reactive silicon nitride, incorporating a densification aid.

3. Isostatically hot pressing the formed rotor to full theoretical density.

A first approximation of anisotropic shrinkage was estimated from studies on round bars, square bars and single airfoil blades from stator assemblies hot pressed to full density in a bed of powdered graphite. A tool was designed and fabricated which produced the segmented turbine wheel assembly shown in Figure 3.13. One of 36 individually molded silicon blades is removed to indicate

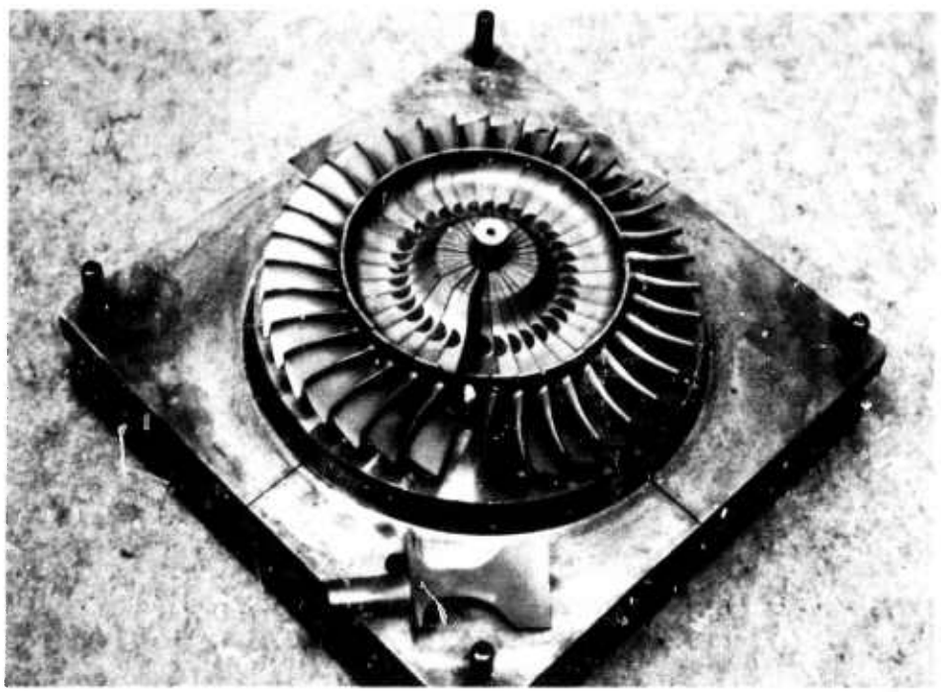

Figure 3.13 — Assembly of Molded Silicon Turbine Rotor Blades

the curved, helical surface forming the bulk of the hub region. The 36 blades are then bonded together by molding the remainder of the hub from the same silicon composition in a separate assembly tool.

Technology currently being developed (refer to Section 3.2.2) enables turbine rotor blade segments pictured in Figure 3.13 to be processed into a silicon nitride turbine rotor preform shown in Figure 3.14. In order to hot press the preform to high strength it is necessary to nitride the silicon into the reactive, high alpha phase form while maintaining dimensional control, homogeneity and a rigid shape sufficiently strong for further processing. An extensive program was formulated to accomplish this goal.

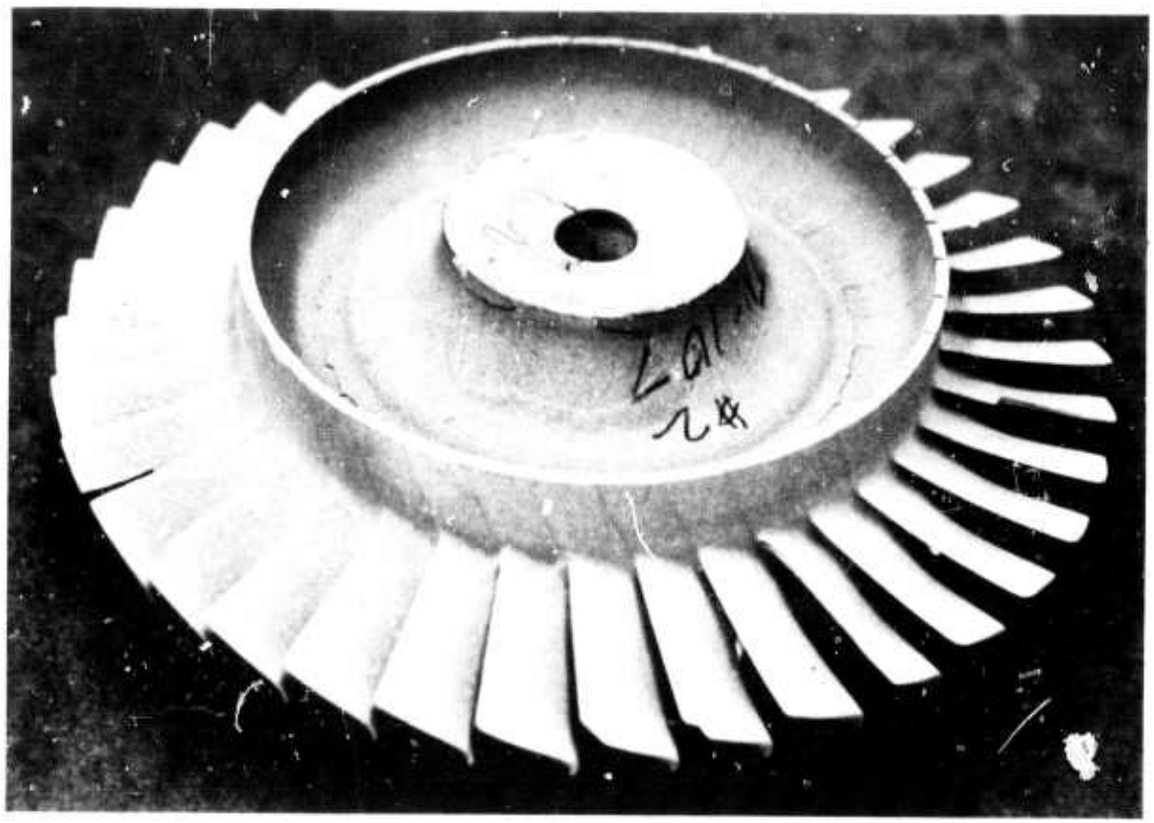

Figure 3.14 — Turbine Rotor Preform After Molding Hub Around Blade Segments and Nitriding

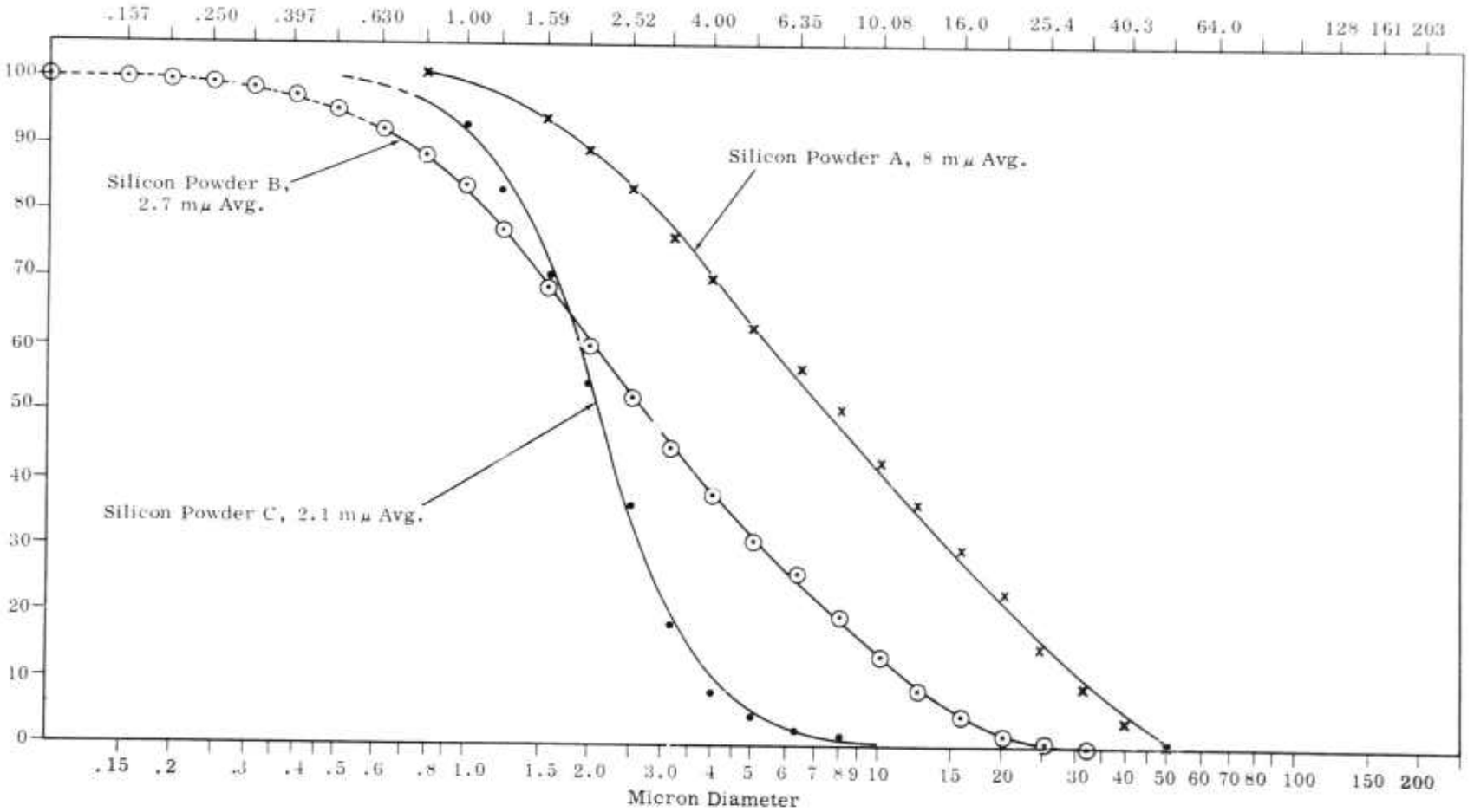

Figure 3.15 — Particle Size Distribution Coulter Counter Model T, Silicon Powders A, B and C

Three grades of readily available silicon were selected having particle size distribution and typical chemical analysis shown in Figure 3.15 and Table 3.3 respectively.

TABLE 3.3

CHEMICAL ANALYSIS OF SILICON METAL POWDERS

Element (ppm)	Powder A GT-196	Powder B GT-209	Powder C GT-22, Milled
Iron	9,000	7,000	2,500
Nickel	200	200	1,000
Copper	200	300	200
Chromium	100	200	<100
Molybdenum	200	NA	<100
Manganese	1,500	450	<100
Titanium	300	300	300
Aluminum	40,000	10,500	1,500
Calcium	4,500	400	400
Magnesium	300	100	200
Cobalt	NA	50	100
Vanadium	NA	100	50
Tungsten	NA	NA	<100
Average particle size	8 mμ	2.7 mμ	2.1 mμ

These represent an inexpensive grade milled in ceramic mills yielding a high Al_2O_3 contamination, a somewhat higher purity grade also milled in ceramic mills, and a higher purity (and higher cost) grade milled in-house using tungsten carbide media for minimum contamination. Additives for use as densification aids during hot pressing were selected on the basis of previous experience. Two approaches were used in a statistical study; 1) mixing of 4 additives in 3 amounts into silicon powder prior to the addition of organic molding materials, and 2) vacuum impregnation of two salts in aqueous solution into porous preformed shapes after nitriding. These combinations can be nitrided in each of the 6 selected atmospheres listed in Table 3.4 introduced at each of 3 experimentally convenient flow rates or on an "as-required" basis. In the latter method, a differential pressure switch and two solenoid valves maintains a constant 3 psi "static" pressure of the desired atmosphere regardless of the gas expansion during heating or the rapid consumption of nitrogen during the initial stages of nitriding in the critical temperature range.

TABLE 3.4

VARIABLES IN NITRIDING STUDY

Additives to silicon powders (3) before molding: MgO, $MgCO_3$, $Mg(OH)_2$, Li_2CO_3

Amount of additive: 1, 2 and 5% based on Si_3N_4

Additives to porous nitride shapes: $Mg(NO_3)_2$, $LiNO_3$ (At about 1%)

Nitriding Atmospheres:	Atmosphere Introduction:
Nitrogen (cryogenic and oil pump tank N_2)	Flowing at 2 CFH
N_2 plus 4% H_2	Flowing at 5 CFH
N_2 plus 10% H_2	Flowing at 10 CFH
N_2 plus 1% CO_2	Static at 3 psi pressure
N_2 plus 1% CO_2 and 4% H_2	
N_2 plus 50% NH_3	

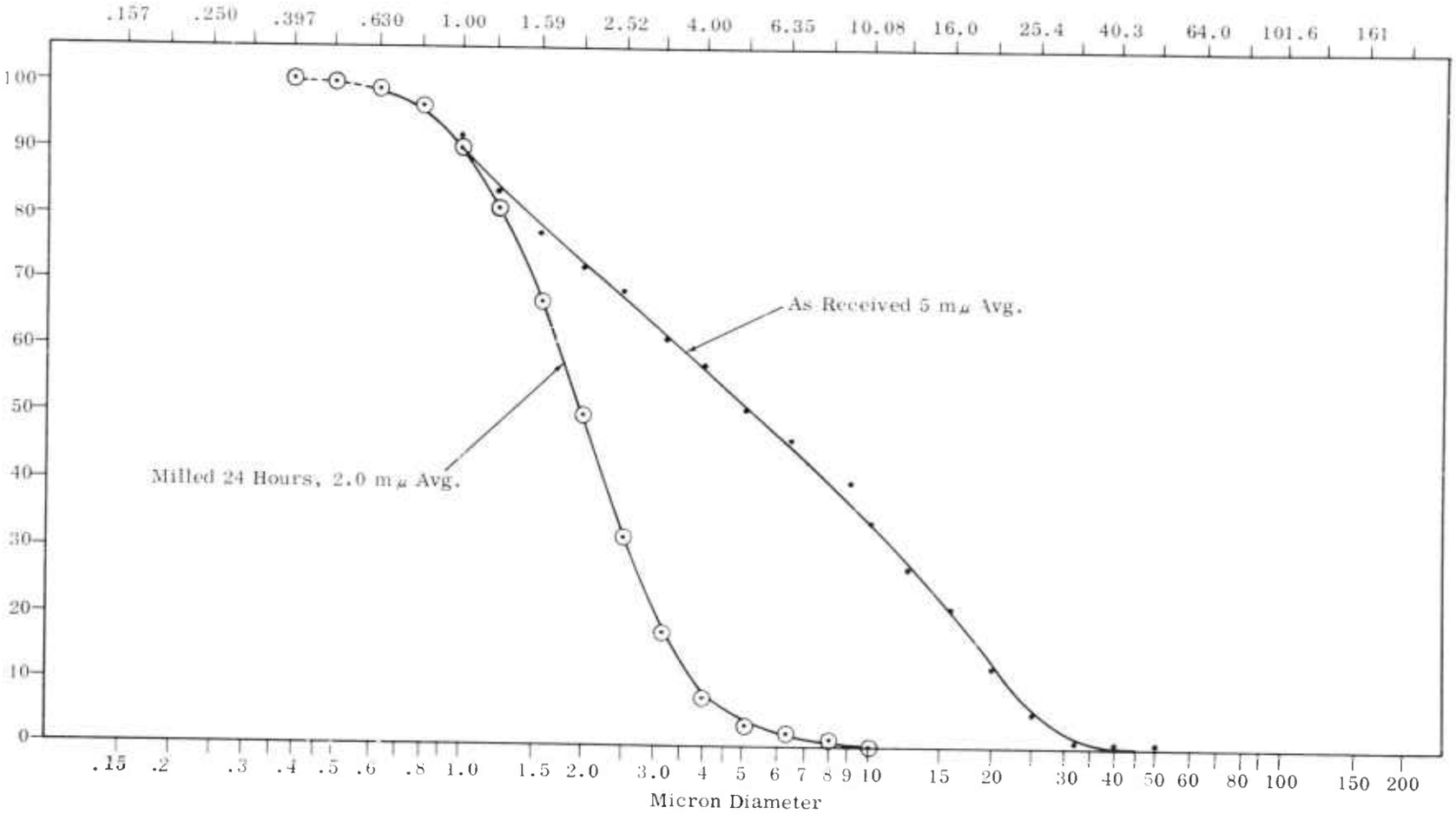

Figure 3.16 — Particle Size Distribution, Coulter Counter Model T AME Silicon Nitride Powder as Received and After 24 Hours Ball Milling

Neither Lucas nor Norton have made their starting reactive powders available for purchase. However Advanced Materials Engineering, Ltd., (AME) is producing a reactive powder for sale. This AME powder when milled with 2% MgO to the particle size distribution shown in Figure 3.16 may be readily hot pressed by conventional methods to theoretical density and high strength. The microstructure of the material, hot pressed to a density of 3.192 gm/cc at Ford is shown in Figure 3.17. Other characteristics are listed in Table 3.5 along with the chemical and crystallographic composition of 3 lots of AME powder received over a six month period of time.

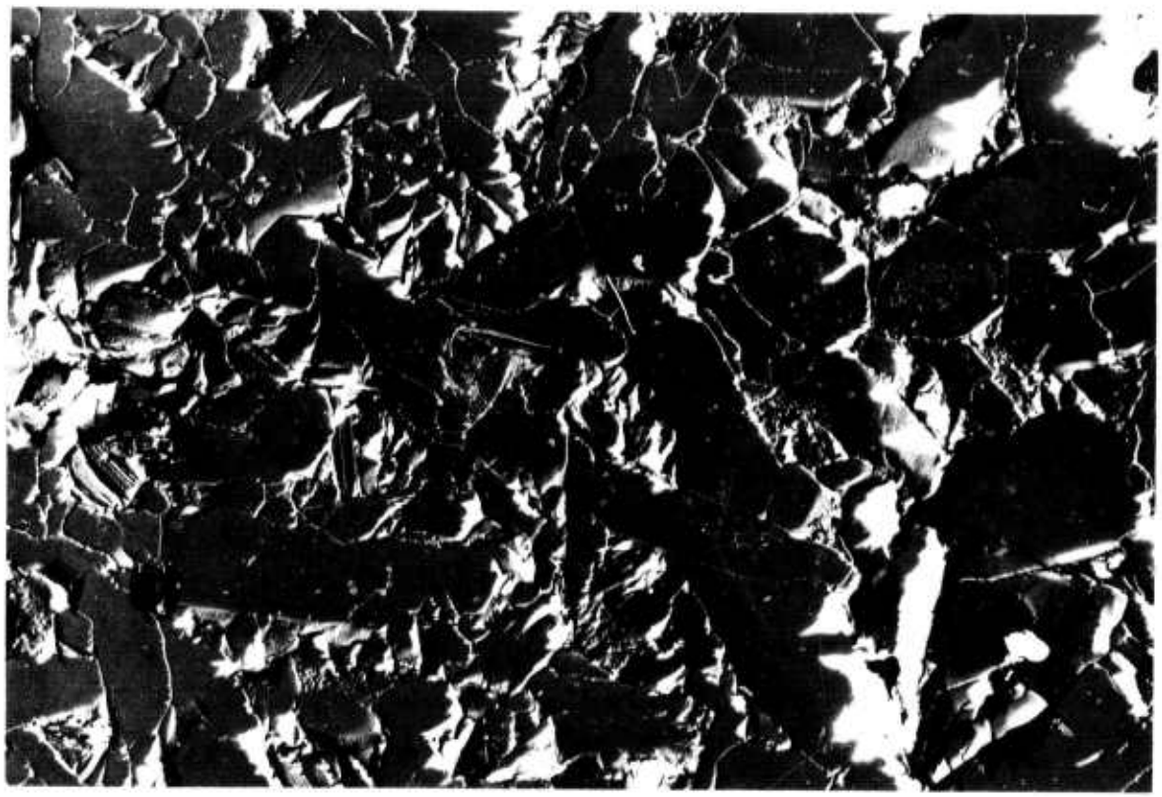

Figure 3.17 — Electron Micrograph, 13,200X, Silicon Nitride Hot Pressed From AME Powder

TABLE 3.5

CHARACTERISTICS OF AME POWDER AND HOT PRESSED BILLET

Composition (ppm) Spectrographic	Powder 1	Powder 2	Powder 3
Iron	6000	770	4500
Nickel	1500	1500	500
Copper	200	200	100
Chromium	200	200	200
Molybdenum	NA	NA	500
Manganese	NA	NA	< 100
Titanium	200	200	300
Aluminum	6000	6600	7000
Calcium	2500	2500	9000
Tungsten	NA	NA	< 100
Magnesium	200	200	1000

Phases Present X-Ray (Peak Height %)	Powder 1	Powder 3	Product of 1
α Si_3N_4	80	83	10
β Si_3N_4	13	12	77
Si_2ON_2	7	5	14
FeSi	-	-	9

Properties of billet from Powder 1	
Density (g/cc)	3.192
MOR (psi)	95,000
Magnesium by atomic absorption (ppm)	8,800

Since it was shown that the crystallographic composition of AME reactive powder is desirable for hot pressing, primary goals were to match this composition as closely as possible. Typical X-ray data of combinations tested which indicate promise of success are listed in Table 3.6.

It should be stated that all X-ray percentages listed in this report are by peak height of a selected peak in the diffraction pattern of each compound. Standards for all constituents were not available, therefore relative sensitivities could not be applied to yield weight percentages. Although preliminary standards have now been established and a computer program for converting peak height percent to weight percent is available, the volume of data (over 600 X-ray patterns to date, not including standardization data) would present a formidable conversion task. Since the goal is to match a specific pattern, units of measurement are less important than duplication of a pattern, postponing the need to dilute the current experimental effort by converting all data.

TABLE 3.6

NITRIDING RESULTS

PERCENT BY X-RAY PEAK HEIGHT

	αSi_3N_4	βSi_3N_4	Si_2ON_2	Si
AME Powder	80	13	7	-
TN 9 - 2450°F 40 hrs N_2 at 5 CFH				
Powder A	61	25	-	14
Powder A w/5% MgO	53	36	-	11
TN 11 - 2450°F 40 hrs N_2 + 4% H_2 at 5 CFH				
Powder A	84	16	-	-
Powder A w/5% MgO	63	32	-	5
TN 12 - 2500°F 40 hrs N_2 + 4% H_2 at 5 CFH				
Powder A	89	11	-	-
Powder A w/5% MgO	63	37	-	-
Powder B	24	76	-	-
TN 13 - 2450°F 40 hrs N_2 + 50% NH_3 at 5 CFH				
Powder A	83	12	5	-
Powder A w/5% MgO	92	8	-	-
TN 38 - 2450°F 60 hrs N_2 + 4% H_2 static, 3 psi				
Powder A	71	21	-	-
Powder A w/5% MgO	56	44	-	-
Powder B	38	62	-	-
TN 46 - 2375°F 24 hrs N_2 + 4% H_2 static, 3 psi				
Powder B	18	82	-	-
Powder B w/5% MgO	50	50	-	-
Powder B w/2% Li_2CO_3	94	-	-	6
TN 49 - 2450°F 40 hrs N_2 + 4% H_2 at 12 CFH (300 in^3 Furnace)				
Powder B	18	82	-	-
Powder B w/5% MgO	50	50	-	-
Powder B w/2% Li_2CO_3	91	4	-	5

TABLE 3.6 (Continued)

	αSi_3N_4	βSi_3N_4	Si_2ON_2	Si
TN 62 - 2450°F 24 hrs				
N_2, static at 3 psi				
Powder A	56	44	-	-
Powder B	11	86	-	-
Powder C	67	33	-	-
TN 58 - 2450°F 24 hrs				
N_2 + 4% H_2, static, 3 psi				
Powder A	76	24	-	-
Powder B	24	76	-	-
Powder C	88	12	-	-
TN 57 - 2450°F 24 hrs				
N_2, static, 3 psi				
Powder B, w/2% Li_2CO_3	96	4	-	-
Powder C, w/2% Li_2CO_3	93	7	-	-
TN 59 - 2450°F 24 hrs				
Tank N_2 static, 3 psi				
Powder B, w/2% Li_2CO_3	88	7	5	-
Powder C, w/2% Li_2CO_3	88	6	6	-
TN 80 - 2450°F 20 hrs				
N_2 + 1% CO_2, static, 3 psi				
Powder B, w/2% Li_2CO_3	84	10	6	-
Powder C, w/2% Li_2CO_3	81	4	15	-
TN 66 - 2450°F 2 hrs				
N_2 static, 3 psi				
Powder C, w/2% Li_2CO_3	82	4	14	-
TN 68 - 2350°F, no soak				
N_2 + 4% H_2 static, 3 psi				
Powder C, w/2% Li_2CO_3	85	6	9	-
TN 86 - 2450°F 24 hrs				
(300 Cu In Furnace)				
N_2 + 1% CO_2, static, 3 psi				
Powder C, (test bar)	90	5	5	-
Powder C, (2 lbs disc)	89	11	-	-
TN 89 - 2450°F 16 hrs				
(300 Cu In Furnace)				
N_2 + 1% CO_2, static, 3 psi				
Powder A Molded Wheel				
Surface	65	13	12	10
Interior of Hub	18	76	-	6

The first group of five nitriding runs listed in Table 3.6 compares powder A with and without a 5% MgO additive under various atmospheres. Note that a 4% addition of hydrogen to nitrogen increase the αSi_3N_4 while lowering the βSi_3N_4 and free silicon. A higher temperature (TN 12) eliminates the remaining free silicon in the MgO containing preform, while the 50-50, N_2 - NH_3 atmosphere (TN 13) nitrides this powder to near the desired 80-13-7 ratio listed at the top of the table. The static condition, while probably more controllable, decreases the alpha content perhaps because less total gas is exposed to the samples; therefore less total oxygen (as a trace impurity in the gas) is available. Two powder B results are included in the group to show the effect of decreased particle size (increased surface area). There is some evidence that a more rapid exothermic reaction due to higher surface area increases temperature locally, producing a higher beta content.

The second group of 2 nitriding runs compares powder B with two selected additives under a static atmosphere in the small furnace and under flowing N_2 + 4% H_2 in the larger furnace. The two furnaces can produce similar results while the additives illustrated have widely different effects on the nitriding results.

The next two runs show the effect on all three powders, without additives, of pure cryogenic nitrogen and tank nitrogen containing 4% H_2, both under static 3 psi positive pressure conditions. The hydrogen increases the alpha content of all three powders but the surface area and purity of the powders cause different nitriding results.

The fourth group of five runs illustrate the effect of a 2% Li_2CO_3 (to initial Si content) addition to powders B and C. The tank nitrogen (TN 59) contained a slightly higher oxygen impurity than the cryogenic line nitrogen (TN 57) causing some Si_2ON_2. A 1% CO_2 additive (TN 80) causes even higher Si_2ON_2. The rate of nitriding is increased by the presence of Li_2CO_3 as illustrated by the grossly shortened two hour soak (TN 66) and zero soak time of TN 68. In the latter case, the power was shut off as soon as the pressure switch no longer called for additional gas to maintain 3 psi pressure. The reaction had gone to completion, at least for the small test bars.

The last two runs listed show that test bars and large pieces molded from the same powder behave somewhat differently. The phase gradient from the surface to the center of a large, molded dummy turbine wheel is a further indication of an exothermic reaction and illustrates the need for further control of the nitriding process.

Hot pressing or pressure sintering is the simultaneous application of heat and pressure to the objeet in question. Several methods may be used to transmit the load to the object, the most common being direct eontaet with the die interior and the ram faees. The elose thermal expansions of Si_3N_4 and graphite plus a reaetion to form an SiC interface ean eause stieking problems. Reaction barrier layers such as BN retard the latter while a thin soft graphite sleeve or hot ejeetion of the part eireumvent the former. Another approach is to bury the object in a powder bed which transmits the load at temperature. Both natural flake graphite and boron nitride accomplish this and have been used suecessfully with silicon nitride. The powder bed approach has shown some promise in producing complex shapes, without the need for eomplex shaped dies and punches, and is therefore being pursued for this program. Sinee the powder bchaves as a first approximation of an isostatic fluid, it is b[illegible]g ealled a pseudo-isostatic hot pressing method.

In order to prove the feasibility of the method test bars of AME Si_3N_4 powder milled with 2% MgO were dry pressed and buried in graphite within the die eavity. After one hour at temperature and pressure the bar was removed, cleaned by sand blasting away the graphite, and density and strength were measured. A density of 3.19 g/cc and a strength 95,000 psi were reproducibly obtained using a 1-1/2" long speeimen on a 1" span in 3 point bending. The mierostrueture of such material is very similar to that powder hot pressed by conventional closed die methods and to the Norton or Lueas hot pressed silicon nitride.

A major portion of the development work on the pseudo-isostatic method has been accomplished using molded bars, 1/4" diameter by 4" long. The bars are readily molded from the various silicon/additive mixes deseribed and nitrided under the many conditions listed. They not only serve as eonvenient samples for X-ray diffraction, chemieal analysis, ete., but are readily hot pressed by the powder bed method for shrinkage and strength determination. The normal 4 point load MOR formula is easily converted for the eliptical eross section of the bar after hot pressing.

Some preliminary experiments on pseudo isostatic hot pressings may be summarized as follows: Lithium earbonate additions to silicon before nitriding are not useful as densification aids because of lithium content drops to 0.09% from 0.85% after 24 hours at 2450°F. Six test bars containing lithium earbonate hot pressed to only 2.43 to 2.62 g/ee, with very low strength. MgO additions to silicon before nitriding remains, but do not yield high strength at the 1% level perhaps beeause homogenity is difficult to aceomplish at the low level. The vacuum impregnation of a saturated aqueous solution of magnesium nitrate, into silicon nitride molded without additives yielded promising results at the same low level. Bars molded from powder B and nitrided to 45%α, 52%β Si_3N_4 and 2% silieon and containing 0.69% Mg whieh had been added by impregnation had an average strength of 57,000 psi at a 2.98 g/ce density when measured in 4 point bending on a 3 in. x 2 in. span. The sample analyzed 8% α and 89% β Si_3N_4 with traces of SiC and FeSi after hot pressing in flake graphite. Similar bars vacuum impregnated with lithium from a saturated solution of lithium nitrate hot pressed to 3.09 to 3.11 g/ec density. While these had very nearly the same strength as the bars containing magnesium, the lithium content after hot pressing was only 0.17% Li suggesting an aporoaeh to improve strength at high temperature.

A large disc, 6" diameter by 1" thick, was dry pressed from powder A and nitrided to a 63% α, 37% β Si_3N_4 composition. This was hot pressed in a flake graphite bed to 3.21 g/cc density after vacuum impregnation with magnesium. Test bars 1/4" square by 4" long sliced from the billet exhibited strength of 50,000 psi on a 3" x 2" 4 point bending fixture. A similar disk nitrided to 87% α and 13% β under otherwise similar conditions was hot pressed to only 3.04 g/cc density but with higher strength (up to 61,000 psi).

A major problem with the pseudo-isostatic method has been non-uniform flow of the powder and subsequent fracture of parts having thin cross sections. Several stator assemblies and thin disks have been hot pressed near theoretical density using a single 100 ton ram pushing from the top while the die (14" diameter ATJ graphite) "floats" on compressible graphite felt. In some cases stator blades which fractured early in the pressing cycle were welded back onto the assembly in a distorted position during hot pressing. The press has now been modified by adding a second 100 ton ram at the bottom and fixing the position of the die firmly in the center of the induction coil. Two matched flow control valves were added in the hydraulic return lines of the two opposed rams so that relative travel of the two rams can be adjusted to be equal in spite of small differences in resistance between upper and lower rams. In this way, a neutral plane can be established in which the assembly may be located and equal pressure applied to both sides. This modification has only recently been made operational and flow control settings have not yet been optimized. One disk, 4" diameter by 3/16" thick was successfully hot pressed to 3.19 g/cc density without fracture when ram travel was held within 1/4" of each other. All previous attempts using the single ram on this size disk had resulted in fracture.

Ford - Energy Research Corp. CVD Silicon Carbide Program

A unique fabrication method for a silicon carbide turbine rotor is to grow the shape molecule by molecule from a gaseous state by chemical vapor deposition (CVD). If theoretically dense, very pure, stress free and inclusion free material can be produced in this manner, much higher strength than that obtained with conventional silicon carbide shapes can be expected.(11)

Energy Research Corporation had earlier reported strength in bending (MOR) values of 109,800 $\pm$ 16,000 psi on samples of cross section 0.05" by .38" supported by knife edges 0.63" apart. Although this is an unusual specimen size and results cannot be readily compared with test results on other materials, the values are sufficiently high for CVD SiC to be considered as a candidate material for turbine rotors.

In order to establish the feasibility of producing a turbine rotor, Energy Research fabricated a turbine blade with an airfoil section as shown in Figure 3.18. A program was therefore initiated to supply samples for the evaluation of physical properties. Simultaneously a fixture is being fabricated to allow deposition of first stage turbine rotors sufficiently within dimensional tolerance to allow testing in an engine.

Figure 3.18 — Turbine Rotor Blade Made From CVD Silicon Carbide
(Courtesy of Energy Research Corp., Bethel, Conn.)

Energy Research has reported that equipment for producing the items described is under construction and checkout.

Ultrasonic Machining of Hot Pressed Silicon Nitride

It would be relatively simple to hot press disks of dense silicon nitride sufficiently large to permit machining into a turbine rotor. If a suitable machining technique could be developed, this method would be a reasonable way to fabricate prototype rotors for the testing and development program. A program was initiated to evaluate ultrasonic machining of a turbine rotor from a solid billet of hot pressed silicon nitride.

An ultrasonic machining study was undertaken to develop methods of machining blade and disk contours to exacting tolerances. The cutting rate of the material has been established at .300 inch per minute with a tool wear rate of 0.002 inches per minute. Tools are being fabricated for cutting the cavities between the blades.

Conclusions

All four parallel efforts described will be further pursued during the next six month report period. The Norton Company is confident that they can produce airfoil shapes from hot pressed Si_3N_4 and can accomplish a weld between hot pressed blades and a hub in a second operation. They expect to evaluate the process on full size rotors by June 30, 1972 and deliver prototypes shortly thereafter.

In the Ford pseudo-isostatic process, it is concluded that silicon molded shapes can be nitrided to any form (alpha, beta, oxynitride, etc.) desired, at least in thin cross sections. Methods need to be developed to solve a major problem of distortion of the airfoil shape during pseudo-isostatic hot pressing. To be investigated are control of powder flow, expendable support tooling, or permanent hard tooling. Further material development for improving strength at high temperature will be investigated.

Chemical vapor deposition was shown to be capable of producing high strength silicon carbide and can be used to deposit airfoil shapes. The feasibility of depositing a full size turbine rotor of dense silicon carbide with all blades formed in one operation will be established by mid 1972. Strength of the deposited material will be measured on samples of more conventional geometry than previously available.

Of several machining methods investigated, an ultrasonic method appears most promising with a cutting rate for dense Si_3N_4 150 times that of the tool wear rate. If warranted by the results of a current program of ultrasonically machining three adjacent blades to size and shape, a group of rotors will be fabricated for spin testing and attachment studies.

3.2 CERAMIC STATORS, SHROUDS, AND NOSE CONES

3.2.1 DESIGN AND ANALYSIS

SUMMARY

Several basic design concepts and material variations have been considered for the stationary hot flow section. Four variations of the nose cone and first stage stator were considered for reaction sintered silicon nitride and Dow Corning transfer molded silicon carbide. One concept has been selected for initial testing.

This selection was based on an analysis of the stationary hot flow section for three engine operating conditions, using two-dimensional finite element and finite difference heat transfer and stress analysis computer programs. Currently under consideration is a more detailed three-dimensional finite element analysis of the stator assemblies including the stator vanes.

Introduction

In Section 3.1.1 aerodynamic design aspects for ceramic turbine rotors were discussed and reasons given for the modification of these components to the Design B and C configurations. Apart from aerodynamic modifications, structural changes of stator platforms and turbine shrouds were incorporated in Design B to improve fabrication processing and provide more uniform response of these structures to transient thermal loadings.

In this section the heat transfer and stress analyses of Design B flow path stationary components are discussed. Specifically, the components analyzed were the nose cone, first stage stator assembly, first stage rotor shroud, second stage stator assembly and second stage rotor shroud. (See Figure 3.19) The materials used were Ford injection molded silicon nitride and Dow Corning transfer molded silicon carbide. Table 3.7 shows the properties of these materials used in this study. The objectives of this analysis were (1) to determine the points and levels of maximum stress and temperature, (2) to evaluate ways of reducing any critical stresses and temperatures, (3) to establish critical hot and cold clearances, (4) to determine the optimum configuration of the first stage stator-nose cone resulting in the least gas leakage thru the stator shrouds compatible with minimum stresses. The same analytical models were used for both materials. The models for stator assemblies and for the nose cone were based on two-dimensional axisymmetric analysis.

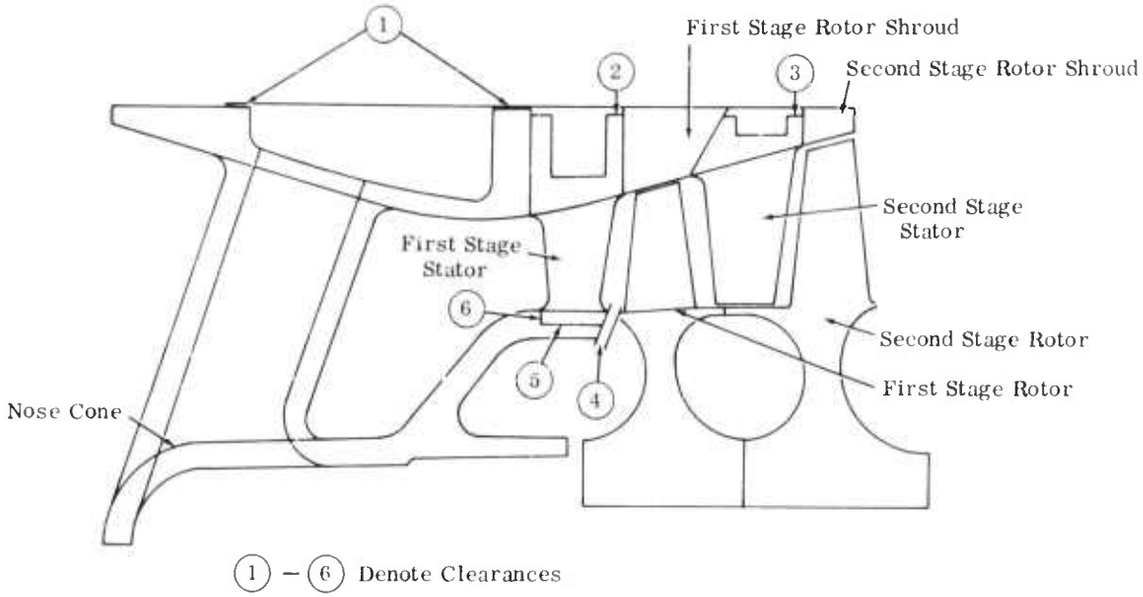

Figure 3.19 — Design B Hot Flow Gas Section with Critical Clearances

TABLE 3.7

MATERIAL PROPERTIES
FORD INJECTION MOLDED SILICON NITRIDE

Temp.	Modulus of Elasticity	Poisson's Ratio	Coeff. of Thermal Expansion	Thermal Conductivity	Specific Heat
(^{o}F)	(psi)		(In/In/^{o}F)	(B/hr in ^{o}F)	(B/lbm ^{o}F)
R.T.	16×10^{6}	.25	$.36 \times 10^{-6}$	.451	.255
500	16×10^{6}	.25	$.82 \times 10^{-6}$	.401	.255
1000	16×10^{6}	.25	1.22×10^{-6}	.356	.255
1500	16×10^{6}	.25	1.54×10^{-6}	.315	.29
2000	16×10^{6}	.25	2.10×10^{-6}	.285	.33
2500	16×16^{6}	.25	2.50×10^{-6}	.264	.36
	DOW CORNING TRANSFER MOLDED SILICON CARBIDE				
R.T.	23×10^{6}	.22	4.35×10^{-6}	.792	.200
500	23×10^{6}	.22	3.50×10^{-6}	.736	.218
1000	23×10^{6}	.22	3.22×10^{-6}	.660	.239
1500	23×10^{6}	.22	3.15×10^{-6}	.590	.259
2000	23×10^{6}	.22	3.13×10^{-6}	.521	.280
2500	23×10^{6}	.22	3.12×10^{-6}	.465	.300

Except in the immediate vicinity of circumferential discontinuities such as vane-shroud or strut-shroud junctions, the analytical models are considered representative of structures analyzed. Accurate determination of stress distribution at vane and or shroud junction will necessitate a full three dimensional analysis. As analytical tools are made available, such analyses will be performed in areas where test experience has indicated the need.

It should be pointed out that, with materials and processing being constantly improved, the analyses reported here are to be considered as development aids, aimed at locating probable problem areas. The assessment of a structure's integrity and its strength will be evaluated and appropriate design codes formulated, once the materials and fabrication proecsses have been finalized.

The analyses contained in this report were based on the elastic to fracture criterion and a linear stress-strain relation (Hooke's law).

Design B Hot Flow Section

The Design B hot flow path with all of the stationary components are shown in Figure 3.19. The parametric studies conducted during this report period involved structural variations on the first stage stator and nose cone.

The nose cone and first stage stator assembly were analyzed in certain configurations where the stresses in each component were affected by the thermal deformations and constraints of the other component. Two basic configurations were considered. (1) The first stage stator assembly was either an integral part of the nose cone structure, or (2) separated from it at the inner shroud pilot. The following variants of these two configurations were analyzed, as shown in Figure 3.20.

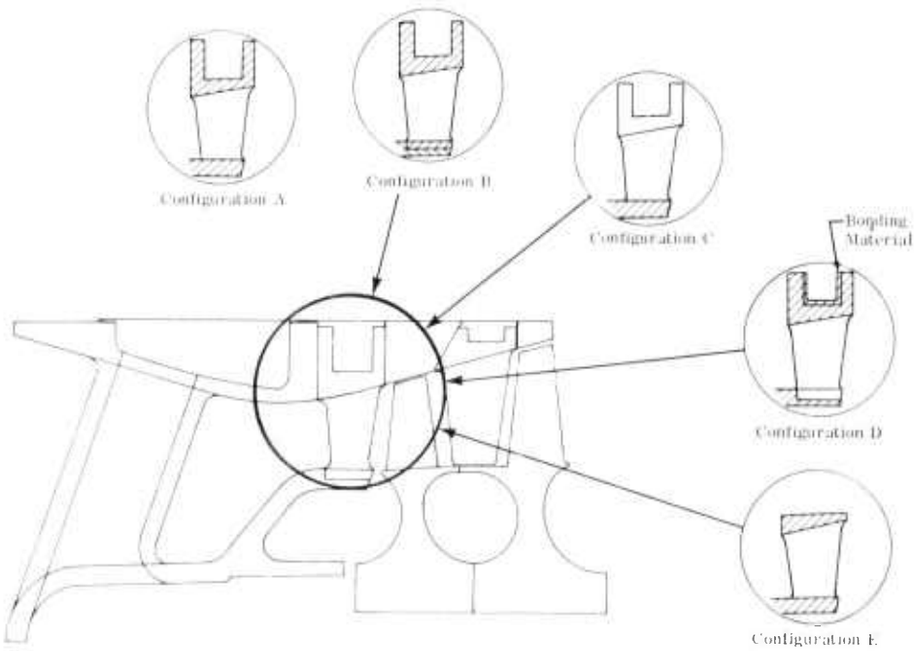

Figure 3.20 — Design B First Stage Stator/Nose Cone Configuration Analyzed

A. The stator outer and inner shrouds were solid rings; the inner shroud was integral with the nose cone.

B. The stator outer and inner shrouds were solid rings; the inner shroud was not integral with the nose cone.

C. The stator outer shroud was segmented; the inner shroud was integral with the nose eone.

D. The stator inner shroud was segmented, and was not integral with the nose eone; the outer shroud was a bonded solid ring.

E. The stator outer and inner shrouds were solid rings; the outer shroud was reduced to .2-.3 inch radial thiekness, and the inner shroud was integral with the nose cone.

The eoncentricity of the first stage stator assembly affects engine performanee. It is therefore desirable to maintain it throughout the engine operating range. From this standpoint, eonfigurations A, C, and E would be the most desirable because the coneentrieity of the first stage stator depends only upon the clearanees at the nose eone outer diameter. These elearanees are designated by 1 in Figure 3.19. For eonfigurations B and D, the stator assembly is piloted on the nose eone and its eoneentricity depends upon clearanee 1, Figure 3.19 and upon elearanees at the stator inner shroud. These clearanees are designated by 5 and 6 in Figure 3.19.

The axial elearance 4 between the nose eone inner shroud and first stage rotor platform is also a funetion of clearance 1; in addition it depends upon whether metallie or ceramie rotors are used sinee there is a signifieant difference in the axial expansion of the rotor platform.

The first and seeond stage rotor shrouds are slotted rings which are assembled with a tight slip fit. The shrouds are free to grow circumferentially with no appreciable change in radial thiekness.

The seeond stage stator assembly is positioned between the rotor shrouds and is held eoncentrie with respect to the rotors by means of a conieal surface. A small axial spring foree is provided to maintain eontaet between these eonieal surfaees and to position all the components axially. The second stage stator assembly is free to grow radially and suffieient clearance must be maintained at the stator outer diameter to prevent interference when hot. This elearance is designated by 3 in Figure 3.19.

At the time this analysis was initiated several methods of cooling the first stage rotor and bolt were considered, for use of either metallic or ceramic turbine rotors. With metallic rotors 22.2 lbm/hr of cooling air from the compressor discharge was directed at the center of the rotor bolt. The method of cooling and the amount of cooling air required for cooling the rotor bolt used with ceramic rotors were not known at the time this analysis was conducted, so it was assumed that conditions existed identical to the metallic rotors at idle speed and that no disk cooling was used for the ceramic rotor at 100% speed. The nose cone cavity adjacent to the first stage rotor is filled with fiberous insulation providing a controlled gap for flowing cool air.

The small arrows in Figure 3.21 trace the path of the inlet air, the hot gas, and cooling air as seen by the components analyzed.

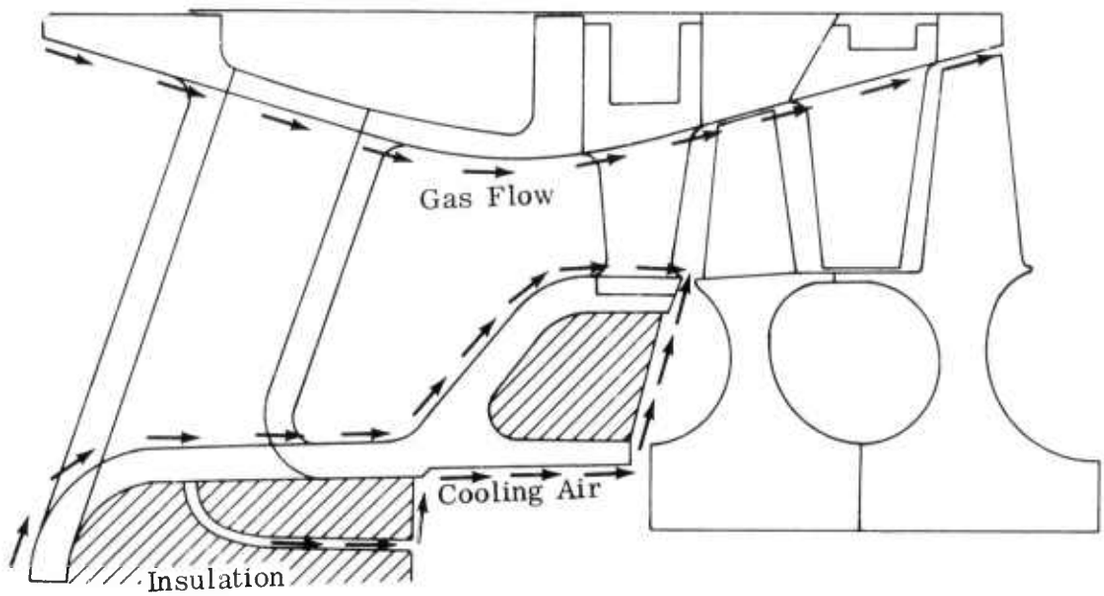

Figure 3.21 — Boundary Cooling Flow Paths Used in Analyses of Ceramic Nose Cone and Turbine Stators

Method of Analysis

A finite element heat transfer program and a finite element stress program were used for the analysis. The same element grid as shown in Figure 3.22 was used in both programs. The heat transfer program was run first and a magnetic tape was generated with the nodal point temperatures. This in turn

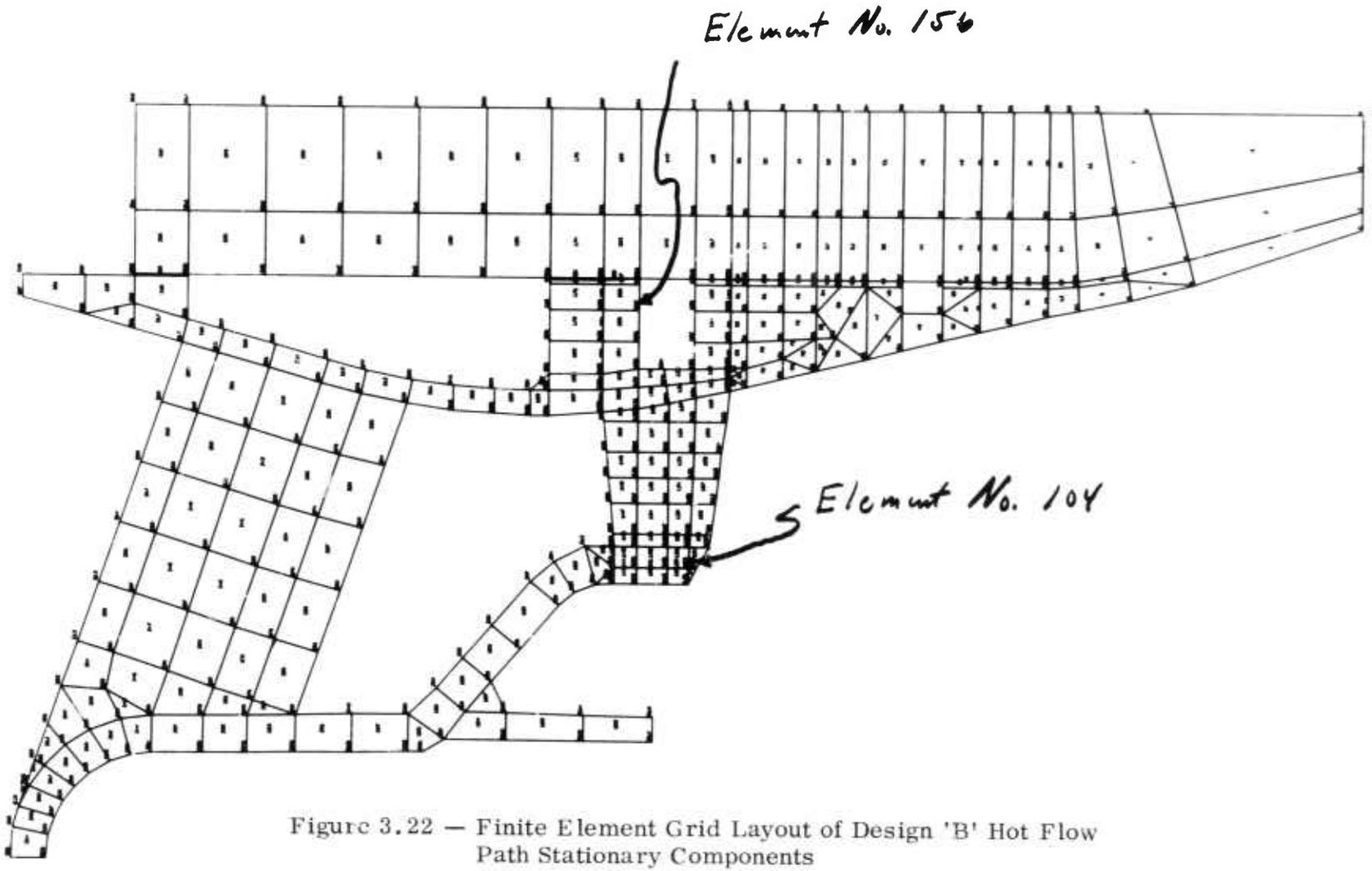

Figure 3.22 — Finite Element Grid Layout of Design 'B' Hot Flow Path Stationary Components

was used as input for the stress program. Heat transfer and stress analyses were obtained simultaneously for either steady state or transient conditions by feeding the output from the heat transfer program directly into the stress program. Nodal point deflections were also part of the stress program output and were used to determine the proper clearances for the various components. Both computer programs are set up for axi-symmetric solids, but they are not capable of directly solving for the heat transfer and stress of the stator vanes and nose cone struts. To account for stiffness and loading effects in the stress analysis, the stator vanes and struts were treated as bodies of revolution with quasi-elastic properties. Employing this method it is expected that the results for the first stage stator with its large number of vanes (25) is good to a first approximation. In the case of the nose cone with only 3 struts the results are probably not as valid.

In the heat transfer program the material properties of the finite elements representing the vanes and struts were adjusted so that there was no heat transfer by conduction into the shrouds. The increased heat transfer due to the fin effect of the vanes and struts was included by adjusting the convective heat transfer coefficients in these areas.

The three basic engine operating conditions investigated are listed below:

A. Idle speed with turbine inlet temperature (T.I.T.) at 2000°F.

   1. Transient - all components initially at room temperature.

   2. Steady state

B. 100% rotor speed with T.I.T. at 1900°F (this applies for use with metallic rotors only).

   1. Transient - all components initially at idle steady state temperature.

   2. Steady state

C. 100% rotor speed with T.I.T. at 2500°F (this applies for use with ceramic rotors only).

   1. Transient - all components initially at idle steady state temperature.

   2. Transient - all components initially at room temperature.

   3. Transient - all components initially at temperature corresponding to peak idle stress point.

   4. Steady state

Convective heat transfer coefficients were calculated for each of these basic operating conditions. For the front 60° spherical portion of the nose cone, the film coefficient was calculated from:

$$h_{c\theta} = .194\ T_f^{.49}\ (V\rho\ /Do)^{.5}\ \left[1 - (\theta/90)^3\right]$$

(See p. 373 reference 3)

where:

$h_{c\theta}$	=	local value of unit thermal convective conductance
Θ	=	angle from leading edge of sphere
T_f	=	arithmetic average of absolute temperatures of free stream and surface
V	=	free-stream velocity
ρ	=	free-stream density
Do	=	outside diameter of body

Film coefficients for the gas flow section from the combustor exit through the diffuser were estimated by using a time sharing computer program which estimates the convective film coefficients for a fluid flowing through a heated annulus. The coefficients obtained by these two methods for the point of transition from spherical to cylindrical geometry agree rather well. For example, at 100% rotor speed with T. I. T. = 1900°F, the spherical section of the nose cone at $\Theta = 80^o$ gives $h_{c\theta} = .237$ Btu/hr-in^2-°F and the heated annulus approximation gives $h_c = .236$ Btu/hr-in^2-°F. These coefficients were corrected in the areas of the nose struts and stator vanes to account for the increased heat transfer due to their fin effect. This was done by using the concept of equivalent convective coefficients which use the film coefficients on the fin surfaces. The film coefficients for the nose cone strut surface were calculated from:

$$h_b = .26k/D_o\ \left[DoV\rho/\mu\right]^{.6}\ \left[Cp\mu/k\right]^{.3}$$

where:

h_b	=	unit thermal convective conductance
k	=	thermal conductivity of gas at film temperature
D_o	=	outside diameter of tube
V	=	velocity thru minimum free area
ρ	=	density of gas at film temperature
C_p	=	specific heat of gas at constant pressure
μ	=	viscosity of gas at film temperature

This equation applies to flows of a warm fluid over a cooler tube and was assumed to be valid for the entire surface of the strut. The first and second stage stator vane surface film coefficients were estimated by using a time sharing computer program based on the empirical formulae for cascades:

$$h = \left[.11\ k_{air}\ \pi/P_w\right](Pr)^{.3}\ (Re)^{.69} \qquad \text{for Re} \geq 30{,}000$$

$$\text{and } h = \left[.664\ k_{air}\ \pi/P_w\right](Pr)^{.3}\ (Re)^{.5} \qquad \text{for Re} < 30{,}000$$

where:

h	=	unit thermal convective conductance
K	=	thermal conductivity of air
P_W	=	wetted perimeter
Pr	=	Prandtl number
Re	=	Reynolds number

The increase in the value of the film coefficients directly opposite the turbine rotor tips was neglected. The effect of any error incurred at the rotor tips should be small since no critical stresses exist in these areas.

For film coefficients near the bolt area, flow through an annulus was assumed and according to reference 3, page 343 the Stanton number $St = .023\ Re^{-.2}$ which results in $h_c = .023\ Re^{.8}\ Pr^{1/3}\ k/D_H$ for turbulent flow. Where D_H = hydraulic diameter, with all other terms as defined above.

The stator vane and strut temperatures were calculated by first solving transient and steady state heat transfer analyses of the complete flow path to determine the boundary temperatures at the base of the vanes and struts. Using in turn these boundary conditions as input to a two-dimensional finite difference heat transfer program, temperature of the vanes and struts was computed as a function of time. To account for the effects of the vanes and struts on the shrouds, these temperatures were used as inputs back at the corresponding nodal points in the finite element program. As anticipated, the vanes were found to increase in temperature rapidly relative to the rest of the stator assembly. The nose cone struts responded much slower than the stator vanes due to their greater bulk and their response was nearly the same as the rest of the nose cone in the strut area. The steady state temperature profile for the vanes and struts were used as inputs into the analysis only after the temperature of the stator shroud areas approached the vane temperatures. A separate analysis was conducted for several discrete points in time, from the cold start, until this convergence was achieved. The stator vane temperature profile was determined for each of these discrete points. For the Si_3N_4 analysis this point corresponded to approximately 50 seconds from cold start and was somewhat less for the SiC analysis because of the greater thermal conductivity of that material. Since the nose cone strut responded at about the same rate as the rest of the nose cone in the strut area and no history of repeated failure occurred in this area, results were not evaluated quantitatively.

As shown in Figure 3.22 the entire gas flow section was analyzed as a whole by using a finite element grid layout which included all components. To correctly model the interaction of individual structures, an elemental layer of negligible thickness and having pseudo elastic properties was introduced at the interface between each component. These pseudo properties were such that the components were able to move freely without imposing stresses on neighboring components and yet allowed the proper heat transfer from one component to the other. Where no surface contact was expected, elements with air properties were assumed or surfaces were treated as free boundaries.

A similar elemental layer of negligible thickness was used between the first stage stator inner shroud and nose cone. This allowed analysis of the various stator-nose cone configurations by using air properties when the inner shroud was not integral with the nose cone, and actual material properties when it was.

Discussion of Results

Results obtained from initial analyses of the Design 'B' hot flow path showed that the highest stresses occurred in the first stage stator and the nose cone. Subsequent analyses were conducted for structural variations of the first stage stator and the nose cone, with all the other components remaining unchanged.

The results and discussion of the various nose cone-stator configurations investigated for the Design 'B' hot flow path follows.

Configuration 'A' — The first stage stator with a solid outer ring, and a solid inner ring integral with the nose cone.

The transient and steady state analyses showed that the maximum stresses occur during the transients, with the steady state stresses being small. Transient thermal conditions at the first stage stator vanes resulted in a more rapid increase of temperature in the stator vanes and inner ring than in the outer ring, inducing stresses due to differential thermal growth and the internal restraints of the structure. The outer ring is stretched by tangential stresses and the inner ring is compressed tangentially. The maximum tensile stress in this configuration is a tangential hoop stress and occurs at the outermost fibers of the upstream portion of the first stage stator outer shroud. (Element No. 156 in finite element grid, Figure 3.22). The maximum compressive stress occurs at the downstream edge in the inner shroud at the stator vane trailing edge. (Element No. 104 in the finite element grid, Figure 3.22.) These stresses are plotted in Figures 3.23, 3.24 and 3.25 for silicon nitride and silicon carbide.

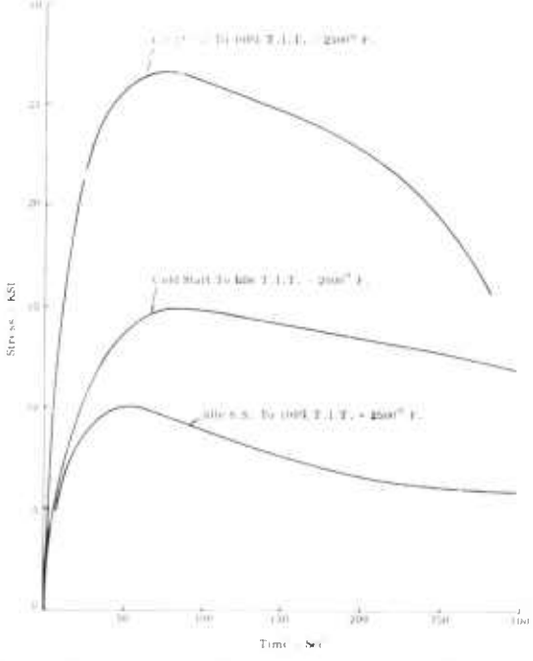

Figure 3.23 — Maximum Tensile Stress First Stage Stator Configuration 'A' Silicon Nitride

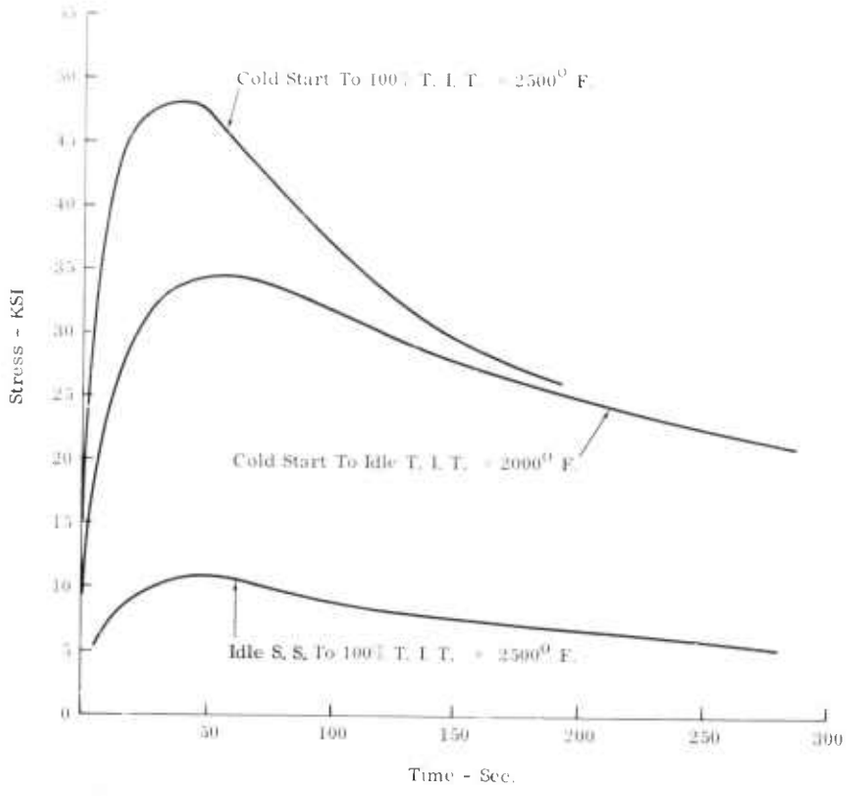

Figure 3.24 — Maximum Compressive Stress First Stage Stator Silicon Nitride Configuration 'A'

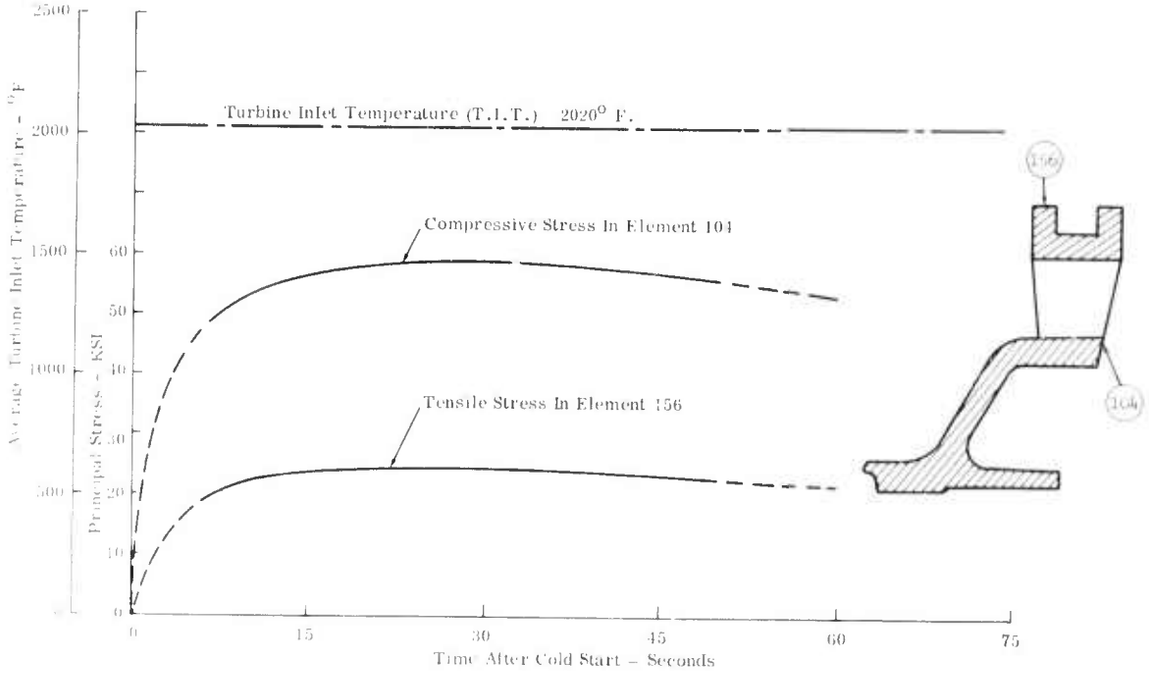

Figure 3.25 — Maximum Stresses in First Stage Configuration 'A' Silicon Carbide

As a rule, compressive stresses have been assumed to have little or no bearing on the structural integrity of components investigated except for stability or buckling considerations.

In this particular configuration the tensile stresses exceed flexural strength values of corresponding materials. Therefore, it was necessary to modify the structure in an attempt to reduce these stresses to acceptable values.

Configuration 'B' (Si_3N_4 Only) — The first stage stator with both outer and inner shrouds as solid rings, the inner shroud not integral with nose cone.

The maximum tensile stress in this configuration (Figure 3.20) again occurs at the outermost fiber of element No. 156, (Figure 3.22) but now is reduced by approximately 25% (see Figure 3.26). The maximum compressive stress has, however, increased to 41,000 psi as shown in Figure 3.27. Comparing this to the previous case indicates that the nose cone is expanding rapidly and this radial expansion is transferred through the vane to add to the tensile stress at the outer shroud. This same trend is shown for all transient conditions as can be seen by comparing Figures 3.23 and 3.26.

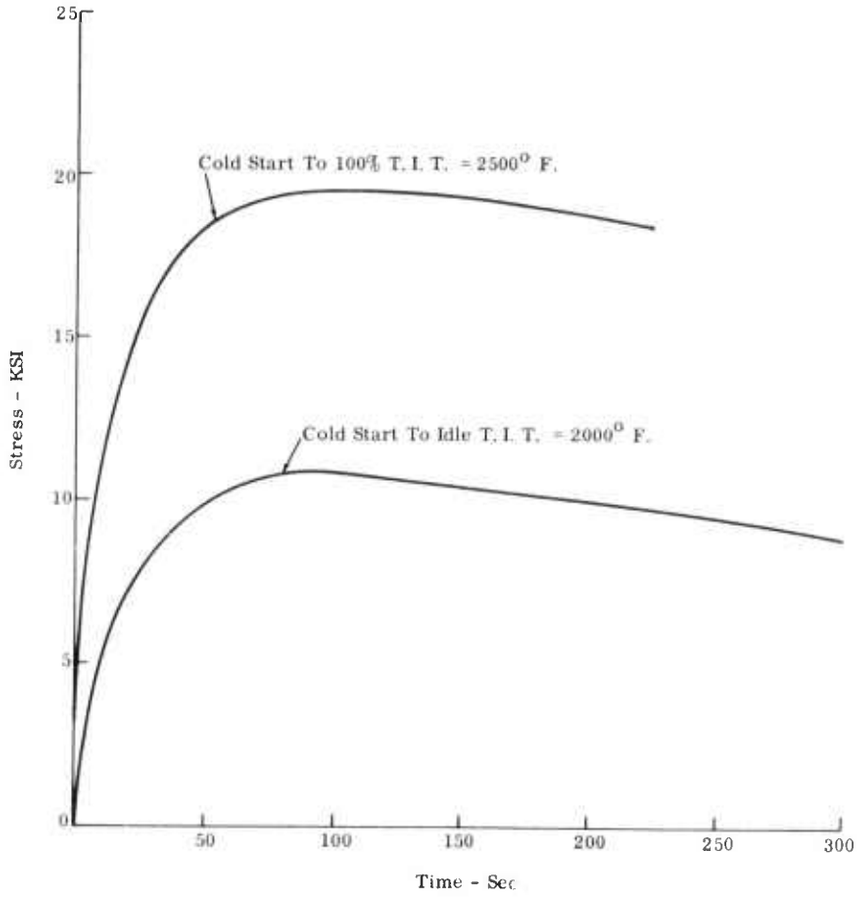

Figure 3.26 — Maximum Tensile Stress First Stage Stator Silicon Nitride Configuration 'B'

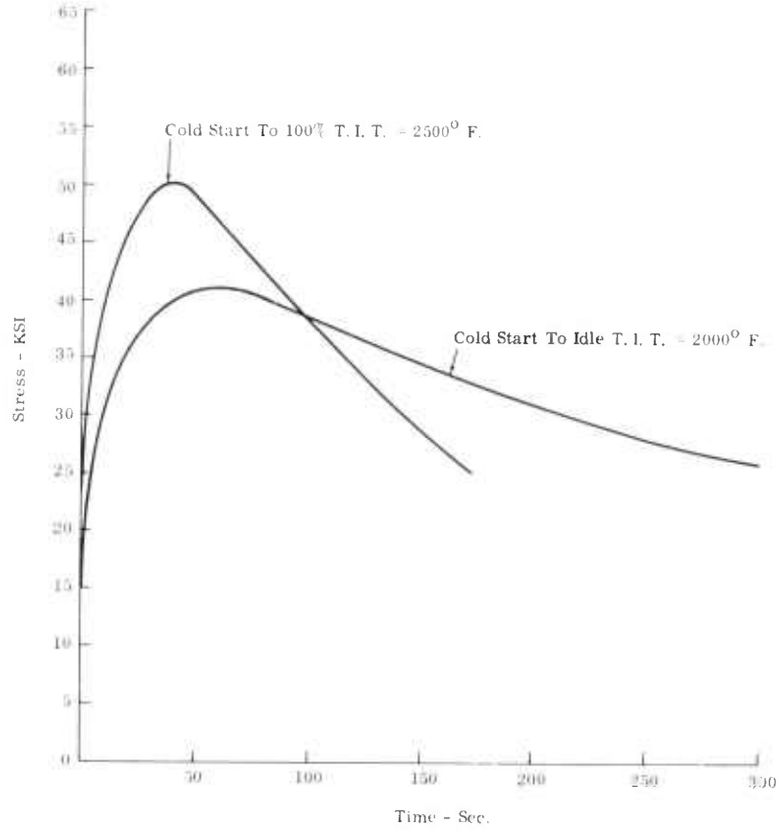

Figure 3.27 — Maximum Compressive Stress First Stage Stator Silicon Nitride Configuration 'B'

Configuration 'C' — The first stage stator outer shroud is segmented; the inner shroud is integral with the nose cone.

This design configuration (Figure 3.19) was investigated to determine the effect of segmenting the outer shroud ring of the first stage stator. In this structural arrangement the thermal growth is no longer restrained by the stiffness of a continuous hoop. The high tensile stresses in the outer ring and compressive stresses in the inner ring are reduced to acceptable levels, however, excessive gas leakages are expected.

Configuration 'D' — The first stage stator inner shroud is segmented; the outer shroud is a bonded, solid ring.

This design configuration (Figure 3.20) has the lowest stress levels of all the design configurations investigated at comparable engine operating conditions. Segmenting the inner ring of the first stage stator assembly limits the maximum tangential stresses in the outer ring to within acceptable levels. Figure 3.31 shows the maximum stress levels in the silicon nitride stator assembly at the transient operating conditions. Figures 3.28, 3.29 and 3.30 show the maximum stress levels in the silicon carbide stator assembly. The silicon carbide stresses are considerably below the flexural strength of that material (26,000 psi).

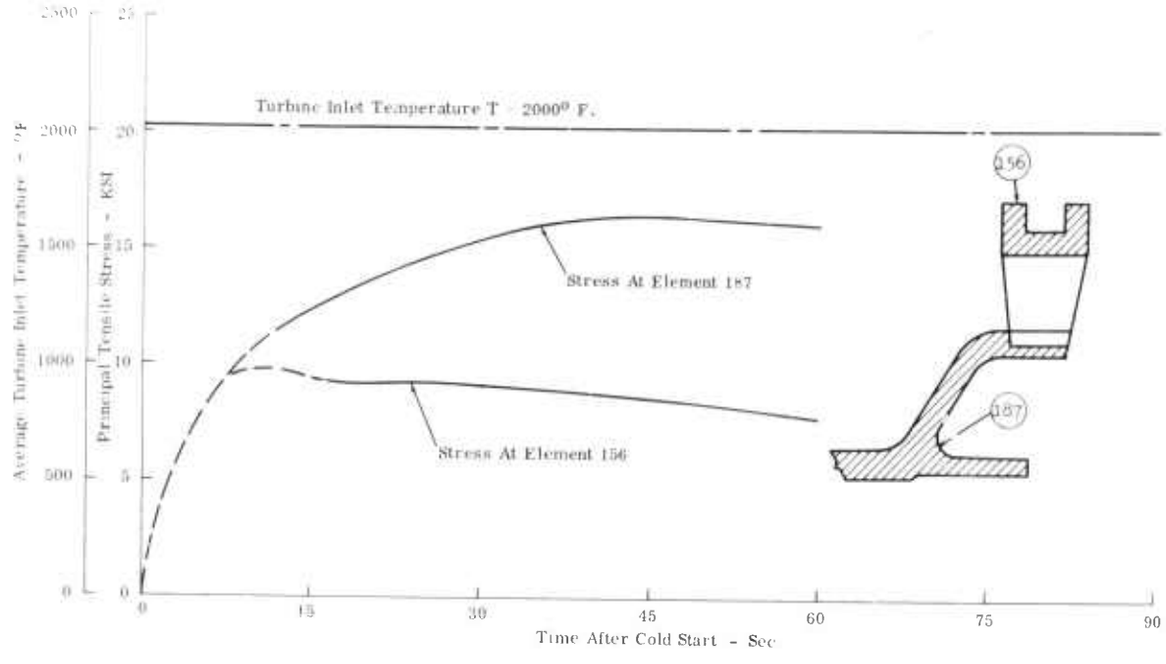

Figure 3.28 — Maximum Stresses First Stage Stator and Nose Cone Silicon Carbide Configuration 'D'

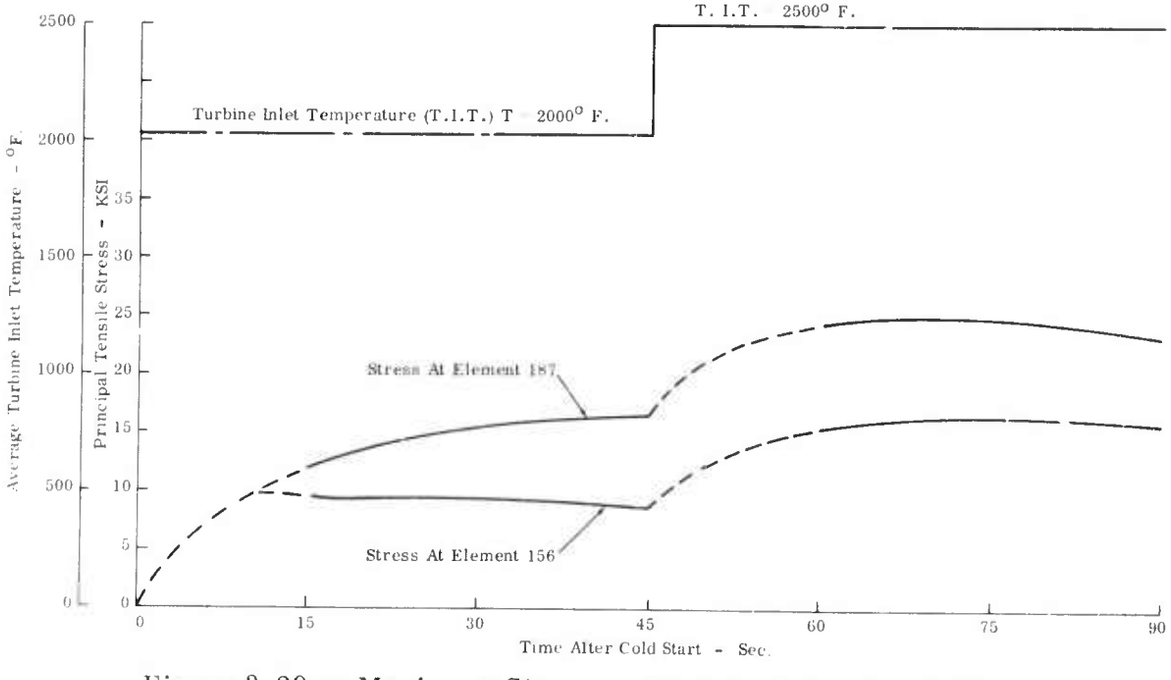

Figure 3.29 — Maximum Stresses First Stage Stator and Nose Cone Silicon Carbide Configuration 'D'

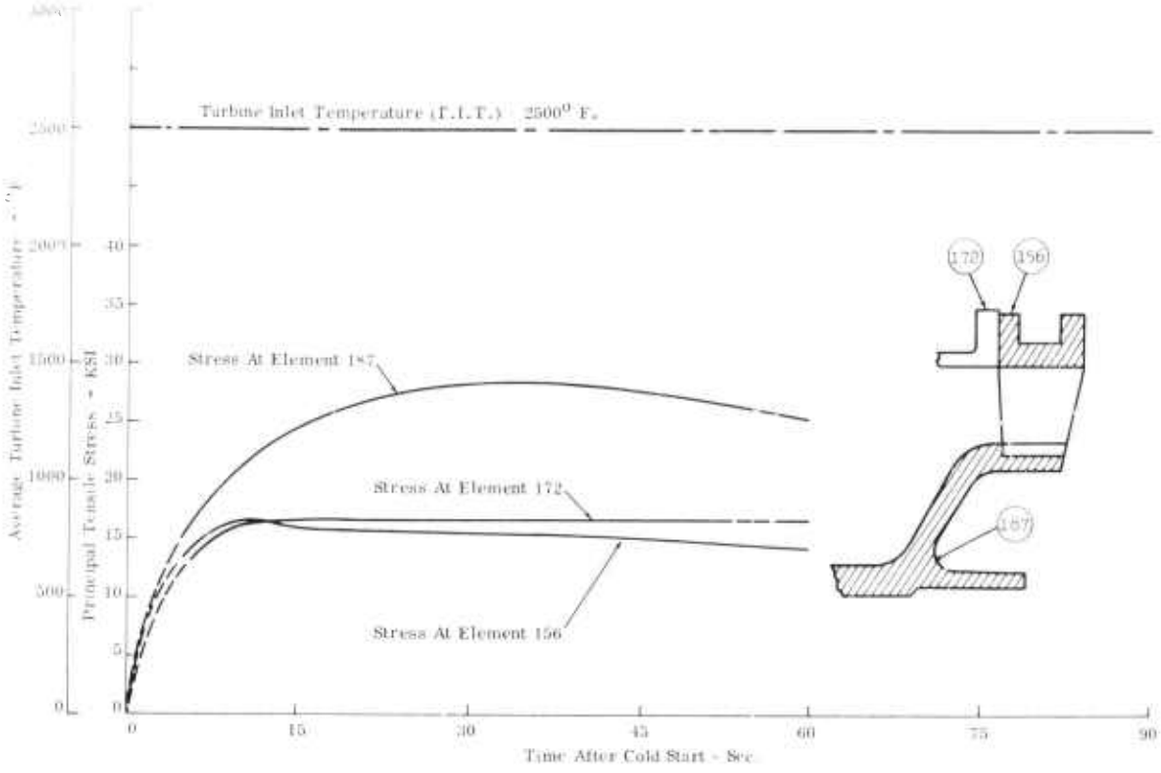

Figure 3.30 — Maximum Stresses First Stage Stator and Nose Cone Silicon Carbide Configuration 'D'

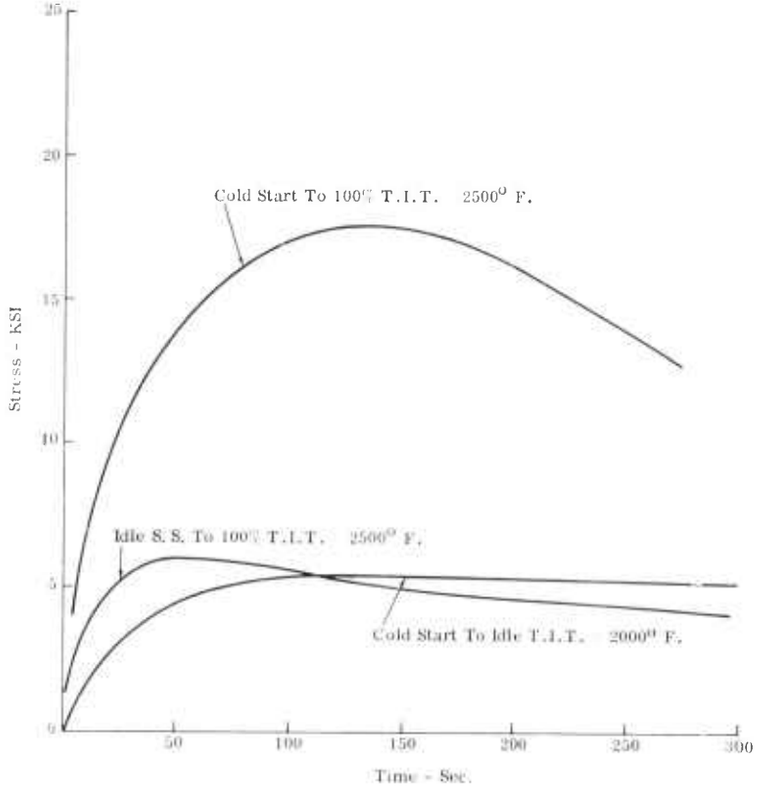

Figure 3.31 — Maximum Tensile Stress First Stage Stator Silicon Nitride Configuration 'D'

During the cold start transient the two shrouds lag in temperature considerably behind the fast responding vanes and constrain its free thermal growth. Figure 3.32 shows typical temperature response of stator components for the cold start to idle transients. As seen from the figure, the more massive the component the slower its response. In the case of the vane, its response is further enhanced by increased heat transfer surface, because the whole vane is submerged in the hot gas steam.

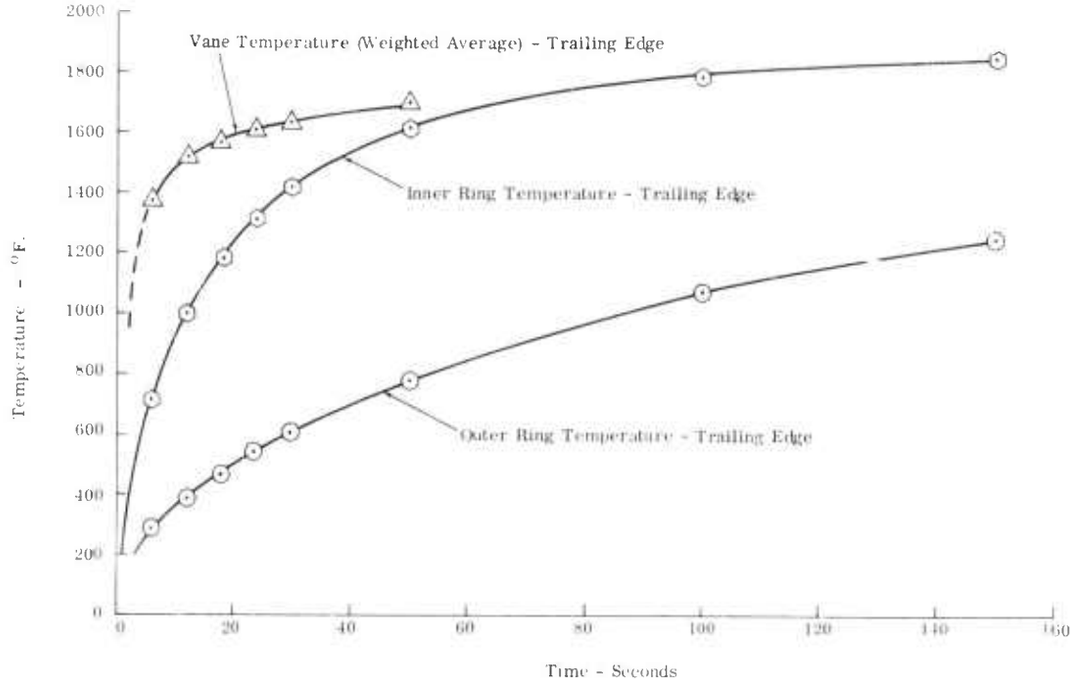

Figure 3.32 — Temperature Response First Stage Stator Silicon Carbide Cold Start to Idle Operation

A solid inner ring having hoop stiffness will resist this growth incompatibility, producing radial interaction loads and tensile and compressive hoop stresses in the outer and inner shrouds respectively. By segmenting the inner shroud, the hoop stiffness resistance to the mismatch of growths is eliminated resulting in lowering of stresses. To prevent the shroud segments from acting as a continuous hoop under thermally induced compression loads the inner shroud segments have been designed to maintain a tangential clearance under the anticipated thermal growth conditions. Radial clearances between the inner surface of the segments and the mating surface of the nose cone structure have also been maintained to prevent restrictions of thermal growth in the radial direction.

To minimize mechanical loads on the vane, an axial clearance has been provided between the inner shroud and the nose cone. This allows the axial thrust resulting from the pressure drop across the nose cone and other upstream structures to be transmitted directly via the outer shroud. The resulting hot and cold clearances necessary to use this shroud-nose cone configuration with either metallic or ceramic rotors is summarized in Table 3.8.

TABLE 3.8

CONFIGURATION D HOT AND COLD CLEARANCES Si_3N_4

	Cold	Steady State at 2000°F	Steady State at 2500°F
Radial clearance between nose cone and 1st stage stator inner shroud	.0055-.0063	.0051-.0063	.0039-.0052
Axial clearance between nose cone and 1st stage stator inner shroud (with metallic rotors)	.0008-.0018	.0000-.0010	NA
Axial clearance between nose cone and 1st stage stator inner shroud (with ceramic rotors)	.0036-.0046	.0028-.0038	.0000-.0010
Circumferential clearance between stator inner shroud segments	.0017-.0024	.0016-.0023	.0014-.0021
Clearance between nose cone and metal rotor platform	.0438-.0679	.0184-.0425	NA
Clearance between nose cone and ceramic rotor platform	.0438-.0679	—	.0283-.0524
Radial clearance 1st stage stator outer shroud	.0185-.0238	.0083-.0135	.0038-.0090
Radial clearance at nose cone O.D.	.0156-.0161	.0046-.0057	.0000-.0012
Radial clearance at 2nd stage stator outer shroud	.0135-.0163	.0038-.0066	.0026-.0053

Note that the axial dimension of the stator inner shroud must be reduced to .0028" when changing from metal rotors to ceramic rotors. This is necessary to minimize leakages through the shroud in both metallic and ceramic rotor configurations.

As previously stated the vane stresses were not directly attainable from this analysis since the computer programs were set up for axi-symmetric solids and only the loading and stiffening effects of the vanes on the shrouds were included. Vane boundary temperatures in the shroud were obtained by using the finite element axi-symmetric heat transfer program and were used in a 2-dimensional finite difference heat transfer analysis to obtain the vane temperature at desired time increments. By using differences between the boundary temperatures and the adjacent vane temperature the maximum axial shear stress in the vane was estimated to be approximately 11,000 psi for the silicon nitride stators. This thermal shock stress level was calculated in the vane trailing edge at the outer shroud interface for the peak temperature difference which occurs at approximately 2 seconds after cold start. It must be emphasized that this stress estimate does not include the effects of aerodynamic loads and vibrations that will depend upon the interaction of the stator assembly with the nose cone and rotors.

Configuration 'E' — The first stage stator outer and inner shrouds are solid rings; the outer shroud is reduced to .2-.3 inch radial thickness; the inner shroud is integral with the nose cone.

This analysis was run by substituting air properties for material properties in the outer shroud elements.

The configuration (Figure 3.20) was essentially identical to Design A except for the first stage stator outer flange which was reduced in radial depth to permit more rapid heating of the ring and increase its hoop flexibility. Contrary to expectations, this modification did not significantly reduce the stresses in the outer shroud ring. The tangential stress distribution was more uniform, indicating the stress due to radial temperature differences across the shroud was reduced. However, the ring was too flexible compared to the rest of the structure, and was being stretched beyond the limits of the material. Stresses are shown in Figures 3.33 and 3.34. Examination of the transient temperatures

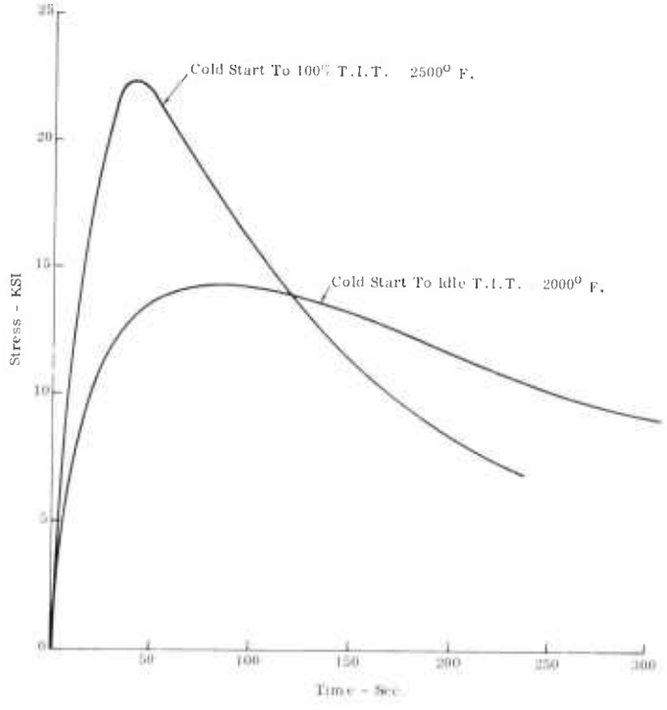

Figure 3.33 — Maximum Tensile Stress First Stage Stators
Silicon Nitride Configuration 'E'

does show that the response of the shrouds are more evenly matched, indicating that thinning the outer shroud and increasing the thickness of a portion of the nose cone inner shell may significantly reduce the maximum tensile stress in the outer shroud.

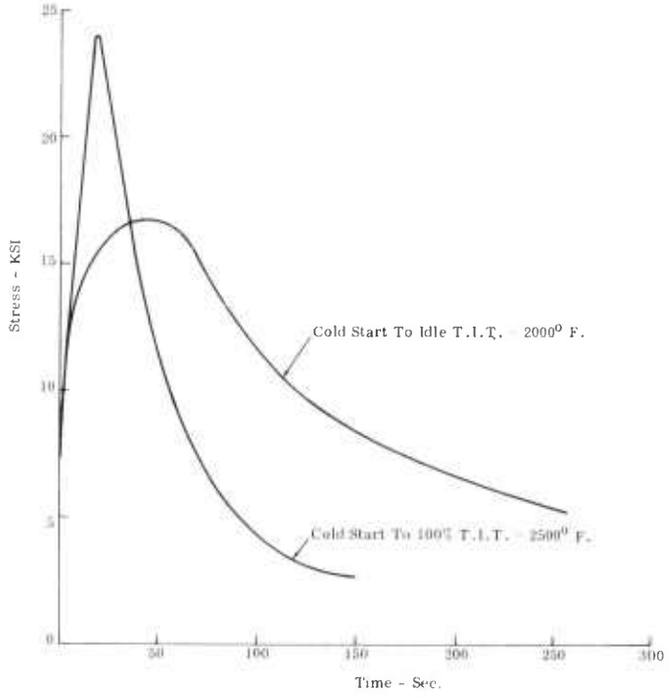

Figure 3.34 — Maximum Tensile Stress First Stage Stator Silicon Nitride Configuration 'E'

Configuration 'D,' first stage stator inner shroud segmented and outer shroud bonded solid ring, was selected for initial testing. This configuration was the least stressed of the five considered. However, the material strength of bonding may be of some concern. This is discussed in more detail in the next chapter.

Nose Cone Structure

The nose cone structure of the hot flow section in general showed significant changes in critical stress levels with variations of design configuration of the first stage stator assembly. The highest stresses indicated were compressive.

Points of highest tensile stress in the nose cone were at the outermost fiber of the downstream pilot (finite element No. 172, Figure 3.22) and at the junction of the cooling air sleeve and the conical portion of the nose cone (finite element No. 187, Figure 3.22). During transient conditions the rim of the conical section increases in temperature more rapidly than the bore of the cone. The cooling air sleeve, which is integral with the cone at the bore, is washed by cooling air directed towards the turbine rotor. The thermal growth differential is manifested in a high bending stress in a fillet at the junction. Figure 3.35 shows the transient temperature response of the nodal points located in the fillet. The stresses for these points are plotted in Figures 3.36 and 3.37 for the silicon nitride design and in Figures 3.28, 3.29 and 3.30 for silicon carbide.

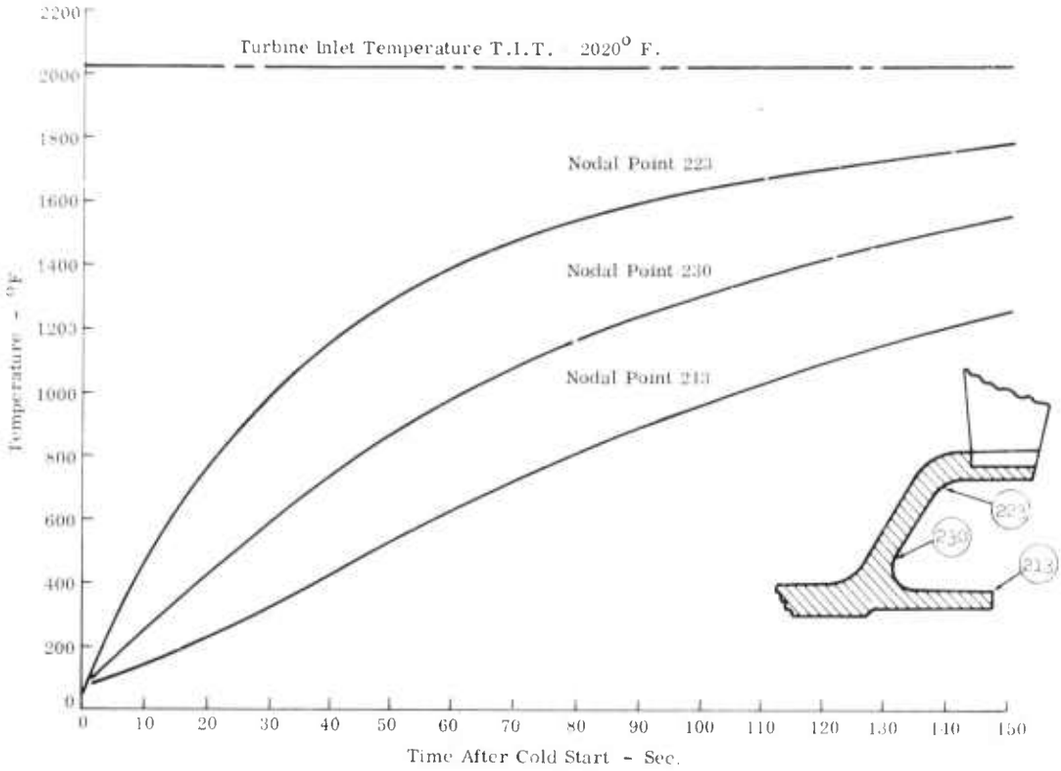

Figure 3.35 — Transient Temperature Response First Stage Turbine Stator & Nose Cone Silicon Carbide

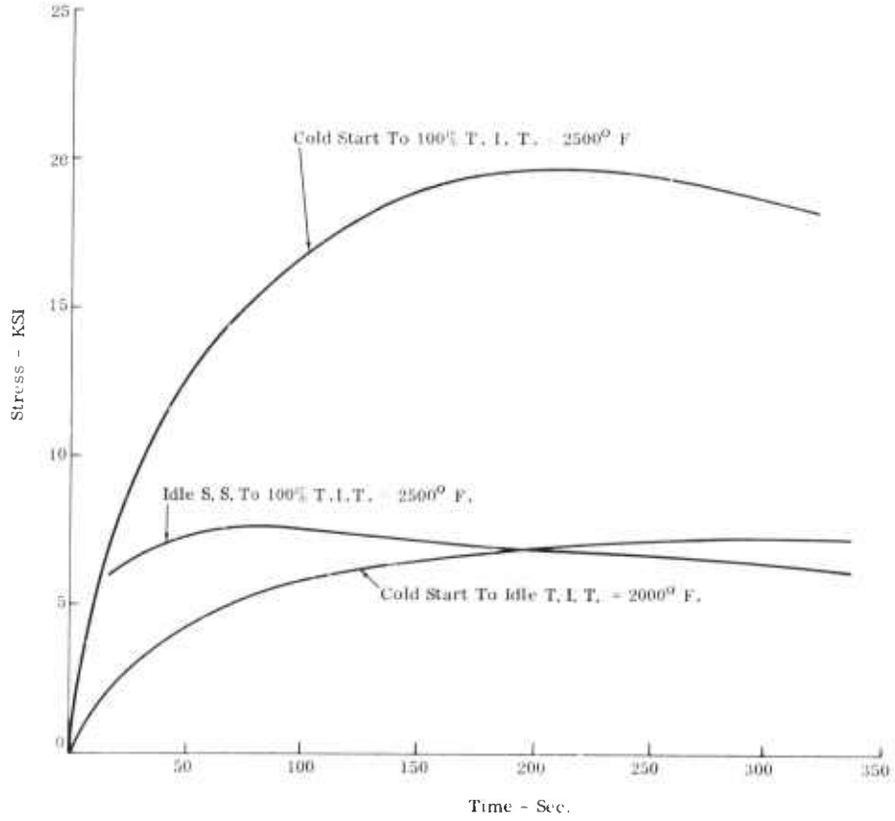

Figure 3.36 — Maximum Tensile Stress at Nose Cone Downstream Pilot Silicon Nitride

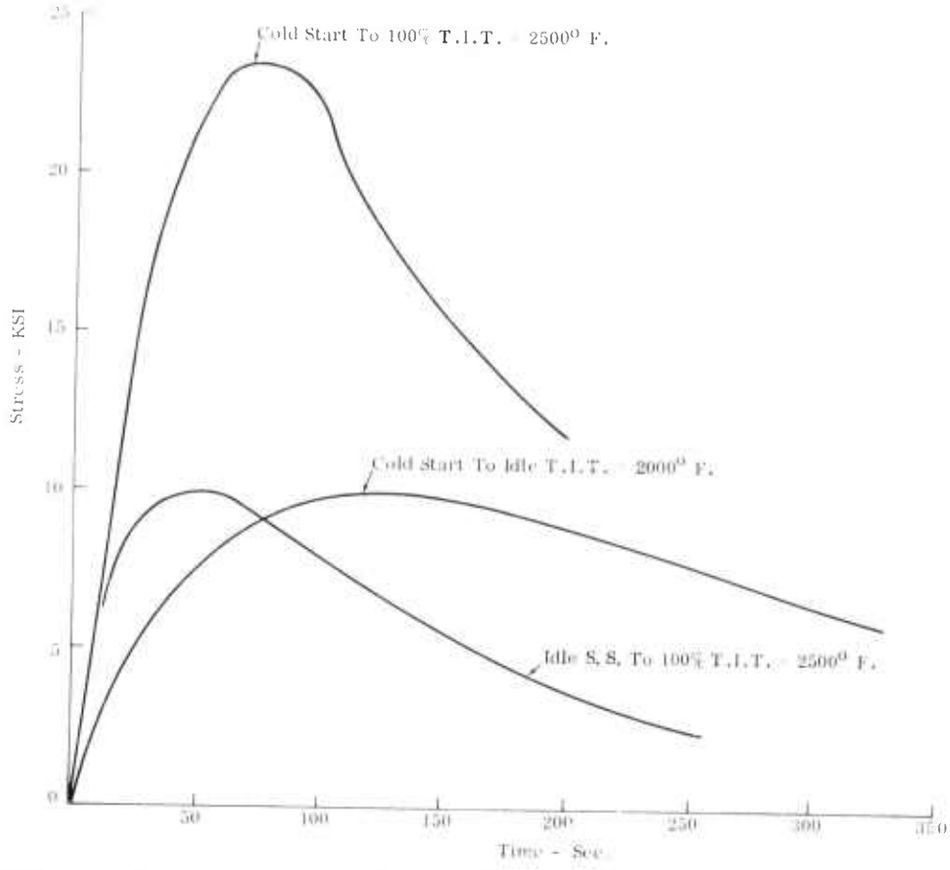

Figure 3.37 — Maximum Tensile Stress Nose Cone Cooling Air Sleeve Silicon Nitride

The critical nose cone stresses at the outermost fibers of the downstream pilot were reduced within acceptable limits by substituting a thin section with lugs for the downstream pilot. The stresses at the junction of the cooling air sleeve and conical portion of the nose cone were reduced to acceptable limits by removing the cooling air sleeve.

At this stage of the design analysis it was learned that the finite element analysis being used may not always be valid for shells subjected to bending loads. A separate analysis showed that excessive errors could be avoided in cases of moderate bending, such as in the case of nose cone, by refining the mesh. Accordingly the analytical model of the nose cone was refined in order to more accurately determine the stress at the extreme fiber by establishing a more precise stress gradient. Since bending flexibility may be very important in the thermal stress analysis of the conical shell, the representation of the wall thickness by smaller elements was evaluated. Figure 3.38 shows the model used to calculate these effects. Figure 3.39 is a plot of the stresses in the junction at 30 seconds after a cold start and Figure 3.40 shows this point and a 45 second point relative to the basic model stress variation. Other stresses using this refined model showed no significant change. Additional computer runs were used to evaluate the effects of this model on the analysis of the other design configurations, and it was concluded that the original model (Figure 3.22) and the refined model (Figure 3.38) gave comparable results in all other areas.

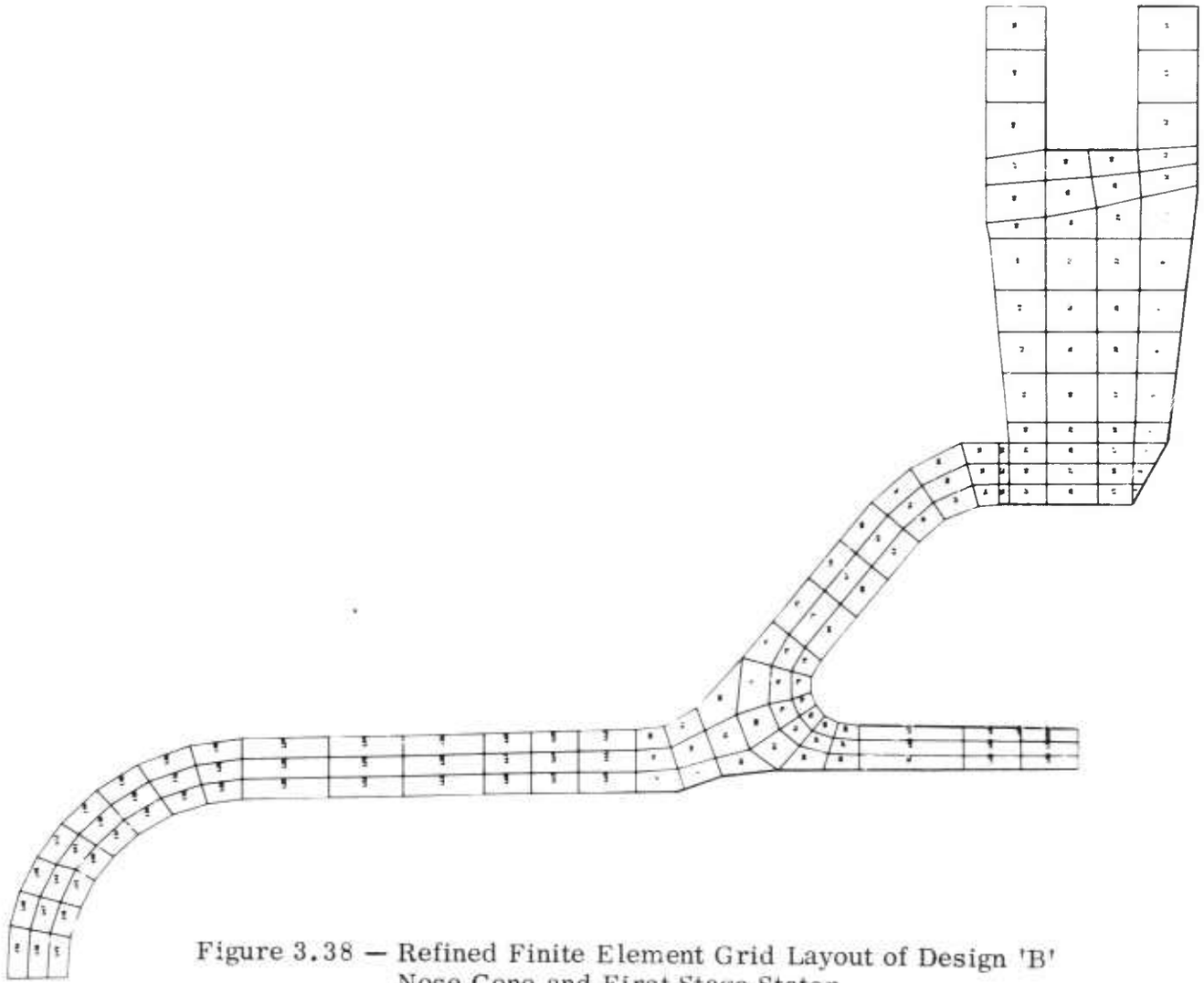

Figure 3.38 — Refined Finite Element Grid Layout of Design 'B' Nose Cone and First Stage Stator

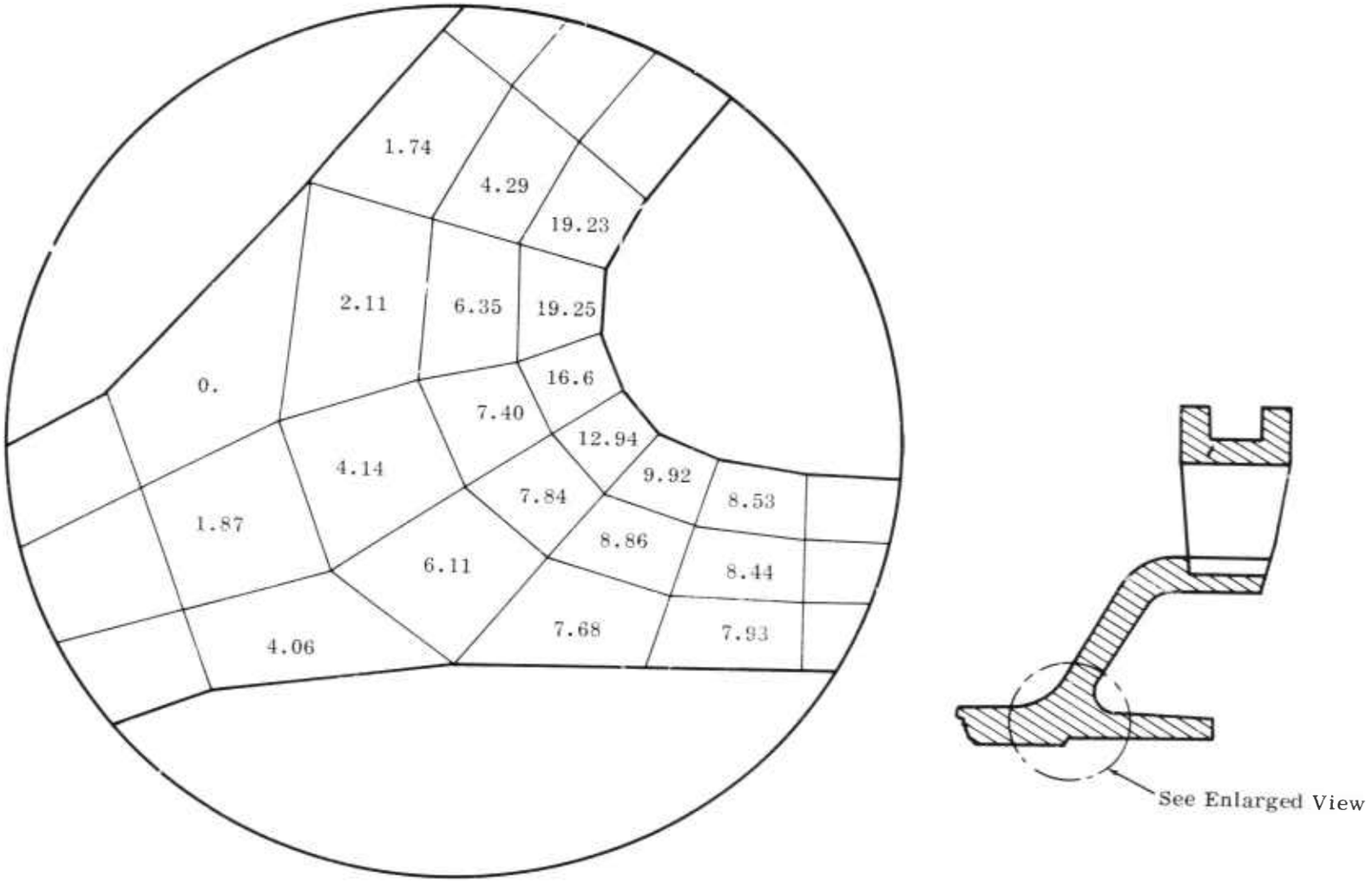

Figure 3.39 — Stresses (KSI) in Refined Model Nose Cone Silicon Carbide

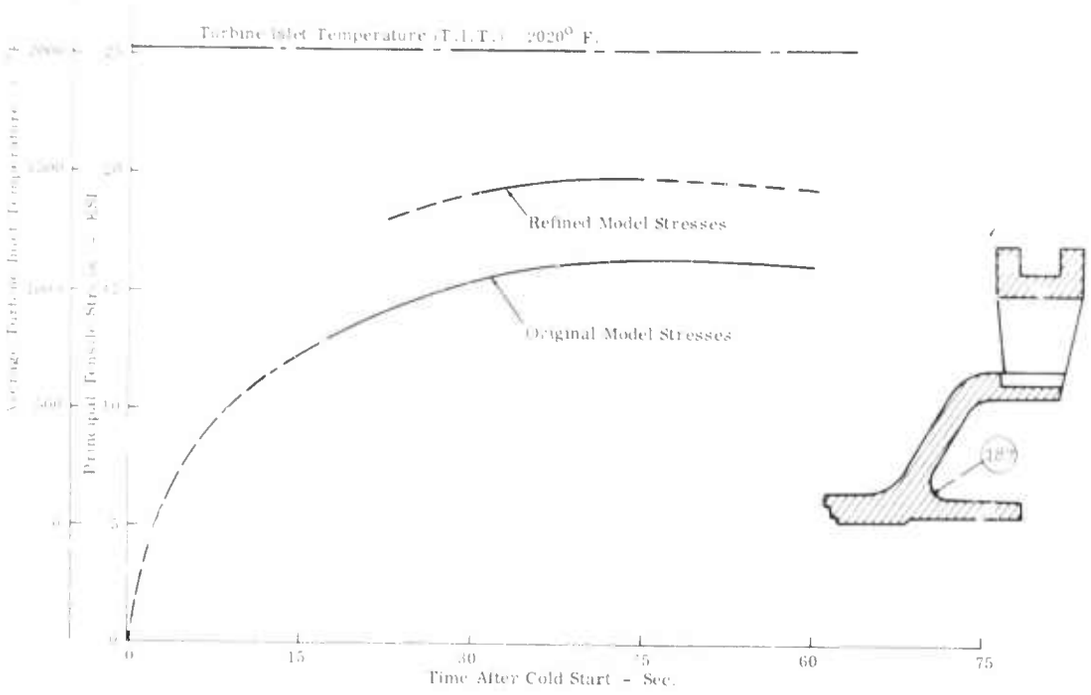

Figure 3.40 — Comparison of Stresses in Original Model and Refined Model - Nose Cone Element 187 - Silicon Carbide

In the fillet of the conical section-cooling air sleeve junction, however, the stresses exceeded the average modulus of rupture during the transient from the cold start to 100% rotor speed with T. I. T. = 2500°F, indicating a possible design problem. Removal of the sleeve virtually eliminated these higher stresses, indicating a possible solution.

The nose cone outer and inner shells in the area of the three canted struts comprise a structure which is difficult to analyze. Using the axisymmetric finite element analysis it was necessary to consider the struts as bodies of revolution in an attempt to maintain their loading and stiffening effects. With a great number of struts (or vanes) it is reasonable to assume that the inner and outer shells are in effect loaded uniformly around their circumference. This 3 strut configuration, however, has loading applied at three discrete locations on the outer and inner shells introducing circumferential bending. The bending flexibility would be added to the hoop flexibility reducing the loads due to thermal incompatibilities. However, because bending stresses may locally be higher, the significance of the reduced loading effects is not known. A three dimensional structural analysis would be necessary to realistically evaluate this area.

Turbine Rotor Shrouds

The rotor shrouds are rings with a single radial saw cut interrupting the hoop continuity. The first stage rotor shroud is cold assembled with a tight slip fit at its outer diameter. A male conical surface on the downstream side positions the second stage stator ring. To maintain critical rotor tip clearances, the shroud must pilot at its outer diameter throughout the full range of engine operating conditions. Because of thermal mismatch, excessive hoop stresses would be encountered if the rotor shroud had hoop continuity. Therefore, the ring was split with a single saw cut. When heated, the split ring is restrained from freely expanding and undergoes curvature change resulting in bending stresses. Because of the uncertainty of actual load distribution, various loading modes were assumed and for each of these the corresponding maximum bending moment stresses were evaluated for a given thermal mismatch. The lowest bending stress calculated for a comparable ring deflection resulted from a uniform internal moment which produces the best curvature match. A loading mode consisting of a laterally applied external pressure in the direction of closing the gap produces bending stresses which are approximately 50% higher. Table 3.9 shows that the stresses determined for all loading modes were less than the corresponding MOR values of silicon nitride and silicon carbide.

TABLE 3.9

ROTOR SHROUD STRESS SUMMARY

- TENSILE BENDING STRESS (PSI) -

Operating Condition	Material	First Stage Loading		Second Stage Loading		MOR
		A	B	A	B	
Cold Start to 100%N.	Si_3N_4	7000	10700	2100	3200	14000
Cold Start to 100% N	SiC	12100	21400	5300	9600	26000

Loading A = Uniform Distribution of Internal Bending Moment

Loading B = Laterally Inward Pressure Loading

Conclusions

Of the four nose cone/stator configurations studied, configuration 'D' has been selected for the Design 'E' hot flow path. Reaction sintered silicon nitride material has been selected for initial testing along with a sliding conical surface pilot mechanism. This approach was selected to facilitate a rapid transition to engine testing. Transfer molded silicon carbide is attractive as a back-up material in the event unanticipated problems arise with the silicon nitride components. The material and fabrication techniques used in the stationary hot flow section are discussed in the next chapter.

3.2.2 MATERIALS AND FABRICATION

SUMMARY

Injection-molding of silicon nitride has been developed for the fabrication of complex stationary ceramic turbine engine components. Process details and the properties of molded silicon nitride are presented. Tooling was obtained for the new Design 'B' nose cones and stators, and parts successfully fabricated.

Introduction

Ceramic materials for vehicular gas turbines have been under development at Ford for sometime prior to the beginning of this contract. (1) Over 300 compositions have been examined as potential candidates for various components. This field was narrowed by the development of design requirements and actual testing. Silicon carbide and silicon nitride were determined to possess properties suitable for use in nose cones and stators. Along with this materials evaluation, processing studies were also conducted. However, it became evident that these components would be of such complexity that a major fabrication development effort was needed.

A survey of known ceramic fabrication processes - i.e. slip casting, extrusion, cold pressing, isostatic pressing, etc. showed that such forming methods were not capable of fabricating the hot flow path components to close tolerances without resorting to expensive and time-consuming finish machining operations. It was decided that adapting the injection molding process used in the plastics industry to the forming of these ceramic components would lead to rapid and economical production of these complex shapes to close tolerances.

Injection molding of ceramics is essentially the extrusion of a heated mixture of fine-grained ceramic powders and thermoplastic organic carriers into an unheated closed metal die. The thermoplastic carriers harden quickly in the die, and the formed article may be removed and safely handled.

This injection molding technique has been applied to the fabrication of prototype turbine engine components in silicon nitride.

In this process fine-grained silicon metal is mixed with organic constituents and the components are molded on standard injection molding machines. The organics are removed by gradual heating to 600° F at the rate of 8° F per hour in an air atmosphere oven. After burnout, nitriding is carried out in a box furnace using silicon carbide heating elements. An atmosphere of flowing nitrogen is maintained, and is drawn from a tank of -80°F dew point liquid nitrogen. The normal firing cycle consists of 24 hours at 2100°F followed by 24 hours at 2660°F. Typical room temperature physical property data of the latest molded silicon nitride is shown in Table 3.10.

TABLE 3.10

PROPERTIES OF INJECTION MOLDED
REACTION SINTERED SILICON NITRIDE

Density	2.3 gm/cc
Modulus of Rupture, RT	17,000 psi
Modulus of Elasticity	20×10^6 psi
Poisson's Ratio	0.25
Coefficient of Thermal Expansion RT to 900°C	2.78×10^{-6}/°C
Thermal Conductivity RT 2000°F	65 BTU/in/Hr/ft.^{2}/°F 41
Specific Heat	0.26 BTU/lb.°F

The sintered density of 2.3 gm/cc is lower than the density of 2.6 gm/cc obtained for reaction sintered silicon nitride made by slip casting. The green density of the molded components is lower due to the volume occupied by the organic constituents. Since there are no changes in the overall dimensions of the article during the reaction sintering, the final density of the molded part is lower because there is less silicon available for reaction.

Stator Fabrication

Silicon nitride stators are fabricated by the injection molding of individual segments which are then assembled into rings. Figure 3.41 illustrates the first and second stage segments as molded in the Design 'A' configuration. The assembly into rings is accomplished by placing the individual segments into a fixture containing piloting surfaces to accurately locate the ring. While held in this fixture another injection molding operation forms a complete ring of material in the U-shaped base channel, resulting in a one-piece accurately formed stator. Figure 3.42 shows a completed ring, with the base channel partially filled with the material molded during the assembly operation.

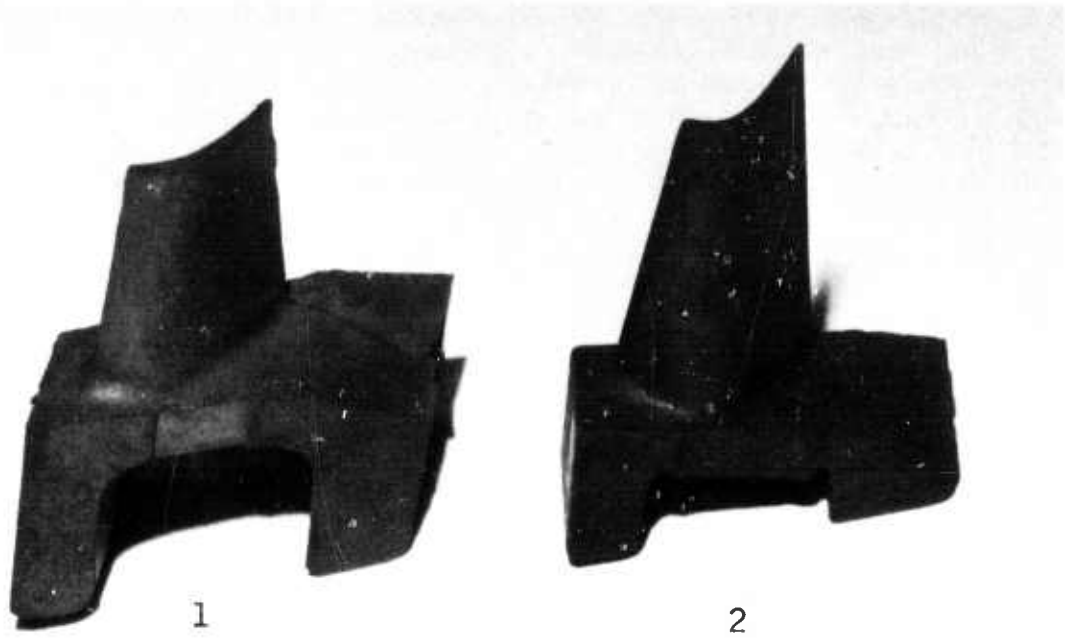

Figure 3.41 — First Stage (1) and Second Stage (2) Design 'A' Stator Segments as Molded

Figure 3.42 — Assembled First Stage Design 'A' Stator

It was determined that adequate bonding between the molded segments and the assembly ring could be obtained only if as-molded or "green" segments were used. Because of the relatively low strength of these green segments, a reduced viscosity material was needed for assembly so that the segments could physically withstand the pressures exerted during molding. The viscosity was reduced by adding additional polymeric materials to the molding batch at the expense of silicon metal, which reduced the required molding pressure from 5000 psi down to only 200 psi. While this modified material is of lower density, and hence lower strength after nitriding, the thermal expansion remains constant. The strength appears adequate for the purpose of holding the ring together, since a good chemical bond is achieved.

After completion of firing, the stator rings are diamond ground to final dimensions. All surfaces with the exception of the airfoils are final machined.

New tooling was procured for the molding of the improved Design 'B' stators. While the same concept of molding individual segments was retained, the tools were designed for semi-automated operation. The die cavity sections were pivoted and cam operated to open and close with the clamping platens of the press. The finished part is then extracted by hand. Figure 3.43 illustrates the first and second stage segments as molded in the Design 'B' configuration.

1 2

Figure 3.43 — First Stage (1) and Second Stage (2) Design 'B' Stator Segments as Molded

Assembly of the Design 'B' stators was accomplished in the same manner as previously used for Design 'A' components, except that less material was used in the base area in order to reduce mass and increase thermal response of the stator. Polymer removal and nitriding operations were the same as previously used for the Design 'A' stators.

Nose Cone Fabrication

Earlier in the Ford ceramic turbine program the injection molding process was extended to the fabrication of larger hot flow path components, such as the nose cone. Tooling procured for the fabrication of Design 'A' nose cones was modified to produce the Design 'B' version. Because of the complexity of the part, this tool contains many small inserts which must be removed by hand. While future production tools could be automated, it was advantageous to construct developmental tooling such that design changes could be accommodated by fast and relatively inexpensive modifications.

The nose cone, illustrated in Figure 3.44 in the as-molded condition, was formed on a 450 ton Reed Prentice injection molding machine of 80 oz. ceramic shot capacity. The parts are molded with extra stock in critical areas to permit finish machining, although this would be minimized or eliminated for volume production.

Figure 3.44 — Nose Cone as Molded

Another very useful facet of reaction-sintered silicon nitride is the machineability of the material in the partially nitrided state. The finish machining of the nose cone is done after nitriding for only the first portion of the schedule — 24 hours at 2100°F. Enough nitriding occurs to somewhat harden and strengthen the part so that it can be handled and mounted in machining fixtures. At this stage diamond tools are not needed — carbide cutting tools work very well. For example, the nose cone is chucked in a lathe and surface machined with the carbide tools much like any other machineable material. After machining, the part is finish nitrided at 2660°F. If any machining is needed at this point, it must be accomplished by diamond grinding.

Thus far in the contract period, a number of nose cones have been successfully fabricated in silicon nitride. The material and the nitriding operations are the same as previously described in the preceeding section on stator fabrication.

Conclusions

The injection molding process has proven to be very useful for the fabrication of prototype silicon nitride engine components, and should be capable of use with a wider range of ceramic materials. Future work is being planned to improve the silicon nitride through development of purer starting materials and the use of better furnacing equipment which will reduce the amount of available oxygen during reaction sintering. The fabrication of engine components from moldable silicon carbide materials, having better mechanical properties than silicon nitride, is also being planned.

3.2.3 TESTING

SUMMARY

The testing and development of ceramic nose cones and stators is conducted under actual engine conditions.

Throughout this test and development effort, ceramic nose cones have accumulated several hundred hours. Design 'B' silicon nitride first and second stage stators and their associated shrouds have successfully survived initial static and dynamic testing. Failures experienced with Design 'A' first stage stators have been apparently eliminated in the Design 'B' stators.

Introduction

The nose cone, stators, and their associated shrouds are the ceramic parts classified as the hot gas flow path stationary components. These components, located directly downstream from the combustor, must be developed to withstand (a) the maximum gas temperature in the engine, (b) the maximum cold start thermal gradients, and (c) severe shut down thermal gradients. Establishment of the integrity of these components is imperative prior to the incorporation of ceramic turbine rotors. Consequently, a major portion of the development effort has been expended in (a) an initial evaluation of Design 'A' components, (b) failure analysis of Design 'A' components, and (c) the initial evaluation of Design 'B' components.

Throughout this development effort, ceramic nose cones have been employed and several hundred hours have been accumulated on these components. However, it should be pointed out that these components have not been failure-free. Except for one instance, nose cone cracking has not influenced the evaluation of Design 'A' and 'B' ceramic stators and shrouds. Although nose cones may develop a hair-line crack, they do not fall apart catastrophically.

Test Rig Configurations

Ceramic components testing is conducted in an engine test rig. Since the engine design features bolt-on turbine rotors, testing is carried on with or without the rotors. Testing of these ceramic components in the engine test rig without turbine rotors is referred to as "static." Engine testing with turbine rotors is referred to as "dynamic." Pre-balancing of the high speed spool during the initial assembly allows for the addition of turbine rotors in the test cell. Thus "static" or "dynamic" tests can be conducted with minimum down time.

Test Conditions

The following is a summary of the various test conditions under which the ceramic stators were evaluated:

- Static testing - 55% engine speed with turbine inlet temperature (T_7) limited to 1800°F.
- Dynamic testing - 55% engine speed with turbine inlet temperature (T_7) limited to 2000°F.
- Cold testing (static or dynamic) - 70% engine speed with no combustion.
- Cyclic testing (static or dynamic) - a sequence of (1) light-off and acceleration to 55% speed. (2) Shut down (zero fuel) and speed reduction to light-off condition. This condition is held until the indicated temperature falls to 1200°F whereupon the sequence is repeated for the desired number of cycles. One of these cycles in termed the "one light test."

Test Results

The initial evaluation of Design 'A' hardware was done in a complete engine. Figure 3.45 shows the Design 'A' ceramic nose cone and stators. The Design 'A' stators have integral turbine rotor shrouds. Testing of these stators resulted in failures.

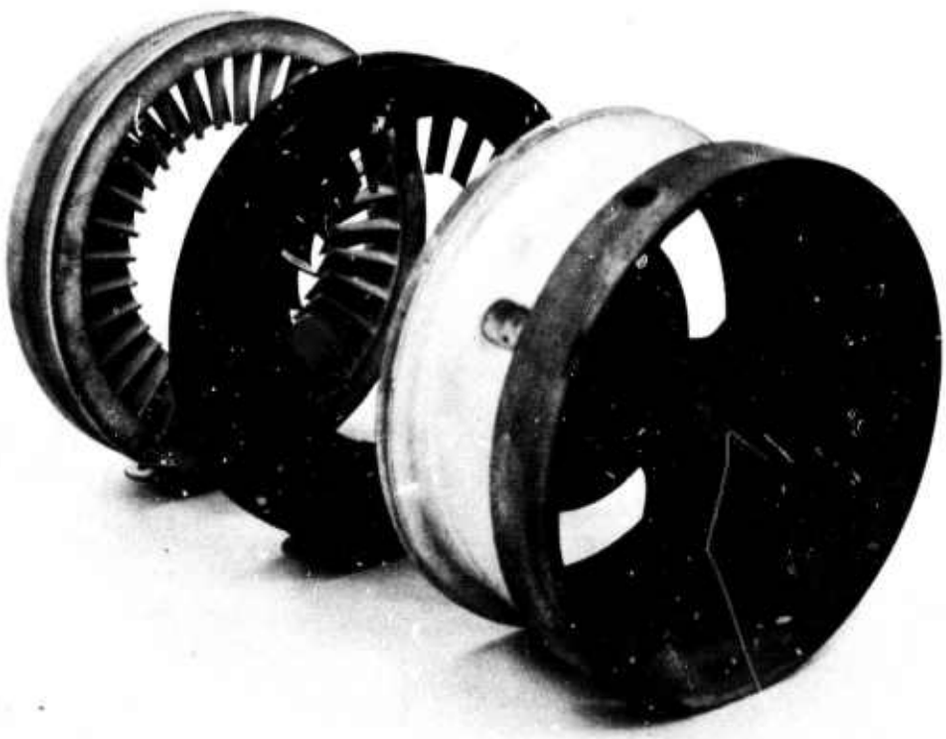

Figure 3.45 — Design 'A' Ceramic Nose Cone and Stators

A test program was outlined to analyze the ceramic stator failures. The evaluation of stators in statie testing was initiated to eliminate possible failures due to:

- Turbine rotor rub (axial or radial)
- Aerodynamic interferenee
- Partiele rebound

Additionally all design elearances were relaxed to eliminatc possible failures due to:

- Hot running interferenees
- Shut down interferenee

This then left the following as possible causes of failure to be isolated in the statie testing:

- Pressure loading
- Light-off thermal shock
- Wake exeitation (from nose eone struts)
- Partiele impingement
- Material deterioration from meehanical loading
- Material deterioration from thermal loading

Those stator assemblies whieh survived the statie testing were then subjeeted to dynamie testing. This introdueed additional possible eauses of failure to be isolated:

- Aerodynamie interferenee
- Partiele impingement and/or partiele rebound

During the ceramic stator failure mode identifieation program, three general types of failures were experienced.

- Thermal — the failure classified as thermal was the most frequent and can be identified by the relatively smooth fracture surface. At the leading and trailing edges of the vane, the fraeture is below the surface of the base while a slight upward curvature is noted at mid-ehord. Figure 3.46 shows a typical thermal failure.

- Meehanieal — the failure elassified as mechanical is charaeterized by the irregular surface of fraeture. Figure 3.46 also shows a typieal meehanieal failure.

- Impurity or defeetive material — small areas of unreacted silicon or impurities.

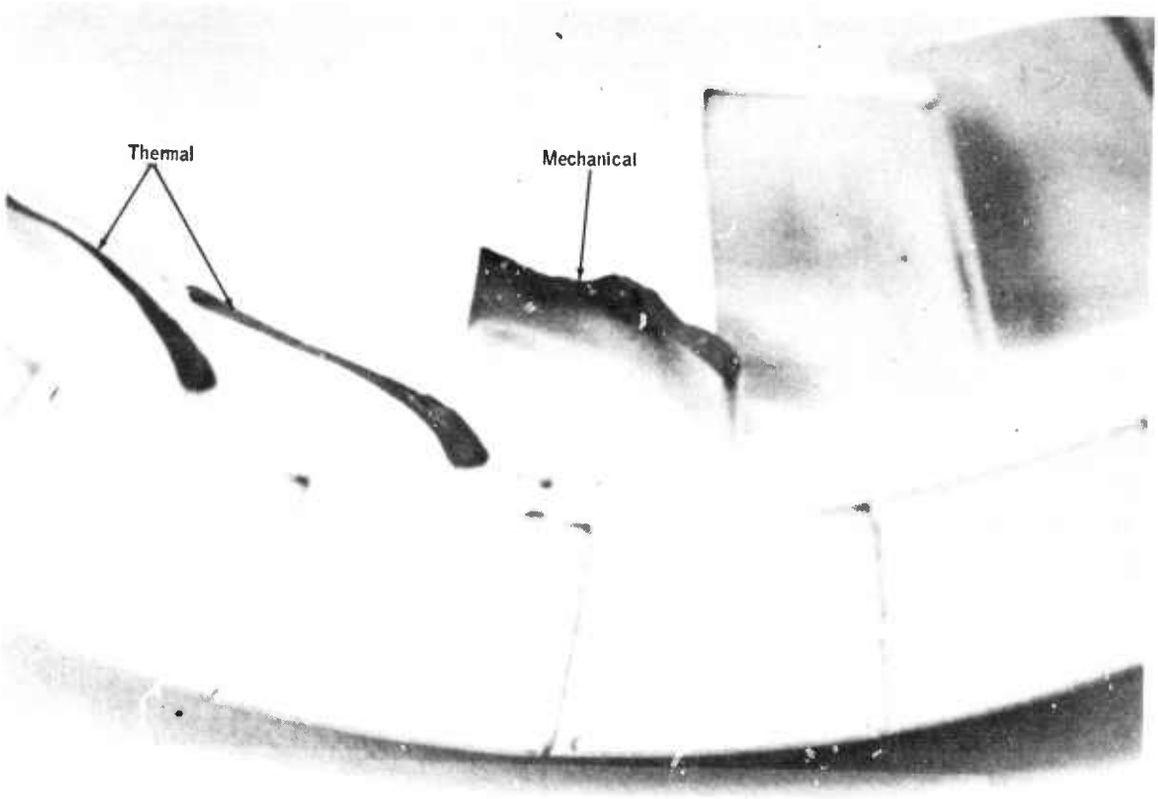

Figure 3.46 — Typieal Failures of Design 'A' Stator Blades

During the investigation very few seeond stage stator failures were experieneed. One explanation of this is that the seeond stage stator does not experienee as severe a thermal shoek as does the first stage. Thus, any advantageous design fea tures of the seeond stage stator eould be evaluated merely by reversing the seeond and first stage stators in the flow path. This was done and statie tests on seeond stage stators in the first stage stator location were eompleted without failure.

Modifieation of the first stage stator followed whieh redueed the mass of the stator by 40 pereent in the vane base area. This modifieation more elosely matehed the thermal response of the vane base to the vane. Seven of the modified stators were tested under statie test eonditions. All seven stators survived all eyelie statie tests and aeeumulated at least 25 hours enduranee eaeh with one of the stators aeeumulating 109 hours. Midway through the testing of these seven stators, a standard first stage stator was tested resulting in failure of one vane at the six o'eloek position after the one-light test. This was done to eonfirm that no changes, other than stator eonfiguration, were being evaluated.

These seven stators were then subjected to the dynamic tests. All seven stators failed. It can be theorized that the addition of turbine wheels subjected the vanes to some degree of wake rebound or similar mechanical (vibratory) loading. Further investigation of mutual aerodynamic interference may be warranted pending results of the Design 'B' stators.

Testing of Design 'B' stator hardware has commenced. Static testing of a modified Design 'B' first stage stator and Design 'A' second stage stator resulted in endurance accumulation of 74.5 hours before failure of the first stage stator. This particular silicon nitride stator was of poor quality, having been nitrided in a leaky furnace resulting in the formation of unusually large amounts of SiO_2. Static tests were conducted on a second first stage stator for 34.5 hours without failure. Design 'B' second stage hardware has since replaced Design 'A' hardware and dynamic tests have commenced. To date, 2.0 hours of dynamic tests were run without failure.

Evaluation of Results

Testing of nose cone and stators, to date, has exhibited the following:

(a) Ceramic nose cones, although not failure-free, exhibit sufficient life such that stator evaluations can be made without detrimental effects from the nose cone.

(b) Ceramic Design 'A' first stage stators exhibit repeatable failures under thermal loading.

(c) Ceramic Design 'A' modified first stage stators and Design 'A' second stage stators do not exhibit failures under thermal loading.

(d) Ceramic Design 'A' modified first stage stators exhibit immediate, repeatable failures under hot dynamic loading.

(e) Ceramic Design 'B' stators consistently survive testing under thermal loading, and initial testing under hot dynamic loading was successful.

Future Plans

Testing, development, and ultimately qualification of these ceramic components will continue. The emphasis will be on Design 'B' components.

Since static testing of Design 'B' silicon nitride components has been very encouraging and no outstanding problems have been encountered, the major area of investigation will be under hot dynamic conditions.

4. PROGRESS ON STATIONARY TURBINE PROJECT

Parametric analysis of a 60 MW gas turbine revealed that the use of uncooled stator vanes would halve the cooling air requirements at 2400°F turbine inlet temperature. If both stator vanes and rotor blades were uncooled, the cooling air requirements at this temperature would be decreased by two-thirds. In terms of specific power output, uncooled stator vanes used together with cooled rotor blades would result in a 20% greater power output. Using both uncooled vanes and blades, the increase in specific power at 2400°F would be 30% greater than is possible with cooled components.

Stress analysis and design concept together determine the strength level required of the ceramic material. On the other hand, current materials technology sets an upper limit on what can be achieved today. Thus, the vane design selected reflects our ability to calculate the stresses in each discrete volume element of the vane and our ability to fabricate a ceramic that can survive the operating stresses.

4.1 STATOR VANES

SUMMARY

Transient thermal stresses of 47,000 and 44,000 psi were calculated for full size SiC and Si_3N_4 stator vanes, under emergency shut down conditions from 2500°F. These stresses are reduced to 28,000 and 31,000 psi, respectively, when vane chord is reduced by 50%. Gas bending stresses increase to 3300 psi for the 1/2 chord solid vane. These combined thermal and mechanical stresses appear well below the strength of the candidate materials.

Introduction

Because the largest single reward can be achieved using uncooled stator vanes and because of the low mechanical stresses involved, an engine testing program is being undertaken to demonstrate the feasibility of using ceramic stator vanes at a 2500°F turbine inlet temperature in a 30 MW test turbine. The test turbine and flow path are shown schematically in Figure 4.1.

The working fluid subjects the vane to steady mechanical loads and, during start-up and shutdown, the vane is subjected to thermal stresses caused by unequal internal thermal expansion. Solid cross section and smaller or larger vane size can often improve the stress distribution.

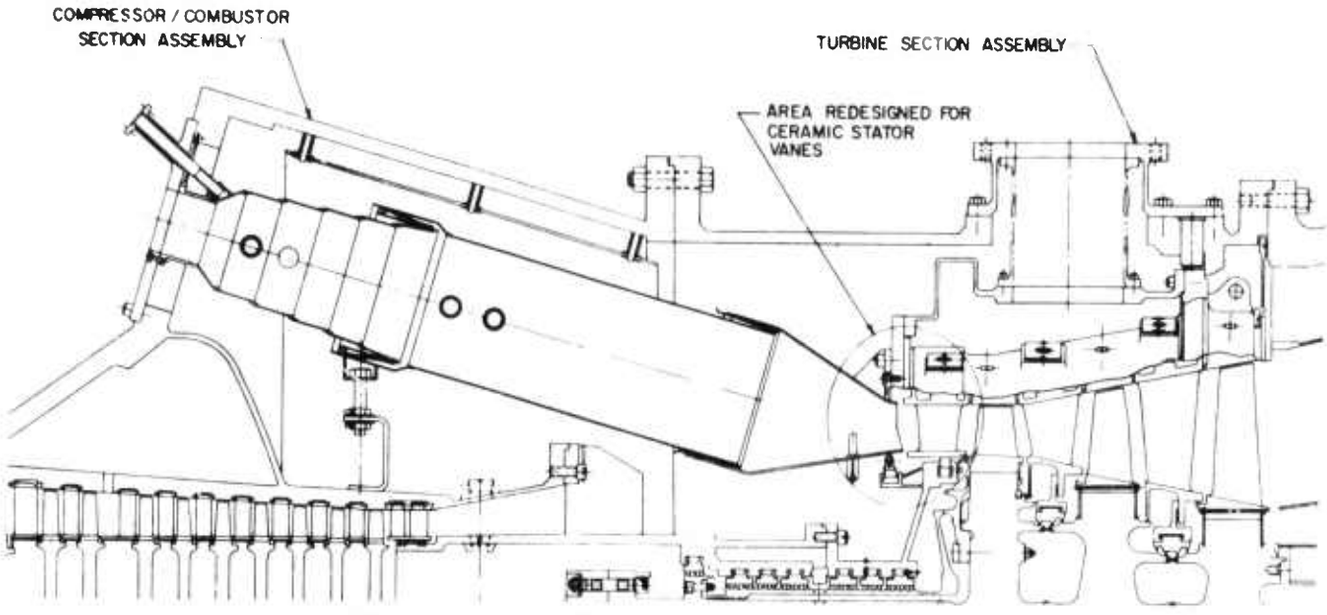

Figure 4.1 — 30Mw Test Turbine Flow Path

THERMAL STRESSES

The transient thermally induced stresses were computed in both the cross-sectional plane and the out-of-plane directions. Since ceramics are weakest in tension, only tensile stresses were considered. Silicon carbide in both hollow and solid cross-sections and silicon nitride in solid cross section were analyzed. Hollow Si_3N_4 vanes were not analyzed because fabrication technology for such shapes has not been demonstrated. The thermal boundary conditions were known from earlier design programs. Figure 4.2 gives typical values of the heat transfer coefficient (h) as a function of time during emergency shutdown while Figure 4.3 gives the distribution of (h) on the surface of a standard 1st stage stator vane.

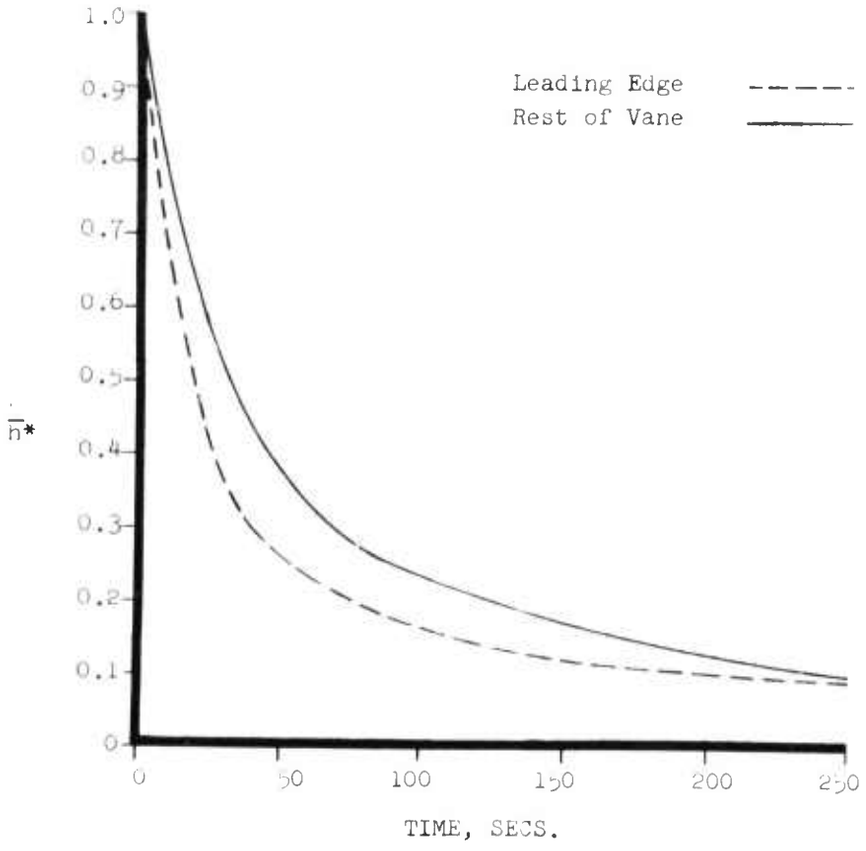

Figure 4.2 — Heat Transfer Coefficient Ratios - vs - Time for a Row 1 Vane Emergency Shutdown Condition

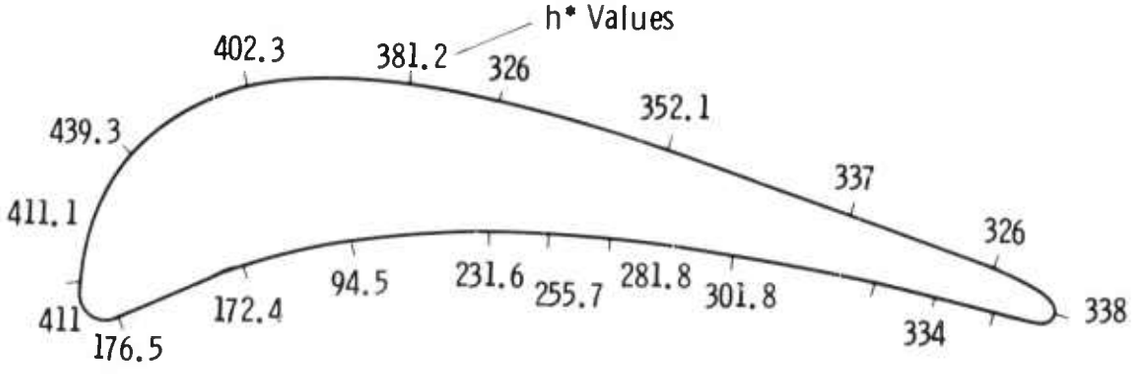

Figure 4.3 — Distribution of Maximum Heat Transfer Coefficients for a Stator Vane Cross Section Under Emergency Start Up and Shut Down Conditions

The computational method simulating cooling consists of the following: (1) the temperature distributions in the cross-sectional plane are determined by a two-dimensional finite difference program using the previous temperature solution for each time frame; (2) out-of-plane tensile stresses are computed by numerical integration from the temperature distribution (see Figure 4.4); (3) a two dimensional finite element plane strain program calculates the stresses in the cross sectional plane (see Figure 4.5.) The analytical model treats the airfoil as infinite length and does not consider the end conditions.

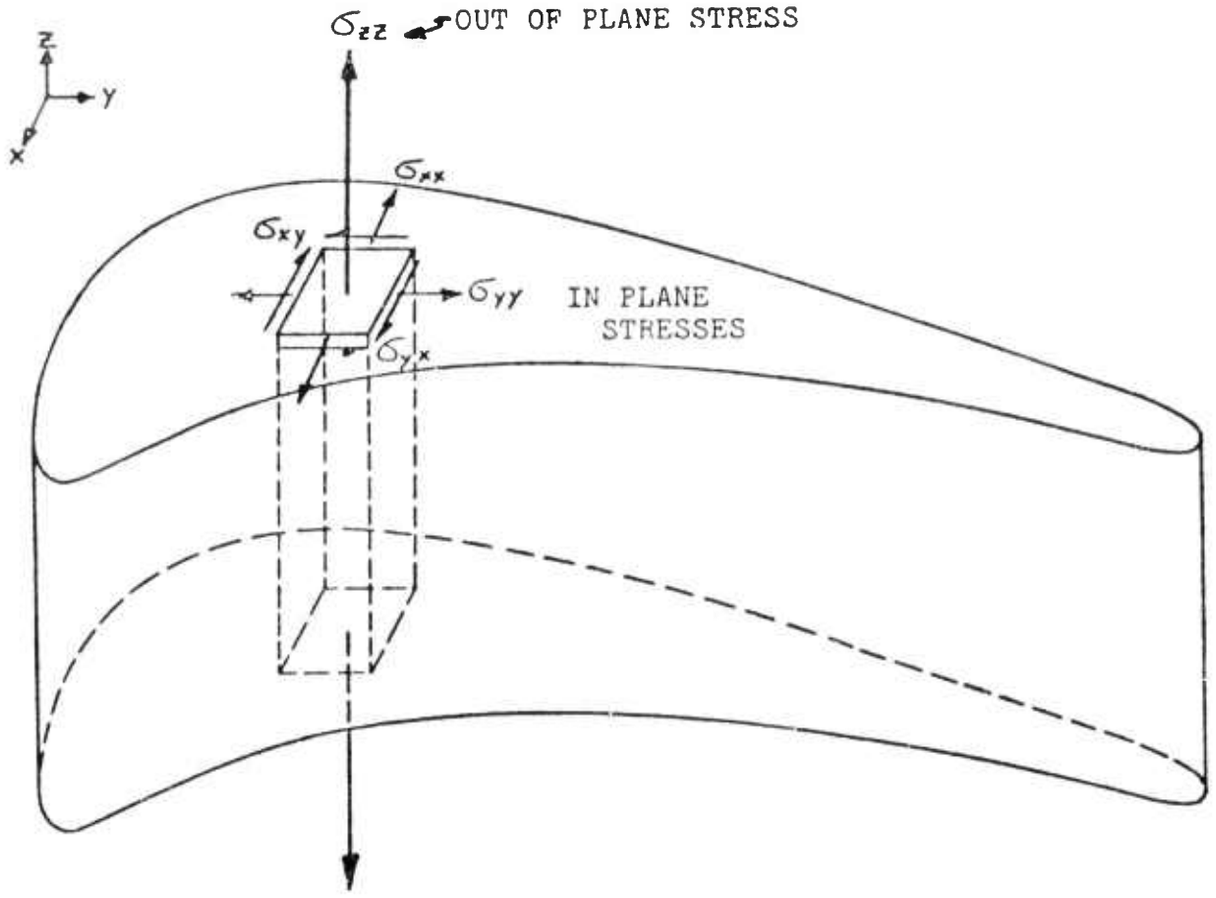

Figure 4.4 — Thermal Stresses in a Vane

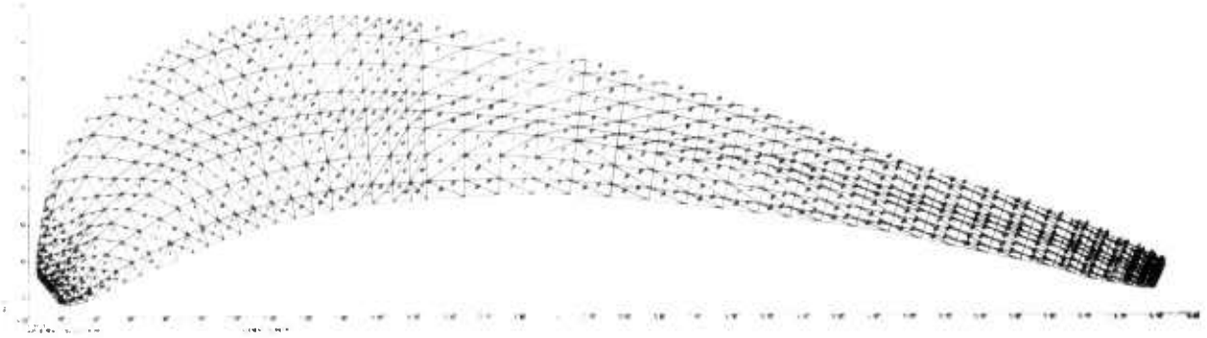

Figure 4.5 — Two-Dimensional Finite Element Mesh for Solid Vane

TABLE 4.1

MAXIMUM TENSILE STRESSES FOR
FULL AND HALF SIZE SiC AND Si_3N_4 VANES

Case	Vane Parameter	Material	Size	Cross Sectional Geometry	Shutdown Temp. °F	Maximum Tensile Stress Psi	Percent Difference In Stress
1	Material	Si_3N_4	Full	Solid	1955	27,000	10
		SiC	Full	Solid	1955	24,000	
2	Material	Si_3N_4	Half	Solid	1955	15,000	0
		SiC	Half	Solid	1955	15,000	
3	Size	Si_3N_4	Full	Solid	1955	27,000	20
		Si_3N_4	Three Qtrs.	Solid	1955	21,500	
4	Size	Si_3N_4	Full	Solid	1955	27,000	45
		Si_3N_4	Half	Solid	1955	15,000	
5	Size	SiC	Full	Solid	1955	24,000	38
		SiC	Half	Solid	1955	15,000	
6	Size	SiC	Full	Hollow	1955	35,000	37
		SiC	Half	Hollow	1955	22,000	
7	Cross Sectional Geometry	SiC	Full	Hollow	1955	35,000	31
		SiC	Full	Solid	1955	24,000	
8	Cross Sectional Geometry	SiC	Half	Hollow	1955	22,000	32
		SiC	Half	Solid	1955	15,000	
9	Shutdown Temp.	Si_3N_4	Full	Solid	2500	44,000	39
		Si_3N_4	Full	Solid	1955	27,000	
10	Shutdown Temp.	Si_3N_4	Half	Solid	2500	31,000	52
		Si_3N_4	Half	Solid	1955	15,000	
11	Shutdown Temp.	SiC	Full	Solid	2500	47,000	49
		SiC	Full	Solid	1955	24,000	
12	Shutdown Temp.	SiC	Half	Solid	2500	28,000	47
		SiC	Half	Solid	1955	15,000	
13	Shutdown Temp.	SiC	Full	Hollow	2500	51,000	31
		SiC	Full	Hollow	1955	35,000	
14	Shutdown Temp.	SiC	Half	Hollow	2500	39,000	44
		SiC	Half	Hollow	1955	22,000	

For both materials, the maximum out-of-plane tensile stress is approximately twice the value of the maximum in-plane stress. In subsequent calculations for various size vanes, only the out-of-plane stresses were computed. For the full size solid vane under shutdown conditions from 2500°F the maximum tensile stress is 47,000 psi for silicon carbide and 44,000 psi for silicon nitride. The full size hollow silicon carbide vane calculations give tensile stresses as high as 51,000 psi. This is due to shape factors which contribute to a stress concentration at the inside trailing edge radius even though local thermal gradients are reduced.

By performing the same calculations for one-half size vanes, the stress levels are generally reduced by 37 to 45% depending upon the material used. (See Table 4.1).

MECHANICAL STRESSES

Gas pressure causes steady bending stresses of the order of 1000 psi for simply supported vanes or 3000 psi for cantilevered full size vanes. Reducing the size of the components generally results in higher bending stresses so that a compromise between thermal and gas stresses was needed. Decreasing the vane size requires more vanes to complete the stator row. Consequently, forty full size vanes become eighty half size vanes. The only requirement is that the pitch to chord ratio remains constant. A comparison of stresses for various size vanes is given in Figure 4.6. Half size vanes seem to offer the best compromise in stress reduction without adding too many parts to the machine. Another factor was the present unavailability of blank material billets large enough to yield full sized components. Larger billets may be available in the future according to Norton Co.

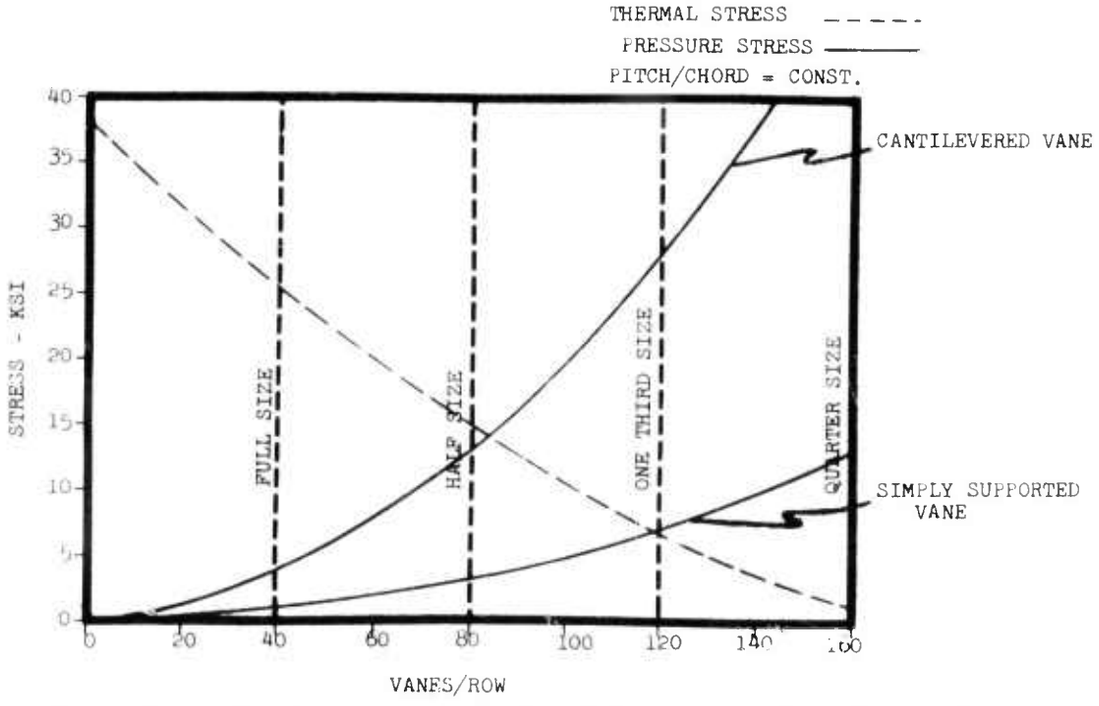

Figure 4.6 — Maximum Stresses in Solid Vane as a Function of Size

Conclusions

Parametric analyses revealed that the transient thermal stresses, during start up and emergency shut down conditions, are most critical to ceramic stator vane performance. For half size solid vanes under shutdown conditions from 2500°F, the maximum tensile stresses are 31,000 and 28,000 psi for silicon nitride and silicon carbide, respectively. These values represent reductions in stress levels by 52 and 47% for the corresponding full size solid vanes.

4.2 ROTOR BLADES

A design and computer evaluation only will be carried out on the turbine rotor blades. Rotor blade design requires three-dimensional elastic stress analysis capabilities. If high temperature test results show the presence of a plastic-creep phenomena, at stress levels anticipated a three-dimensional elastic-plastic-creep analysis will be required. Furthermore, this capability is needed to optimize the three-piece, first-row, stator vane design as well. The required analysis can be made using a digital computer and a finite element technique. However, the three-dimensional programs currently available are based on a flat-sided, constant-strain tetrahedral element, and they lack the capability for analyzing the contact between two adjacent components.

While it is possible to incorporate an appropriate three dimensional element and to analyze the contact between adjacent components into an existing program like NASTRAN, considerable time would be required and the results would be very cumbersome to handle. Westinghouse, alternately, chose to develop its own three-dimensional finite element program that is based on a higher order iso-parametric element, which can have curved sides and variable strains. The program will have a capability for analyzing three-dimensional, elastic-plastic-creep problems having contact faces between several parts.

Three-Dimensional Finite Stress Analysis

A three-dimensional iso-parametric element was selected that allows the user to vary the number of nodes on the sides of the element. This capability facilitates the generation of graduated element networks.

The derivation of the stiffness matrix and load vectors for this element was completed and programming of the corresponding subroutines has begun. Work is progressing on the computer programming of an equation solver. The program is based on the Gaussian elimination method and uses a technique known as the wave-front technique. With this technique, the formation and solution of the finite element equations are intimately connected. Using this program, we should be able to solve systems of linear equations having several thousand unknowns.

5. MATERIALS TECHNOLOGY - VEHICULAR AND STATIONARY TURBINE PROJECTS

5.1 MATERIALS ENGINEERING DATA

SUMMARY

The room temperature strength of Norton hot pressed silicon nitride is 56,900 and 98,600 psi as measured in tension and flexure, respectively. The flexural strength decreases with temperature to 16,700 psi at 2550°F. High cycle flexural fatigue tests indicate endurance limits of 30,000 psi at 1800°F and 20,000 psi at 2200°F. The static and dynamic coefficients of friction for Si_3N_4 against itself vary from 0.2 to 1.6 from RT to 1900°F. Both Si_3N_4 and SiC display outstanding corrosion-erosion resistance in long term tests in a turbine environment at 2000°F.

Introduction

The use of brittle materials in turbo-machinery is such a departure in materials application and design philosophy from metals that a system is being devised for relating specific material properties with loading conditions existing in a gas turbine. This system consists of identifying all possible turbine operating conditions such as stresses, temperatures, heat fluxes, etc., and all material constants such as fracture strength, thermal conductivity, fatigue endurance limit, etc. By evaluating all of the material properties against each turbine operating condition, previously undetected areas may be identified that will prove to be critical to the effective utilization of brittle materials in gas turbines.

One method for doing this is to include all possible turbine operating conditions on one axis and all possible material properties on a second axis. Combinations of properties are then produced in a systematic fashion by the intersection of the lines joining the two axes. Of course, many of these combinations are trivial but others should prove to be significant. Table 5.1 lists the various turbine operating conditions under input coding and the material physical properties under material coding. Figure 5.1 shows a typical output card. The physical and engineering data that may be needed in the design of turbine components are listed on the right side. In the example shown, a load-temperature combination might cause the material to change phase, which could cause other property changes. For example, a decrease in the corrosion resistance may result.

TABLE 5.1

TURBINE CONDITIONS VS PHYSICAL PROPERTY
INPUT CODING CORRELATIONS

			Code
I.	Loading	tension	1
		compression	2
		shear	3
		bending	4
II.	Ballistic Impact	modulus of elasticity of impactor	5
		change of momentum	6
III.	Chemical Environment		7
IV.	Temperature		8
V.	Time	period of cycle	9
		number of cycles	10
VI.	Geometry	gross size	11
		notch radii	12
		orientation (to loads)	13
		crack size, orientation	14
		surface finish	15

MATERIAL CODING
(Experimental Observations)

I.	Strains	elastic tension	a
		elastic compression	b
		elastic shear	c
		viscous tension	d
		viscous compression	e
		viscous shear	f
II.	Cracks	crack energy	g
		crack length	h
		crack geometry	i
		crack orientation	j
		crack nucleation	k
III.	Basic Material Properties (thermodynamics; phase, grain size damage; thermal expansion etc.)		l
IV.	Corrosion		m
V.	Erosion		n
VI.	Solubility (or binary reactions)		o

CODE 1 1

Input Variables		Material Measurements	Physical & Engineering Data		
Type	Range	(Experimental observations)	Thermal Cond.	K	
Tension Stress	Up to 100,000 psi	Material Properties	Coef. of thermal expansion	α	
Important values of other variables		Example-phase Change	Specific heat	c	All may change ↓
			Surface tension	Γ	
Temperature			Surface hardness	M_S	
Time			Damping coef.	ζ	
Environment?			Young's modulus	E	
			Poisson's ratio	ν	
			Yield or fracture stress	ρ	
			Maxwell creep constant	μ	
			Fatigue stress	σ_f	
			Friction coef.	μ	
			Phase change	may cause corrosion	

Figure 5.1 Typical Engineering Data Output Card

5.1.1 PHYSICAL PROPERTIES

Testing configurations and specimen geometries are being modeled to reflect, as closely as possible, actual turbine conditions in order that the test data will be significant. For example, temperature gradients induce thermal stresses that can cause tensile stresses in certain regions of the vane and compressive stresses in others. Since stress cycling results from thermal cycling, fatigue failure may occur. This stress pattern of tension-to-compression can be closely approximated by a bending beam mechanical fatigue test as illustrated in Figure 5.2. The bending beam fatigue test also has a shear stress imposed by the external driving force P. However, the shear stress is generally 1% or less of the bending stress.

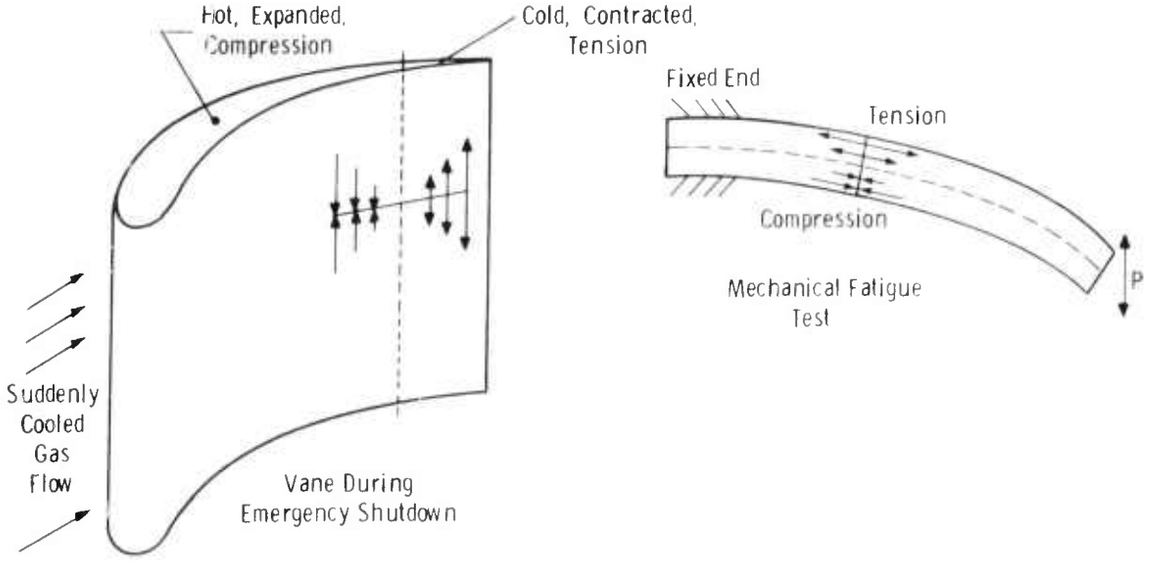

Figure 5.2 — Modeling Tests After Actual Machine Conditions

Statistically significant physical property data will be established eventually for both the silicon nitride and silicon carbide that are being considered for turbine stator vanes. The data presented in this report represents the first lot of 6" x 6" x 1" billets of hot pressed silicon nitride supplied by Norton Company. Preliminary data on the latest lot indicate substantial improvements.

Tensile Strength

Tension tests of silicon nitride were performed at room temperature using the specimen and fixture shown in Figure 5.3. The "Fiberfrax" washer helps to distribute the stresses under the specimen's end cap. To insure proper alignment and reduce bending, three strain gauges were bonded to the specimens 120^{o} apart and parallel to the long axis. All three gauge readings were made to agree to within about 3% (max. 7%) by mechanically adjusting the fixture while under a small (50 pound) load. Two more strain gauges wrapped circumferentially about the specimen were used in conjunction with the axial gauges to measure Poisson's Ratio (ν). The gauge readings, with a sensitivity of 2×10^{-6} were plotted as functions of load on X-Y recorders.

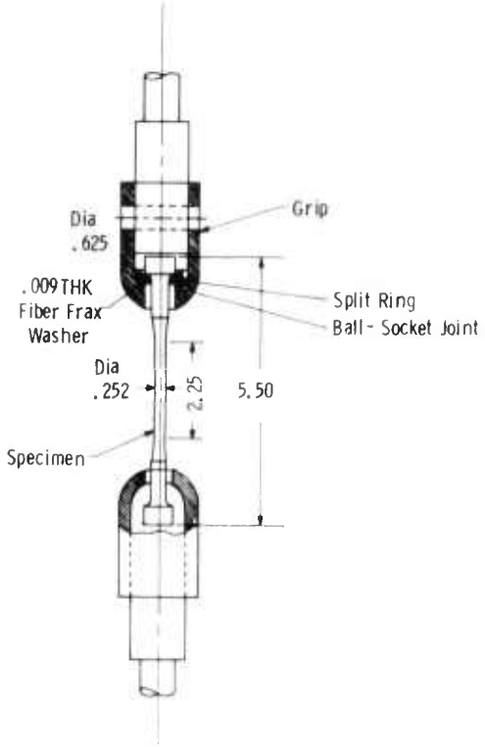

Figure 5.3 — Tensile and Creep Specimens and Gripping Arrangement

The specimens were loaded in 10,000 or 20,000 psi increments with unloads to 1000 psi until failure occurred. The average fracture strength, 56,900 psi (see Table 5.2), is approximately 60% of the fracture strength in a four-point bend test. This may illustrate the importance of "volume effect." The error introduced by specimen misalignment varies from 1700 to 3980 psi at 3% to 7% of the maximum strain, respectively. Therefore, the reported tensile results are conservative. Since the error approximates the standard deviation it is not considered too serious.

TABLE 5.2

SUMMARY OF TENSILE TESTS, R.T.
(Specimens machined from Norton material, received July 1971)

Specimen #	Density g/cc	Strain Rate 10^{-4}/ min.	Elastic Modulus E, 10^6 psi	Shear Modulus G, 10^6 psi	Poisson's Ratio ν	Fracture Stress ^{O}F, psi
S_3N_4-TS-01	3.33	6.6	44.2	17.4	0.27	59,650
S_3N_4-TS-02	3.20	6.6	43.9	17.4	0.26	54,650

The stress-strain curve is shown in Figures 5.4 through 5.7. Within a strain resolution of 5×10^{-6}, a linear retrace was obtained for the loading and unloading cycles. Specimen #1 fractured on the sixth run at 59,650 psi after having sustained a stress of 62,000 psi on the fifth run (see Figure 5.4). Specimen #2 fractured about 2 seconds after reaching a maximum stress on the fifth run.

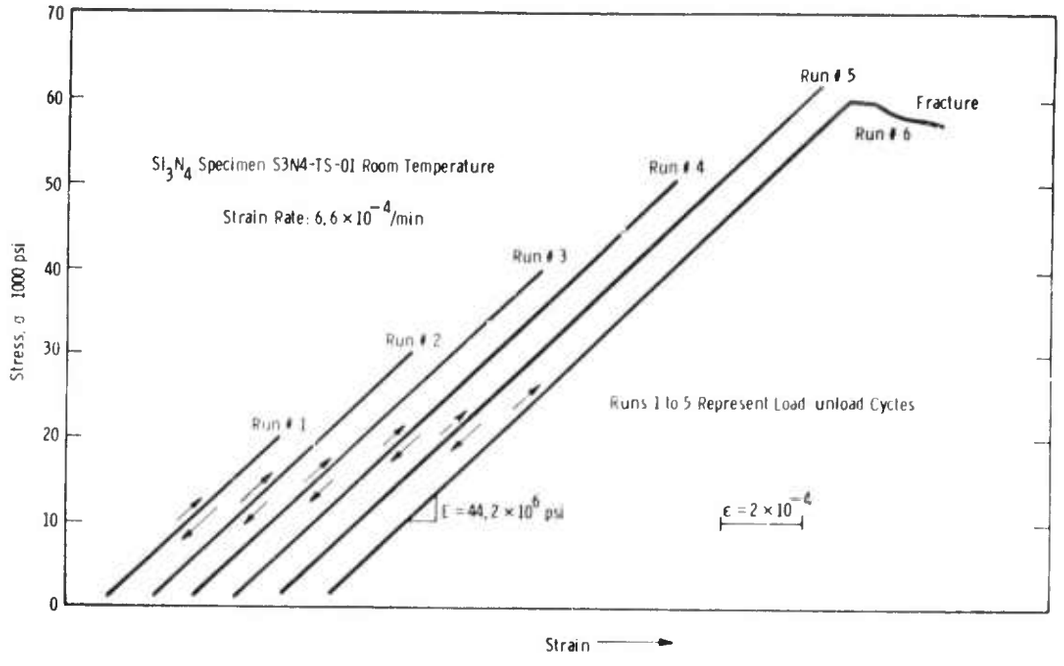

Figure 5.4 — Stress-Tensile Strain Curves for Specimen #1

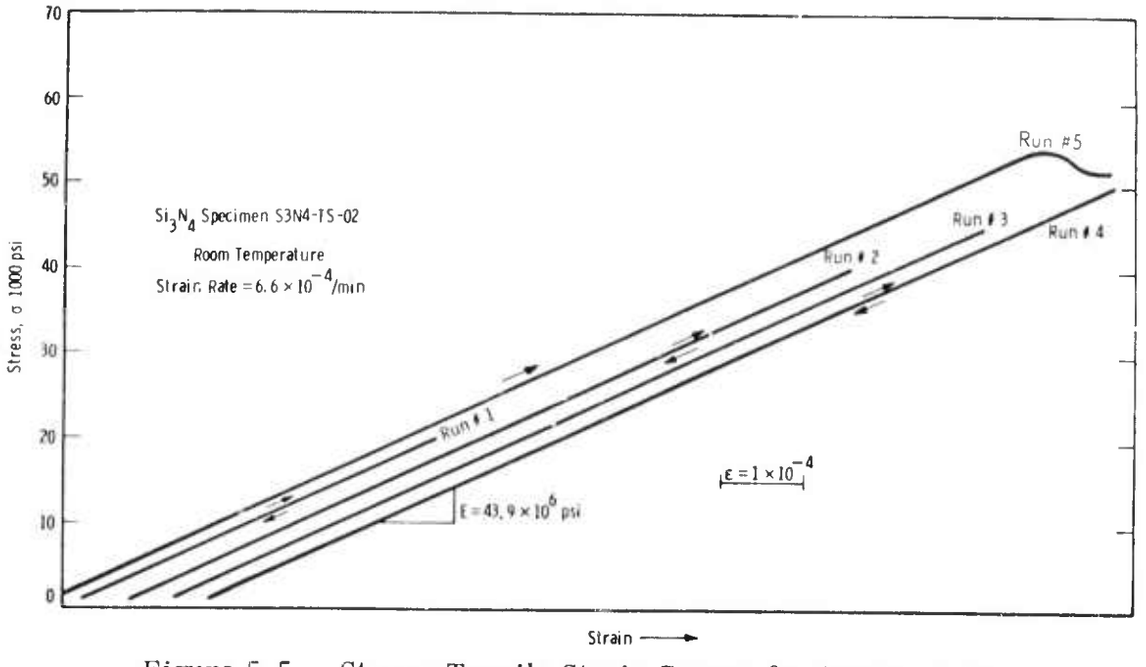

Figure 5.5 -- Stress-Tensile Strain Curves for Specimen #2

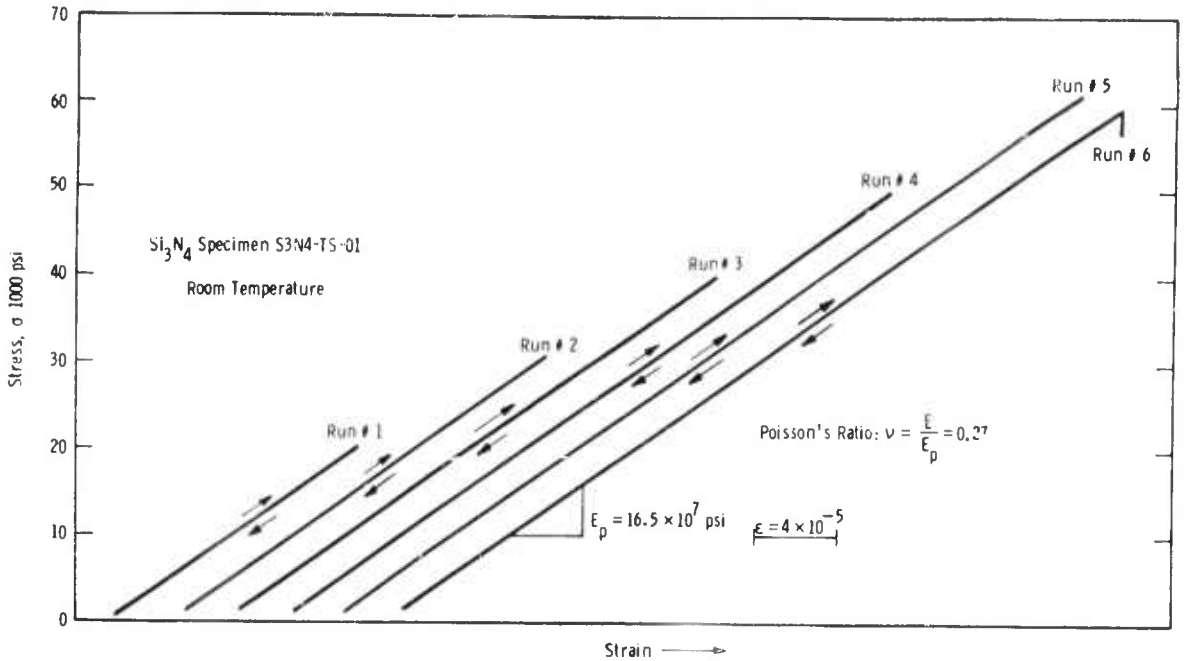

Figure 5.6 -- Stress-Radial Strain Curves for Specimen #1

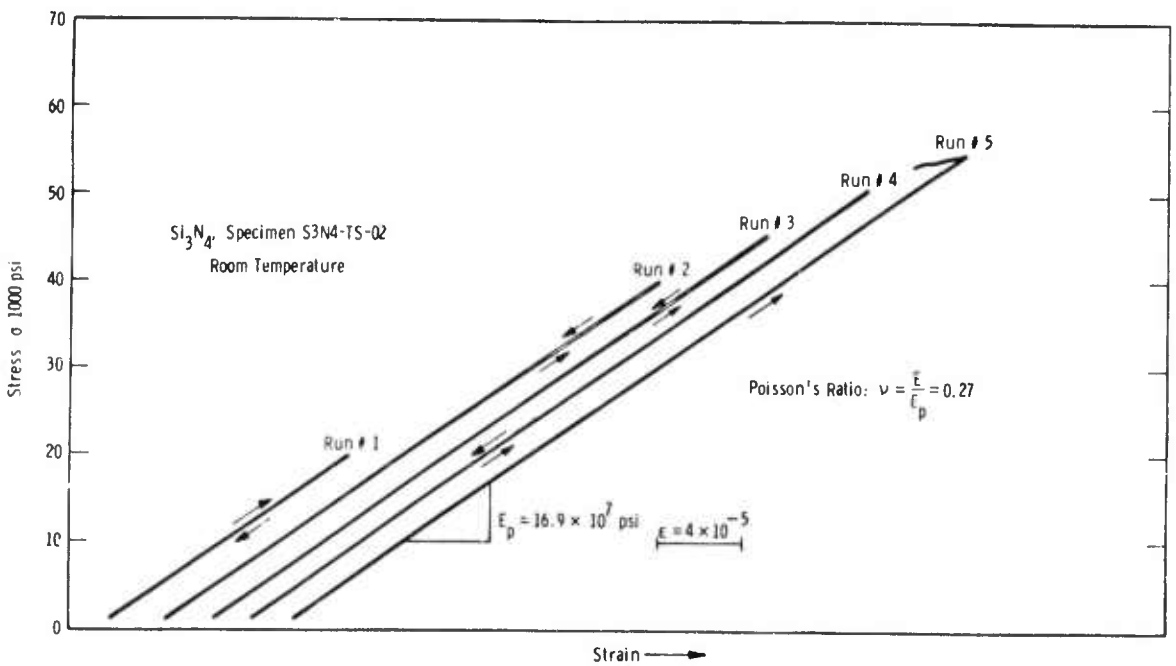

Figure 5.7 -- Stress-Radial Strain Curves for Specimen #2

Flexural Strength

The flexural strength of Norton hot-pressed silicon nitride from the first lot was measured by 4-point loading using an Instron tester at a strain rate of 0.02 inch/min. In one set of tests, the specimen dimensions were 0.25" x 0.25" x 2.00" with maximum and minimum span distances of 1.5" and 0.5", respectively. In the other set, the specimen dimensions were 0.25" x 0.125" x 1.375" with maximum and minimum span distances of 1.0" and 0.5", respectively. The critical tensile sides of all specimens were diamond ground with a 200 grit wheel to insure surface uniformity. Specimens used in elevated temperature tests were brought to temperature and held 15 minutes before testing.

The average room temperature flexural strength of the first lot of Norton supplied silicon nitride, when measured normal to the hot-pressing direction, was 98,800 psi $\pm$ 6%, which compared to a mean value of 109,570 psi $\pm$ 8%, reported by Norton using 3-point loading (see Table 5.3).

TABLE 5.3

ROOM TEMPERATURE FLEXURAL STRENGTH

NORTON SILICON NITRIDE LOT #1

Specimen	Flexural Strength* psi 4 pt loading	Norton Data psi 3 pt loading
1	105,700	95,970 min.
2	97,700	123,727 max.
3	98,100	109,570 mean
4	91,600	

*Direction - normal to hot pressing axis

The average flexural strength measured parallel to the pressing direction decreased from 74,900 psi $\pm$ 4% at room temperature to 54,000 psi $\pm$ 7% at 1800°F to 16,700 psi $\pm$ 11% at 2550°F (see Table 5.4). Anisotropy exists in all of the lots of hot-pressed silicon nitride made by Norton.

The strength of the Norton material has improved significantly from the first lot. Using 3-point bend tests, Norton reported flexural strengths of 125,000 $\pm$ 15,000 psi, 126,000 $\pm$ 8800 psi and 131,400 $\pm$ 7100 psi on the last three billets of silicon nitride that were shipped to us. They also reported a strength of 45,000 psi normal to the pressing direction and 40,000 psi parallel to the pressing direction at 2500°F.

TABLE 5.4

THE EFFECT OF TEMPERATURE ON FLEXURAL STRENGTH OF NORTON SILICON NITRIDE LOT #1

Temperature °F	Average Flexural Strength* psi	Deviation %
R.T.	74,800	4
1000	51,800	12
1450	66,800	6
1800	54,000	7
2000	50,300	6
2150	43,700	9
2350	27,200	11
2550	16,700	11

*Direction parallel to hot pressing direction

Fatigue Strength

Westinghouse designed a cantilever type flat specimen with a reduced gauge section for the cyclic flexural fatigue testing of hot pressed silicon nitride (Figure 5.8). The specimen is clamped at one end (Figure 5.9) while load is applied at the other end in a Balwin (BLH) model SF 2 universal fatigue machine. The load is provided by an eccentric weight rotating at 1800 rpm. A small furnace, which permits testing up to 1300°C (2370°F) in air, is fitted over the gauge section. The stress at the fracture point is calculated from the classical beam equation:

$$\sigma = \frac{6Pl}{bh^2}$$

where P is the applied load, l is the distance from the end of the specimen (at the point of applied load) to the fracture point, b is the specimen width at the fracture point and h is the specimen thickness.

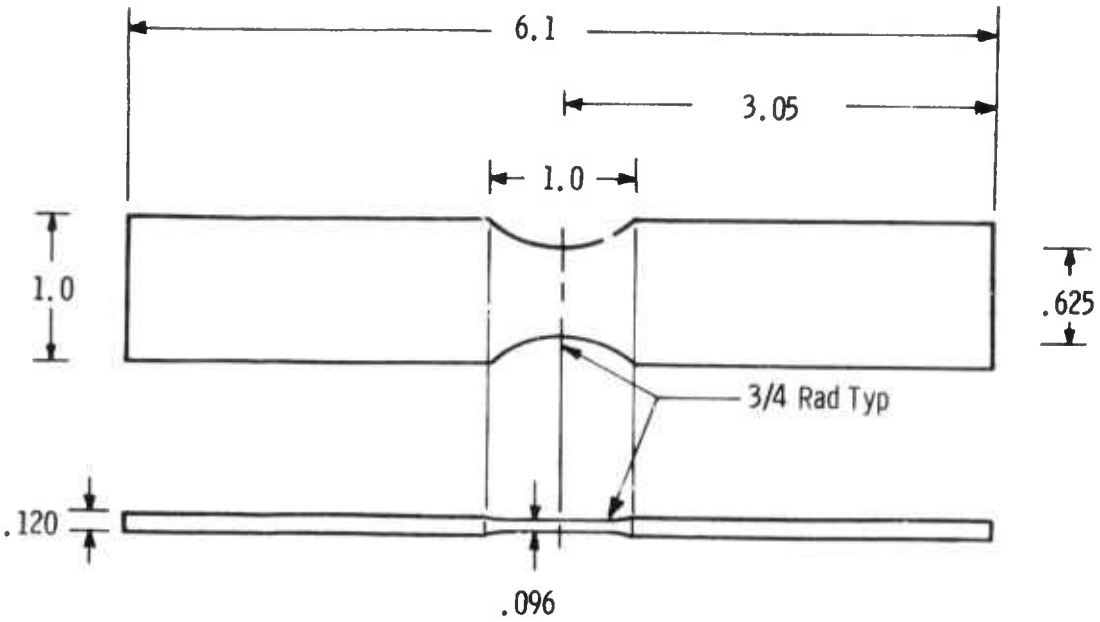

Figure 5.8 — Silicon Nitride Fatigue Specimen

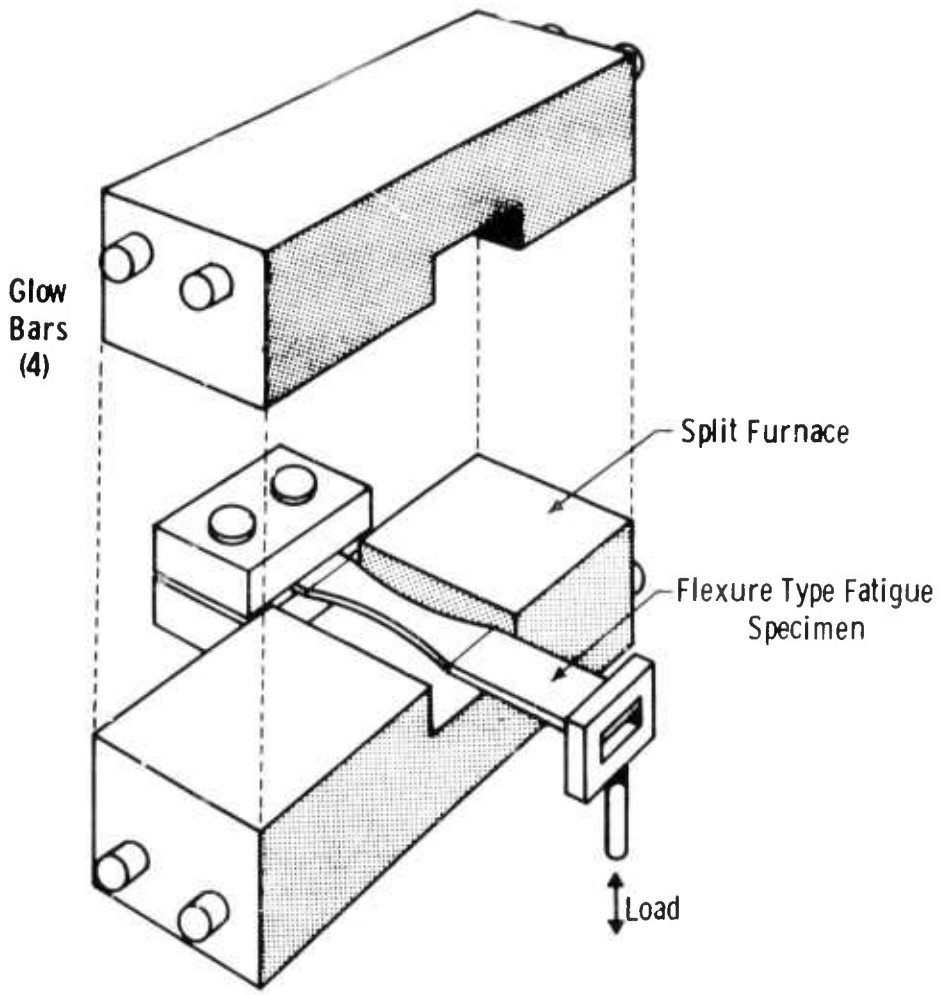

Figure 5.9 — Fatigue Test

Thirteen specimens have been tested thus far at various stresses and at three temperatures. The results are summarized in Table 5.5 and displayed in σ -N curves in Figure 5.10. The data indicate endurance limits for the 1800°F and 2200°F tests of 30,000 psi and 20,000 psi, respectively. The low temperature test data indicate a sharp transition stress of about 75,000 psi.

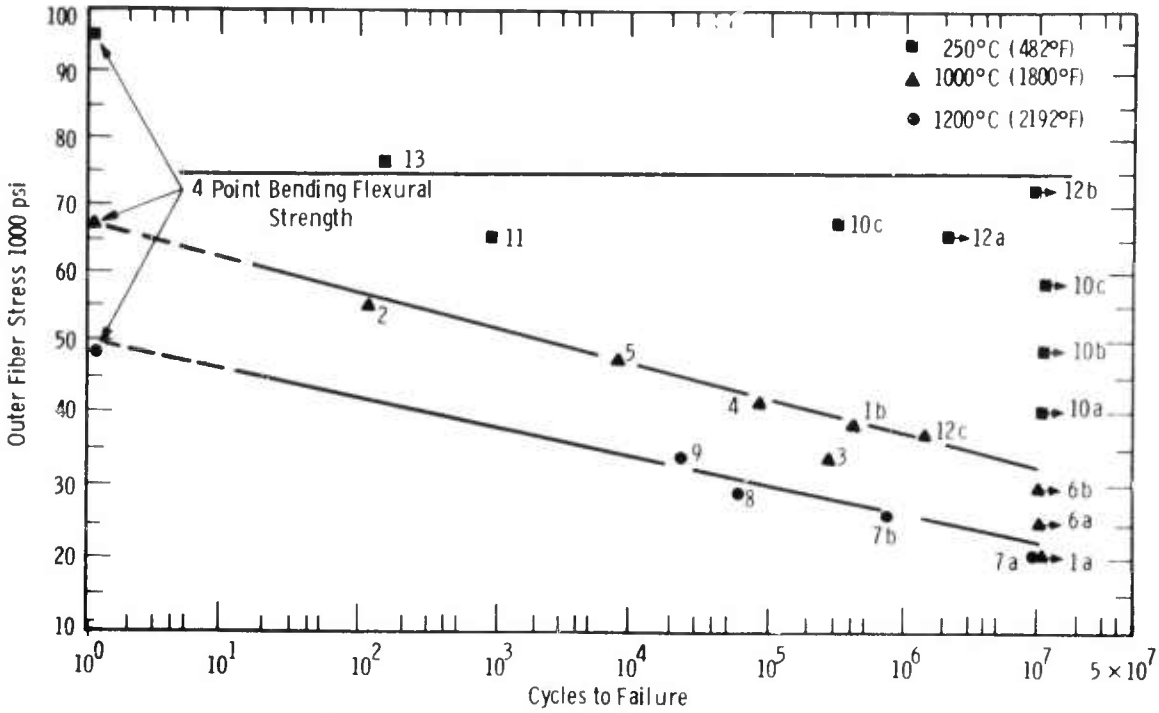

1800 cpm, in air. Specimens S3N4-FT-01 to S3N4-FT-13

Figure 5.10 — Tentative Flexural Fatigue Curves

A few specimens were subjected to more than one loading condition. For example, specimen #12 did not fail after 10^6 cycles at 70,000 psi and 482°F. The stress was then raised to 75,000 psi and the specimen was subjected to additional 10^7 cycles without failure. The specimen finally failed after 1.5 x 10^6 cycles at 1800°F.

TABLE 5.5

SUMMARY OF FLEXURAL FATIGUE TESTS, 1800 cpm, ZERO MEAN STRESS

(Specimens machined from Norton material, received July 1971)

Specimen #	Temperature	Stress psi	Cycles to Fracture (*) = run out, no failure	Remarks
S_3N_4-FT-01	1000°C (1800°F)	20,000	1.0×10^7 (*)	broke outside gauge section
S_3N_4-FT-01	1000°C (1800°F)	37,000	4.5×10^5	
S_3N_4-FT-02	1000°C (1800°F)	55,000	1.9×10^2	
S_3N_4-FT-03	1000°C (1800°F)	33,000	2.8×10^5	
S_3N_4-FT-04	1000°C (1800°F)	41,000	8.5×10^4	
S_3N_4-FT-05	1000°C (1800°F)	46,000	8.6×10^3	
S_3N_4-FT-06	1000°C (1800°F)	25,000	1.0×10^7 (*)	
S_3N_4-FT-06	1000°C (1800°F)	28,000	1.0×10^7 (*)	
S_3N_4-FT-07	1200°C (2192°F)	20,000	1.0×10^7 (*)	
S_3N_4-FT-07	1200°C (2192°F)	26,000	8.1×10^5	
S_3N_4-FT-08	1200°C (2192°F)	28,000	7.0×10^4	
S_3N_4-FT-09	1200°C (2192°F)	35,000	2.8×10^4	
S_3N_4-FT-10	250°C (482°F)	39,000	1.0×10^7 (*)	
S_3N_4-FT-10	250°C (482°F)	47,000	1.0×10^7 (*)	
S_3N_4-FT-10	250°C (482°F)	56,000	1.0×10^7 (*)	
S_3N_4-FT-10	250°C (482°F)	68,000	3.3×10^5	foreign object fell on machine
S_3N_4-FT-11	250°C (482°F)	65,000	8.5×10^2	large free Si particle
S_3N_4-FT-12	250°C (482°F)	64,000	2.2×10^6 (*)	
S_3N_4-FT-12	250°C (482°F)	73,000	1.0×10^7 (*)	
S_3N_4-FT-12	1000°C (1800°F)	37,000	1.4×10^6	
S_3N_4-FT-13	250°C (482°F)	75,000	1.5×10^2	

Friction

The three piece vane design permits some freedom of motion between the stator vane airfoil and its restraining end caps. Because this motion is affected by tenon geometry and friction at the surface, both static and dynamic coefficients of friction must be measured for high density silicon nitride against itself. The initial friction measurement consisted of rubbing a silicon nitride stylus, having a 1/16 inch diameter flat nose, against a flat block of silicon nitride. A motor drives the flat block past the stylus, which is loaded with a 5 lb weight. A strain gauge in the stylus mount measures the force necessary to overcome friction (see Figure 5.11). Temperatures up to 600°F are achieved by blowing hot air against the friction surface and temperatures up to 1900°F are obtained by using a gas burner.

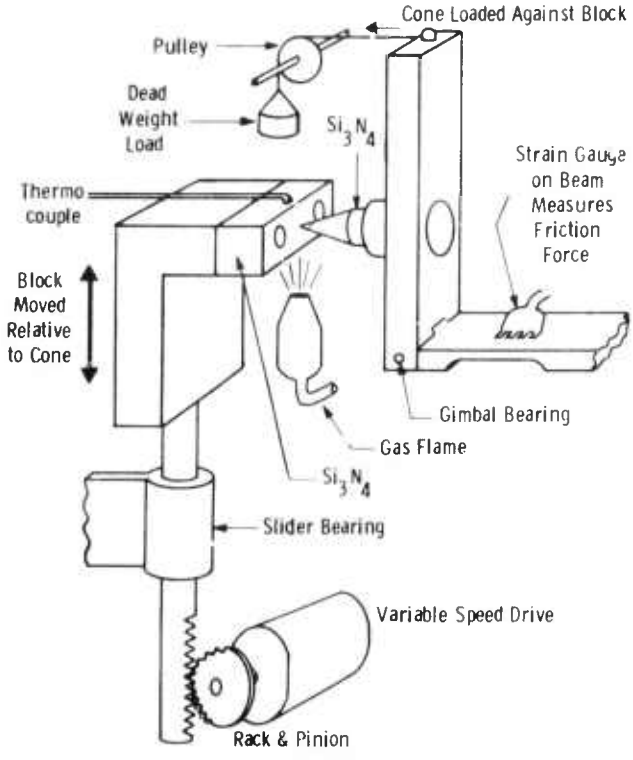

Figure 5.11 — Schematic Drawing of Friction Apparatus

The static or breakaway coefficient of friction is 0.22 at room temperature, and it increased to 1.58 at 1900°F (see Table 5.6). At room temperature, the dynamic or sliding friction coefficient is also 0.22, but it becomes unsteady at higher temperatures as a stickslip behavior develops. Generally, its average value is 20 to 40% lower than the static coefficient (see Figure 5.12).

TABLE 5.6

STATIC AND DYNAMIC FRICTION CHARACTERISTICS

Si_3N_4 vs Si_3N_4

Run No.	Load Lbs	Load psi	Speed inch/min	Temp °F	Static Friction Force Lbs	Static Friction Coefficient	Dynamic Friction Coefficient
1	5	1700	10	R.T.	1.0	0.20	0.20
2	5	1700	10	R.T.	1.2	0.24	0.24
3	5	1700	10	600	1.3	0.26	stick-slip
4	5	1700	10	600	1.4	0.28	stick-slip
5	5	1700	10	1000	1.8	0.36	stick-slip
6	5	1700	10	1000	2.3	0.46	stick-slip
7	5	1700	10	1800	8.5	1.70	stick-slip
8	5	1700	10	1850	7.3	1.46	stick-slip
9	5	1700	10	1900	7.9	1.58	stick-slip

NOTE: Apparent contact area - 0.003 $in.^2$

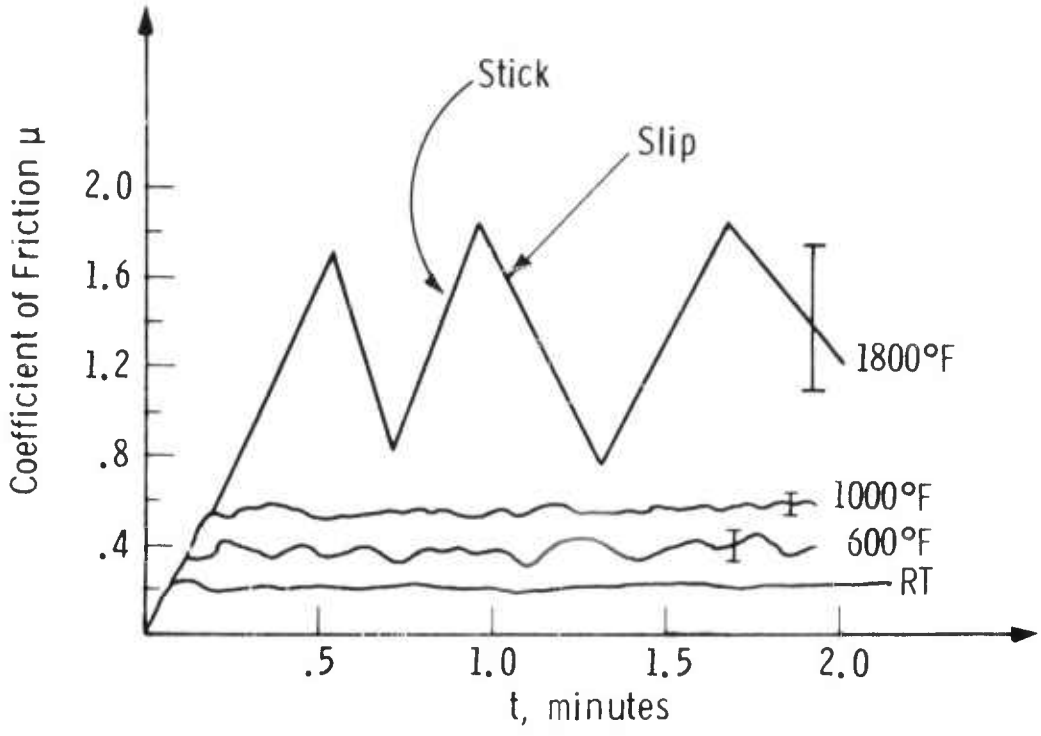

Figure 5.12 — Static and Dynamic Friction Characteristics of Si_3N_4 vs Si_3N_4

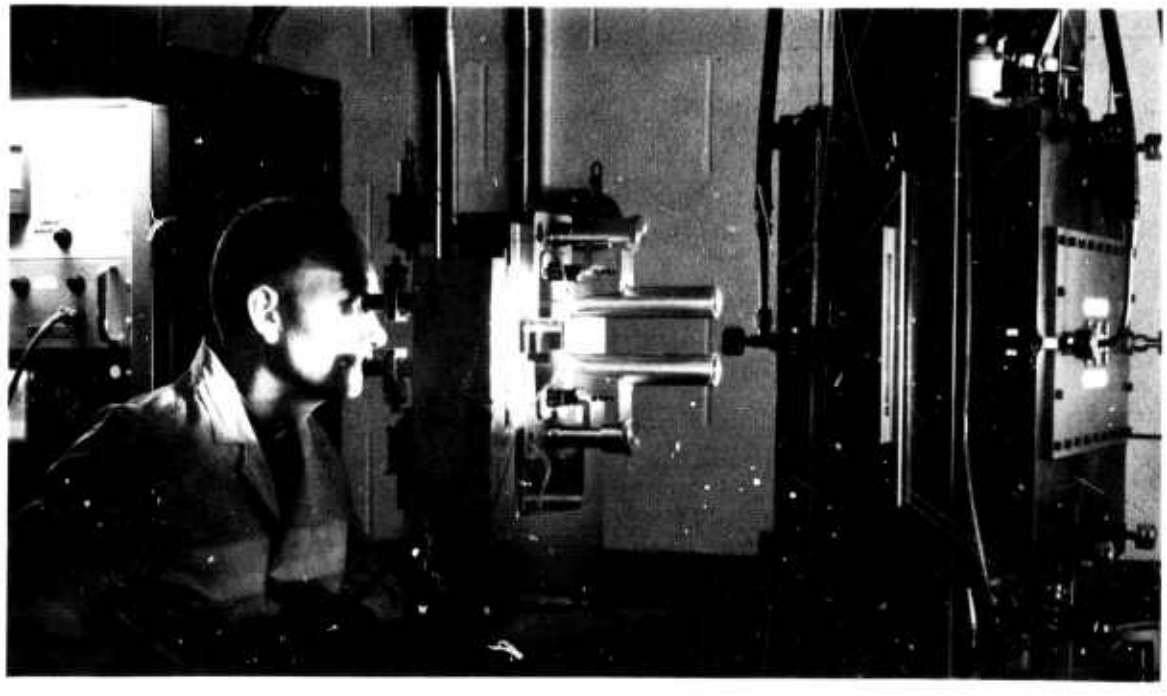

Figure 5.13 — Multispecimen Thermal Expansion Measuring System

Thermal Expansion

A multi-specimen system is being used to measure the thermal expansion of both silicon nitride and silicon carbide at temperatures between room temperature and 2600°F (see Figure 5.13). Measurements are made by two interlocking microtelescopes that sight on the upper and lower edges of the specimen. Monitoring of specimen dilation is achieved through motor-driven filar eyepieces and transmitting potentiometers. Temperature is measured by either a pyrometer that sights on the specimen or Pt/Pt-13Rh thermocouple attached directly to the specimen. The outputs from the telescope potentiometers and pyrometer, or thermocouples are fed to a digital data acquisition system. Up to 10 samples can be measured automatically in sequence, with a precision of $\pm$ 1% at 2500°F.

Specimens are being machined from billets of the third lot of hot-pressed silicon nitride prepared by Norton. This is substantially better material than the first lot. Measurements will be made on samples with axes either parallel or perpendicular to the pressing direction in order that any anisotropy can be detected.

5.1.2 DYNAMIC HOT CORROSION TEST

Pressurized Test Passage

A test passage which reproduces the operational environment of a large stationary gas turbine was used to determine the corrosion-erosion resistance of Si_3N_4 and SiC specimens at 2000°F. Air compressed to 45 psi in a bank of 30 hp rotary compressors is preheated in an indirectly fired air heater to 600°F and fed into a 6 inch diameter combustion chamber (see Figure 5.14). Fuel is injected into the combustor through a bayonet-mounted nozzle and burned with the compressed air. At the combustor exit, an array of 16 thermocouples is positioned to measure the gas temperature. Downstream of the thermocouple array, a transition section reduces the flow area to a 2" x 3-3/4" rectangular cross-section and increases the velocity to 500 fps, which is typical of the turbine inlet velocities in stationary gas turbines. At this location, the test specimens are exposed to the hot gas stream. A test section holds a pack of eight specimens that are held at their ends in the fixture shown in Figure 5.15. Downstream of the test section, a damper valve located in the passage maintains typical turbine pressures; and finally, the combustion products are cooled by a water spray before passing to a muffler.

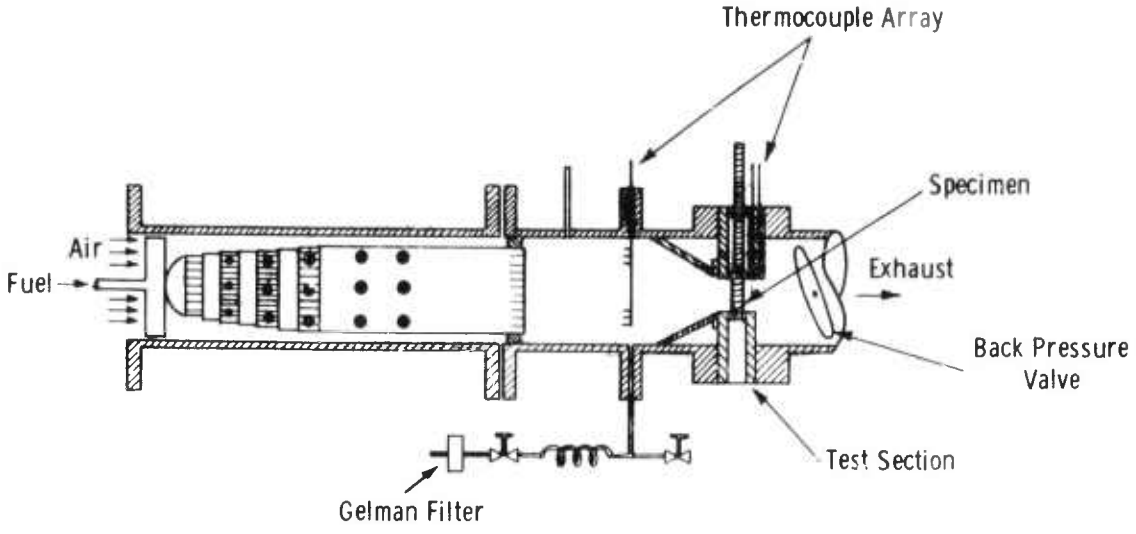

Figure 5.14 — High Pressure Corrosion Test Passage

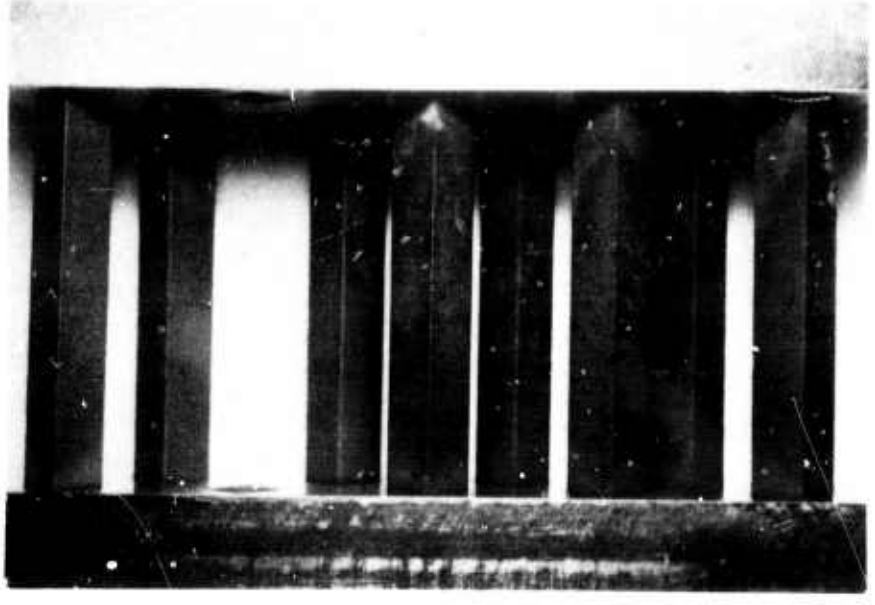

Figure 5.15 — Specimens and Holding Fixture

Testing Program

For the initial test, four specimens measuring 1/4 by 1/4 by 2 inches of the hot-pressed Si_3N_4 (Lucas) and SiC (Ceradyne) were exposed to a 1200°F temperature gas stream for 100 hours. Air and fuel flow rates were adjusted so that the gas stream velocity approaching the specimens was 500 fps at the passage pressure of 45 psi.

The combustion gas contained sulfur, sodium, vanadium, and magnesium compounds, which were introduced with the fuel. The fuel oil contained 0.5 wt% sulfur, 5 ppm sodium, 2 ppm vanadium, and 0.6 ppm magnesium, corresponding to the ASTM fuel specification #3-GT. This is the level of contaminants found in fuel that is currently used in industrial gas turbines and which causes severe corrosion of super-alloys such as Udimet-500 and X-45.

Ceramic specimens were cleaned, weighed, and measured before the test. After test periods of 10, 20, 30, 50, 70, 92, and 100 hours, each specimen was visually examined and weighed.

Figure 5.16 illustrates the surface appearance of a Si_3N_4 specimen after 100 hours of exposure. Deposits on the front surface had a different appearance from those on the back. Front surface deposits were black and relatively soft whereas those on the back were brown and glassy, an indication that they were once molten. X-ray diffraction analysis indicated that both front and back deposits consist of a spinel-type structure and α-Fe_2O_3. Emission spectroscopy revealed the presence of Si, Mg, V, Fe, Mn, Cr, and Ni. Apparently most of the surface deposits came from both the fuel and by erosion of the passage liner. Visual examination of the specimens showed no loss of original material in either SiC or Si_3N_4. Figures 5.17 and 5.18 illustrate the weight changes observed for Si_3N_4 and SiC, respectively. The results for each specimen are shown to illustrate the scatter of the data. Both ceramics gained weight either by deposition of material or by oxidation. In contrast to ceramics, superalloys experience significant weight loss after 50 hours of exposure, even at test temperatures several hundred degrees lower than 2000°F.

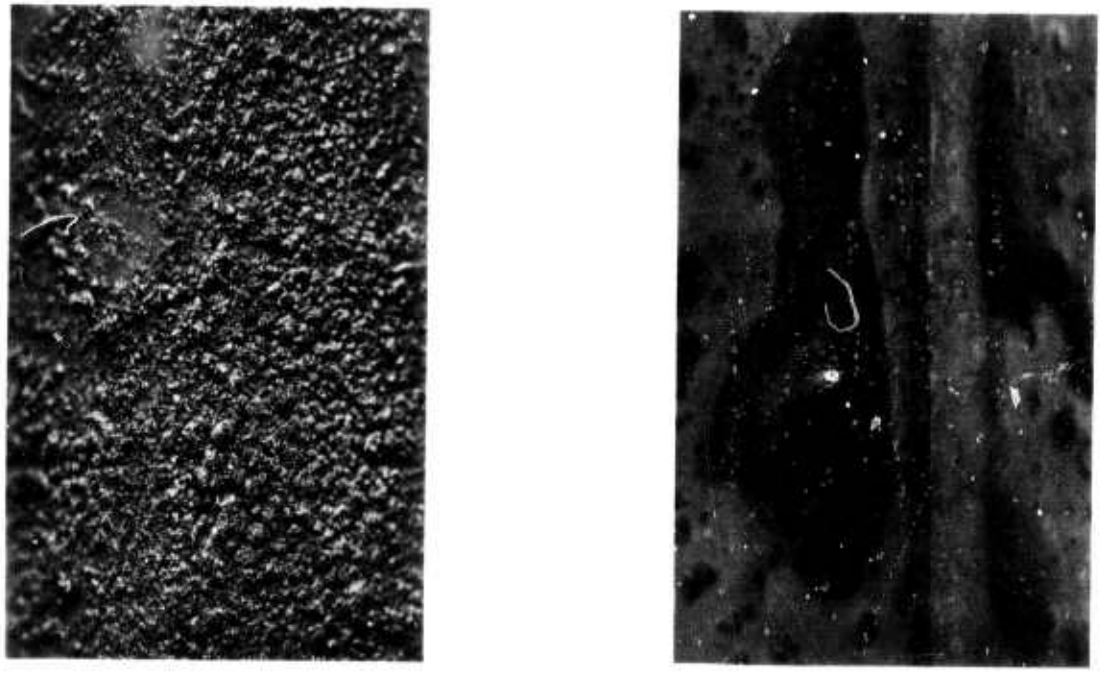

Figure 5.16 — Magnified view of a Si_3N_4 specimen after 100 hours of test showing different deposit characteristics on front and back surfaces. 10X

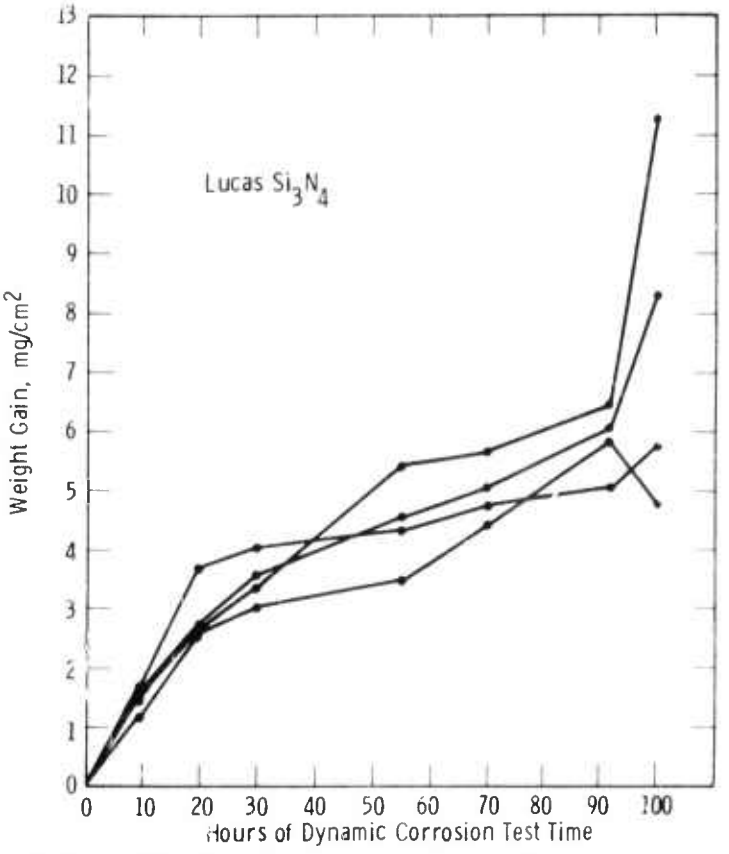

Figure 5.17 — Weight Change vs Hours of Exposure Time for Si_3N_4 Tested at 2000°F and 3 Atmospheres

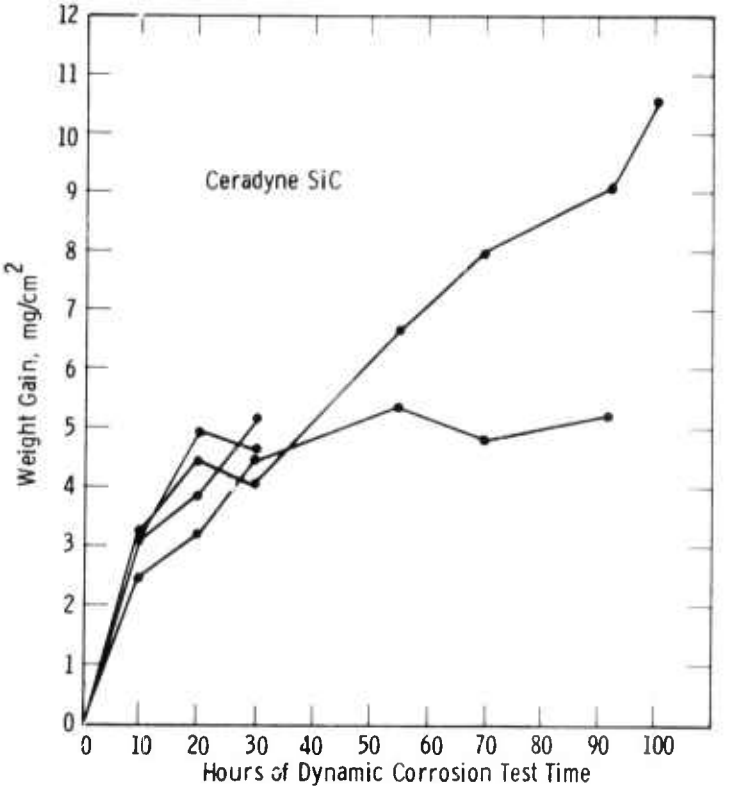

Figure 5.18 — Weight Change vs Hours of Exposure Time for SiC Tested at 2000°F and 3 Atmospheres

Conclusions

The flexural, tensile, and fatigue strengths of Norton hot pressed silicon nitride have been reported. Weibull statistics are being used to correlate vendor data from 3 point bend tests with 4 point bend and tensile tests. Static and dynamic coefficients of friction for Si_3N_4 increase with temperature from 0.2 at RT to 1.5 at 1900°F. Dynamic hot erosion-corrosion tests indicate both silicon nitride and silicon carbide are superior to superalloys.

All of the mechanical and thermal properties of silicon nitride and silicon carbide will be determined statistically from room temperature to 2550°F to provide engineering input for the final vane design. The testing will then be continued using the billets from which the vanes are fabricated. Special tests will be used to simulate component performance and assess pertinent effects such as wear and fretting at the airfoil-end cap interface.

5.2 MATERIAL FABRICATION

SUMMARY

Norton Company will fabricate billets of silicon nitride by hot pressing from which they will machine stator vanes to Westinghouse specifications. Energy Research Corporation, on the other hand, will fabricate hollow vanes of silicon carbide by in-situ chemical vapor deposition.

5.2.1 NORTON SILICON NITRIDE

Norton Company will blend a 100 lb lot of high quality, alpha silicon nitride powder, deliver three prototype 6.3" x 6.3" x 1.3" thick billets when the process is optimized for reproducible strength, and measure flexural strength and density on these billets in the first phase of their program.

An additional 100 lb lot of powder and 37 hot-pressed billets, certified with respect to strength and density, will be prepared in the second phase of their program. Twenty airfoils and 20-40 end caps will be machined from these hot-pressed billets. Billets not consumed in machining and remnants from vane fabrication will be used for the statistically designed materials characterization study at Westinghouse.

Billet certification guarantees minimum hot-pressed densities of 3.10 gm/cc and a mean room temperature flexure strength, less 3 standard deviations, greater than 90,000 psi in the strong direction of the material. Strength is measured by three-point loading over a 3/4" span. The mean strength and standard deviation are determined from 20 1/8" x 1/8" x 1" specimens per billet. Billet dimensions of 6.3" x 6.3" x 1.3" are specified.

Norton delivered three billets that were hot-pressed from the first 100 lb lot of silicon nitride powder completing Phase I. An average flexural strength of 127,800 ± 9700 psi was reported by Norton, and an average density of 3.18 ± 0.01 gm/cc, which is well within the range specified for certification. The data in Table 5.7 was adjusted to eliminate a low value of 83,000 psi which resulted from a specimen with surface damage according to Norton.

TABLE 5.7

PROPERTIES OF HIGH STRENGTH, HOT PRESSED NORTON SILICON NITRIDE

Billet No.	No. of Tests	Average Flexural Strength psi	Standard Deviation psi	Range psi	Density gm/cc
309902-1	24	125,000	15,900	154,000 / 83,000	3.19
309902-1 adjusted	23*	129,000	13,200	154,000 / 103,000	3.19
309902-2	20	126,600	8,800	140,000 / 110,000	3.17
309902-3	20	131,400	7,100	148,000 / 120,000	3.18

*Test run 24 - 83,000 psi flexural strength - not used because of surface damage on specimen.

Norton is producing silicon nitride billets for this program at the rate of 2 billets per week from a pilot plant facility. Billet fabrication and airfoil machining are scheduled for completion by April 30, 1972, and May 31, 1972, respectively.

5.2.2 ENERGY RESEARCH SILICON CARBIDE

Energy Research will optimize the CVD process for making wall thickness > 0.125" and prepare modulus of rupture specimens in the first phase of their program. Later on, flexural and tensile specimens will be cut from actual CVD deposited silicon carbide vanes. Finally, five hollow silicon carbide vanes will be supplied for evaluation in the pressurized test passage.

The material and vanes produced in the first year is on a best effort basis. Certain general requirements must be met, however. All silicon carbide material will be deposited on the inside surface of a mandrel large enough to prepare 0.125" x 0.25" x 4.0" specimens. Room temperature modulus of rupture tests will be made using four-point loading using 1-1/8" inside and 3-3/8" outside span lengths.

Energy Research is presently optimizing their chemical vapor deposition process to give thick wall sections. An average flexural strength of 62,000 ± 11,800 psi was achieved from the first 19 specimens (see Table 5.8).

TABLE 5.8

ENERGY RESEARCH CVD SILICON CARBIDE
MOR TEST RESULTS USING FOUR POINT BENDING FIXTURE
INSIDE CENTER DISTANCE 1-1/8 INCHES
OUTSIDE CENTER DISTANCE 3-3/8 INCHES

CVD Run No.	Specimen Width-b Inches	Specimen Thickness-d Inches	Breaking Load Pounds	4 Point MOR Stress psi
C-71-10-24				
A	.245	.155	105	60,200
B	.222	.156	72	45,000
C	.251	.157	54	29,400
C-71-11-7				
X	.255	.125	72	61,000
Y	.231	.117	65	69,400
C-71-11-10				
1	.260	.164	136	65,600
2	.237	.173	137	65,200
3	.258	.173	96	42,000
C-71-11-11				
1	.259	.164	184	89,100
2	.251	.163	146	73,900
C-71-11-12				
1	.260	.174	110	47,100
2	.257	.125	52	48,700
3	.246	.144	70	46,300
C-71-11-13				
1	.257	.136	95	67,500
2	.257	.143	126	80,900
3	.256	.123	86	74,900
4	.246	.146	104	66,900
5	.249	.138	96	68,300
6	.247	.143	95	63,500

$$S = \frac{3.375 \times \text{Breaking Load}}{bd^2}$$

Energy Research expects to deliver vanes for evaluation in the turbine passage by June 30, 1972. Process optimizati will be eompleted by February 15, 1972. Specimens cut from hollow airfoil and the data deseribing them will be available after May 30, 1972.

Conclusions

Norton has improved the quality of hot pressed silieon nitride significantly sinee the beginning of its contract. The strength of the CVD silicon earbide deposited by Energy Research has not met expectations up to this point.

5.3 MATERIALS SCIENCES

SUMMARY

Norton hot pressed silicon nitride is predominately a fine grain (1-4 μ m) material with oeeasional evidence of longer (8-10 μ m) equiaxed and clongated grains. Calcium and magnesium represent major cation impurities which apparently affect the high temperature properties of the material. Dislocations and slip bands have been identified in the mierostructure of both hot pressed and reaction-sintered silicon nitride.

The oxidation of hot pressed silicon nitride is pure oxygen is shown to follow the parabolic rate law with constants of 3.5×10^{-14} and 6.6×10^{-13} at 1800 and 2000°F, respectively. Weigh gains of 260 μ gm/cm^2 (2000°F) and 105 μ gm/em^2 (1800°F) after a 40 hour exposure are reported.

Introduction

The criterion used in seleeting areas for scientific investigation was to ask the question: assuming the answer was known, how would it affect the engineering deeision to use ceramics in gas turbines? Both microstruetural charaeterization and gas-solid reaetion kinetics are of first order importance. Correct interpretation of microstructural detail is required to be able to correlate fabrication procedures with physieal properties, sinee the fabrieation procedures originally determine the microstructure and ultimately affeet the engineering performance of the eeramie. Likewise, the gas-solid reaetion kineties are important beeause the oxidation resistanee of both silicon nitride and silicon earbide depends on the stability of an oxide surfaee layer.

5.3.1 MICROSTRUCTURAL CHARACTERIZATION OF Si_3N_4

The microstructure of Norton hot pressed Si_3N_4 was determined from 1 cm x 1 cm x 3 mm specimens mounted in Kold Mount. Wet paper was used for rough polishing down to 600 grit. Final polishing was done on cloth with Linde B solution. The specimens were preheated, etched in a eutectic mixture consisting of 93 gm K_2CO_3 and 15 gm Na from 1/2 to 4 minutes and then cleaned ultrasonically. Surface replicas were prepared using a two-stage carbon replication shadowed with palladium. The replicas were examined in a Siemans Micrograph operating at 100 kV. (The high voltage was used so that diffraction patterns could be obtained from grains and other debris extracted from the surface.)

Figures 5.19 through 5.23 show the typical microstructure of hot-pressed Si_3N_4 as revealed by optimal etching conditions of 75 sec. at 1350°F. There are basically four types of grains. The most frequent are the small equiaxed grains, with sizes varying from about 1 μ m to 4 μ m. A few larger equiaxed grains, with sizes of the order of 8-10 μ m, and a few elongated grains, with typical dimensions of 2 x 10 μ m were observed. All of the grains in these groups that were examined by electron diffraction were identified as the β phase (see Figures 5.22 and 5.23). This is in agreement with the observations of Evans and Sharp [13]. It should be noted that occasionally small round dimples were seen inside the grains (Figure 5.22). This could be due to surface pitting during etching or polishing. However, it is more likely that these dimples are small subgrains also frequently observed by transmission microscopy. A fourth type of grain was only occasionally observed; a rough estimate would put these grains at less than 1% by volume. They were very large, elongated grains about 10 μ m wide and up to 50 μ m long (Figure 5.23). These large grains were indexed predominantly as α-Si_3N_4. The grain boundaries are deeply etched (as revealed by the long, white shadow and the torn off pieces of replica material left inside the boundary grooves). The grain boundaries appear continuous although discontinuties were observed occasionally (arrows, Figures 5.22 and 5.23).

A typical grain morphology as revealed by transmission electron microscopy is shown in Figure 5.24. The diffraction pattern was taken through the largest diffraction aperature covering the entire micrograph area. One should note the absence of a ring pattern indicating a non-random distribution of grain orientations.

Impurities in High Density Silicon Nitride

Although hot-pressed silicon nitride is nominally only 98% pure, the distribution of impurities is apparently not random. Macroscopically, one occasionally finds "large" chunks of silicon or particles of iron. On a microscopic scale, impurities were generally found to be unassociated with grain boundaries. Only occasional individual particles or clusters of particles were observed; typical examples are shown in Figure 5.25 through 5.27. A row of small particles in a α-grain, which were less than 300Å in diameter, are shown in Figure 5.27.

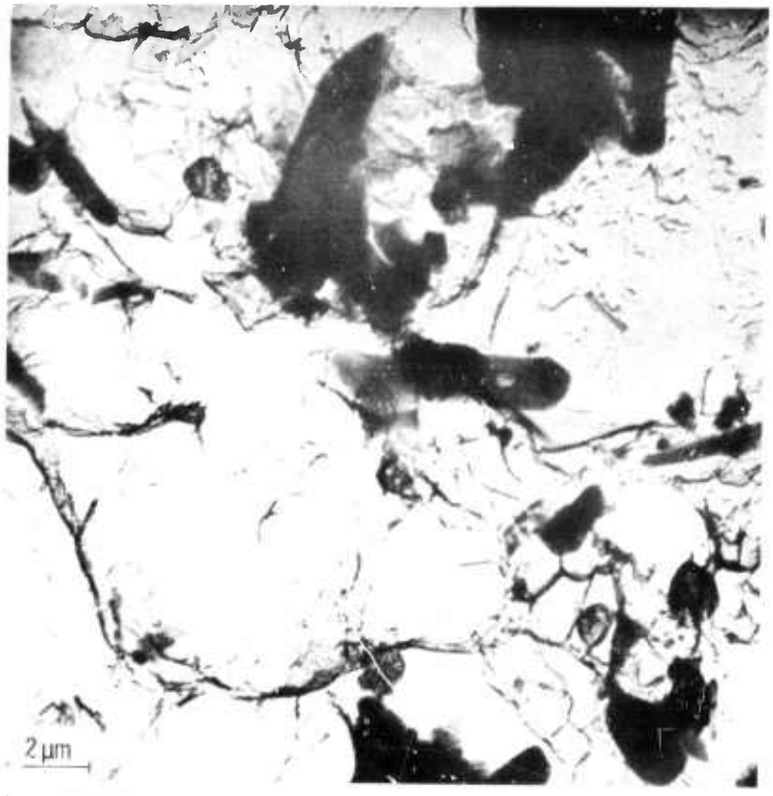

Figure 5.19 -- Replica transmission micrograph of an over etched surface of hot pressed Si_3N_4. Etched 4 min at 740°C

Figure 5.20 — High magnification detail of an over etched surface of hot pressed Si_3N_4. Two stage carbon replica

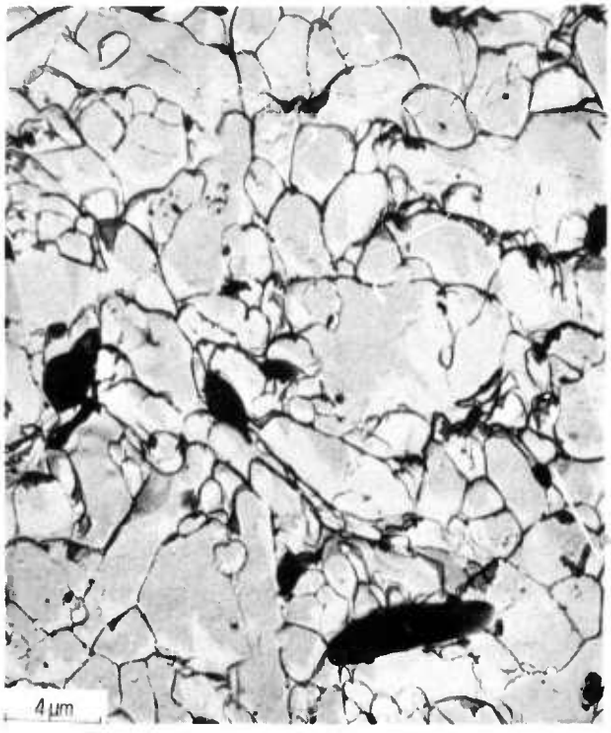

Figure 5.21 — Typical microstructure of hot pressed Si_3N_4. Etched 75 sec. 740°C. Two stage carbon replica

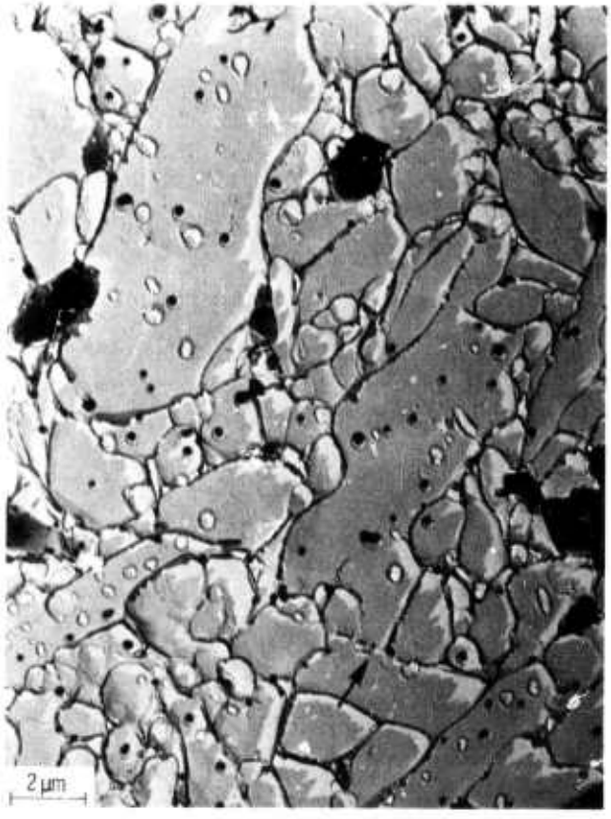

Figure 5.22 — Typical microstructure of hot pressed Si_3N_4. Etched 75 sec. 740°C. Two stage carbon replica

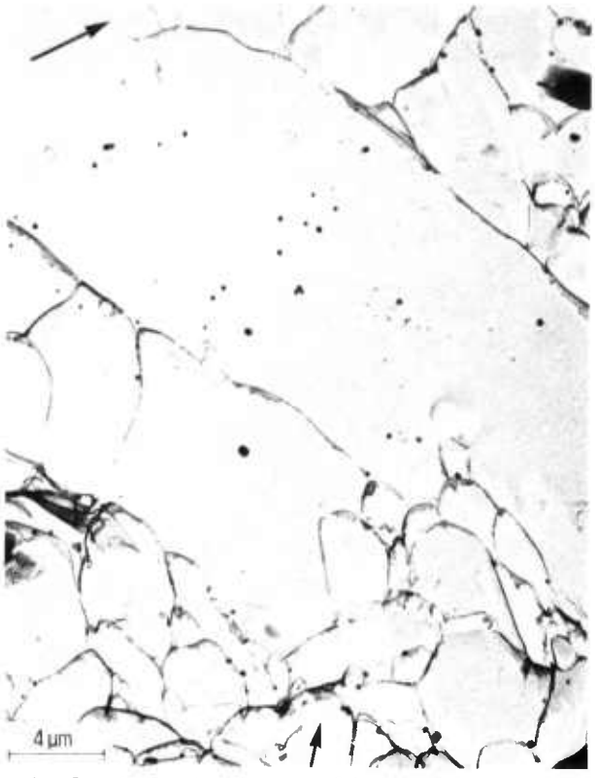

Figure 5.23 — Typical microstructure of hot pressed Si_3N_4. Etched 75 sec. 740°C. Two stage carbon replica

Figure 5.24 — Transmission micrograph (100 kV) showing general grain morphology of hot pressed Si_3N_4. Note the absence of a ring pattern, indicating non-random grain orientations

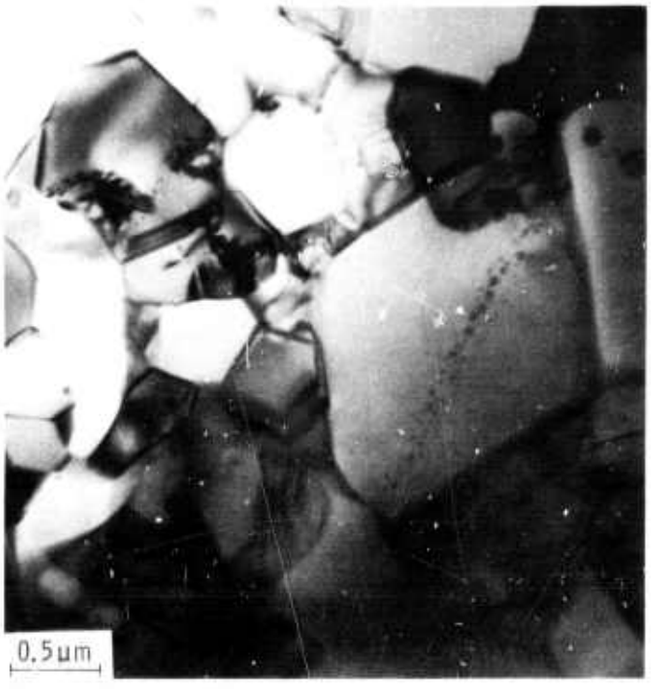

Figure 5.25 — Chain of impurities across a grain occasionally observed in transmission microscopy. (100 kV)

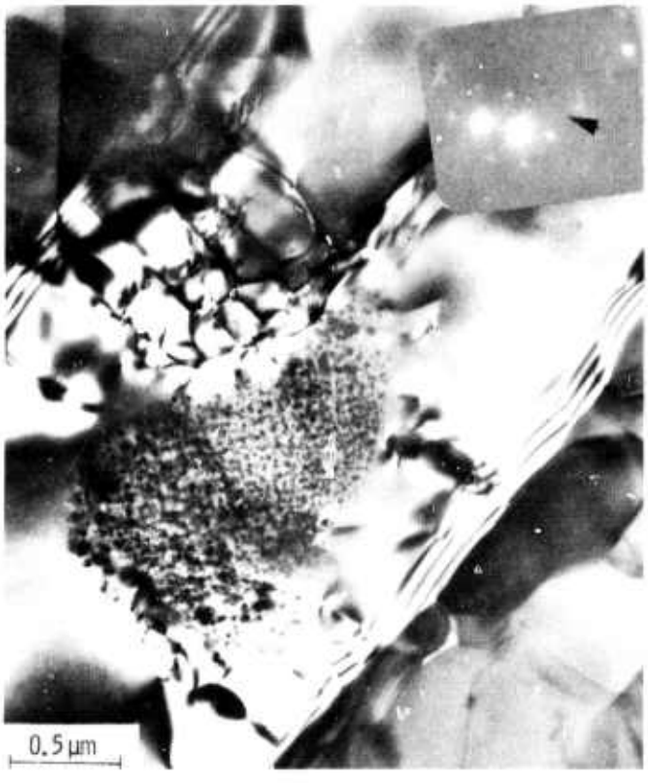

Figure 5.26 — Dark field image of $\overline{g}$ showing a cluster of impurities (α grain, 800 kV)

These particles are too small for identification by electron diffraction. Similarly, a cluster of impurities of less than 200Å in diameter are shown in an α grain by dark field illumination in Figure 5.26. One or two extra spots were observed in the diffraction pattern (arrow), however, positive identification was impossible. Larger particles about 1000Å in diameter are shown in Figure 5.27. Elastic strain fields were associated with these larger particles. Also a few particles were located in grain boundary defined by the dislocation network (marked gb in the micrograph).

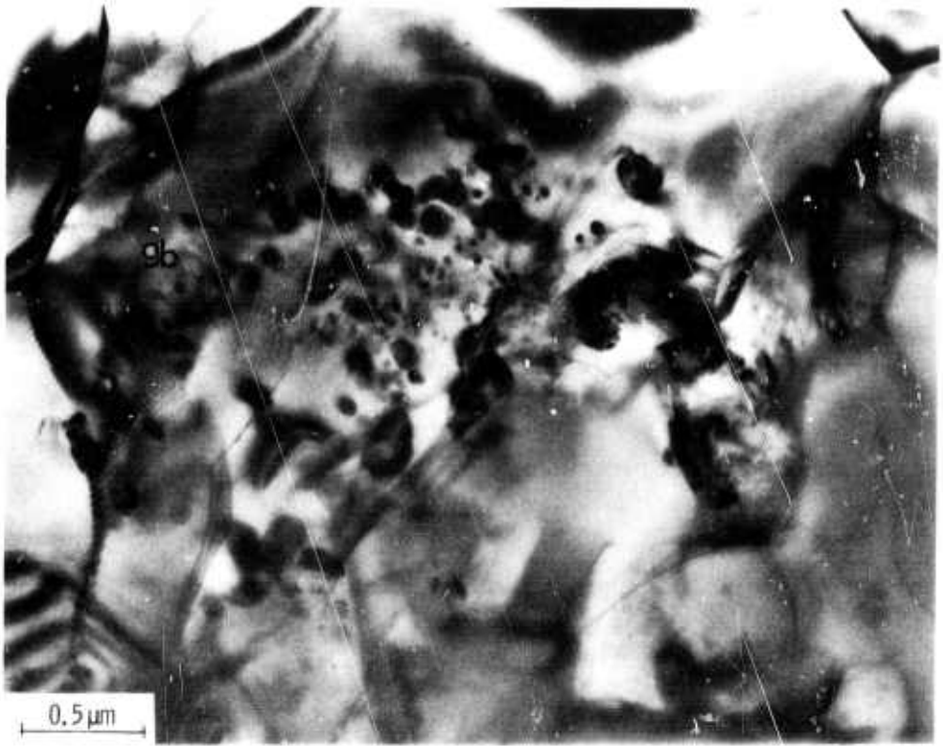

Figure 5.27 — Occasionally observed round impurities with associated strain fields. Also impurity particles in grain boundaries (g.b) 800 kV)

Voids were only occasionally observed. It was difficult to decide whether a void was originally present or whether it was the result of a grain being lost during thinning and handling. Since the voids shown in Figure 5.28 display a sharp contrast transition, they are true voids, rather than being a result of thinning. Otherwise, low angle ion bombardment would have produced a more gradual transition in contrast across the edge of the void.

Dislocation Structures in High Density Silicon Nitride

Evans and Sharp[13] and Butler[14] reported on the dislocation structures that they found in β phase. The present observations on β phase are in general agreement with their work. However, dislocation structures were observed as well in the very large, elongated α grains. From the limited information that has been gathered so far, it seems that the dislocation structures in both phases are similar.

Figure 5.28 — Typical pores in hot pressed silicon nitride. The sharp transition in contrast at the edge of a pore indicates that it was not due to thinning effects (800 kV, 15^{o} thinning)

To determine Burger vectors in both the α and β phases, grains extracted during surface replication were examined. These extracted grains were thin enough for high voltage transmission work, and by the nature of their formation, they present suitable conditions for examining slip behavior at room temperature. Normally, in a brittle material like Si_3N_4, the critical stress for dislocation motion is much higher than the fracture stress (at least at low temperatures). Only at the fracture surface do sufficiently high stresses develop to cause dislocation motion. Consequently, the thin extracted grains provided the fracture surfaces for transmission microscopy.

Examples of slip bands observed in α and β grains are shown in Figure 5.29. In both examples, the dislocations are mostly of the screw type. Furthermore, the conditions of $\bar{g}.\bar{b} = 0$ or $\bar{g}.\bar{b} \neq 0$ are consistent only with a Burger's vector of the type c [0001]. Other examples of tilting experiments are given in Table 5.9, from which the conclusion is made that the most common Burger's vector for both α and β is c [0001]. This has been previously observed for the β phase only.

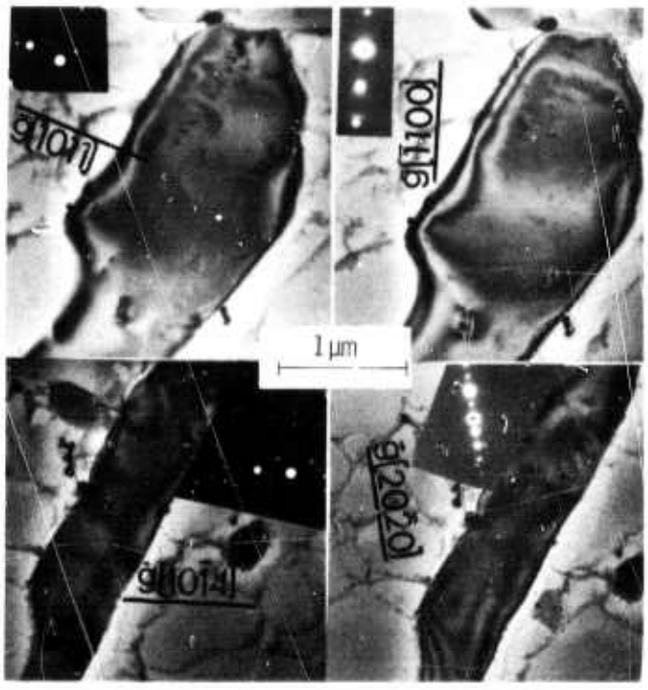

Figure 5.29 — Room temperature slip traces in extracted Si_3N_4 grains. Tilt analysis consistant with B. V. C[0001]. Note that dislocations are almost all of the screw type. (800 kV)
Top row: β grain $[1\bar{1}01]$ ZA. Bottom row: α grain $[01\bar{1}0]$ ZA
Left: $g.b \neq 0$ Right: $g.b = 0$

TABLE 5.9

CONDITIONS FOR DISLOCATION VISIBILITY AND NON-VISIBILITY FOR $\bar{b} = c$ [0001]

g	$\bar{g}.\bar{b}=O$	$\bar{g}.\bar{b}\neq O$	Phase
$\bar{2}022$		X	β
$3\bar{3}00$	X		β
$02\bar{2}2$		X	β
$2\bar{2}00$	X		β
$10\bar{1}4$		X	α
$20\bar{2}0$	X		α
$10\bar{1}2$		X	α

Two more examples of commonly observed dislocations in the large α grains are shown in Figures 5.30 and 5.31. The dislocation segments that are in contrast and the segments that are out of contrast (arrows Figure 5.30) probably comprise a low angle twist boundary. Near edge dipoles are shown in Figure 5.31 (note dislocations of opposite signs pointed by arrow). Common dislocation boundaries in β grains are shown in Figure 5.32. Other common features observed in β grains are shown in Figure 5.33. Note dislocation tangles, Figure 5.33a, b, and what might be bundles of stacking faults in Figures 5.33c and 5.33d.

More work is required to fully characterize the dislocation and fault structures in both the α and β phases.

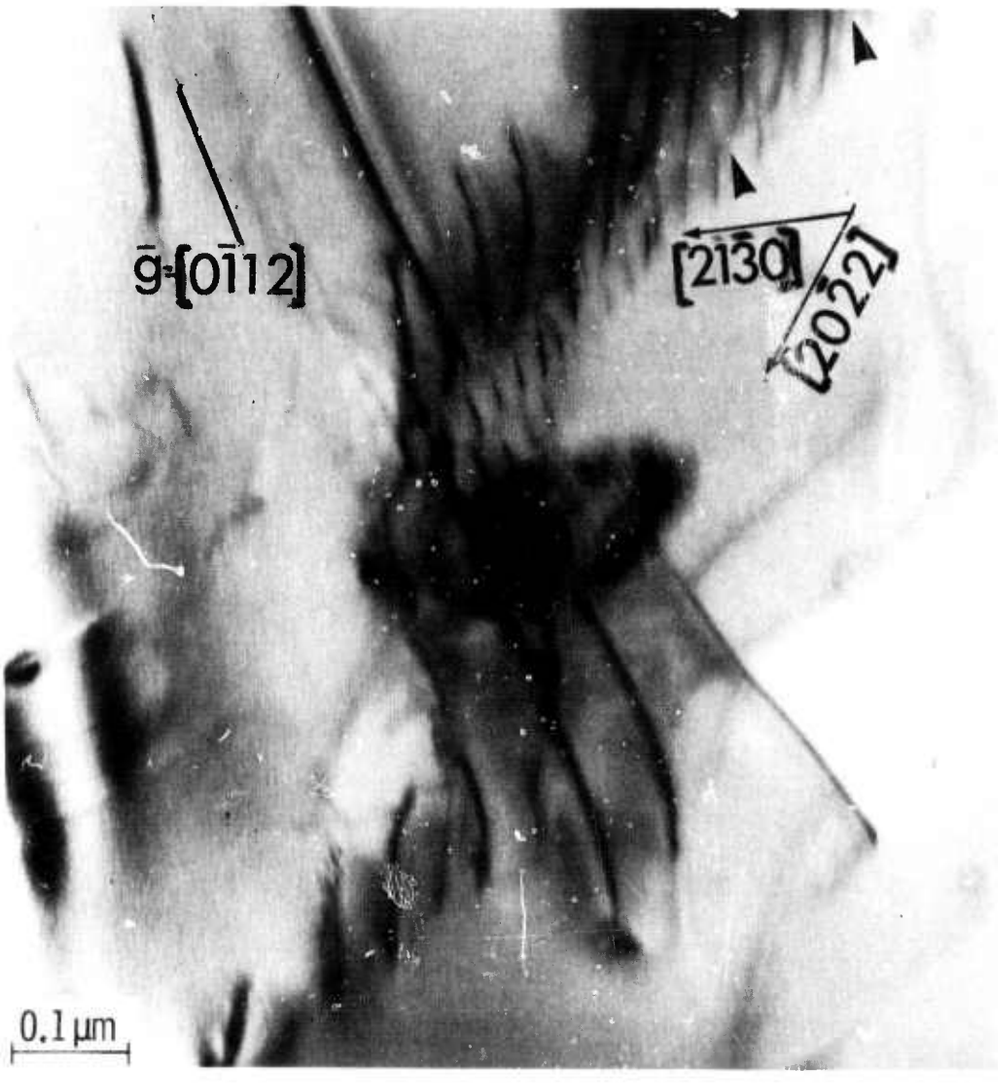

Figure 5.30 — Example of dislocations in an α grain $\bar{g}=[0\bar{1}12]$, $[\bar{1}2\bar{1}1]$ ZA (100 kV)

Figure 5.31 — Near dipoles (arrow) in an α grain $\overline{g} = [10\bar{1}2]$, $[\bar{1}3\bar{2}2]$ $\overline{ZA}$ (100kV)

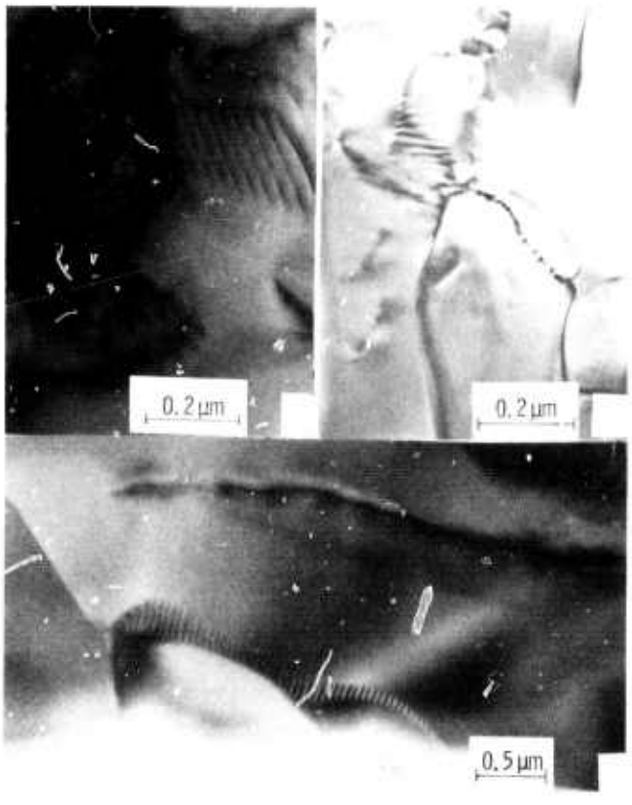

Figure 5.32 — Examples of Frequently Observed Grain Boundary Dislocation Networks and Faults

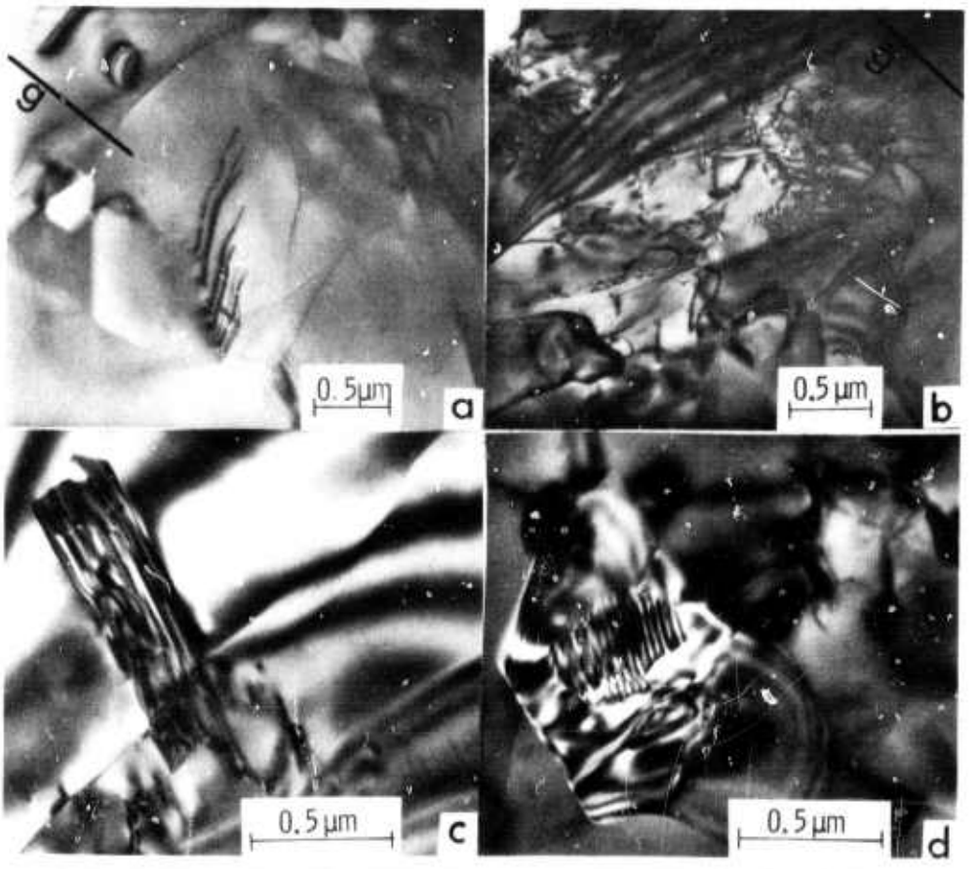

Figure 5.33 — Examples of disloeation (a and b) and possible fault struetures (c and d) in β grain. Note tangles in b and grain boundary network in a. (800 kV)

Low Density Silieon Nitride

Four stator seetions from the vehieular gas turbine projeet were analyzed; two seetions from eaeh of the stators designated #125 and #156, respeetively. General views of these stator sections are shown in Figures 5.34 and 5.35. The six grids shown in Figure 5.34 were taken from the "white" and "grey" colored areas; X-ray samples were seraped from the same areas as well as from the blades, Figure 5.34b Blade 7 in stator #125 was fraetured intentionally for mieroscopie and X-ray analyses of the interior of a blade. A similar proeedure was followed with stator #156 (Figure 5.35). Note that blade 16 (Figure 5.35a) failed during engine tests whereas blade 17 was fractured for analysis. The "white" and "grey" surfaces are better identified in Figure 5.35b.

The white surface is the edge of the base of the blade; the grey material is below the inner ring that holds the blades together to form the stator assembly.

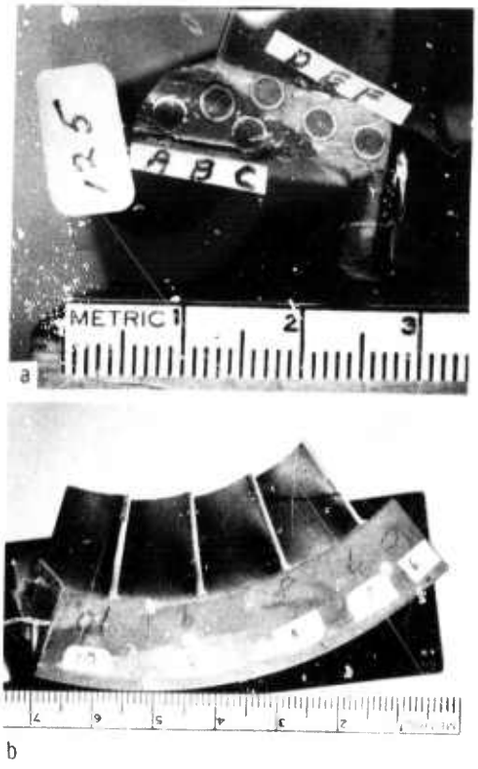

Figure 5.34 — Identification of location of grids and blades for replication and scanning microscopy. Ford Stator #125

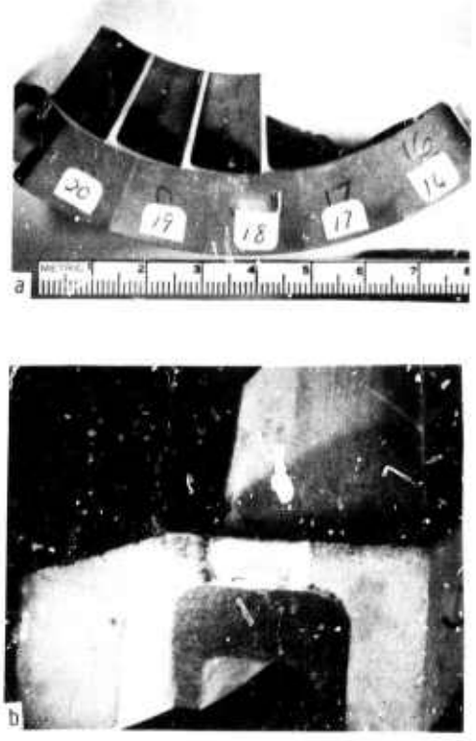

Figure 5.35 — Ford Stator #156, fresh fracture surface of blade #17 examined by replica and seanning eleetron mieroscopy and white and grey areas from whieh replication grids and x-ray sample were taken

A summary of the X-ray results is given in Figure 5.36. The outer surface of the base of the blade is pure α-Si_3N_4 (Figure 5.36). Deeper scraping (Figures 5.36c, g) showed that the blade base is composed of a mixture of 80% α and 20% β . The grey material has a slightly higher content of β than the white material (30% vs 20%)(Figures 5.36b, d, f, h). Scrapings from freshly fractured surfaces showed that in stator #125 the composition of the blades is high in α (90%), (Figure 5.36) while in stator #156, the α content of the blade is only about 60%. The high oxide content in blade 7, stator #125 (Figure 5.36i), is the result of long engine testing.

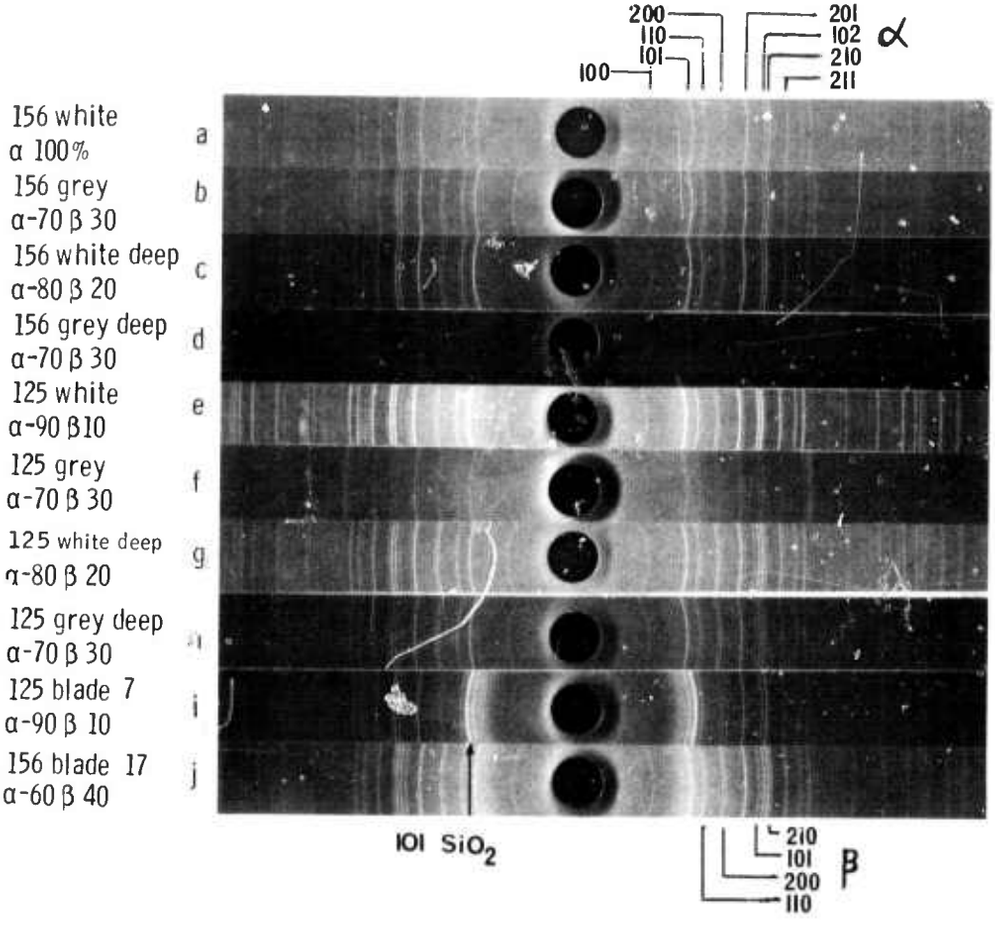

Figure 5.36 — Powder X-Ray diffraction patterns, Ford Stator #125 & 156

Fractographs taken of stator #125 are shown in Figures 5.37 through 5.39. The grey fractured surface appears to be smooth and it contains occasional patches of silicon-oxynitride (Figure 5.37) while the white surface has a much rougher appearance (Figure 5.38), and also contains patches of silicon-oxynitride (Figure 5.40). Also note the elongated grains (Figure 5.38) which are typical to the α phase.

Scanning electron micrographs of the fresh fracture surface of blade 7 are shown in Figure 5.41. The entire cross section of the blade reveals a uniform microstructure, a small grain size and a smooth fracture surface.

In contrast to blade 7, the scanning micrographs of the fresh-fractured surface of blade 17 stator#156 (Figures 5.41 and 5.42) reveal a non-uniform microstructure specifically in the area of the leading edge (Figure 5.41). The inner area of the leading edge reveals elongated whisker-like grain associated with large pores. Also note the round particle inside the pore, Figure 5.42, which is either an oxynitride or free silicon.

These preliminary results suggest that compositional differences (α content), grain structure and porosity are the important factors to be considered.

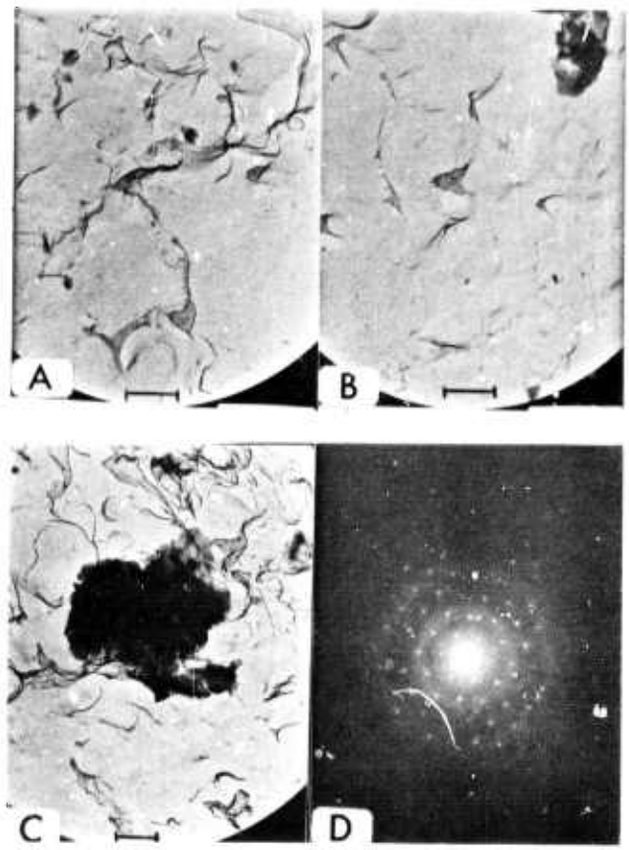

Figure 5.37 — Ford Stator #125, Grid A, gray fracture (α & β)
A, B: Typical surface replicas. Note smooth appearing fracture
C: Occasionally found patches of Si_2N_2O
D: Diffraction pattern off C, (002) ZA
1 μ m scale bars

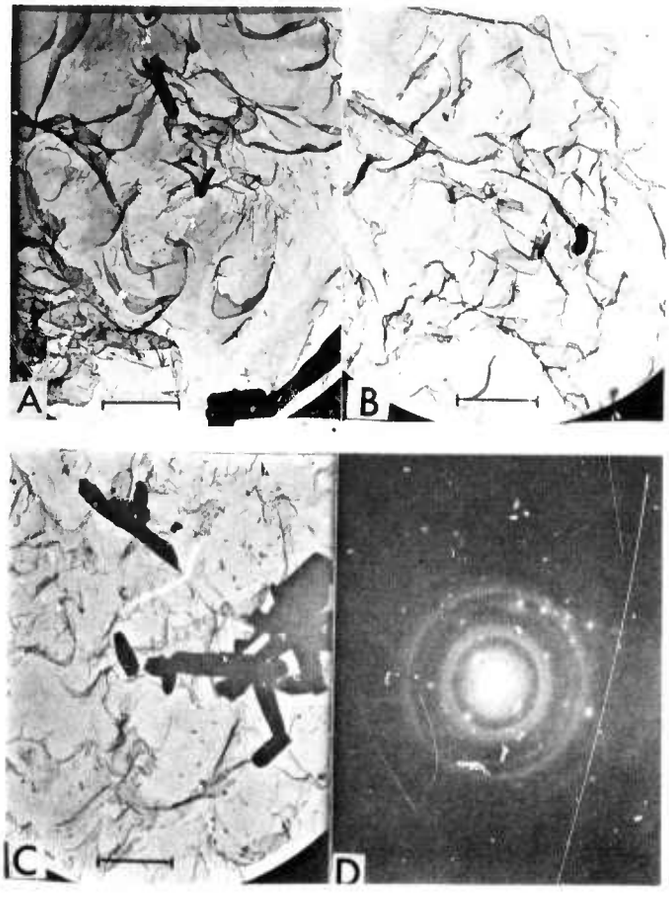

Figure 5.38 — Ford Stator #125, Grid F, white fracture (all α)
A, B, C: Typical surface replicas. Note ruggid appearance and elongated α grains (C)
D: Diffraction pattern off C. Dominant (100) ZA
5 μm scale bars

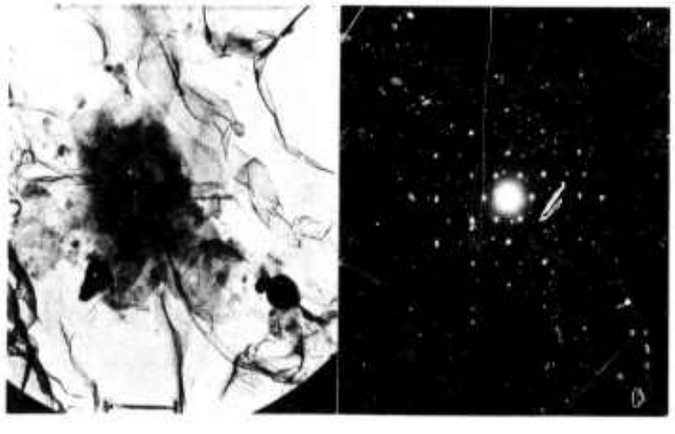

Figure 5.39 — Ford Stator #125, Grid F, white fracture (all α). Occasional collection of small particles of Si_2N_2O. Dominant (002) ZA
2 μm scale bar

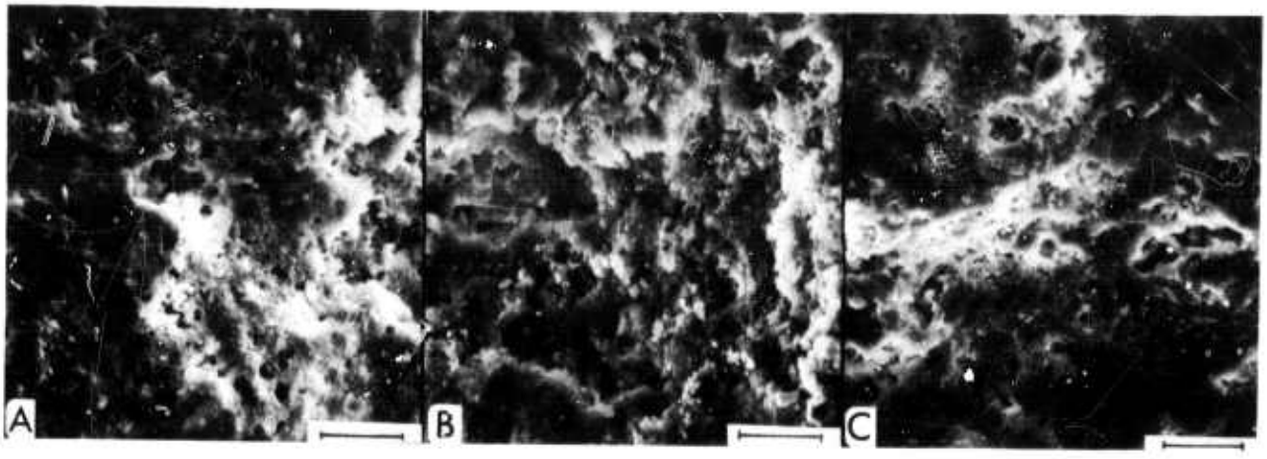

Figure 5.40 — Ford Stator #125. Scanning micrographs of fresh fracture surface, blade #7
A: Inner area of leading edge
B: Outer area of leading edge
C: Inner area of trailing edge

10 μm scale bars

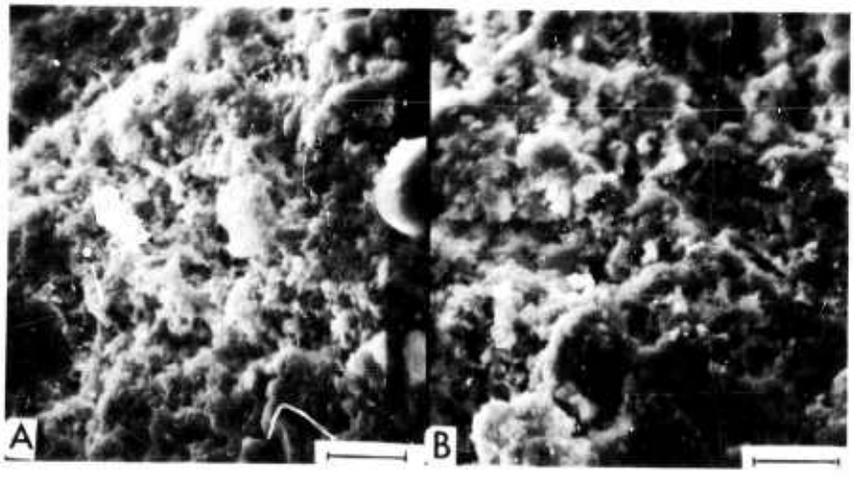

Figure 5.41 — Ford Stator #156. Scanning micrographs of fresh fracture surface, trailing edge of blade #17
A: Outer area B: Inner area

10 μm scale bars

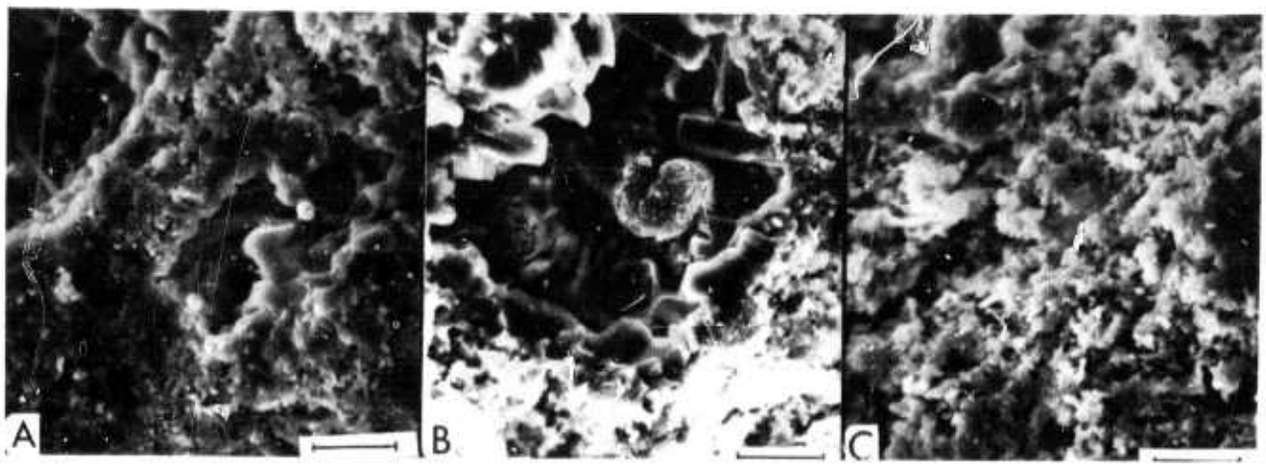

Figure 5.42 — Ford Stator #156. Seanning mierograph of fresh fracture surfaee, leading edge of blade #17
A, B: Inner area C: Outer area
10 μ m scale bars

5.3.2 GAS-SOLID REACTIONS

Introduetion

Compared to the thousands of hours expeeted from gas turbine components, the few hundred hours of testing possible in the pressurized test passage leaves unanswered questions about the effect of impurities on the long term corrosion-erosion resistance of silieon nitride and silieon carbide. For this reason, the kineties of aceelerated oxidizing and sulfidizing gas mixtures containing various impurities on these two eeramies are being studied in the temperature range between 1300°K (1800°F) and 1600°K (2370°F). Initially, these studies were performed at low gas stream veloeities for experimental convenience. When the results are compared with the eorrosion-erosion data obtained in the pressurized test passage, the importanee of the stream veloeity on the kineties of the gas-solid reaetions ean be established.

Thermochemical Analysis

Using the free energy data (ΔG_f^o) and the equilibrium constant data (log K_p) for silicon-nitrogen-oxygen and silicon-carbon-oxygen systems at 1300° and 1600°K, the oxidizing potentials of the reactive gas mixtures and the thermochemical stability of the condensed phases were determined as a function of the oxygen potentials of the gas mixtures. The free energy of formation (ΔG_f^o) and the equilibrium constant (log K_p) data for silicon compounds, carbon monoxide, carbon dioxide and carbon monomer gas were taken from the JANAF tables,[15] and are shown in Table 5.10. The diagrams were constructed by calculating the equilibrium expressions for coexistence of different condensed phases using the following thermodynamic equations:[16]

$$\Delta G = \Delta G^o + RT \ln K \quad (1)$$

$$\Delta G^o = -RT \ln K_p \quad (2)$$

$$\Delta G_R^o = \epsilon \Delta G^o \text{ (products)} - \epsilon \Delta G^o \text{ (reactants)} \quad (3)$$

The mass action constant K for a reaction

$$\alpha A + \beta B \rightleftarrows \gamma C + \delta D$$

is given by:

$$K = \frac{a_C^{\gamma} \; a_D^{\delta}}{a_A^{\alpha} \; a_B^{\beta}} \quad (4)$$

where a_A, a_B, a_C, a_D represent the activity of A.

At equilibrium: $K = K_p$ (5)

TABLE 5.10

THERMOCHEMICAL DATA FOR THE Si-N-O AND Si-C-O SYSTEM

Compounds & Species	$\Delta G^o f$ cal. mole^{-1}		Log Kp	
	1300°K	1600°K	1300°K	1600°K
Si_3N_4 (s)	-75,161	-51,850	12.636	7.082
SiC (s)	-14,636	-14,085	2.461	1.924
SiO_2 (s)	-162,207	-150,027	27.269	20.493
CO (g)	-54,126	-60,284	9.099	8.234
CO_2 (g)	-94,701	-94,739	15.920	12.940
C (g)	122,276	110,948	-20.558	-15.154
Si O (g)	-50,590	-56,244	8.505	7.683
Si O_2 (g)	-73,758	-73,722	12.400	10.070

Figures 5.43 and 5.44 summarize the thermochemistry for the condensed phases in the silicon-nitrogen-oxygen system at 1300° and 1600°K, respectively. The ordinate scale gives the nitrogen and the abscissa gives the oxygen partial pressure, both scales being logarithmic. The various lines in the diagram separate the regions of existence for Si(s), Si_3N_4(s) and SiO_2(s). The Si_3N_4-SiO_2 coexistence lines in Figures 5.43 and 5.44 give the nitrogen to oxygen pressure ratio at the nitride-oxide interface, and will be useful in evaluating the role of nitrogen diffusion outward through the oxide layer on the oxidation kinetics of Si_3N_4. If the nitrogen pressure builds up at the nitride-oxide interface, it can rupture the protective oxide layer causing further rapid oxidation of silicon nitride.

The pressures of SiO (g) or SiO_2 (g) which can form at the Si_3N_4-SiO_2 interface or over SiO_2 (g) during oxidation of Si_3N_4 in pure oxygen at 1 atmosphere are negligible. The formation of these volatile silicon oxides, therefore, will not affect the oxidation kinetics of Si_3N_4.

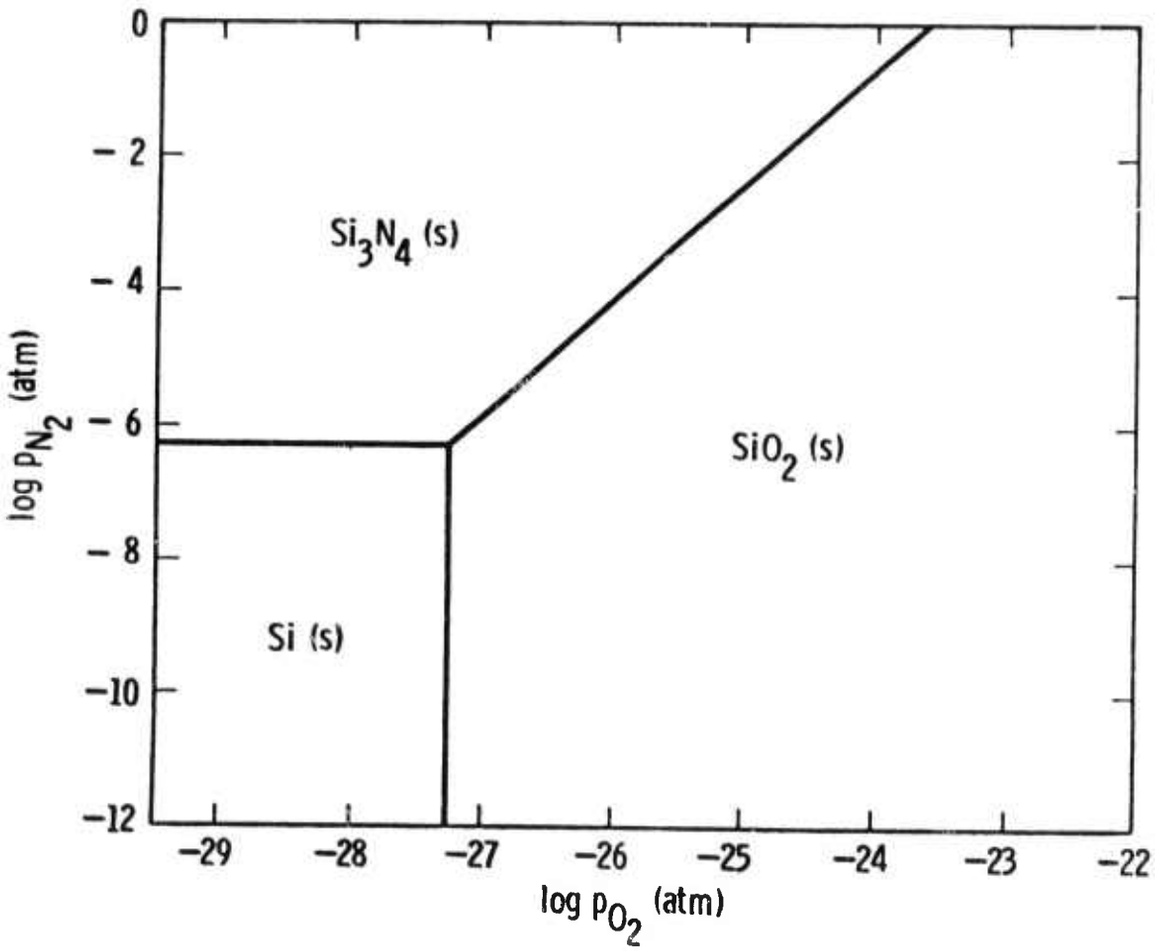

Figure 5.43 — Thermochemical Data for the Silicon-Oxygen-Nitrogen System at 1300°K

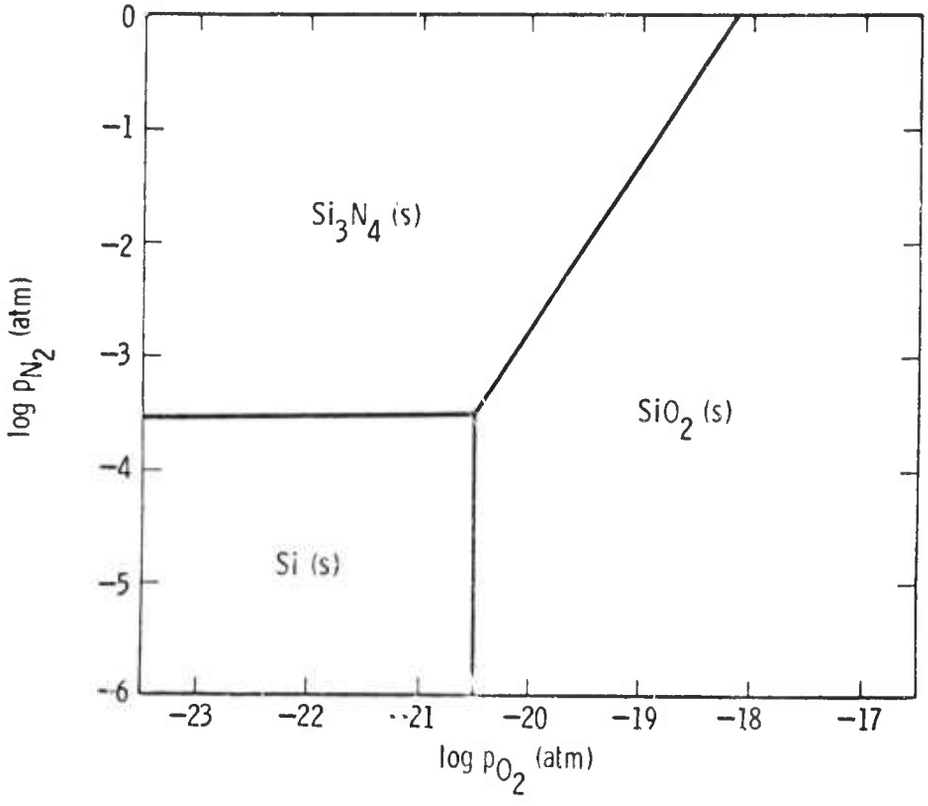

Figure 5.44 — Thermochemical Data for the Silicon-Nitrogen-Oxygen System at 1600°K

Figures 5.45 and 5.46 show the thermochemical diagrams for the silicon-carbon-oxygen system at 1300° and 1600°K, respectively. The ordinate scale gives the pressure of the carbon monomer; the abscissa gives the oxygen partial pressure and the pressure ratio for carbon monoxide to carbon dioxide. The thin diagonal lines in the diagrams give the carbon monoxide pressures. The thicker lines separate the regions of existence for Si(s), SiC(s), and SiO_2(s). Carbon monomer pressures higher than those for solid carbon have no meaning. These diagrams predict the oxidation behavior of SiC at various oxygen potentials which may be encountered in gas turbine environments. The SiC-SiO_2 line in the diagrams give the oxygen and carbon gas pressures at the carbide-oxide interface which are needed for solving the diffusion equations to evaluate the role of C(g) or oxygen diffusion through the SiO_2 layer.

The formation of SiO (g) on SiO_2 (g) is not expected to have an effect on the oxidation kinetics of SiC in pure oxygen at 1 atmosphere pressure.

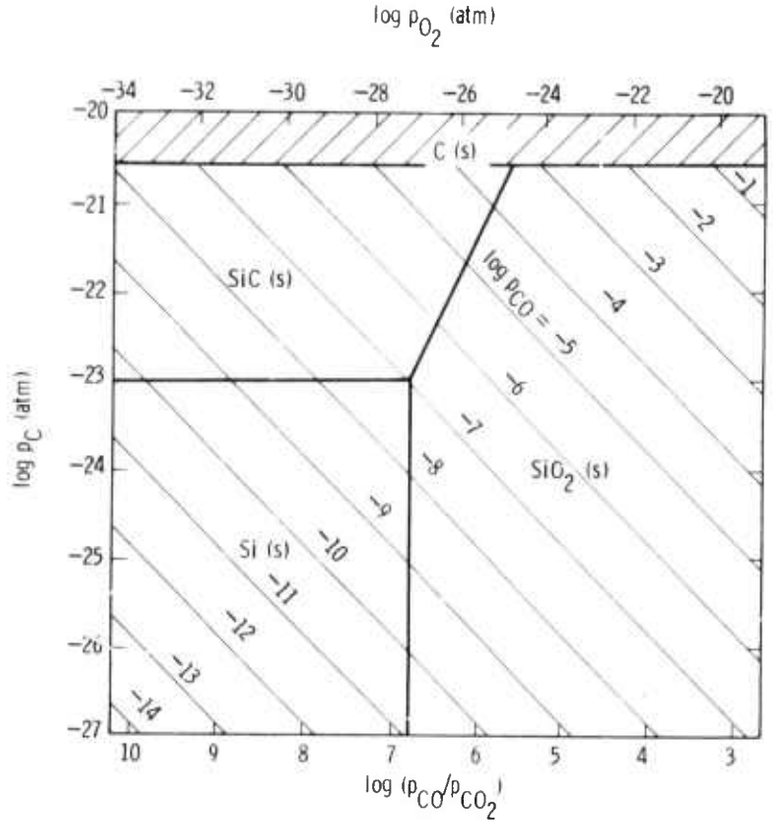

Figure 5.45 — Thermochemical Data for the Si-C-O System at 1300°K

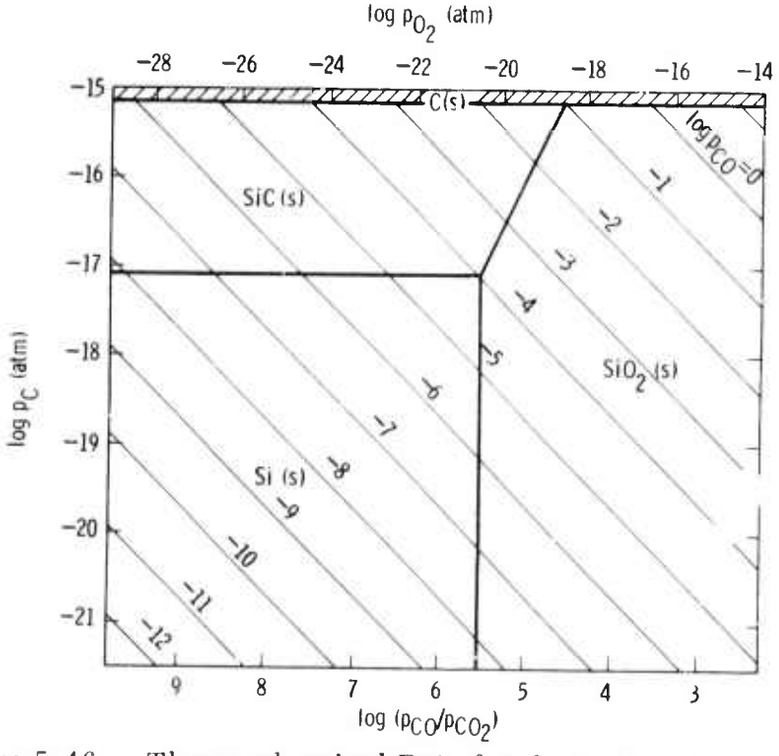

Figure 5.46 — Thermochemical Data for the Si-C-O System at 1600°K

Experimental Approach

The oxidation kinetics are being studied by continuously measuring the changes in the weight of a silicon nitride sample as a function of time in different gas mixtures using a Cahn automatic recording electrobalance. The maximum capacity of the balance is 100 gr with a sensitivity of 2×10^{-6} gr. The experimental arrangement is shown in Figure 5.47. The electrobalance is positioned above a vertical platinum resistance furnace. The temperature of the furnace is controlled to within $\pm$ 1°C using a Pt/Pt-10% Rh thermocouple connected to a proportionating temperature control system.

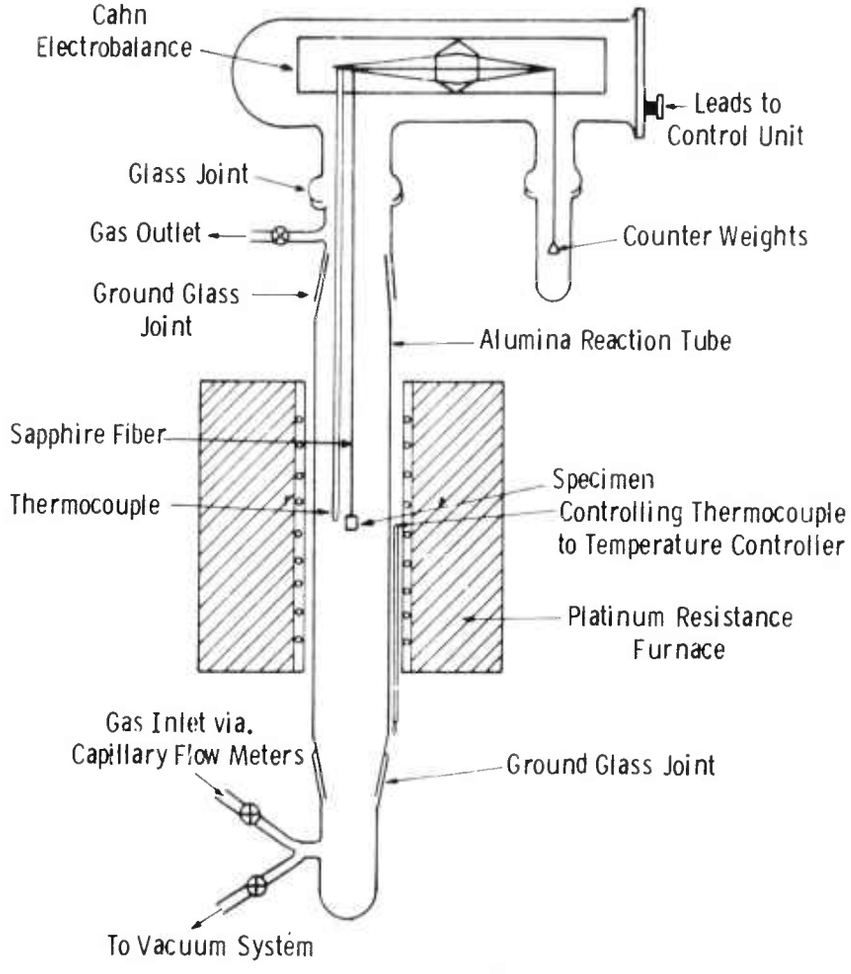

Figure 5.47 — Static Gas-Solid Kinetic Experimental Apparatus

The sample to be studied is cut to a 1" x 0.5" x 0.050" plate and polished metallographically with up to 3 micron size diamond paste to obtain a smooth surface finish. The polished and cleaned specimen is suspended from the microbalance with a single crystal sapphire fiber of 0.010" diameter, bent at each end into a U-shaped hook. The temperature of the sample is measured with a Pt/Pt-10% Rh thermocouple held in place adjacent to the specimen.

The preliminary experiments were conducted on Norton's hot pressed Si_3N_4 in pure oxygen at 1 atm pressure. After suspending the specimen from the microbalance, the alumina reaction tube was alternately evacuated and purged with purified argon several times to obtain a clean system. A flow of purified argon at the rate of 511 ml/min., measured with a pre-calibrated capillary flowmeter, was then started and the furnace heated up slowly to prevent any cracking of the Si_3N_4 sample or the alumina reaction tube. After the furnace had reached the desired temperature, argon flow was stopped and dried oxygen gas passed through the system at the rate of 500 ml/min. The change in the sample weight was automatically recorded as a function of time on a strip chart recorder.

After completion of the run, oxygen was cut off from the system and argon flow started again to prevent any further oxidation of the sample. The furnace was then cooled slowly to room temperature and the oxidized samples were analyzed by metallographic and x-ray diffraction techniques.

Static Oxidation

Preliminary experiments were carried out to study the rate of oxidation of hot pressed Si_3N_4 as a function of time at 1800°F and 2000°F. Figure 5.48 shows the weight gain curves at 1800°F and 2000°F for the oxidation of silicon nitride in pure oxygen at 1 atm pressure.

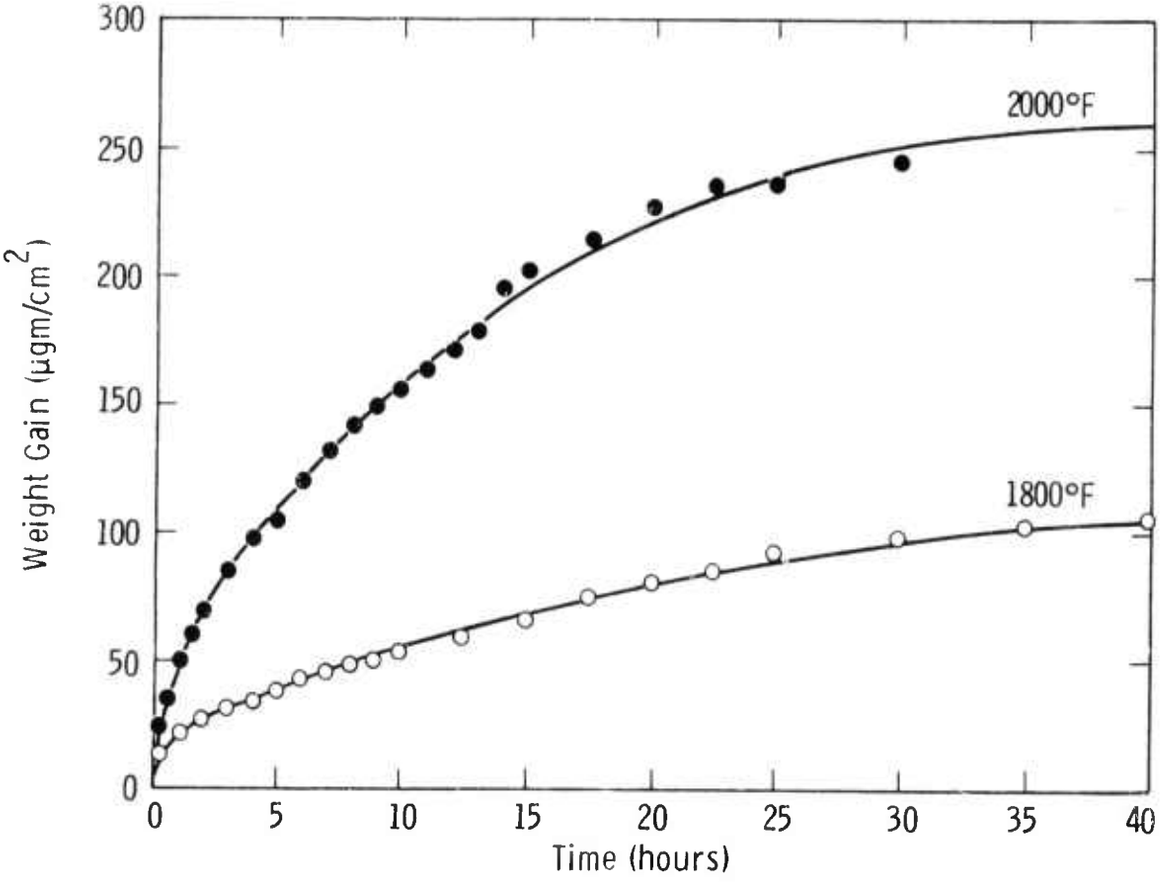

Figure 5.48 — Oxidation of Hot Pressed Si_3N_4 in Oxygen at 1 atm

The parabolic rate law[16,17] was used to interpret the oxidation data, according to which:

$$W^2 = At + C$$

where W is the weight gain at time t, A is the parabolic rate constant, and C is another constant. Figure 5.49 shows the plots of the square of the weight gain (W^2) as a function of time for the oxidation of Si_3N_4 at 1800° and 2000°F. These plots are straight lines showing that the oxidation of silicon nitride in pure oxygen follows the parabolic rate law with parabolic rate constants of about 3.5×10^{-14} and 6.6×10^{-13} $g^2cm^{-4}sec.^{-1}$ at 1800 and 2000°F, respectively. Since the parabolic rate law is derived assuming oxidation involves diffusion of some species, it suggests that the oxidation of Si_3N_4 is controlled by the diffusion of oxygen through the initial oxide layer.

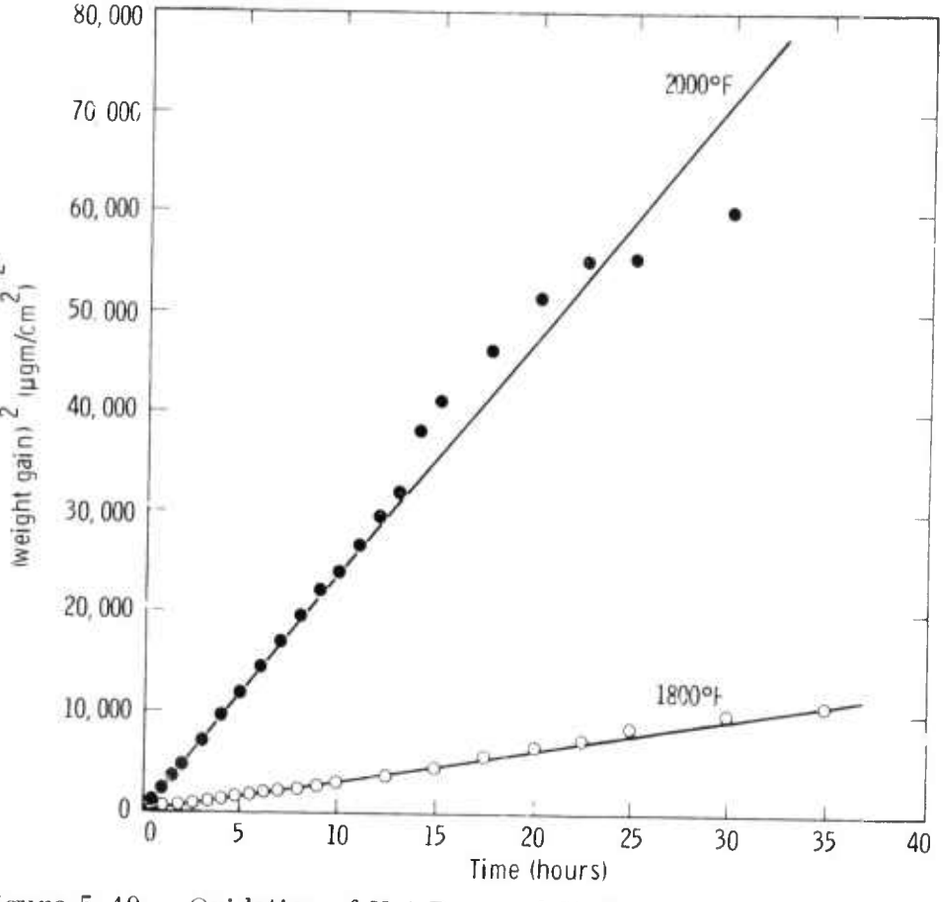

Figure 5.49 — Oxidation of Hot Pressed Si_3N_4 in Oxygen at 1 atm

The surface layers on the oxidized samples were analyzed using x-ray diffraction techniques. It was found that cristobalite formed on silicon nitride samples oxidized at 2000°F. The oxide layers on future oxidized samples will be completely characterized using metallographic, x-ray diffraction and scanning electron microscopic techniques.

Figure 5.49 shows that the weight gain values at 2000°F after about 12 hours deviate considerably from the parabolic rate law plot. This experiment was conducted using a quartz rod for suspending the specimen from the microbalance. The devitrification of the quartz rod and subsequent loss in its weight due to loss of SiO_2 particles probably caused the weight gain measurements after about 12 hours to be erroneous. The oxidation experiments at higher temperatures are now being conducted using single crystal sapphire fiber for suspending the specimen from the microbalance. The oxidation behavior of Si_3N_4 will be completely investigated from 1800° to 2550°F in pure oxygen, oxygen-argon and oxygen-nitrogen mixtures to understand the oxidation mechanism and the effect of nitrogen at the nitride-oxide interface on the oxidation kinetics.

Conclusions

The correct interpretation of microstructure and how it relates to fabrication is important to the understanding of material performance at elevated temperatures. Many microstructure details of high density silicon nitride have been identified and similar work is in progress for silicon carbide. Future work will be directed toward correlating microstructure and mechanical properties and to use this information for improving the high temperature properties of both silicon nitride and silicon carbide.

The study of kinetics of gas-solid reactions was initiated for silicon nitride and silicon carbide, including experimental determination of the oxidation rate of silicon nitride. These studies will continue for both of these materials in order to provide a basis for understanding long term stability in high temperature gas turbine environments.

5.4 NON-DESTRUCTIVE EVALUATION OF MATERIALS

5.4.1 ULTRASONIC NDT

SUMMARY

Ultrasonic evaluation has proven to be an NDE method which provides sensitive location of internal flaws. Ceramic components are evaluated for subsurface defects by C-scan methods, and homogeniety is determined by measuring sonic velocity. Procedures were established to optimize the testing technique on simple shapes of representative material. This included fabricating standards with known sound energy reflectors to represent flaws.

Introduction

The development of the vehicular gas turbine engine, as was pointed out in the introductory section of this report, is an iterative process. The actual testing of ceramic engine components becomes a vital step in this process. While much effort is being spent on developing materials with good mechanical properties, and fabrication methods which consistently yield high quality components, it is additionally desirable to be able to detect the presence of unknown flaws and defects in these components prior to use. The purpose of the work on non-destructive evaluation is to develop techniques which will quickly and accurately determine whether ceramic engine components have acceptable quality.

Ultrasonic evaluation of polycrystalline ceramic bodies has been chosen as the method offering the greatest sensitivity in locating subsurface flaws as well as providing qualitative information. This data, coupled with radiographic, dye penetrant, proof testing, and destructive analysis and testing, is deemed necessary to determine the quality of ceramic hardware and to evaluate the effects of processing and fabrication variables.

Magnaflux ultrasonic C-scanning equipment (Figure 5.50) with an operating frequency of .5-15 MHZ, was selected and a program initiated to establish the instrumentation parameters necessary to evaluate two ceramic systems which currently are used in the vehicular gas turbine engine. Reference blocks with artificial flaws were made from lithium-aluminum silicate (which is the material used to make ceramic heat exchangers) and silicon nitride, to represent standards from which C-scan techniques could be developed. The optimized ultrasonic evaluation procedures were then applied to test specimens fabricated from the two ceramic systems.

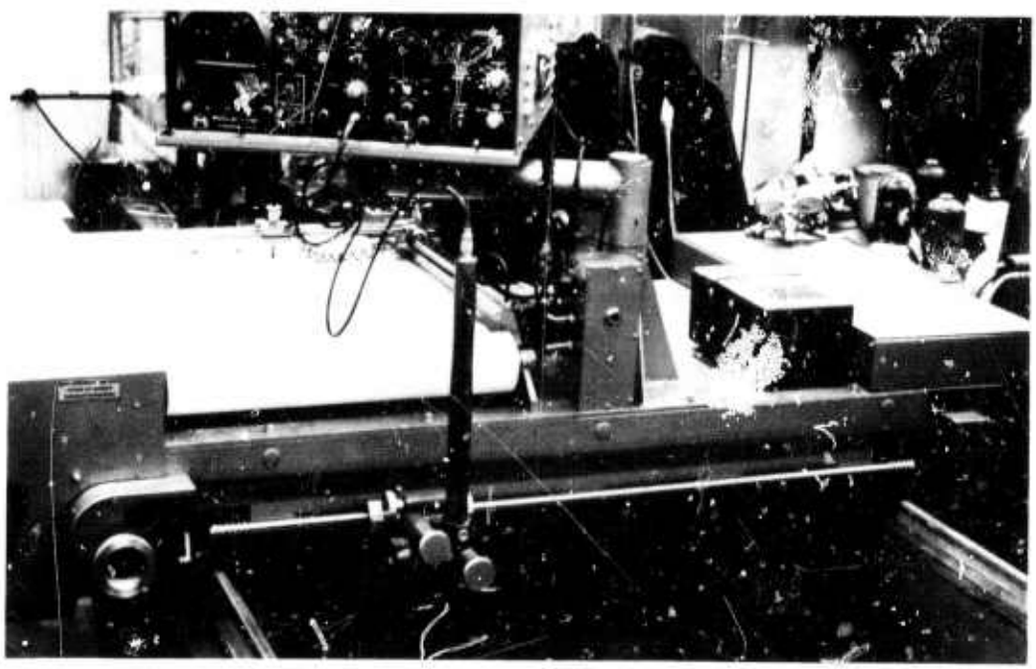

Figure 5.50 — Ultrasonic Defect Detection Equipment

Procedures were also developed to measure the sonic velocity in both longitudinal and transverse directions in order to determine the dynamic modulus of elasticity of these and other ceramic materials. This information was then used as one of the parameters in evaluating candidate materials as well as providing an indication of the quality of ceramic components.

Standards and Procedure Optimization

The reference blocks, used to establish the procedures for the lithium-aluminum-silicate material were approximately 1.25 x 1.25 x 4.0 inches (Figure 5.51). Flat bottomed holes [illegible]4, 4/64, 6/64, and 8/64 inch in diameter were ultrasonically drilled in the ceramic reference samples to represent identifiable sound energy reflectors. Three hole depths were selected to represent flaws located at 25%, 50% and [illegible]% of the reference thickness of 1.25 inches.

A similar procedure was used for preparing silicon nitride components. Flat bottomed holes were drilled by conventional means in a block of unfired material .75 x 1.75 x 4.5 inches which was later reaction-sintered. (Figure 5.51) This did not produce as flat a reflector as was achieved by ultrasonic drilling and resulted in a slight distortion in the resulting C-scans. The reference block contains three rows of flat bottomed holes machined to a depth of 30%, 50% and 70% of the total thickness of .75 inch. Each row contains holes with diameters ranging from 8/64 inches to 1/64 inches, in 1/64 inch increments.

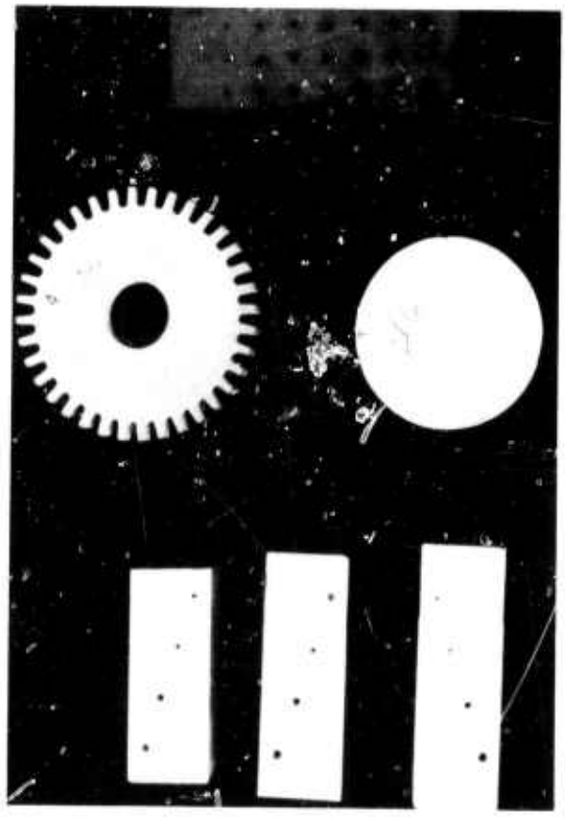

Figure 5.51 — Test Samples for Ultrasonic Defect Detection

Several transducers, varying in frequency, size and element material were evaluated to determine those best suited for the ceramic materials. The best C-scans for both materials were obtained using a focused 5 MHZ lithium sulphate transducer with a focal length of 4.0 inches in water. This provided the best resolution while retaining good sensitivity and penetration. Variables such as part geometry, porosity and the characteristic attenuation of sound energy for a given material were found to be most troublesome in optimizing the evaluation procedures.

Applications

Round spin test samples (Figure 5.51) fabricated from lithium-aluminum-silicate and slip cast silicon nitride were selected to determine the applicability of the reference scanning techniques. The geometries were relatively simple and with the exception of the tooth-like area on the silicon nitride specimens, minimized the problem of interpreting edge effects in the scanning results. All C-scans were made at a 1:1 recording ratio.

Typical C-scans of the silicon nitride specimens are shown in Figure 5.52, 5.53 and 5.54. Figure 5.55 indicates no flaws in the part, and a scan of the reference block made at the same time indicates the attenuation of the signals with depth as well as insufficient reflected energy, relative to the instrumentation settings, from the smaller flat bottomed holes. Figures 5.53 and 5.54 show the C-scan results after increasing the sensitivity. Flaws are now visible in both the spin disk and reference block.

Figure 5.55 shows the C-scan results for the lithium-aluminum-silicate spin disks. Four disks with flaws varying in number and size indicate the defects which may be found in this material. Sectioning was performed on several similar disks to verify the flaws found ultrasonically. It was found that porosity segregation of relatively small magnitude reflected sufficient sound energy, such as to appear on the final C-scan the same as a shrinkage crack or an impurity-matrix interface. This points out that while ultrasonic scanning is very sensitive, other techniques are needed to interpret the nature of the types of flaws indicated.

Radiographic analysis, using a 140KV x-ray unit, indicate fewer flaws than the ultrasonic inspection in specimens of both materials. No attempt was made, other than establishing exposure times, to further refine the radiographic process for these test specimens.

Dynamic Modulus of Elasticity Measurements

Sonic velocity measurements in a longitudinal and transverse mode were made to determine sample block and component homogenity. These measurements were also used to determine the dynamic elastic modulus and comparisons were made between representative sample blocks and actual components.

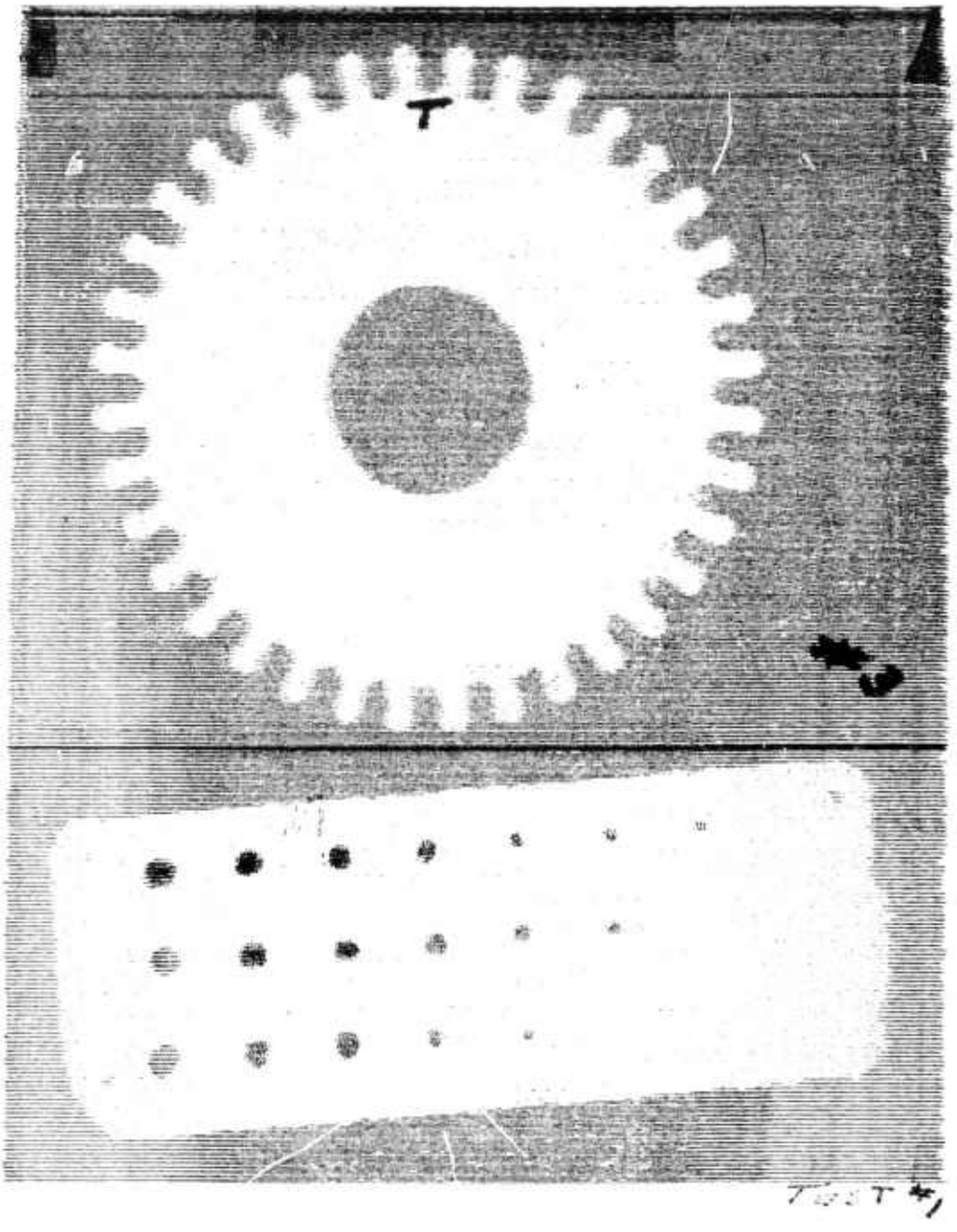

Spin Disk #3 Vern. Set. 1.2

No Flaws

Figure 5.52 — C-Scan of Silicon Nitride Test Samples

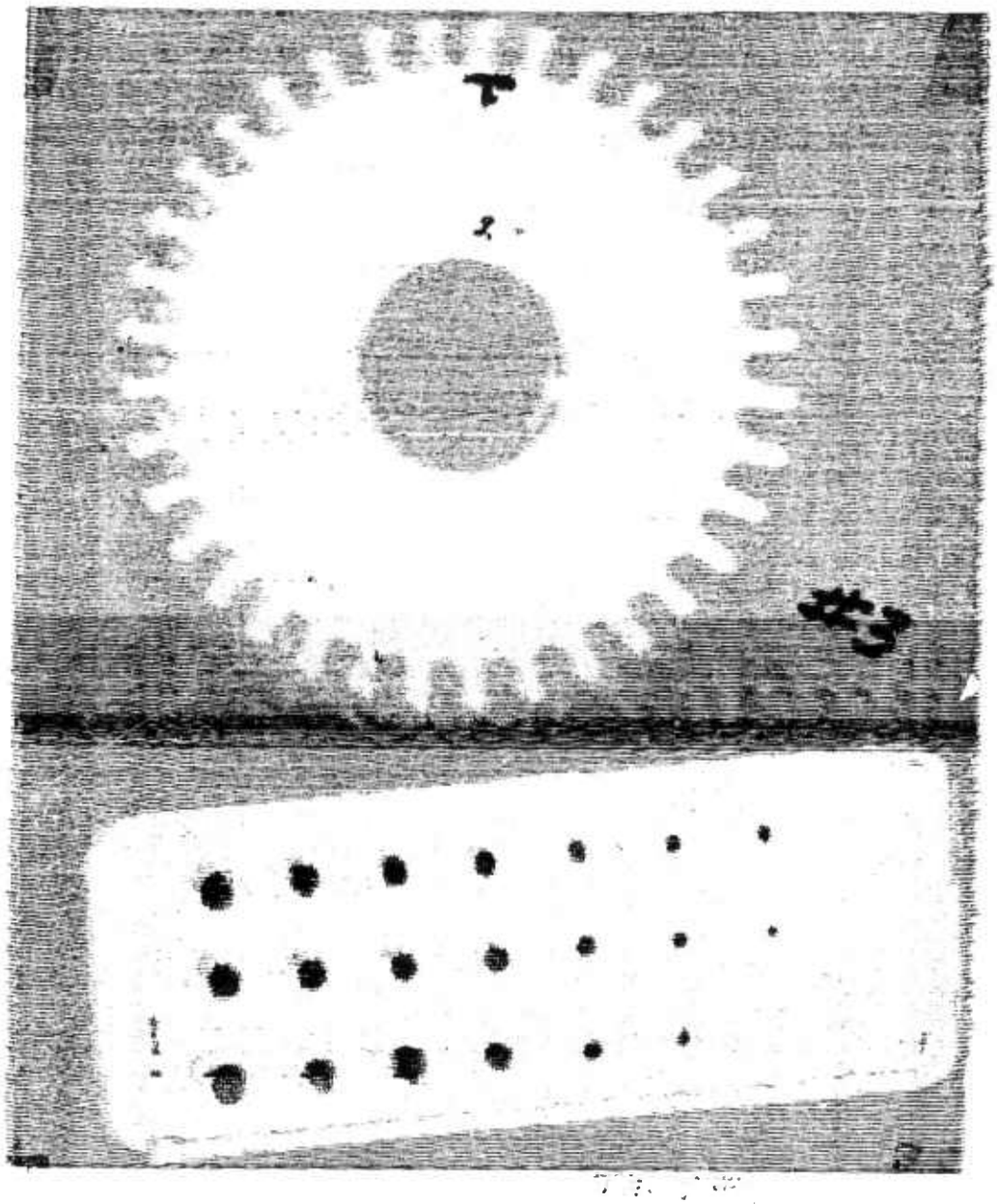

Spin Disk #3 Vern. Set. 1.5

Flaw No.	Depth (In.)
1.	.55

Figure 5.53 — C-Scan of Silicon Nitride Test Samples

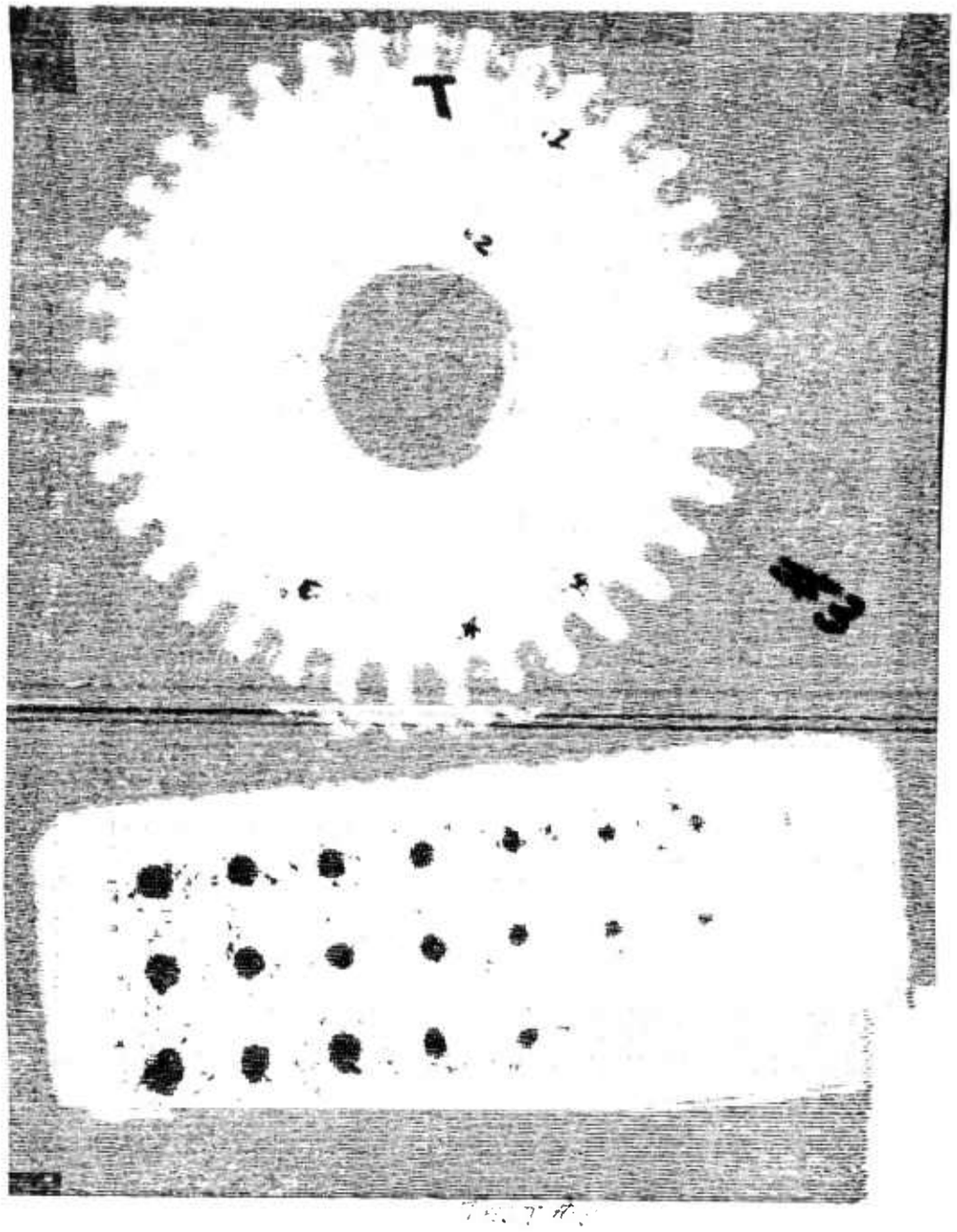

Spin Disk #3 Vern. Set. 1.8

Flaw No.	Depth (In.)
1.	.38
2.	.55
3.	.35
4.	.42
5.	.28

Figure 5.54 — C-Scan of Silicon Nitride Test Samples

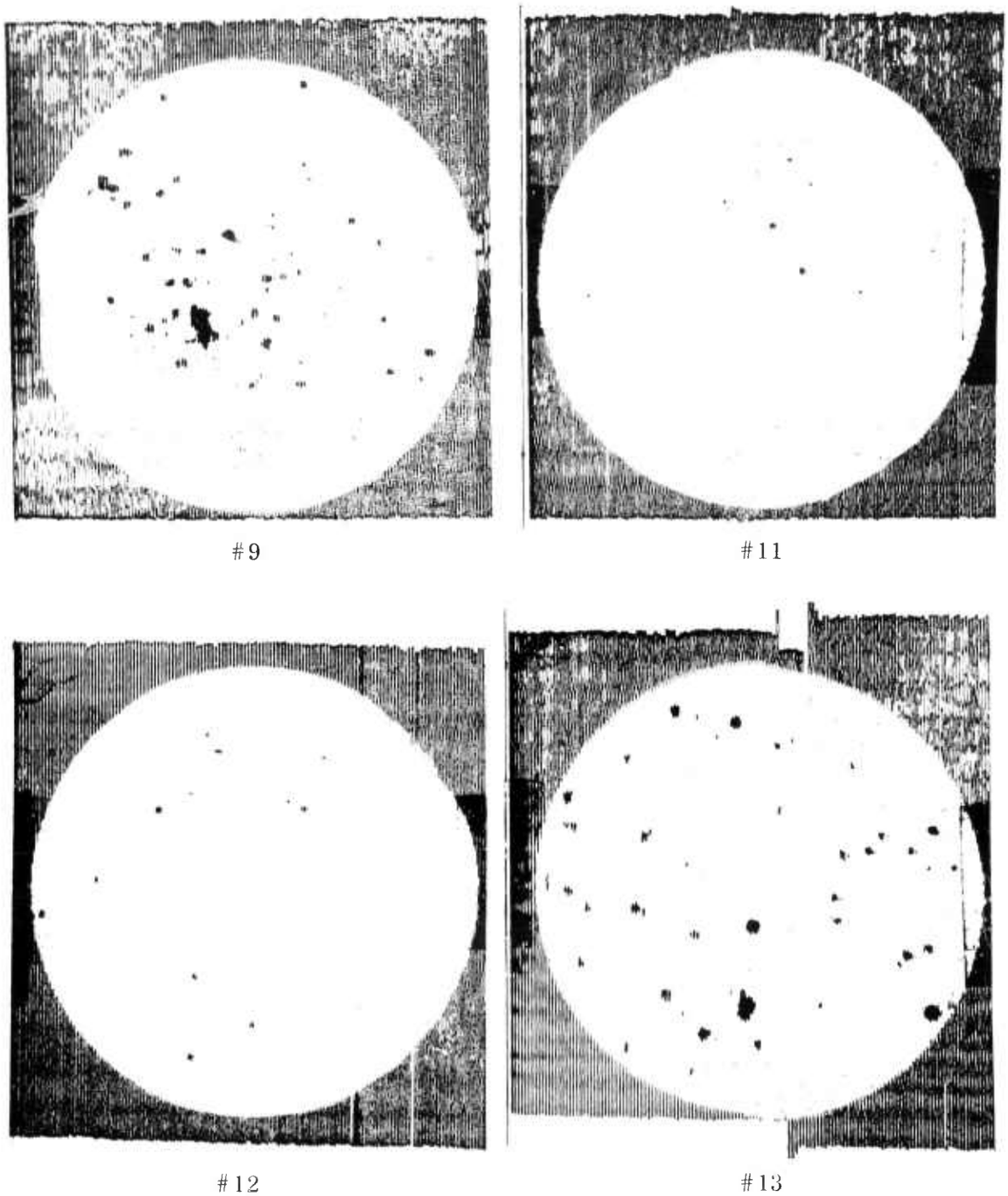

#9 #11

#12 #13

Figure 5.55 — C-Scan of Lithium Aluminum Silicate Disks

Sonic velocity measurements on lithium-aluminum-silicate material were accomplished using contact techniques, with a Magnaflux PS-902 display unit, a 5 MHZ PZT longitudinal wave transducer, and a 5 MHZ quartz shear wave transducer. A reference piece of aluminum, .50 inch thick, with a longitudinal velocity of 6.34 (10^5) cm/sec. and a transverse velocity of 5.10 (10^5) cm/sec, was used to display three back reflections on the display unit corresponding to 3.0 cm. on the CRT horizontal scale. From the three back reflections displayed, the scale factor was determined.

The equations used to calculate the sonic velocities were,

$$V_L = 6.34\ (10^5)\ (3.0/F_L)\ (\text{Thick}/.50)\ \text{cm/sec}$$

$$V_T = 5.10\ (10^5)\ (3.0/F_T)\ (\text{Thick}/.50)\ \text{cm/sec}$$

where F_L and F_T are the longitudinal and transverse scale factors for the ceramic material being measured, V_L is the longitudinal velocity and V_T is the transverse velocity. The elastic modulus was then calculated using the following equation,

$$E = (V_L^2)\ (e)\ (1 + \mu)\ (1 - 2\mu)/(1 - \mu)\ \text{dynes/cm}^2$$

where:

e = the density in gms/cc

μ = Poisson's ratio calculated from the equation:

$$\mu = \left[1 - 2\ (V_T/V_L)^2\right] / \left[2 - 2\ (V_T/V_L)^2\right].$$

The longitudinal and transverse sonic velocity of this material varied from 5.18 to 6.25 (10^5) cm/sec. and 2.99 to 3.41 (10^5) cm/sec respectively. These values indicate the variation which can be expected for this ceramic and depict the effects of processing and thermal history.

Conclusions

The ultrasonic detection of subsurface flaws has proven to be more sensitive than radiographic analysis. There is a definite need to categorize the ultrasonically-detected flaws, since their effect on component performance is not known.

The most troublesome, but not insurmountable, variables encountered in optimizing the evaluation procedures were part geometry, inherent porosity, and the characteristic attenuation of sound energy.

Sonic velocity measurements have proven quite useful in depicting the effects of fabrication variables. Any inhomogeniety present is readily verified by these measurements.

The procedures developed to date will be applied to various engine components. This includes subsurface flaw detection by C-scanning and velocity measurements by the immersion techniques. Quality acceptance levels will be ultimately established for all ceramic hardware.

5.4.2 ACOUSTIC EMISSION

SUMMARY

Acoustic emission techniques can be applied to detect the onset of catastrophic failure in ceramic materials. The AE response to stress, for material tested in four point bending, has exhibited a precusor to final failure. This implies a transition from microcracking to unstable macrocracking, resulting in catastrophic failure of the test bar. During this series of tests, an unstable crack was monitored using acoustic emission rate versus time at a constant load. This type of test is directly applicable to proof-testing actual components, by static means, to determine subcritical and critical crack growth.

Introduction

Acoustic emission tests were initiated in an effort to obtain greater insight into the fracture mechanisms of polycrystalline ceramics. Acoustic emission appears to be a valuable tool for the determination of design limits for ceramics since the relationship of applied stress to material damage can be measured. In addition, this technique should be most useful in relating the influence of flaws to the initiation of microcracks.

Instrumentation was used at the University of Michigan in Ann Arbor and tests were conducted on test bars of lithium-aluminum-silicate, the material used for gas turbine heat exchangers.

Acoustic Emission Instrumentation

The instrumentation used to detect, amplify, and filter the emitted signals is shown in Figures 5.56 and 5.57. The piezoelectric transducer is a lead-zirconate-titanate (PZT) type. The amplifiers provide an overall system voltage gain of 1×10^5 with the filters operating between 100 KHZ and 300 KHZ. The signals to the counting circuitry are externally attenuated by a potentiometer which limits the background noise level. After establishing the proper attenuator setting only slight variations were necessary to continue testing from day to day. An audio monitor was used very effectively in detecting small differences in the acoustic emission rate which were not obvious on the acoustic emission summation curves. The X-Y recorder and Sanborn recorder which monitored the applied load were always started together so that a direct correlation could be made between stress and acoustic emission response. The mechanical loading of a specimen in 4-point bending provides a means of applying a stress while monitoring the acoustic emission response during the test. Teflon tape was used to reduce the effects of relative movement between the test specimen and the knife edges of the bending fixture as shown in Figure 5.58. Adhesive tape was used at all other points of loading within the load frame to reduce noise. The load was applied by a hand pump and hydraulic ram fixed in a framework. This eliminated the possibility of extraneous machine noise, which may be encountered when using automated loading devices.

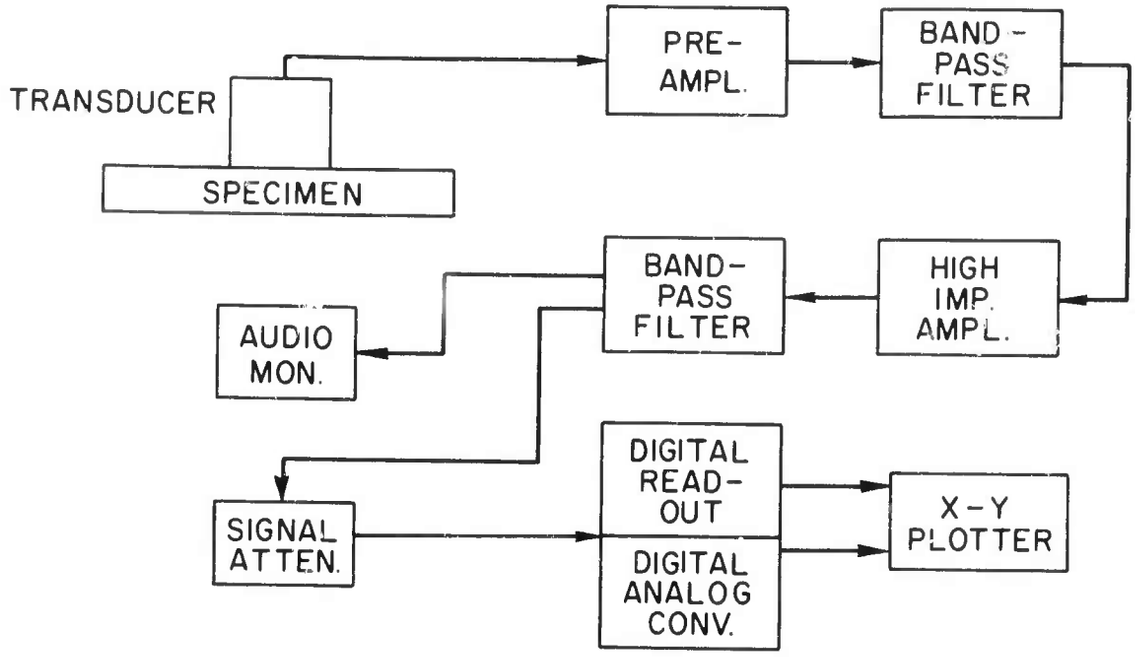

Figure 5.56 — Instrumentation Diagram

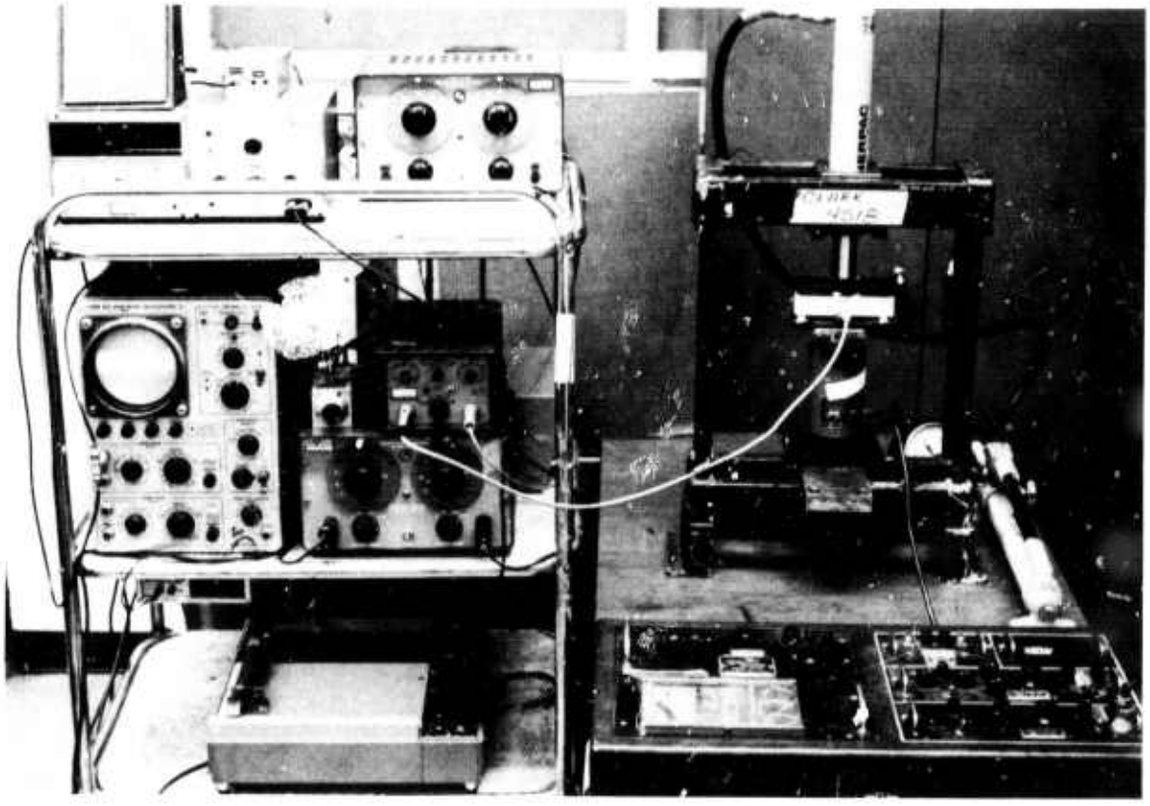

Figure 5.57 — Acoustic Emission Apparatus

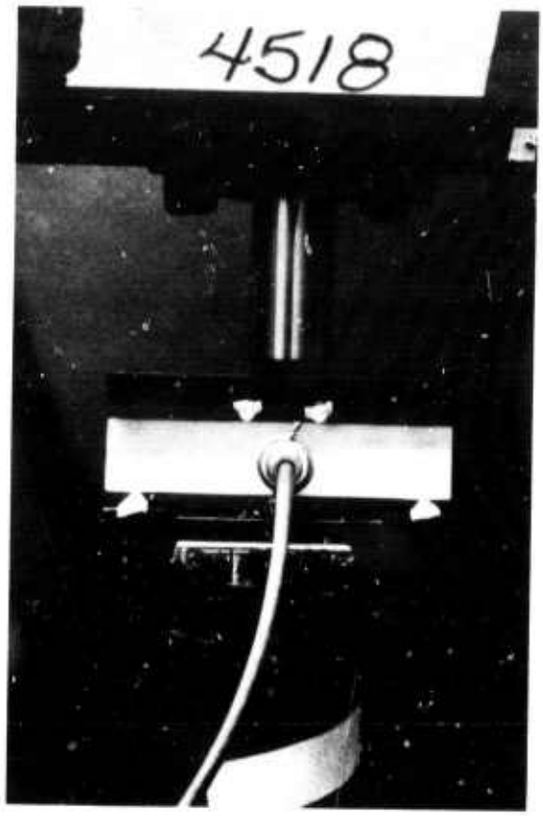

Figure 5.58 — Method of Loading Specimens for Acoustic Emission Testing

The first series of tests were conducted to establish the feasibility of applying acoustic emission techniques to ceramics by mechanical loading. Curves generated during this sequence depict an approximate load since no load cell was used. A calibrated gauge on the hydraulic system reflected the load obtained. During this time, a scale which allowed early detection of the onset of catastrophic failure was established along with an acceptable background noise level prior to testing. It was also concluded that acoustic emission summation provided a better characterizing parameter than acoustic emission rate. A second series of tests included a load cell and a Sanborn recorder which afforded an accurate determination of stress for any given point on the acoustic emission curves.

Materials and Test Procedure

Rectilinear ceramic bars of lithium-aluminum silicate (LAS) material were tested. This material is a polycrystalline ceramic with a closed-cell pore structure. It is made by slip-casting and sintering, a process that produces voids, shrinkage cracks and segregated porosity, which would suggest a "noisy" material when subjected to a specific stress level.

The bars tested had dimensions of 1-1/4 x 1-1/4 x 6 inch. Two attempts were made to reduce the amount of contact area under the knife-edges by chamfering the upper and lower surfaces such that a narrow strip only was in contact. However, it was found that the noise emitted at the ceramic-teflon-knife edge junction was always one order of magnitude lower than that detected during stressing at low loads, so the amount of contact area did not affect the results. Low loads are meant to be less than 40% of the ultimate fracture load for this material. No particular attempt was made to reduce the potential source of noise due to the test bar edges chipping under the knife-edges. This did not appear to be a problem during these tests.

The ceramic bars were cut from sample blocks representing material with a specific composition and thermal history. These sample blocks exhibit segregated porosity with a finite thickness along the center plane, since this area is the last to solidify in the slip-casting process. The bars were oriented in the bending fixture with the porosity plane both perpendicular to and coinciding with the neutral axis. The results are inconclusive as to whether the low density area contributes to the acoustic emission response of the bars.

The dynamic conditions in the test bars were accomplished by incremental loading with the hydraulic ram. Audio monitoring and visual monitoring of the digital readout on the counter and the X-Y recorder indicated the magnitude of acoustic emissions generated. The recorded data are shown in Figures 5.59, 5.60, 5.61, 5.62, and 5.63.

Discussion of Data

Figure 5.59 is indicative of the acoustic emission response of LAS material having a characteristic modulus of rupture of 5000 psi and 7.0% apparent porosity. The increase in acoustic emission is very evident several seconds prior to failure. It should be noted that the bar was preloaded to approximately 1600 lbs. to eliminate the signals generated at lower stress levels. This resulted in clarification of the data output by utilizing the Kaiser effect, defined as the lack of stress wave emission until the previous stress level is exceeded.

The next series of curves, Figures 5.61, 5.62 and 5.63 again indicate impending failure, however, it is detected well before catastrophic failure of the test bar. The effects of loading in the critical stress region where significant damage can occur is also shown in this series of curves. Reducing the load and then reloading results finally in a failure at a reduced level. This suggests that cumulative damage, such as the initiation of many microcracks, ultimately reduced the load bearing area which resulted in the bar reaching a critical stress level at a lower load.

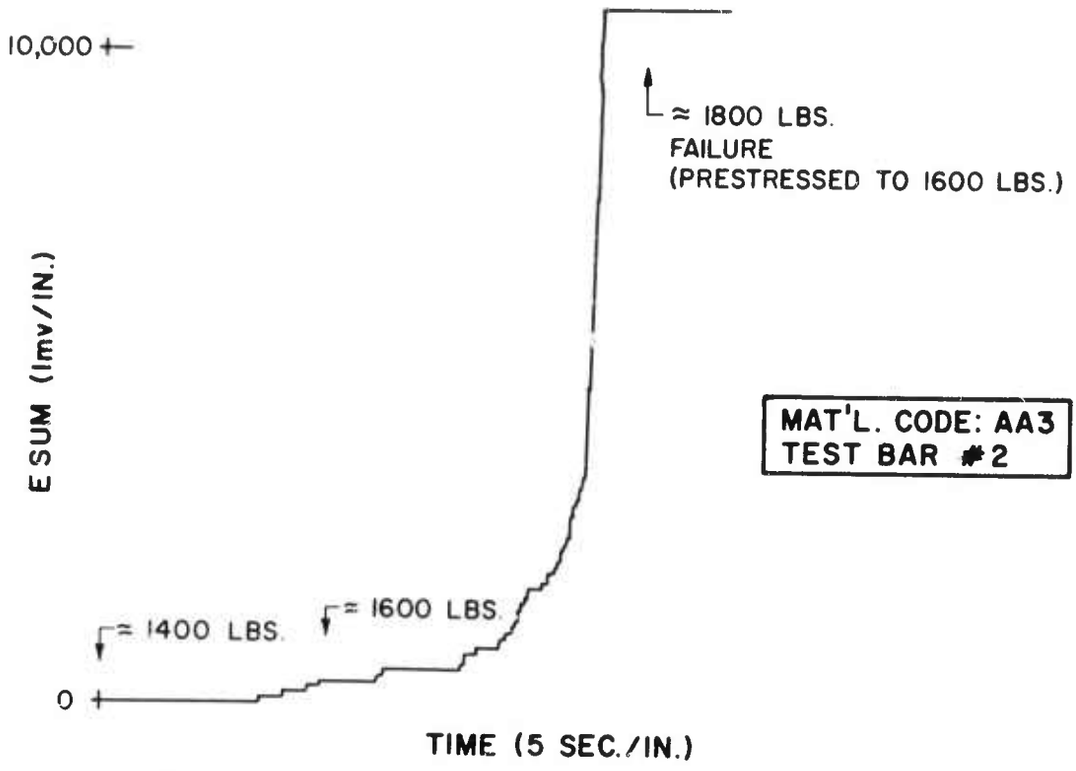

Figure 5.59 — Acoustic Emission Summation vs Time
Corning 9453

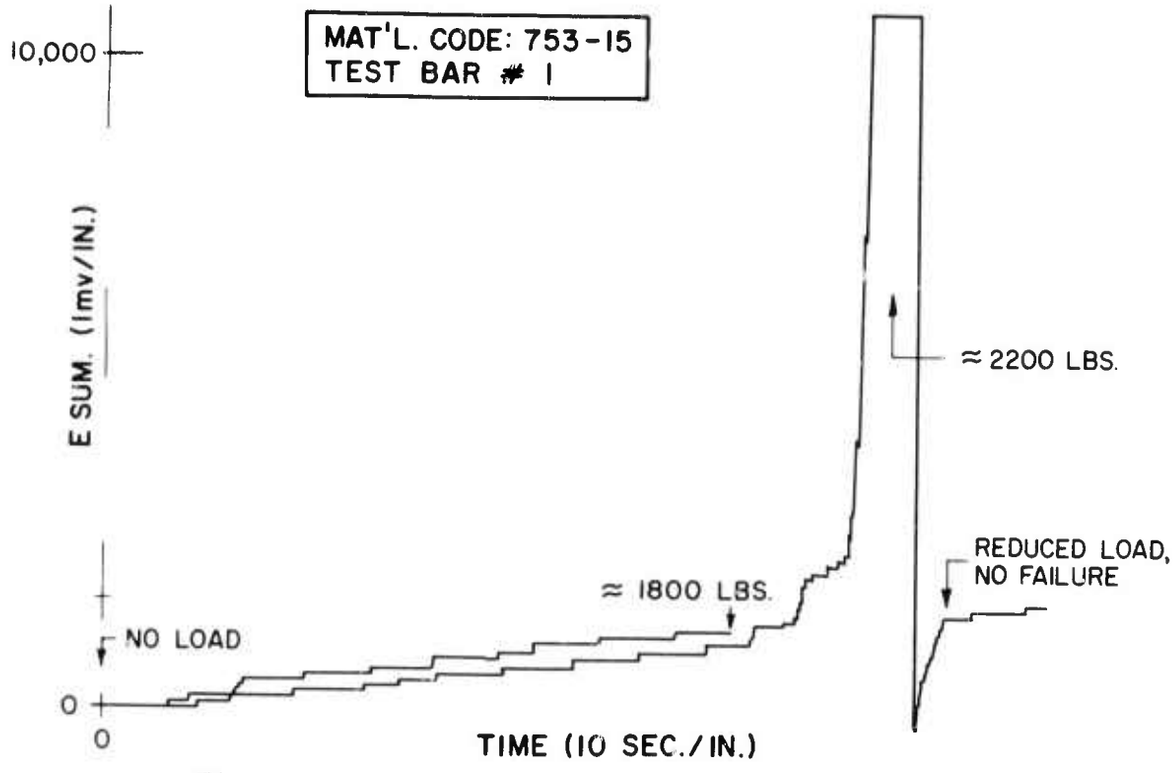

Figure 5.60 — Acoustic Emission Summation vs Time
Corning 9458

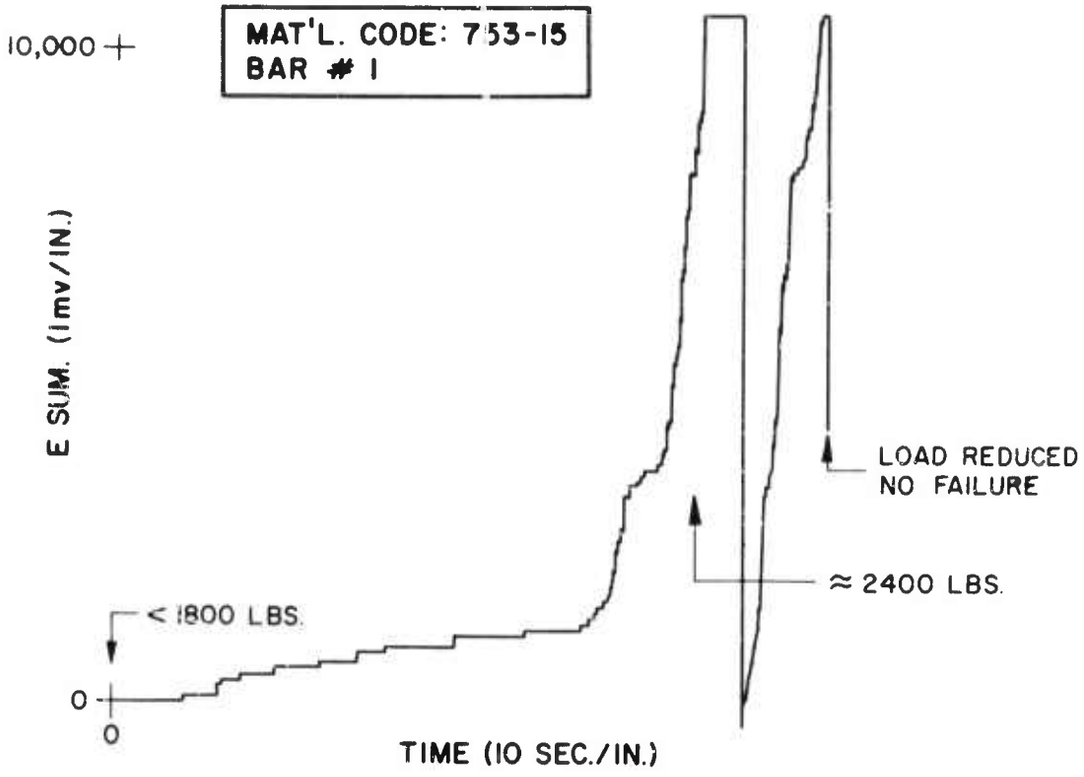

Figure 5.61 — Acoustic Emission Summation vs Time
Corning 9458

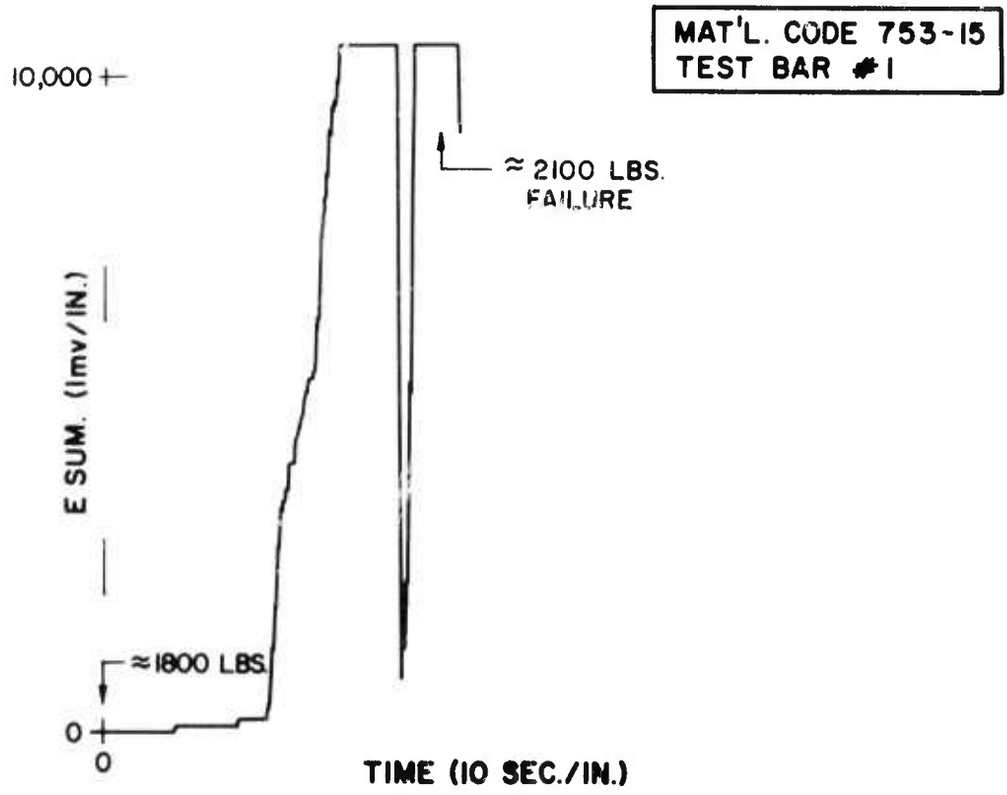

Figure 5.62 — Acoustic Emission Summation vs Time
Corning 9458

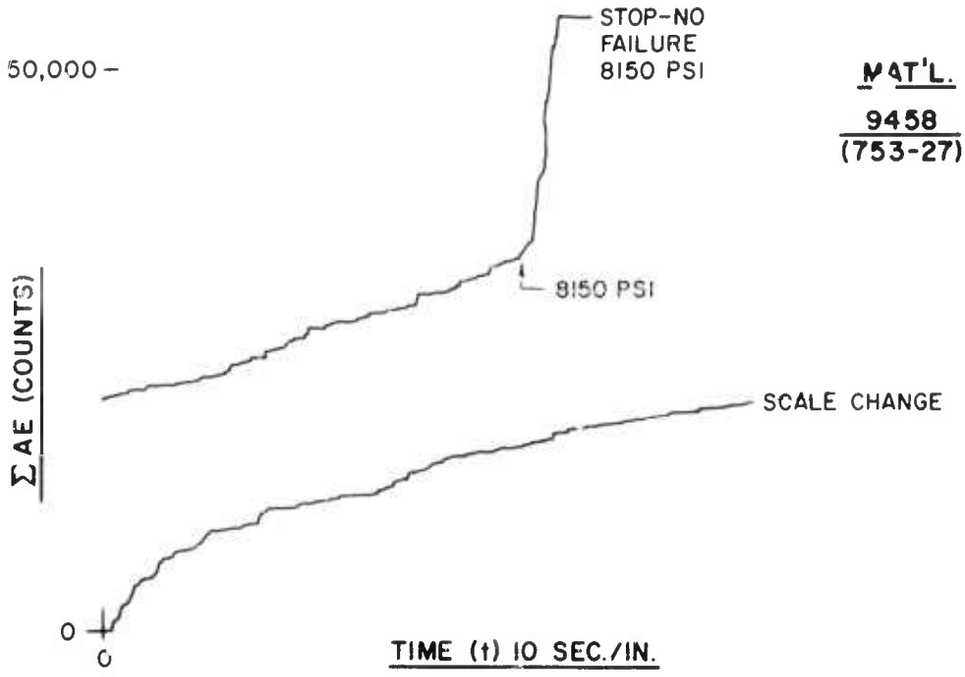

Figure 5.63 — Acoustic Emission Summation vs Time
Corning 9458

In Figure 5.63 the onset of failure is indicated at 8150 psi where a significant change in the slope of the curve of acoustic emission summation versus time is noted. This test bar represents LAS material with an average modulus of rupture of 7700 psi and an apparent porosity of 2.0%. It should be noted that this curve represents no preloading to eliminate the acoustic emissions at low stress levels, and indicates the magnitude of the number of events detected over the entire load range. The test was terminated prior to failure with the intent of analyzing for cumulative damage. Although the transition from microcrack to macrocrack propagation is evident, the total acoustic emission response of the test bar to stress is quite different from the previous tests on similar material. Many variables such as fracture strength, flaw density and morphology, porosity segregation, and the presence of undesirable phases and their specific location within the material structure need to be separated in order to analyze the acoustic emission response of a ceramic body subjected to a specific stress.

Conclusions

It is concluded that acoustic emission techniques can be applied to ceramic materials by mechanical loading. The results point out the potential of establishing design criteria, proof-stressing levels, and in-service integrity of ceramic components.

The areas of future work will include:

1. The determination of the effects of ultrasonically recorded flaws and their specific location in the AE test bars.
2. The effects of loading a ceramic body for periods of time at various stress levels.
3. Determining the relationship between AE response and cumulative damage.

6. REFERENCES

1. McLean, A. F., "The Application of Ceramics to the Small Gas Turbine," ASME Publication, No. 70-GT-105, Presented at the ASME Gas Turbine Conference & Products Show, Brussels, Belgium, May 24-28, 1970.

2. Dunham, J. and Came, P. M., "Improvements to the Ainley-Mathieson Method of Turbine Performance Prediction," ASME Paper No. 70-GT-2, Ibid.

3. Wilson, E. L., "Structural Analysis of Axisymetric Solids," AIAA Journal, Vol. 3, No. 12, December, 1965.

4. Wilson, E. L. and Nickell, R. E., "Application of the Finite Element Method to Head Condition Analysis," Nuclear Engineering and Design 4, North - Holland Publishing Company, Amsterdam, pp 276-286, 1966.

5. Private communication from M. L. Torti, Norton Company, October, 1971.

6. Gardner, K. A., "Efficiency of Extended Surfaces," Trans. ASME, November, 1945, p. 621.

7. Kingery, W. D., "Introduction to Ceramics," John Wiley and Sons, 1960, p. 10.

8. Popper, P., "Recent Developments in Ceramics and Their Application in Engineering," Journal of the Institute of Production Engineers, Vol. 48, No. 1, January, 1969.

9. Lumby, R. J. and Coe, R. F., "The Influence of Some Process Variables on The Mechanical Properties of Hot Pressed Silicon Nitride," Proceedings of the British Ceramic Society, No. 15, January, 1970.

10. Weaver, G. O. and Olsen, B. A., "Hot Pressed Silicon Carbide for High Temperature Applications." To be presented at the American Ceramic Society Annual Meeting, Washington, D.C., May 8-11, 1972.

11. Gulden, T. D., "Deposition and Microstructure of Vapor Deposited Silicon Carbide," Journal of the American Ceramic Society, Vol. 51, No. 8, August 1968, p. 424-27.

12. UKAEA Reactor Group, Risley, Warrington, Lancashire, England.

13. Evans, A. G. and Sharp, J. V., "Microstructural Studies on Silicon Nitride," Journal of Material Sciences, Vol. 6, (1971) p. 1292.

14. Butler, E., "Observations of Dislocations in β-Silicon Nitride," Philosophical Magazine, Vol. 21, (1971) p. 829.

15. JANAF Tables of Thermochemical Data, Dow Chemical Co., Midland, Mi.

16. Darken, L. S. and Gurry, R. W., "Physical Chemistry of Metals," McGraw Hill Book Co., Inc. (1953).

17. Per Kofstand, "High Temperature Oxidation of Metals," John Wiley & Sons, Inc. (1966).

Army Materials and Mechanics Research Center, Watertown, Massachusetts 02172

BRITTLE MATERIAL DESIGN, HIGH TEMPERATURE GAS TURBINE

Arthur F. McLean, Eugene A. Fisher, Ford Motor Company, Dearborn, Michigan 48121, Don E. Harrison, Westinghouse Electric Corporation, Pittsburgh, Pennsylvania 15235

Technical Report AMMRC CTR 72-3, March 1972, 162 pp - illus. - tables, Contract DAAG 46-71-C-0162, ARPA Order Number 1849, Interim Report, July 1, 1971 to December 31, 1971

AD _____

Distribution Limited to U.S. Government agencies only; Test and Evaluation data; March 1972. Other requests for this document must be referred to the Commanding Officer, Army Materials and Mechanics Research Center, Attn: AMMXMR - STL, Watertown, Massachusetts 02172

Key Words

Gas turbine engine
Brittle design
Ceramics
High temperature materials
Silicon nitride
Silicon carbide
Non-destructive tests

The "Brittle Materials Design, High Temperature Gas Turbine" program is to demonstrate successful use of brittle materials in demanding high temperature structural applications. A small vehicular gas turbine and a large stationary gas turbine, each utilizing uncooled ceramic components, will be used in this iterative design and materials development program. Both the contractor, Ford Motor Company, and the prime subcontractor, Westinghouse Electric Corporation, have had in-house research programs in this area prior to this contract.

In the vehicular gas turbine project, ceramic turbine components of improved design were fabricated and engine testing was started. During the first contract reporting period, silicon nitride turbine stators of the new design have shown considerably improved durability in testing to date. New design silicon nitride nose cones were fabricated by injection molding. Design studies on ceramic turbine rotors have shown that computed operating stresses can be withstood by dense silicon carbide and dense silicon nitride. Development programs were started to fabricate rotors in these materials.

Work on the stationary turbine project has concentrated on materials evaluation and initial design of ceramic stator vanes. Maximum calculated vane stresses were reduced 40% by decreasing the stator vane chord. The strength of hot-pressed silicon nitride, one of the candidate materials, has been significantly improved. A variety of microstructural details of this material have been identified. Physical property data were obtained on hot pressed silicon nitride.

Army Materials and Mechanics Research Center, Watertown, Massachusetts 02172

BRITTLE MATERIAL DESIGN, HIGH TEMPERATURE GAS TURBINE

Arthur F. McLean, Eugene A. Fisher, Ford Motor Company, Dearborn, Michigan 48121, Don E. Harrison, Westinghouse Electric Corporation, Pittsburgh, Pennsylvania 15235

Technical Report AMMRC CTR 72-3, March 1972, 162 pp - illus. - tables, Contract DAAG 46-71-C-0162, ARPA Order Number 1849, Interim Report, July 1, 1971 to December 31, 1971

AD _____

Distribution Limited to U.S. Government agencies only; Test and Evaluation data; March 1972. Other requests for this document must be referred to the Commanding Officer, Army Materials and Mechanics Research Center, Attn: AMMXMR - STL, Watertown, Massachusetts 02172

Key Words

Gas turbine engine
Brittle design
Ceramics
High temperature materials
Silicon nitride
Silicon carbide
Non-destructive tests

The "Brittle Materials Design, High Temperature Gas Turbine" program is to demonstrate successful use of brittle materials in demanding high temperature structural applications. A small vehicular gas turbine and a large stationary gas turbine, each utilizing uncooled ceramic components, will be used in this iterative design and materials development program. Both the contractor, Ford Motor Company, and the prime subcontractor, Westinghouse Electric Corporation, have had in-house research programs in this area prior to this contract.

In the vehicular gas turbine project, ceramic turbine components of improved design were fabricated and engine testing was started. During the first contract reporting period, silicon nitride turbine stators of the new design have shown considerably improved durability in testing to date. New design silicon nitride nose cones were fabricated by injection molding. Design studies on ceramic turbine rotors have shown that computed operating stresses can be withstood by dense silicon carbide and dense silicon nitride. Development programs were started to fabricate rotors in these materials.

Work on the stationary turbine project has concentrated on materials evaluation and initial design of ceramic stator vanes. Maximum calculated vane stresses were reduced 40% by decreasing the stator vane chord. The strength of hot-pressed silicon nitride, one of the candidate materials, has been significantly improved. A variety of microstructural details of this material have been identified. Physical property data were obtained on hot pressed silicon nitride.

Army Materials and Mechanics Research Center, Watertown, Massachusetts 02172

BRITTLE MATERIAL DESIGN, HIGH TEMPERATURE GAS TURBINE

Arthur F. McLean, Eugene A. Fisher, Ford Motor Company, Dearborn, Michigan 48121, Don E. Harrison, Westinghouse Electric Corporation, Pittsburgh, Pennsylvania 15235

Technical Report AMMRC CTR 72-3, March 1972, 162 pp - illus. - tables, Contract DAAG 46-71-C-0162, ARPA Order Number 1849, Interim Report, July 1, 1971 to December 31, 1971

AD _____

Distribution Limited to U.S. Government agencies only; Test and Evaluation data; March 1972. Other requests for this document must be referred to the Commanding Officer, Army Materials and Mechanics Research Center, Attn: AMMXMR - STL, Watertown, Massachusetts 02172

Key Words

Gas turbine engine
Brittle design
Ceramics
High temperature materials
Silicon nitride
Silicon carbide
Non-destructive tests

The "Brittle Materials Design, High Temperature Gas Turbine" program is to demonstrate successful use of brittle materials in demanding high temperature structural applications. A small vehicular gas turbine and a large stationary gas turbine, each utilizing uncooled ceramic components, will be used in this iterative design and materials development program. Both the contractor, Ford Motor Company, and the prime subcontractor, Westinghouse Electric Corporation, have had in-house research programs in this area prior to this contract.

In the vehicular gas turbine project, ceramic turbine components of improved design were fabricated and engine testing was started. During the first contract reporting period, silicon nitride turbine stators of the new design have shown considerably improved durability in testing to date. New design silicon nitride nose cones were fabricated by injection molding. Design studies on ceramic turbine rotors have shown that computed operating stresses can be withstood by dense silicon carbide and dense silicon nitride. Development programs were started to fabricate rotors in these materials.

Work on the stationary turbine project has concentrated on materials evaluation and initial design of ceramic stator vanes. Maximum calculated vane stresses were reduced 40% by decreasing the stator vane chord. The strength of hot-pressed silicon nitride, one of the candidate materials, has been significantly improved. A variety of microstructural details of this material have been identified. Physical property data were obtained on hot pressed silicon nitride.

Army Materials and Mechanics Research Center, Watertown, Massachusetts 02172

BRITTLE MATERIAL DESIGN, HIGH TEMPERATURE GAS TURBINE

Arthur F. McLean, Eugene A. Fisher, Ford Motor Company, Dearborn, Michigan 48121, Don E. Harrison, Westinghouse Electric Corporation, Pittsburgh, Pennsylvania 15235

Technical Report AMMRC CTR 72-3, March 1972, 162 pp - illus. - tables, Contract DAAG 46-71-C-0162, ARPA Order Number 1849, Interim Report, July 1, 1971 to December 31, 1971

AD _____

Distribution Limited to U.S. Government agencies only; Test and Evaluation data; March 1972. Other requests for this document must be referred to the Commanding Officer, Army Materials and Mechanics Research Center, Attn: AMMXMR - STL, Watertown, Massachusetts 02172

Key Words

Gas turbine engine
Brittle design
Ceramics
High temperature materials
Silicon nitride
Silicon carbide
Non-destructive tests

The "Brittle Materials Design, High Temperature Gas Turbine" program is to demonstrate successful use of brittle materials in demanding high temperature structural applications. A small vehicular gas turbine and a large stationary gas turbine, each utilizing uncooled ceramic components, will be used in this iterative design and materials development program. Both the contractor, Ford Motor Company, and the prime subcontractor, Westinghouse Electric Corporation, have had in-house research programs in this area prior to this contract.

In the vehicular gas turbine project, ceramic turbine components of improved design were fabricated and engine testing was started. During the first contract reporting period, silicon nitride turbine stators of the new design have shown considerably improved durability in testing to date. New design silicon nitride nose cones were fabricated by injection molding. Design studies on ceramic turbine rotors have shown that computed operating stresses can be withstood by dense silicon carbide and dense silicon nitride. Development programs were started to fabricate rotors in these materials.

Work on the stationary turbine project has concentrated on materials evaluation and initial design of ceramic stator vanes. Maximum calculated vane stresses were reduced 40% by decreasing the stator vane chord. The strength of hot-pressed silicon nitride, one of the candidate materials, has been significantly improved. A variety of microstructural details of this material have been identified. Physical property data were obtained on hot pressed silicon nitride.

Army Materials and Mechanics Research Center, Watertown, Massachusetts 02172

BRITTLE MATERIAL DESIGN, HIGH TEMPERATURE GAS TURBINE

Arthur F. McLean, Eugene A. Fisher, Ford Motor Company, Dearborn, Michigan 48121, Don E. Harrison, Westinghouse Electric Corporation, Pittsburgh, Pennsylvania 15235

Technical Report AMMRC CTR 72-3, March 1972, 162 pp - illus. - tables, Contract DAAG 46-71-C-0162, ARPA Order Number 1849, Interim Report, July 1, 1971 to December 31, 1971

AD

Distribution Limited to U.S. Government agencies only; Test and Evaluation data; March 1972. Other requests for this document must be referred to the Commanding Officer, Army Materials and Mechanics Research Center, Attn: AMMXMR - STL, Watertown, Massachusetts 02172

Key Words

Gas turbine engine
Brittle design
Ceramics
High temperature materials
Silicon nitride
Silicon carbide
Non-destructive tests

The "Brittle Materials Design, High Temperature Gas Turbine" program is to demonstrate successful use of brittle materials in demanding high temperature structural applications. A small vehicular gas turbine and a large stationary gas turbine, each utilizing uncooled ceramic components, will be used in this iterative design and materials development program. Both the contractor, Ford Motor Company, and the prime subcontractor, Westinghouse Electric Corporation, have had in-house research programs in this area prior to this contract.

In the vehicular gas turbine project, ceramic turbine components of improved design were fabricated and engine testing was started. During the first contract reporting period, silicon nitride turbine stators of the new design have shown considerably improved durability in testing to date. New design silicon nitride nose cones were fabricated by injection molding. Design studies on ceramic turbine rotors have shown that computed operating stresses can be withstood by dense silicon carbide and dense silicon nitride. Development programs were started to fabricate rotors in these materials.

Work on the stationary turbine project has concentrated on materials evaluation and initial design of ceramic stator vanes. Maximum calculated vane stresses were reduced 40% by decreasing the stator vane chord. The strength of hot-pressed silicon nitride, one of the candidate materials, has been significantly improved. A variety of microstructural details of this material have been identified. Physical property data were obtained on hot pressed silicon nitride.

Army Materials and Mechanics Research Center, Watertown, Massachusetts 02172

BRITTLE MATERIAL DESIGN, HIGH TEMPERATURE GAS TURBINE

Arthur F. McLean, Eugene A. Fisher, Ford Motor Company, Dearborn, Michigan 48121, Don E. Harrison, Westinghouse Electric Corporation, Pittsburgh, Pennsylvania 15235

Technical Report AMMRC CTR 72-3, March 1972, 162 pp - illus. - tables, Contract DAAG 46-71-C-0162, ARPA Order Number 1849, Interim Report, July 1, 1971 to December 31, 1971

AD

Distribution Limited to U.S. Government agencies only; Test and Evaluation data; March 1972. Other requests for this document must be referred to the Commanding Officer, Army Materials and Mechanics Research Center, Attn: AMMXMR - STL, Watertown, Massachusetts 02172

Key Words

Gas turbine engine
Brittle design
Ceramics
High temperature materials
Silicon nitride
Silicon carbide
Non-destructive tests

The "Brittle Materials Design, High Temperature Gas Turbine" program is to demonstrate successful use of brittle materials in demanding high temperature structural applications. A small vehicular gas turbine and a large stationary gas turbine, each utilizing uncooled ceramic components, will be used in this iterative design and materials development program. Both the contractor, Ford Motor Company, and the prime subcontractor, Westinghouse Electric Corporation, have had in-house research programs in this area prior to this contract.

In the vehicular gas turbine project, ceramic turbine components of improved design were fabricated and engine testing was started. During the first contract reporting period, silicon nitride turbine stators of the new design have shown considerably improved durability in testing to date. New design silicon nitride nose cones were fabricated by injection molding. Design studies on ceramic turbine rotors have shown that computed operating stresses can be withstood by dense silicon carbide and dense silicon nitride. Development programs were started to fabricate rotors in these materials.

Work on the stationary turbine project has concentrated on materials evaluation and initial design of ceramic stator vanes. Maximum calculated vane stresses were reduced 40% by decreasing the stator vane chord. The strength of hot-pressed silicon nitride, one of the candidate materials, has been significantly improved. A variety of microstructural details of this material have been identified. Physical property data were obtained on hot pressed silicon nitride.

Army Materials and Mechanics Research Center, Watertown, Massachusetts 02172

BRITTLE MATERIAL DESIGN, HIGH TEMPERATURE GAS TURBINE

Arthur F. McLean, Eugene A. Fisher, Ford Motor Company, Dearborn, Michigan 48121, Don E. Harrison, Westinghouse Electric Corporation, Pittsburgh, Pennsylvania 15235

Technical Report AMMRC CTR 72-3, March 1972, 162 pp - illus. - tables, Contract DAAG 46-71-C-0162, ARPA Order Number 1849, Interim Report, July 1, 1971 to December 31, 1971

AD

Distribution Limited to U.S. Government agencies only; Test and Evaluation data; March 1972. Other requests for this document must be referred to the Commanding Officer, Army Materials and Mechanics Research Center, Attn: AMMXMR - STL, Watertown, Massachusetts 02172

Key Words

Gas turbine engine
Brittle design
Ceramics
High temperature materials
Silicon nitride
Silicon carbide
Non-destructive tests

The "Brittle Materials Design, High Temperature Gas Turbine" program is to demonstrate successful use of brittle materials in demanding high temperature structural applications. A small vehicular gas turbine and a large stationary gas turbine, each utilizing uncooled ceramic components, will be used in this iterative design and materials development program. Both the contractor, Ford Motor Company, and the prime subcontractor, Westinghouse Electric Corporation, have had in-house research programs in this area prior to this contract.

In the vehicular gas turbine project, ceramic turbine components of improved design were fabricated and engine testing was started. During the first contract reporting period, silicon nitride turbine stators of the new design have shown considerably improved durability in testing to date. New design silicon nitride nose cones were fabricated by injection molding. Design studies on ceramic turbine rotors have shown that computed operating stresses can be withstood by dense silicon carbide and dense silicon nitride. Development programs were started to fabricate rotors in these materials.

Work on the stationary turbine project has concentrated on materials evaluation and initial design of ceramic stator vanes. Maximum calculated vane stresses were reduced 40% by decreasing the stator vane chord. The strength of hot-pressed silicon nitride, one of the candidate materials, has been significantly improved. A variety of microstructural details of this material have been identified. Physical property data were obtained on hot pressed silicon nitride.

Unclassified

Security Classification

DOCUMENT CONTROL DATA - R & D

Security classification of title, body of abstract and indexing annotation must be entered when the overall report is classified)

1. ORIGINATING ACTIVITY (Corporate author)	2a. REPORT SECURITY CLASSIFICATION
Ford Motor Company Dearborn, Michigan 48121	Unclassified
	2b. GROUP

3. REPORT TITLE

Brittle Materials Design, High Temperature Gas Turbine

4. DESCRIPTIVE NOTES *(Type of report and inclusive dates)*

Interim Report, July 1, 1971 to December 31, 1971

5. AUTHOR(S) *(First name, middle initial, last name)*

Arthur F. McLean
Eugene A. Fisher
Don E. Harrison

6. REPORT DATE	7a. TOTAL NO. OF PAGES	7b. NO. OF REFS
March, 1972	162	17

8a. CONTRACT OR GRANT NO.	9a. ORIGINATOR'S REPORT NUMBER(S)
DAAG 46-71-C-0162	AMMRC CTR 72-3
b. PROJECT NO ARPA Order No. 1849	
c. Project Code No. 1D10	9b. OTHER REPORT NO(S) *(Any other numbers that may be assigned this report)*
d. Agency Accession No. DA OD 4733	

10. DISTRIBUTION STATEMENT Distribution limited to U.S. Government agencies only; Test and Evaluation data; March 1972. Other requests for this document must be referred to the Commanding Officer, Army Materials and Mechanics Research Center, ATTN: AMXMR-STL, Watertown, Massachusetts 02172

11. SUPPLEMENTARY NOTES	12. SPONSORING MILITARY ACTIVITY
	Army Materials and Mechanics Research Center Watertown, Massachusetts 02172

13. ABSTRACT

The "Brittle Materials Design, High Temperature Gas Turbine" program, is to demonstrate successful use of brittle materials in demanding high temperature structural applications. A small vehicular gas turbine and a large stationary gas turbine, each utilizing uncooled ceramic components, will be used in this iterative design and materials development program. Both the contractor, Ford Motor Company, and the prime subcontractor, Westinghouse Electric Corporation, have had in-house research programs in this area prior to this contract.

In the vehicular gas turbine project, ceramic turbine components of improved design were fabricated and engine testing was started. During the first contract reporting period, silicon nitride turbine stators of the new design have shown considerably improved durability in testing to date. New design silicon nitride nose cones were fabricated by injection molding. Design studies on ceramic turbine rotors have shown that computed operating stresses can be withstood by dense silicon carbide and dense silicon nitride. Development programs were started to fabricate rotors in these materials.

Work on the stationary turbine project has concentrated on materials evaluation and initial design of ceramic stator vanes. Maximum calculated vane stresses were reduced 50% by decreasing the stator vane chord. The strength of hot-pressed silicon nitride, one of the candidate materials, has been significantly improved. A variety of microstructural details of this material have been identified. Physical property data were obtained on hot pressed silicon nitride.

DD FORM 1 NOV 1473 REPLACES DD FORM 1473, 1 JAN 64, WHICH IS OBSOLETE FOR ARMY USE.

Unclassified

Security Classification

KEY WORDS	LINK A		LINK B		LINK C	
	ROLE	WT	ROLE	WT	ROLE	WT
Gas turbine engine						
Brittle design						
Ceramics						
High-temperature materials						
Silicon nitride						
Silicon carbide						
Non-destructive tests						